MIXTURE FORMATION AND HEAT RELEASE IN DIESEL ENGINES

by

Meguerdich Meguerdichian

Thesis submitted for the degree of
Doctor of Philosophy
in the
University of London

March 1978

Department of Mechanical Engineering,
Imperial College of Science & Technology,
London, S.W.7.

ACKNOWLEDGEMENTS

The author wishes to acknowledge the paramount guidance and supervision received from Dr. N. Watson.

Thanks are extended to Prof. W. Murgatroyd and academic staff members of the Thermal Power Section.

Special thanks are due to Mr. W. Masters and the technical staff of the Mechanical Engineering Department.

The author wishes to express thanks to his colleagues for suggestions, help and discussions, especially to Dr. M. Marzouk, Dr. T.F. Jones, Dr. N. James, Dr. D. Abizadeh and Mr. Z. Baazaari.

Sincere thanks are also due to Miss D. Day and the Department Librarian, Miss E.M. Archer.

The author is very thankful to Mrs. B. Price for typing most of the manuscript.

Financial assistance received from Arya Mehr University and the British Council is gratefully acknowledged.

ABSTRACT

A mathematical model for predicting the mixture formation and rate of heat release in direct injection diesel engines has been developed. The method is based on a time-dependent multi-zone analysis of the cylinder contents.

Movement and concentration change of small individual zones within the developing fuel spray has been considered on the basis of a jet-mixing model. Attention has been paid to devise a detailed zone-division pattern that allows transition to a wall jet and accounts for the air swirl in the combustion chamber.

The First Law of thermodynamics, the equation of state and the burning rate equation have been applied to individual zones. Pressure is assumed to be equal in all zones at any time. The fuel mass burning rate is calculated by the Arrhenius equation, for all zones from the rich to the lean limits of inflammability.

The zone-division pattern provides the essential structure for a step-by-step computation of the time-dependent zone variables.

The use of an ignition delay correlation has been avoided. It has been shown to be possible to predict ignition on the basis of two phenomena, namely, the jet mixing pattern and temperature dependent reaction rates.

Predicted cylinder pressure, rate of pressure rise and heat release rate diagrams have been compared with experimental data obtained from a turbocharged, direct

injection, 4-stroke truck engine.

The response of the model to changes in injection timing, swirl, air temperature and injection rate has been predicted and discussed.

The initiation and development of combustion has been studied by displaying the predicted temporal and spatial distribution of burning rate, local temperature, air-fuel ratio etc. at two test conditions.

It has been concluded that the model is capable of predicting realistic rate of pressure rise and heat release rates and responds sensibly to parametric changes. Therefore it has been recommended that the distribution of variables predicted by the model will be a valuable tool in future pollutant studies.

CONTENTS

Chapter One - Introduction

1.1 Introduction and scope of work page 1
1.2 General description 2
1.3 Objectives and outline 7

Chapter Two - Literature Review

2.1 Introduction 10
2.2 Combustion models 10
2.2.1 Previous models 11
a) The Lyn model 11
b) The Ikegami model 13
c) The Shipinski model 14
d) The Whitehouse model 20
e) The C.A.V. model 23
2.2.2 Contemporary models 27
a) The Hodgetts model 27
b) The Shahed model 31
c) The Hiroyasu model 35
2.3 Discussion 40

Chapter Three - Mixture Formation

3.1 Introduction 44
3.2 The free jet 44
3.2.1 Definitions 44
3.2.2 Momentum conservation 46
3.2.3 Mass conservation 47
3.2.4 Velocity and concentration decay 48
3.2.5 Growth of the mixing layer 50
3.2.6 Initial region of the jet 51
3.2.7 Fuel and air flow 54
3.3 The wall jet 55
3.3.1 Definitions 55
3.3.2 Wall jet variables related to a free jet 57

page

3.3.3 Wall jet fuel and air flow 58
3.3.4 The wall jet growth, velocity and concentration decay 59

3.4 The starting jet 60
3.4.1 Definitions 61
3.4.2 The free-jet penetration 63
3.4.3 The wall-jet penetration 65
3.4.4 The development time 66

3.5 A multizone spray model 71
3.5.1 Moving zones of equal fuel mass 71
3.5.2 Zones in intermittent jets 79
3.5.3 Air swirl 84
3.5.4 Zones after impingement 88

Chapter Four - Experimental Work

4.1 Introduction 92
4.2 Test facility 92
4.3 Test bed equipment 95
4.4 The injector instrumentation 100
4.5 Data 112

Chapter Five - Heat Release Prediction

5.1 Introduction 119
5.2 The heat release model 119
5.2.1 Assumptions 122
5.2.2 Governing equations 123
5.2.3 Further information 126
a) Heat transfer 126
b) Evaporation 127
c) Numerical constants 129
d) Zone fuel and air mass 130
e) Zone specific heats 133
f) Calculation of the swirl ratio 134

5.3 Solution procedure 138
5.4 The computer program 143

page

Chapter Six - Discussion and Evaluation of Results

6.1 Introduction 150

6.2 Comparison of model prediction with experimental data 150

6.3 Effects of varying certain parameters on model predictions 166

6.4 Investigation of history and distribution of predicted variables 175

Chapter Seven - Conclusions and Recommendations for Future Work

7.1 Summary 209

7.2 Conclusions 211

7.3 Recommendations 212

Appendix A 214

Appendix B 216

Appendix C 217

Publications 218

References 219

NOTATION

A_o	nozzle hole area
A	jet cross sectional area
b	burnt fract (m_{fb}/m_f)
c	concentration (fuel-air by mass)
d_o	nozzle hole diameter
d'	equivalent jet diameter ($d' = d_o \sqrt{\rho_o/\rho_a}$)
E	activation energy
h	enthalpy
K_f, K_j, K_s	constants
K	parameter to define layer number
KR	number of layers in zone-division
L	parameter to define zone number along a layer
LX	number of zones in a layer
m	mass
m_{fb}	mass of fuel burnt
$\dot{m}_f$	fuel injection mass flow rate
n	number of burning zones
p	pressure
q	heat
r	radius
r_i	jet radius at impingement
r_f	positions of the wall jet front
r_m	positions along the wall jet maximum velocity
R	gas constant
s	arc distance along the deflected jet centreline
t	time since injection
t_i	time since impingement

t_o	development time
T	temperature
u	velocity
u_f	penetration velocity (free jet)
u_{mi}	free jet maximum velocity at impingement
U	specific internal energy
V	volume
w	velocity (wall jet)
w_{mi}	wall jet initial maximum velocity
x_f	distance along centreline (hypothetical penetration)
x_s	length of the developed part of the jet
x_{sl}	axial distance in deflected jet
y	non-dimensional radius (free jet)
y_{sl}	tangential displacement in deflected jet
λ	deflection parameter
ϕ	equivalence ratio (c/c_{st})
ρ	density
Δt	time step of computation
Δy_k	layer width

SUFFICES

a	air
b	burnt
f	fuel (or jet-front)
i	impingement (or initial)
j	jet
K	layer
m	maximum (or centreline)

o	nozzle exit
w	wall
z	zone

List of Figures

Fig. 1.1 The heat release rate diagram in diesel engines.

Fig. 1.2 The direct injection engine spray configuration.

Fig. 2.1 Schematic relationship between rate of injection and rate of burning (Lyn - 1962).

Fig. 2.2 a) Schematic diagram ill tration, the relation between B(t), C(t) and Q(t).

b) Block diagram of varying delay mechanism.

c) Block diagram of the model (Ikegami - 1969).

Fig. 2.3 ROHR for fuel injected during each degree crank angle and total heat release curve (Shipinski - 1969).

Fig. 2.4 Comparison of ROHR predicted by Model Tanas II with $C_E \propto p^{-0.12}$ and experimental ROHR (Shipinski 1969).

Fig. 2.5 Comparison of ROHR predicted by Model Tanas II with $C_E \propto p^{0.25}$ and experimental ROHR (Shipinski 1969).

Fig. 2.6 Comparison of ROHR predicted by Model Tanas II with $C_E \propto T^{0.33}$ and experimental ROHR (Shipinski 1969).

Fig. 2.7 Geometric representation of two zone model (Whitehouse - 1974).

Fig. 2.8 Fuel spray free and wall jet model for air entrainment (C.A.V. - 1973).

Fig. 2.9 Schematic representation of combustion zones (C.A.V. - 1973).

Fig. 2.10 Calculated instantaneous values for air entrainment, micromixing, and rate of heat release versus crank angle (C.A.V. - 1973).

Fig. 2.11 a) Calculated positions of point mass centres of zones.
b) Diagram of free jet showing formation of "n" zones (Hodgetts - 1975).

Fig. 2.12 Progressive evolution of combustion zones (Shahed - 1975).

Fig. 2.13 a) Diagram of the divided package of the spray
b) Schematic diagram of the spray combustion (Hiroyasu - 1976).

Fig. 3.1 Schematic diagram of the free jet.

Fig. 3.2 Sketch of the initial jet region.

Fig. 3.3 The relationship between jet variables.

Fig. 3.4 Schematic diagram of the wall jet.

Fig. 3.5 Inner and outer layers of the wall jet.

Fig. 3.6 The developing jet

Fig. 3.7 Jet development and zone-division initial study (Eq. 1)

Fig. 3.8 Jet development and zone-division initial study (Eq. 2)

Fig. 3.9 Variables of a zone-division pattern with unequal layer width.

Fig. 3.10 Relationship between zone residence-time and layer number.

Fig. 3.11 Development of individual zones with time.

Fig. 3.12 Zone labelling code.

Fig. 3.13 The deflected jet in swirling cross-flow.

Fig. 3.14 Visualisation of zone growth

Fig. 3.15 Zone motion with deflection and impingement.

Fig. 4.1 General view of the test-bed.

Fig. 4.2 PDP 15 computer and peripherals.

Fig. 4.3 The Leyland 520 engine.

Fig. 4.4 The data logging interface.

Fig. 4.5 Auxilliary equipment tower.

Fig. 4.6 Test-bed instrumentation panel.

Fig. 4.7 Top view of the test-bed.

Fig. 4.8 Engine control and monitoring units.

Fig. 4.9 Cross-sectional drawing of the instrumented injector.

Fig. 4.10 Injector nozzle geometry.

Fig. 4.11 The flow area at needle lift.

Fig. 4.12 Injection rate and nozzle discharge coefficient vs needle lift.

Fig. 4.13 Variation of fuel to air equivalence ratio with engine speed and load.

Fig. 4.14 Variation of injection duration with engine speed and load.

Fig. 4.15 Variation of fuel/cycle/cylinder with engine speed and load.

Fig. 4.16 Variation of trapped mass with engine speed and load.

Fig. 4.17 Average injection velocity and injection rates versus engine speed and load.

Fig. 4.18 Fuel/degree/FCC versus engine speed and load.

Fig. 4.19 Variation of maximum fuel line pressure and needle lift with speed and load.

Fig. 4.20 Variation of maximum cylinder pressure with engine speed and load.

Fig. 4.21 Cylinder pressure at injection versus engine speed and load.

Fig. 4.22 Air density ratio at injection versus engine

speed and load.

Fig. 5.1 Constant pressure specific heats vs mixture temperature.

Fig. 5.2 Variation of swirl ratio with crank angle.

Fig. 5.3 P - V diagram to illustrate the iteration procedure.

Fig. 5.4 Flow-diagram of the computer program.

Fig. 6.1 Experimental verification of model predictions (case 1) Engines speed 1000 rev/min, bmep 450 kN/m^2

Fig. 6.2 Experimental verification of model predictions (case 2) Engine speed 1000 rev/min, bmep 900 kN/m^2.

Fig. 6.3 Experimental verification of model predictions (case 3) Engine speed 1500 rev/min, bmep 450 kN/m^2.

Fig. 6.4 Experimental verification of model predictions (case 4) Engine speed 1500 rev/min, bmep 900 kN/m^2.

Fig. 6.5 Experimental verification of model predictions (case 5) Engine speed 2000 rev/min, bmep 450 kN/m^2.

Fig. 6.6 Experimental verification of model predictions (case 6) Engine speed 2000 rev/min, bmep 900 kN/m^2.

Fig. 6.7 Experimental verification of model predictions (case 7) Engine speed 2500 rev/min, bmep 450 kN/m^2.

Fig. 6.8 Experimental verification of model predictions (case 8) Engine speed 2500 rev/min, bmep

900 kN/m^2

Fig. 6.9 Jet-front displacement every degree crank angle before wall impingement (case 1 to 8)

Fig. 6.10 Predicted effect of injection timing (case 3).

Fig. 6.11 Predicted effect of swirl ratio (case 3).

Fig. 6.12 Predicted effect of trapped mass (case 3).

Fig. 6.13 Predicted effect of injection rate (case 3)

Fig. 6.14 Percentage of fuel burnt in individual zones (7 to 10 degrees- case 3).

Fig. 6.15 Percentage of fuel burnt in individual zones (11 to 14 degrees- case 3).

Fig. 6.16 Temperature in individual zones (7 to 10 degrees- case 3).

Fig. 6.17 Temperature in individual zones (11 to 14 degrees - case 3).

Fig. 6.18 Fuel burning rate in individual zones (7 to 10 degrees- case 3).

Fig. 6.19 Fuel burning rate in individual zones (11 to 14 degrees- case 3).

Fig. 6.20 Percentage of unburnt air in individual zones (7 to 10 degrees- case 3).

Fig. 6.21 Percentage of unburnt air in individual zones (11 to 14 degrees- case 3)

Fig. 6.22 Unburnt air/zone fuel equivalence ratio (7 to 10 degrees- case 3).

Fig. 6.23 Unburnt air/zone fuel equivalence ratio (11 to 14 degrees- case 3).

Fig. 6.24 Percentage of fuel burnt in individual zones (5 to 13 degrees- case 8).

Fig. 6.25 Percentage of fuel burnt in individual zones (14 to 19 degrees- case 8).

Fig. 6.26 Temperature in individual zones (5 to 13 degrees- case 8).

Fig. 6.27 Temperature in individual zones (14 to 19 degrees- case 8).

Fig. 6.28 Fuel burning rate in individual zones (5 to 13 degrees- case 8).

Fig. 6.29 Fuel burning rate in individual zones (14 to 19 degrees- case 8)

Fig. 6.30 Percentage of unburnt air in individual zones (5 to 13 degrees- case 8).

Fig. 6.31 Percentage of unburnt air in individual zones (14 to 19 degrees- case 8).

Fig. 6.32 Unburnt air/zone fuel equivalence ratio (5 to 13 degrees- case 8).

Fig. 6.33 Unburnt air/zone fuel equivalence ratio (14 to 19 degrees- case 8).

Fig. 6.34 Percentage of fuel burnt vs crank angle for individual zones created during the first half of injection (case 3).

Fig. 6.35 Percentage of fuel burnt vs crank angle for individual zones created during the second half of injection (case 3).

Fig. 6.36 Percentage of fuel burnt vs crank angle for individual zones created during the first half of injection (case 8).

Fig. 6.37 Percentage of fuel burnt vs crank angle for individual zones created during the second half of injection (case 8).

CHAPTER 1

INTRODUCTION

1.1 Introduction and scope of work

Experimental work aimed at the optimisation of engine performance involves successive changes of each of the many parameters concerned, which is both expensive and time consuming.

If the behaviour of the engine can be simulated by a mathematical model, the effect of design changes can be quickly and cheaply estimated by the use of a computer.

Within the past twenty years or so, significant progress has been made in various aspects of engine mathematical modelling in Great Britain and other parts of the world. Yet there is a considerable lack of published literature on the fundamentals of the combustion process, particularly in diesel engines. This part of the engine cycle analysis has proved to be the weakest link in the chain leading to engine performance prediction.

There have been a number of difficulties, mainly in the following areas:

a) The heterogeneous nature of the combustion process in diesel engines offers a complicated problem to be solved as compared to the petrol engine, which usually involves homogeneous mixtures.

b) The time-dependent nature of both the spray and the surrounding air makes the problem entirely different from the usual heterogeneous combustion occurring in the gas turbine.

c) There is an acute shortage of both theoretical and experimental work on complicated jet-mixing processes such as the ones encountered in diesel engines.

It will be a long time before details of such a problem are correctly formulated and exact solutions obtained. Meanwhile the immidiate practical needs of the diesel engine industry remain unfulfilled. Some related factors are as follows:

1) There is widespread concern about pollutants in the exhaust, which are directly affected by mixture formation and the burning pattern in the engine.

2) There are the requirements for improving engine specific fuel consumption, due to recent world-wide economic difficulties and dwindling fuel resources.

3) Considerable attention is being paid to engine noise as another potential invironmental hazard, this being affected by the rapid pressure rise in the engine cylinder due to a particular burning pattern.

4) For engine design, the burning pattern is needed to forecast the peak pressure to which the engine components are to be subjected.

Thus although a number of difficulties are involved, any improvement in the mathematical model which can be obtained could lead to significant practical benefits.

Before discussing combustion models, a general description of the combustible mixture formation process and subsequent burning in a diesel engine is given.

1.2 General description

In diesel engines, fuel and air enter the combustion chamber separately. The air mass is determined at inlet valve closure (IVC) and is termed 'the trapped mass'. The desired mass of liquid fuel is injected into it via an appropriate injection system. The 'static injection timing' is the crank angle position, relative to top dead centre, at which the system is statically set to commence injection. The actual commencement of injection, however, depends on the running condition and is known as 'the dynamic injection timing'. During the compression stroke the charge temperature and pressure are being increased to exceed the self ignition condition of the fuel.

The spatial location at which ignition occurs is not fixed, as it depends on where the correct mixture conditions will have formed at the appropriate local temperature. The mixing process taking place inside the combustion chamber facilitates the formation of desirable local conditions for ignition, even at very low values of the overall fuel/air ratio.

The relatively slow nature of diesel engine combustion is also partly attributed to the mixing process. There is some rapid premixed burning however just after ignition. During this stage, the fuel accumulated at a variety of mixture ratios (from rich to lean limits of inflammability), initially undergoing the slow preflame reactions due to comparatively low local temperatures, is finally subjected to temperatures high enough to create a 'burning-temperature rise-burning' chain of events.

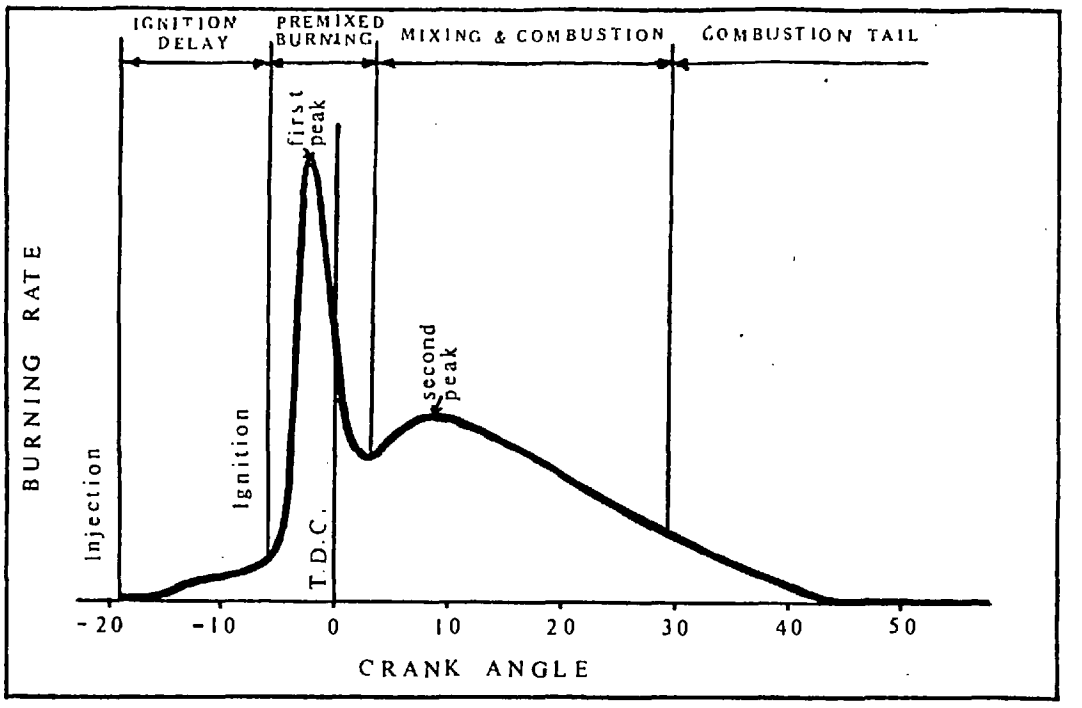

Fig.1.1 The heat release rate diagram in diesel engines.

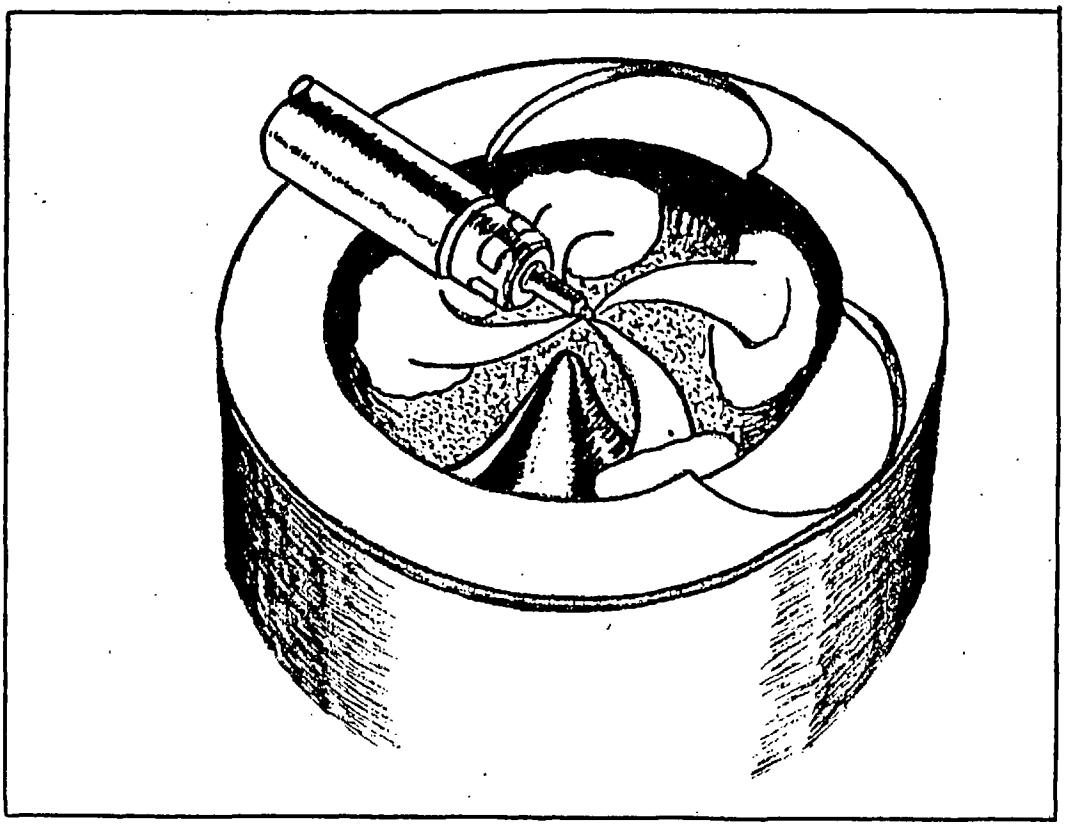

Fig.1.2 The direct injection engine spray configuration.

Fig. (1.1) shows the fuel burning rate in diesel engines diagramatically. This curve is usually considered to consist of four stages. The first stage is known as the 'ignition delay' and involves the preflame reactions. The values of burning rate are very small during this stage but they gradually increase towards the ignition point (shown exaggarated on the curve). Ignition in diesel engines is recognised by the onset of a highly luminous flame with consequent rapid rise in the burning rate.

The duration of the 'premixed burning' stage depends on engine running conditions. Sometimes there may be little premixed burning (high load and speed, turbo-charged non-intercooled engines). At other times, however, when there is a significant amount of premixed fuel, a sharp spike will appear in the fuel burning rate curve. Longer ignition delay results in a higher first peak. Delayed injection (nearer to T.D.C.) reduces it. Higher values of trapped mass also result in a small first peak.

After the premixed burning stage there are no abrupt changes in the fuel burning rate. The temperatures are high enough at this stage to burn the mixture according to its preparation rate. This is called the 'mixing controlled' or the 'diffusion controlled' combustion stage. It may or may not show a second peak on the curve. The existence of the second peak will depend on whether the preparation rate is already decreasing at the end of pre-mixed burning, or is still rising before it finally starts to decrease.

During the next and final stage, known as 'the combustion tail', the temperatures eventually reduce due to

expansion, and any unburnt mixture burns at a much lower rate. The mixture distribution is somewhat irregular and the nature of the reactions rather unknown during this stage. The rate of burning may become temperature dependent once again and possibly show a slight increase towards the end.

The above description is very general; the details, of course, will depend on the particular engine and the running conditions. The studies in this text are carried out by considering a direct injection type engine spray configuration shown schematically in Fig. (1.2).

In this type of a combustion chamber, fuel is injected directly into the piston bowl by means of a multihole nozzle. Depending on the engine geometry and the air swirl present, the resulting plumes usually hit the wall and spread across it in the form of wall-jets. Motion pictures of combustion have revealed that ignition may occur before or after impingement, at a location somewhere behind the jet-front. A luminous flame then flashes back towards the nozzle, forming an off-burner type flame, while injection continues. At the end of injection the flame is swept away along the jet path. Obviously, during injection, the mixture in the vicinity of the nozzle is too rich to hold a flame, even when cylinder temperatures are quite high. The details are best explained when the assumptions are stated and a model is presented.

Cylinder pressure is a variable which is relatively easy to measure and can be used to compute what is known as the 'apparent heat release rate'. This is obtained by

applying the first law of thermodynamics to the cylinder contents together with the knowledge of the instantaneous heat loss to the walls.

The term 'heat release rate' is widely applied to express the heat equivalent of the fuel mass burning rate (burning rate multiplied by the fuel calorific value). The term 'apparent' covers the fact that some assumptions are made for heat transfer and that exact heat transfer rates are unknown. The 'apparent heat release rate' also takes into account the dissociation effects and the latent heat of fuel evaporation and thus may initially show some slightly negative values.

In different published literature, the term 'burning' may have different meanings (i.e. partial oxidation, oxidation to equilibrium products, etc.). In this work, the term 'fuel burning rate' is used only for the rate of fuel liberating its fixed calorific value. (Note: in the literature review, if partial oxidation is referred to as 'burning', it will be specified).

1.3 Objectives and outline

The work described herein was carried out in conjunction with engine performance simulation projects. The objective was to study the mixture formation and heat release in diesel engines in order to develop methods of simulating the combustion part of the engine thermodynamic cycle.

The outcome was intended to be of use in complete engine simulation programmes as well as to be of some help in solving problems in industry.

Experimental work was based on a Leyland 520 turbo-charged engine. The work was carried out in parallel with a dynamic simulation project for this engine (Marzouk, 1976).

The engine was instrumented to supply transient as well as steady-state data under direct computer control, thus providing a variety of information to compare with theoretical predictions.

Some of the previous techniques for the simulation of mixture formation and heat release in diesel engines were studied; a review of relevant published literature is given in the next chapter. It is shown how the traditional approach to diesel engine combustion (droplet evaporation and burning) has been replaced by more recent studies which consider jet-mixing to be the dominating phenomenon.

Most jet-mixing literature deals mainly with steady free or wall jets and does not cover diesel engine type intermittent sprays. In Chapter 3 a model is presented to describe the mixture distribution and motion in these types of jets through a consistent set of relations. In particular the penetrating jet-front, the trancating jet-back as well as the transition to a wall jet under these conditions are considered.

The measured variables for the calculation of the injection-rate as well as other experimental data are explained in Chapter 4 along with descriptions of the test-bed and engine. It is also explained how the required data mainly served the purpose of model evaluation and how those variables needed as initial conditions were reduced to a minimum, in order to obtain a more flexible and general

prediction model.

In Chapter 5 the heat release model, based on a multizone analysis of the cylinder contents, is explained. The fuel injected is divided into discrete elements, each one forming a zone which moves and entrains air according to the pattern explained in Chapter 3. Due to the complexity of the problem, a set of simplifying assumptions had to be adopted and these are stated and discussed. Differential equations are set up and solved numerically to yield the zone temperature and burning rate in addition to the cylinder pressure variation with time.

Predicted results are compared with the experimental data in Chapter 6, together with a discussion of the merits and shortcomings of the model.

In the final chapter, conclusions are drawn and recommendations made for future work on the basis of the experience gained while carrying out the project.

CHAPTER 2

LITERATURE REVIEW

2.1 Introduction

When liquid fuel is injected into a diesel combustion chamber a jet is formed as a result of atomization, evaporation and mixing with air. There is temperature rise due to compression, and favourable mixture conditions preveil when some of the fuel is slowed down and pushed towards the edges of the jet. Ignition then takes place followed by further mixing and burning.

Each of the steps in this simplified pattern has been the subject of several studies in the past. It is the intention of this chapter to analyse those parts of past studies which relate to the problem at hand. A review of some of the contemporary models is also presented.

2.2 Combustion models

It is appropriate to mention the general trend observed in recent developments in diesel engine combustion modelling. Efforts have been made to:

a) employ a more realistic air entrainment pattern;

b) reduce dependence on specific experimental correlations.

For example, experimental correlations can be seen for ignition delay, spray penetration and droplet evaporation in most combustion models. Whether or not their use proves fruitful depends mostly on the range of application and the purpose for which they have been designated.

2.2.1 Previous models

a) The Lyn model

Lyn (1962) proposed a model for the computation of heat release in which the fuel was divided into elements according to their order of entering the combustion chamber.

A certain law was assumed to describe the way each element mixed with air and became 'ready for burning'. This law was entirely empirical, Fig. (2.1). A triangular shape was chosen to represent this for each individual element. The sum of the areas of these triangles was equal to the area under the fuel injection curve (upper part of diagram).

The ignition point was taken from experimental measurements, and the shaded area of the 'ready for burning' triangles were added together in order to give the first peak of the total rate of burning curve.

The rest of the curve was dictated by the shape of the triangles (i.e. any fuel which was ready for burning, in fact burnt instantly). The implication of this model was that, once a suitable relationship between the rate of burning and rate of injection was found for one test condition, it could be applied to predict engine behaviour at others.

From experience, Lyn found that the theoretical burning rate of a single droplet in a free supply of air (rate proportional to droplet diameter) did not fit the above model. However, to avoid a theoretical treatment of the mixing processes, he assumed an empirical pattern for the burning of discrete elements.

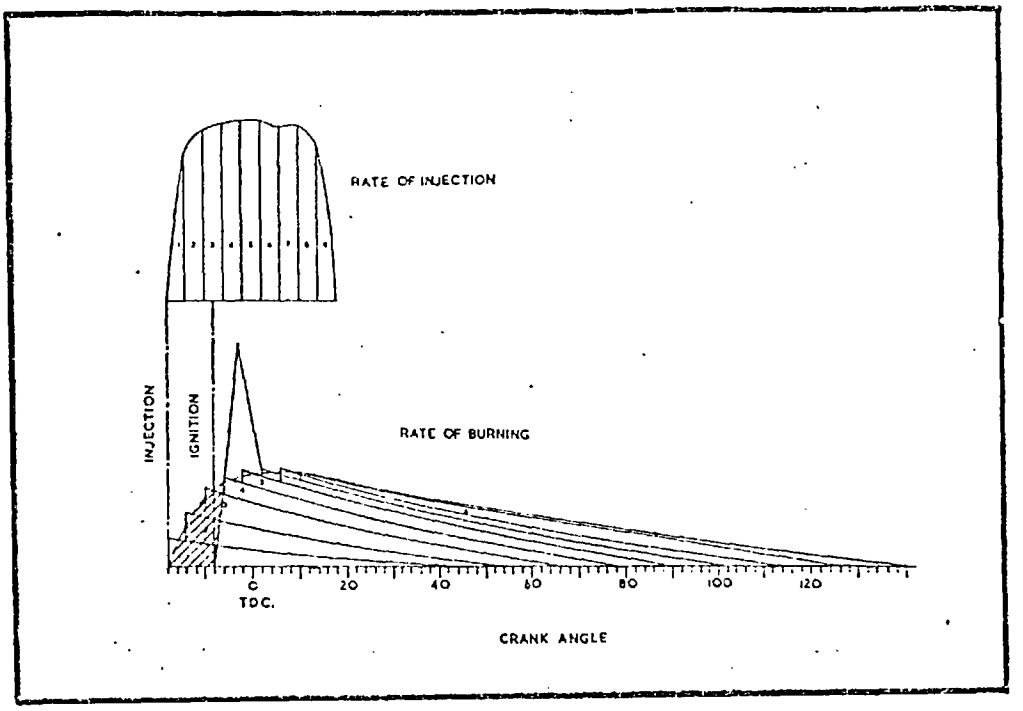

Fig. 2.1 Schematic relationship between rate of injection and rate of burning.

LYN - (1962)

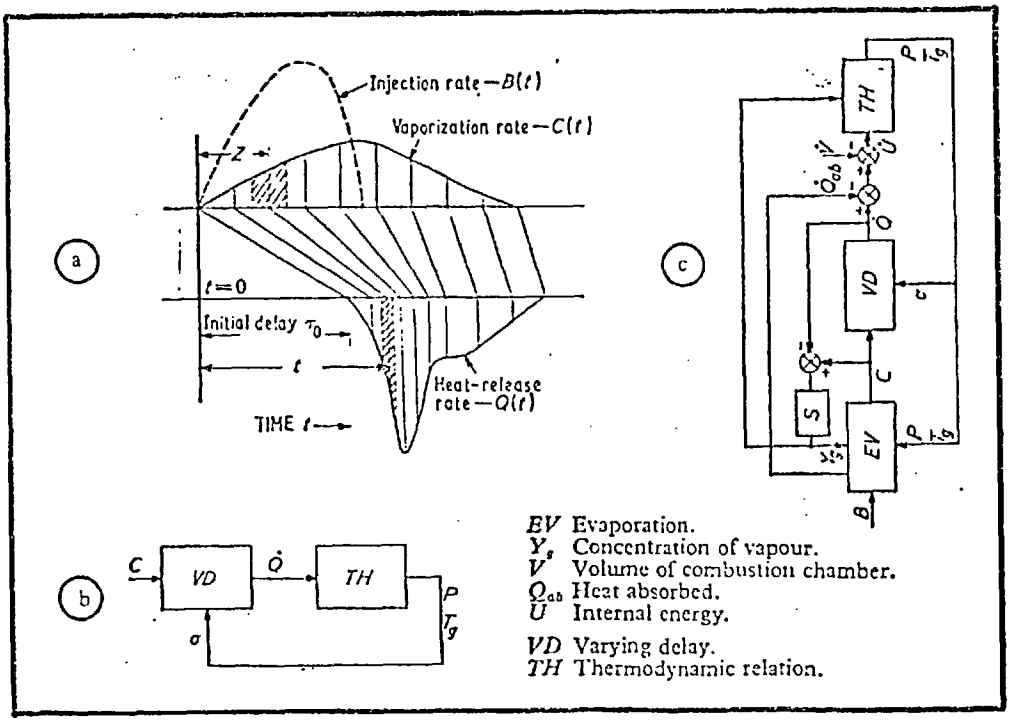

Fig. 2.2. (a) Schematic diagram illustration, the relation between $B(t)$, $C(t)$ and $Q(t)$

(b) Block diagram of varying delay mechanism

(c) Block diagram of the model

IKEGAMI - (1969)

Chemical kinetics, based on activated collisions, was completely ignored. It was argued that if the process was affected by chemical kinetics, the rate of heat release curve would have been more temperature sensitive than the experimental evidence showed. The position and temperature histories of the elements were not considered.

The heat release curves thus obtained were employed to compute cylinder pressure diagrams which were compared with those obtained experimentally. Better predictions were reported when varying the speed and load than when varying ignition timing.

b) The Ikegami model

The model presented by Ikegami and Nagao (1969) was based on droplet evaporation, employing a varying delay mechanism. Fig. (2.2) schematically shows the relationship of fuel injection rate B(t), overall evaporation rate C(t) and the heat release rate Q(t) (t denotes time).

The correlation used for the ignition delay was a modified version of the formula presented by Wolfer (1938).

$$\sigma(p, T) = 0.44\ p^{-1.19}\ .\ \exp(4650/T)\ \{ms\} \qquad (2.1)$$

The delay τ under a changing environment was then

$$\int_0^{\tau} \frac{dt}{\sigma(p, T)} = 1 \qquad (2.2)$$

For the mathematical treatment of the droplet evaporation, the Spalding (1955) theory was applied. It

was assumed that the droplets were uniformly distributed over the combustion space without any interaction between them and without any effect from the chamber wall. The Sauter Mean Diameter and the droplet size distribution were assumed to be constant throughout injection.

The burning of each fuel element was assumed to take place within 1 deg. crank angle after the end of ignition delay for that element (Fig. 2.2).

The pressure and temperature in the chamber were then calculated on the assumption that the gas was an ideal mixture of fuel vapour and air, and that no heat was transferred to the walls. The properties of combustion products were assumed to be the same as those of air.

The block diagram in Fig. (2.2) shows the interrelationship of the variables in the Ikegami model. The model was basically designed to predict diesel combustion knock (rapid pressure rise at ignition). Thus the overall discrepencies between predicted and experimental results were attributed to ignoring parameters such as local gas temperatures, local fuel and air concentrations, air motion and heat losses to the walls.

c) The Shipinski model

This followed from previous models due to Wiebe and Tanasawa and was reported by Shipinski et al (1969). Shipinski first tried to curve fit his experimentally obtained heat release data using a semi-empirical dimensionless relation proposed by Wiebe (1956):

$$w(\theta) = a \cdot a_2(a_1 + 1)\theta^{a_1} \exp\{- a_2(\theta^{a_1+1})\} \qquad (2.3)$$

In this relation, $w(\theta)$ was the heat release rate, (a_1) the Wiebe shape coefficient, (a_2) the Wiebe efficiency-of-combustion coefficient, (a_3) the Wiebe parameter corresponding to ignition delay and θ the normalized crank angle given by:

$$\theta = (\theta - a_3)/(310 - a_3) \qquad (2.4)$$

The value of (a) was given in terms of m (fuel mass/cycle) and q (the higher heating value for fuel).

$$a = m \cdot q/(310 - a_3) \qquad (2.5)$$

The results obtained in this way were unsatisfactory and work based on the Wiebe function was discontinued.

Models Tanasawa and Tanas I were then constructed. Probert (1945) and Tanasawa (1953) had shown the importance of the effect of droplet size on the rate of burning of a spray. Probert had combined a droplet size distribution and single-droplet burning rates to obtain a spray burning rate. He had also assumed that single-droplet evaporation and burning coefficients were valid for the spray (i.e., no interaction between droplets). Tanasawa, on the other hand, had employed his own relation for droplet-size distribution obtained experimentally from a gas turbine nozzle spray. The following empirical relation was proposed:

$$\frac{w_b}{w_o} = 1. - \exp\{(-3c_b.t/4\ SMD^2)^{.75}.(1-c_b.t/4\ SMD^2)^{-.25}\} \quad (2.6)$$

(w_b/w_o = mass fraction burnt at time t, c_b = burning coefficient).

This relation was used by Shipinski to calculate the amount of evaporated fuel.

The rate of injection (ROI) was divided into 1 degree crank angle increments. The fuel injected during each of these increments was treated separately and an appropriate Sauter Mean Diameter (SMD) was calculated using Knight's (1955) formula.

Ignition delay was computed for each increment using a modified version of the Woffer (1938) relationship.

$$I.D. = \left(\frac{6\ RPM}{1000}\right)\left(\frac{0.0271}{p\ 0.386}\right)\left(\frac{40}{CN}\right)^{0.69}\exp\left(\frac{8360}{T}\right) \quad (2.7)$$

(p and T in Imperial units, CN = Fuel Cetane number).

It was assumed that evaporation did not start until the end of the delay period, after which the evaporation and burning rates were equal (i.e. no fuel accumulation during the delay period).

Fig. (2.3) shows the procedure adopted in this model. Each line indicates the heat release rate of the fuel injected during a single crank angle increment.

The failure of this method to predict reasonably representative heat release curves was attributed to the assumption that no fuel evaporated during its delay period. In a further model (Tanas I), therefore, fuel preparation

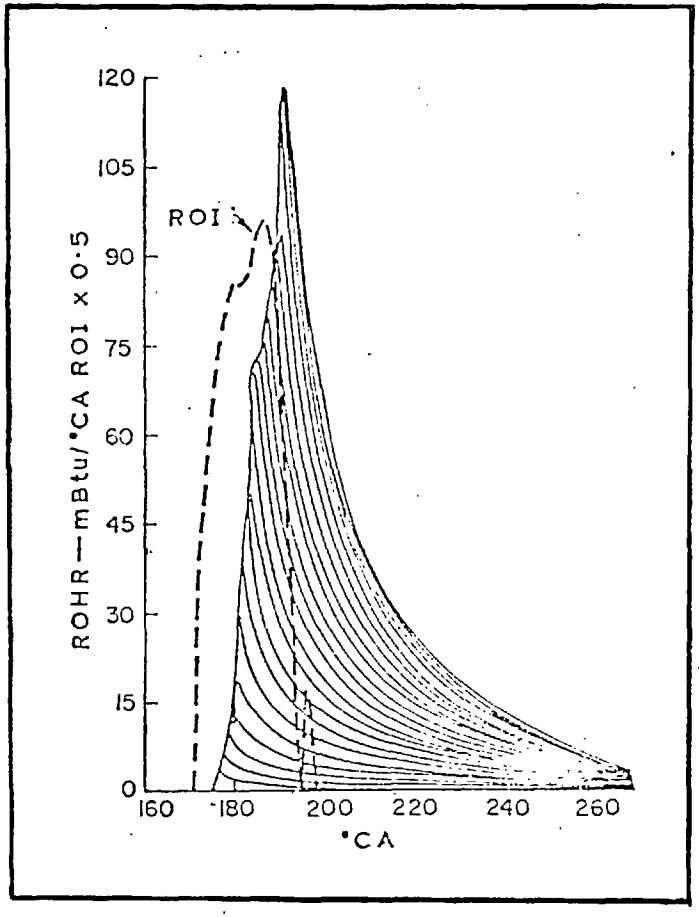

Fig. 2.3. ROHR for fuel injected during each degree crank angle and total heat release curve

SHIPINSKI – (1969)

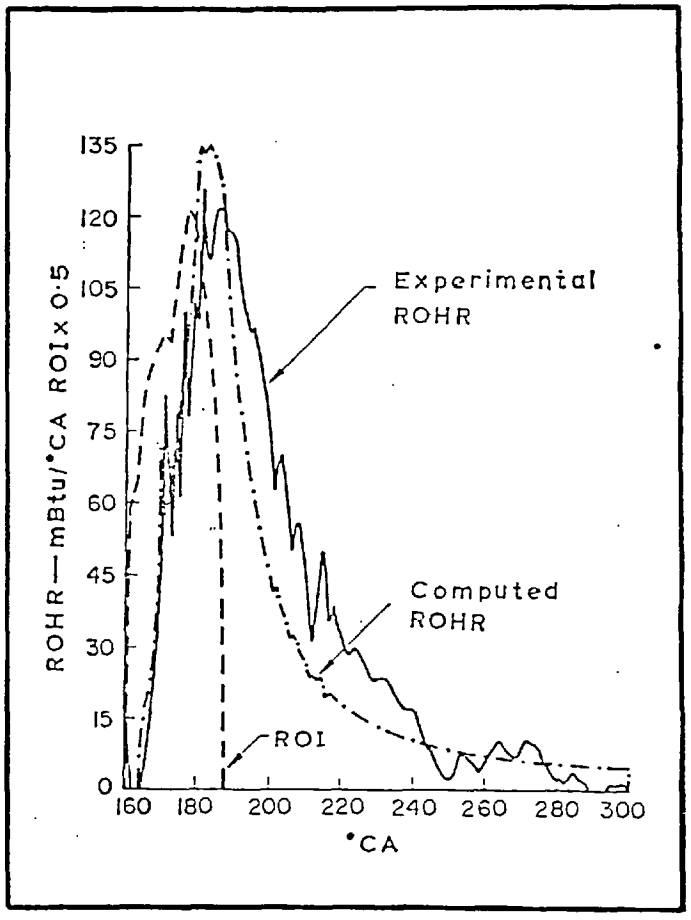

Fig. 2.4. Comparison of ROHR predicted by Model Tanas II with $C_E \propto P^{0.25}$ and experimental ROHR

SHIPINSKI – (1969)

was considered during the delay period, but no significant improvement was shown.

It was judged that the main reason for these failures was that neither model considered mixing or reaction rate relations.

The approach was finally modified in model Tanas II by defining a burning rate coefficient c_E. Effects of mixing and chemical reaction were assumed to be implicitely included in c_E . (c_b . c_E used instead of c_b in equation 2.6).

Shipinski's method of obtaining values for these constants was to keep changing them until the theoretical curve was the best least square fit to the experimental one. Figures 2.4 and 2.5 show the results of investigating a pressure dependence for c_E. Since an index of 0.25 was reported by Hall (1953) for single droplet experiments, this was the first value tried, whilst keeping c_b constant at a value observed by Spalding (1955). Comparison between the values 0.25 and 0.12 was reported, and showed that although the curve was improved in some respects, it was less satisfactory in others (Fig. 2.5). Additional comparisons were made for a variety of manifold pressure ratios at a constant inlet temperature. No significant pressure dependence was found. Attempts to relate c_E to the instantaneous oxygen availability were not fruitful, although the constant c_E was dependent on the trapped air/fuel ratio

(c_E = 0.0041 A/F for $20 < A/F < 60$).

Finally, satisfactory results were obtained by using a relationship describing c_E as a function of cylinder temperature:

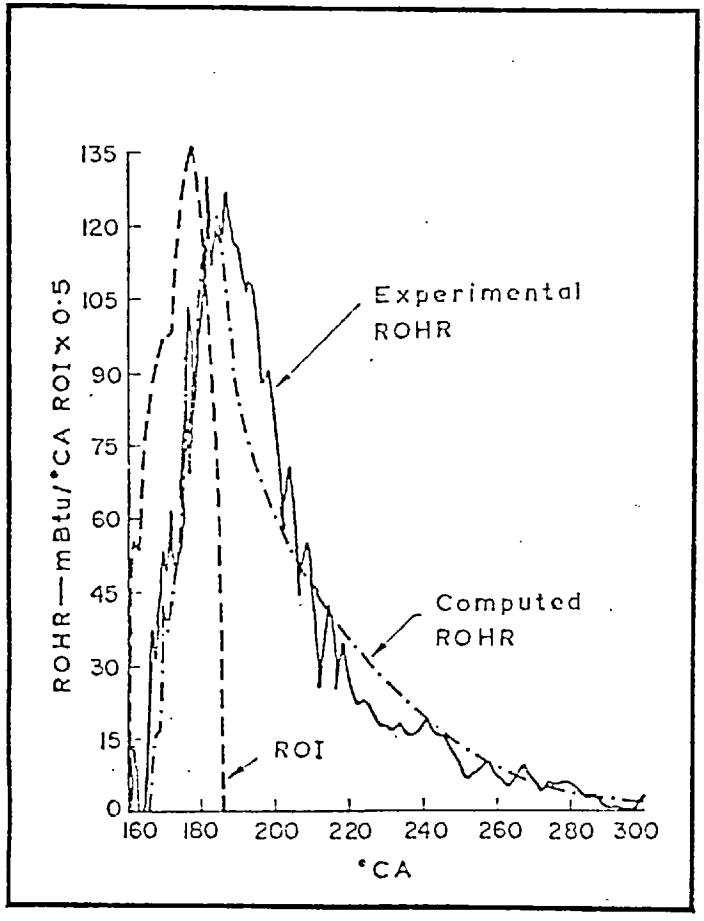

Fig. 2.5. Comparison of ROHR predicted by Model Tanas II with $C_E \propto P^{-0.12}$ and experimental ROHR

SHIPINSKI – (1969)

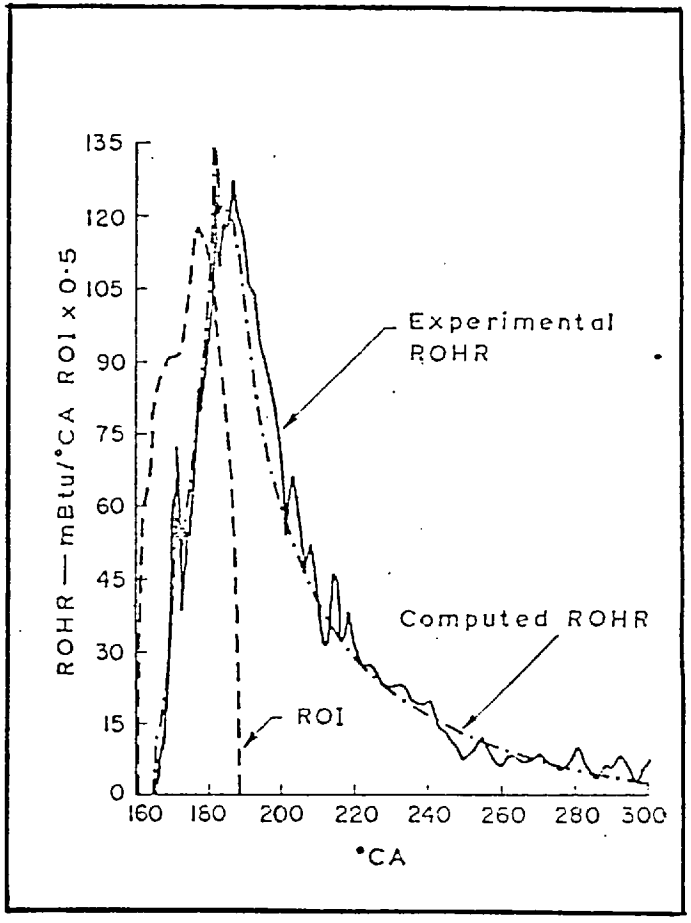

Fig. 2.6. Comparison of ROHR predicted with Model Tanas II with $C_E \propto T^{0.33}$ and experimental ROHR

SHIPINSKI – (1969)

$$c_E = m\ T^n/250 \qquad (2.7)$$

$(4 . < m < 8.$ and $n \simeq 0.33)$

d) The Whitehouse model

Whitehouse and Way (1969) presented a heat release model for use in engine simulation programmes. Fuel preparation and burning was assumed to be proportional to the total surface area of (n) droplets of equal diameter (D), i.e. $(n\ \pi\ D^2)$. Expressing this in terms of the mass of injected fuel $(M_i = n\ \rho\ \pi\ D_o^3/6)$ and the mass of unburnt fuel $(M_u = n\ \rho\ \pi\ D^3/6)$, showed that the fuel preparation rate (M) was proportional to $M_i^{1/3}$ and $M_u^{2/3}$, i.e.

$$(M = n\ \pi\ D^2 = 6M_i^{1/3} . M_u^{2/3}/D_o . \rho).$$

The reaction rate (W) was assumed to be proportional to M multiplied by P_o^m. (P_o being the instantaneous partial pressure of available oxygen).

$$W = k . M_i^{1/3} . M_u^{2/3} . P_o^m \qquad (2.7)$$

By trial and error it was initially found that suitable values for m and k were 1/3 and 0.00625 respectively. Equation (2.7) was used to predict heat release and the results were compared with a variety of experimental data obtained from four different engines (namely, 4.9 inch bore four-stroke Dorman 4LBT, 3.6 inch bore valve in head two-stroke Foden FD6, 3.4 inch bore opposed piston

two-stroke Rolls-Royce K60 and 12 inch bore four-stroke Mirrlees-National FV2).

With the exception of the last engine, all were run using an external compressed air supply, which enabled the boost pressure to be varied independently of speed and load. Nozzles were used in the exhaust pipes to simulate the effect of a turbocharger. Fuel injection characteristics were varied by altering the fuel injection rates (by means of the pump plunger diameter).

The results showed that there was a need for revision of the model to replace the index 2/3 by a value (x) which could vary from one test condition to another.

$$\dot{W} = k\, M_i^{1-x}\, M_u^{x}\, P_o^{m} \qquad (2.8)$$

This was explained in the following manner. If the effective parameter for burning was considered to be the droplet diameter rather than the surface area (Spalding, 1955), then x would be 1/3 instead of 2/3. On the other hand if a droplet size-distribution was taken into account, x would change, values of up to unity then being possible.

An explanation was also given for such cases as the Dorman engine where, for a considerable period of time, the combustion rate remained constant despite great reduction in the quantity of unburnt fuel. It was suggested that a mechanism to produce such an effect could be present in a deep bowl piston where (presumably) the direction of the fuel injection and the effect of swirl will concentrate the fuel in an annulus against the outer wall of the bowl.

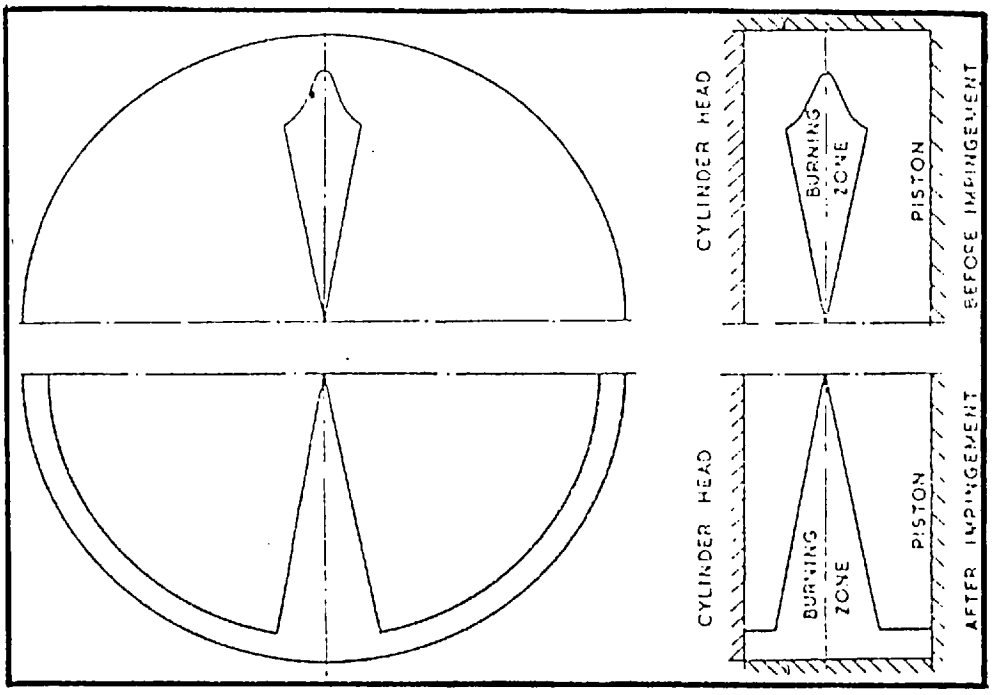

Fig. 2.7. Geometric representation of two-zone model. WHITEHOUSE - (1974)

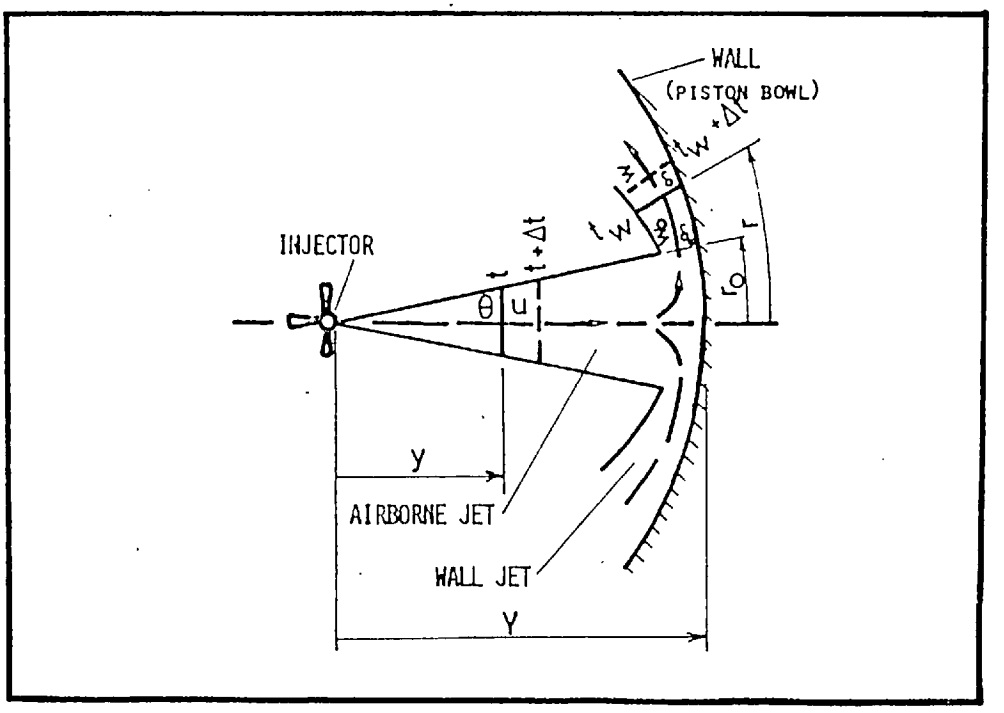

Fig. 2.8. Fuel spray free jet and wall jet model for air entrainment

Thus if a burning rate proportional to fuel surface area was assumed, it would remain constant as long as there was enough fuel left to cover the bowl area. For the same engine, it was stated that the heat release model could be used in two stages. Up to 14^{o} ATDC equation (2.8) could be used in the form of $\dot{W} = 0.004(M_i)^{0.99}(M_u)^{0.01} P_o^{0.4}$ and for the remaining period, in the form of $\dot{W} = k\, M_u\, P_o^{0.4}$ (k should be $0.004\ (M_i/M_u)^{0.99}$ for the two formulae to agree at 14^{o} ATDC).

The same principle was applied to synthesise heat release data in various forms appearing in later publications such as a two zone model by Whitehouse and Sareen (1974).

The necessity of considering chemical kinetics was emphasized,and an Arrhenius type equation of the following form was included in the model, replacing the assumption that burning and preparation rates were equal:

$$\dot{W} = \frac{k'\ P_O}{RPM\ \sqrt{T}} \int_o^{\theta} (\dot{M} - \dot{W})\ d\,\theta .\ \exp\ (-\frac{E}{RT}) \qquad (2.9)$$

(Different values of k' had to be used for different engines).

e) The C.A.V. Model

This model was developed at C.A.V. Ltd, and presented by Grigg and Syed (1970) and Khan (1973). It offered an entirely different approach by taking air entrainment into the spray as the dominating factor in the heat release process. First a conical spray was

considered and its penetration was calculated from the formula proposed by Schweitzer (1938):

$$x_f^2 = 32.7 \frac{P^{\frac{1}{2}} \cdot d.t}{n} \qquad (2.10)$$

In this equation x_f is the distance penetrated by the jet tip, P the fuel injection pressure, d the nozzle hole diameter and t the time measured from the start of injection (S.I. units). The spray half cone angle (a) was given by:

$$\tan^2 a = 0.00075 \cdot n \qquad (2.11)$$

In equations (2.10) and (2.11) n denoted the air density ratio $[\rho_a/(\rho_{a\ NTP})]$.

The rate of air entrainment was then calculated:

$$\dot{A} = \frac{\rho_a}{3} \tan^2 a \cdot \frac{d}{dt}(x_f^3) \qquad (2.12)$$

Thus the mass of air in the spray A(t) was calculated at any time from the integral of $\dot{A}dt$. At the end of injection the motion of the jet-back was assumed to leave a truncated cone according to equation (2.10).

Micromixed air (M_a) and micromixed fuel (M_f) were then calculated by assuming that the rate of micromixing ($\dot{M}_a$ or $\dot{M}_f$) was porportional to the jet-tip velocity (u_f) and a constant (D) which depended on diffusivity.

$$\dot{M}_a = D \cdot u_f(A - M_a)$$
$$\dot{M}_f = D \cdot u_f(F - M_f) \qquad (2.13)$$

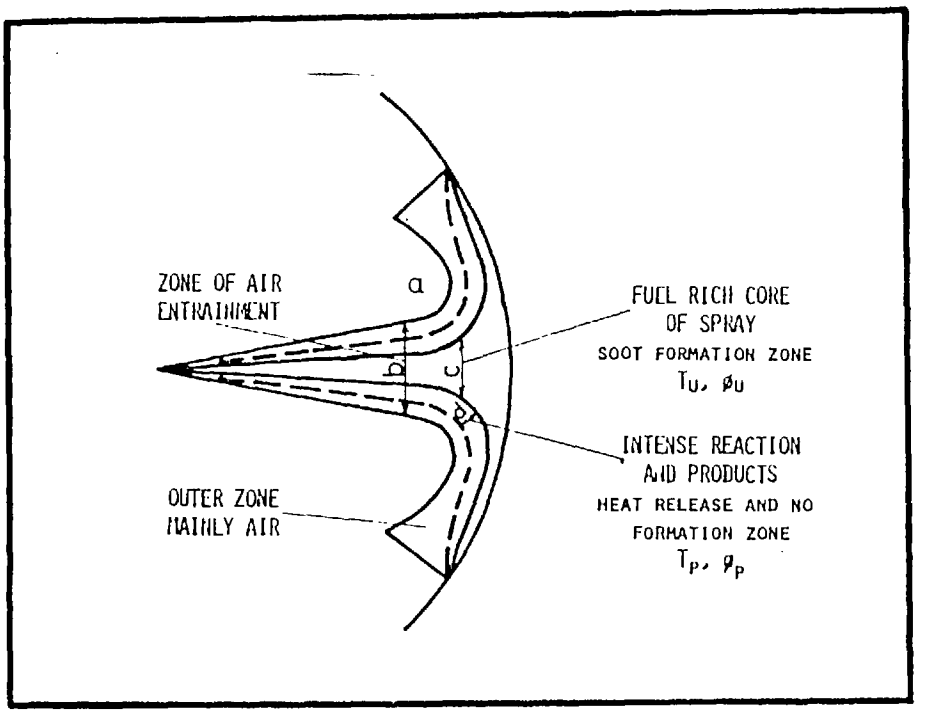

Fig. 2.9. Schematic Representation of Combustion Zones. C.A.V. - (1973)

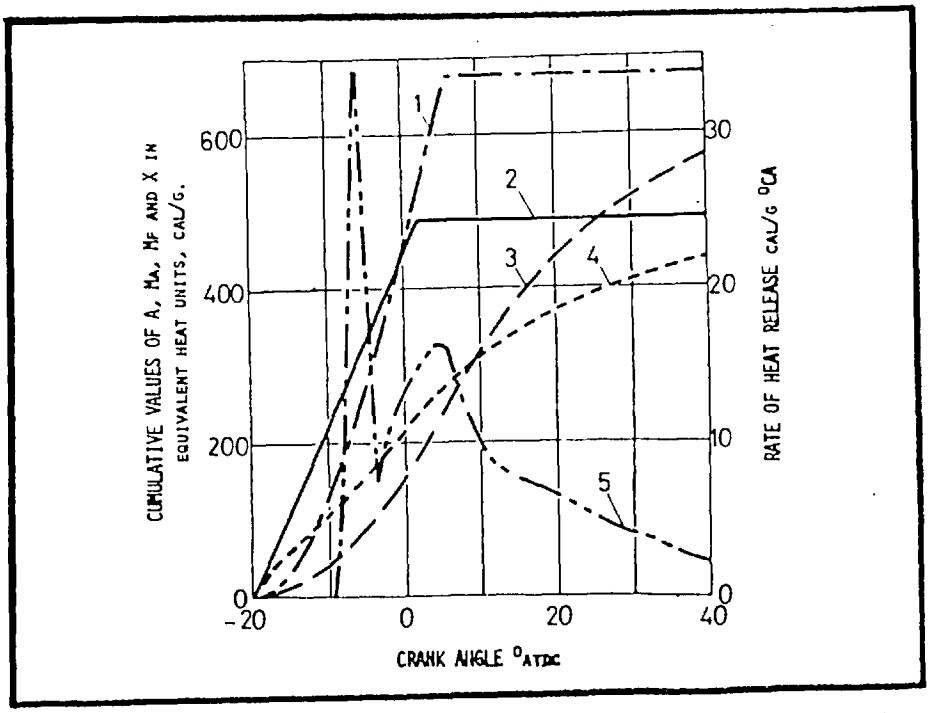

Fig. 2.10. Calculated instantaneous values for air entrainment, micro-mixing, and rate of heat release versus crank angle. C.A.V. - (1973)

A wall-jet model was later included (Khan (1973)) to account for the change in air entrainment if the jet hits the piston bowl (Fig. 2.8). This was based on the turbulent wall jet development reported by Glauert (1956). During transition of the jet front from a free to a wall jet, the loss of kinetic energy in the direction of flow was neglected.

The velocity (w) and thickness (δ) in terms of radius (r) were given by the following relations:

$$W = w_o\left(\frac{r}{r_o}\right)^{-1.06} \tag{2.14}$$

$$\delta = \delta_o (r/r_o)^{1.006} \tag{2.15}$$

The suffix (o) denoted the conditions at the transition radius. The wall-jet front volume flow was then calculated in terms of t_w and t_i (t_w = time since impingement, t_i = time from injection to impingement).

$$\Delta A_w = 4\pi r_o^2 \rho_a w_o \frac{\{(t_w + \Delta t)^{1.459} - t_w^{1.459}\}}{1.459\ t_o^{0.459}} \tag{2.16}$$

$$t_w = t + t_o - t_i \quad \text{and} \quad t_o = \frac{r_o}{2.06\ w_o} \tag{2.17}$$

The model described so far assumed stagnant surroundings for the jet. In order to take some account of the effect of swirl, an entrainment ratio (E_r) was defined which was the ratio of actual air entrained to that entrained in stagnant air ($\Delta A_{actual} = E_r \cdot \Delta A_{stagnant}$).

Fig (2.10) summarises the procedure adopted in the model. Once an estimate of prepared fuel or air was

determined in the way explained (curves 3 and 4), the heat release rate (curve 5) was calculated by one of the following two methods.

An experimental value of ignition delay was suplied and the rate of premixed burning was assumed to form a triangle on a six degrees crank angle base. After this the curve was dictated by the fact that any fuel or air prepared, burnt instantly.

Alternatively the following Arrhenius type equation was employed:

$$\dot{m}_b = K\ N_{AM}\ .\ N_{FM}\{T(1 + \frac{E}{RT})\}^{\frac{1}{2}}\ \exp(\frac{-E}{RT}) \qquad (2.18)$$

where ($\dot{m}_b$) was the fuel burning rate and (N_{FM}) and (N_{AM}) were the concentrations of micromixed fuel and air respectively. (T) was the instantaneous mass averaged temperature, (R) the gas constant and (E) the activation energy. The value of (K), the steric factor, varied from 5×10^5 to 6×10^6 $m^3/kg/s/1^oK^{\frac{1}{2}}$, depending on engine running condition.

2.2.2 Contemporary Models

a) The Hodgetts Model

Directed mainly towards the prediction of nitric oxide formation in diesel engines, this model was reported by Hodgetts and Shroff (1975). It is a multizone model, based on a jet mixing pattern in two dimensions.

The Whitehouse evaporation model was applied to each zone together with a Wolfer type ignition delay formula. An Arhenius type equation was employed to compute reaction

rates which were assumed to be dependent either on evaporated unburnt fuel or unburnt air equivalence ratio whichever was dominant.

The jet-mixing equations were developed on the basis of theories by Squire and Trouncer (1945) and Forstall and Shapiro (1950). A cosine variation of velocity with radial distance from the jet contreline together with a hyperbolic decay of centreline velocity was employed, giving the following relations for the velocity distribution in the two dimensions (r) and (x).

$$u = 0.5u_m\left(1 + \text{Cos}\ \frac{r\pi}{r_{max}}\right) \tag{2.19}$$

$$(u_{mx} - u_{ax})/u_o = 1/s \tag{2.20}$$

In these equations, the axial components of the centreline velocity and the swirl velocity were denoted by u_{mx} and a_{ax} respectively, u being the velocity at a radius r and u_m the centreline velocity.

The length of the potential core (l) was calculated from:

$$l = \text{Const.}(\rho_f/\rho_a)^{\frac{1}{2}} \tag{2.21}$$

The relative distance (s) travelled along the centreline up to an axial distance x, was given by:

$$S = \int_o^l (u_{mx} - u_{ax})dt \tag{2.22}$$

Air swirl was represented by solid body rotation about the point of injection. The zone subdivisions can be

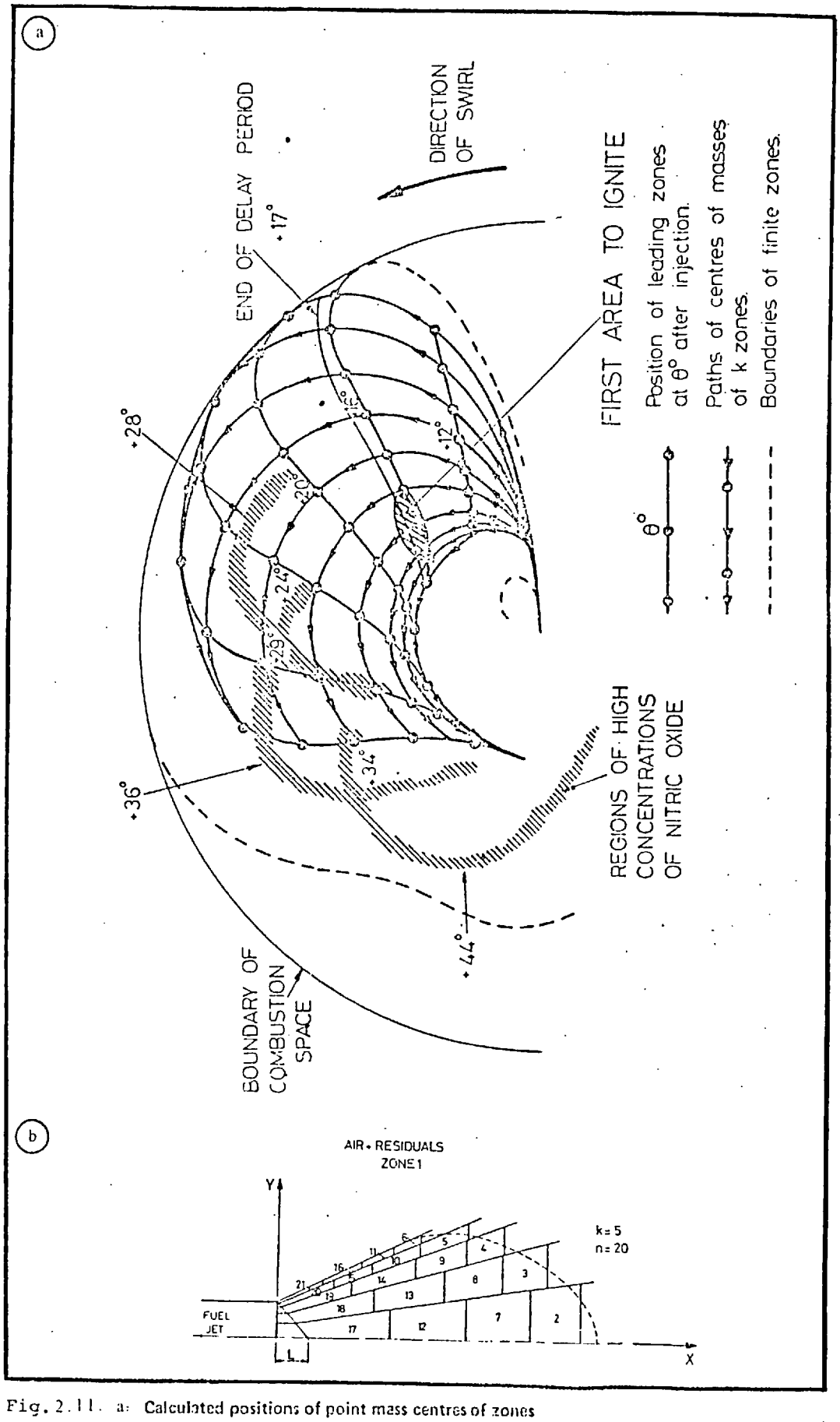

Fig. 2.11. a: Calculated positions of point mass centres of zones

b: Diagram of free jet showing formation of 'n' zones.

HODGETTS - (1975)

seen in Fig. (2.11b). In the radial direction there are (k) divisions to give equal mass flux for the mixture. There are (n) divisions in the axial direction such that each zone accommodates an equal mass of fuel. The velocity of the centre point of each zone was given by $C_f \cdot u_m$, C_f being calculated according to the zone subdivision pattern.

Air entrainment was calculated from:

$$\frac{m_f}{m_a + m_f} = \frac{C_f \cdot l}{s} \tag{2.23}$$

which, in differential form, gives the rate of air entrainment:

$$dm_a = \left(\frac{s}{C_f \cdot l} - 1.0\right) dm_f + \left(\frac{m_a + m_f}{s \cdot l}\right)(lds - sdl) \tag{2.24}$$

dm_f and dl were zero, once the zone was formed; i.e.:

$$dm_a = ds \cdot (m_a + m_f)/s \tag{2.25}$$

For the wall-jet, it was assumed that the path of the zone was tangential to the wall and that the normal component of momentum was lost. The rate of entrainment was thus reduced to 50% of that of a free jet.

The fuel evaporation, varying ignition delay, and the fuel burning rate equations were added to this zone motion model and were solved for the temperature distribution and the pressure change in the cylinder. Fig. (2.11a) shows a typical zone map also indicating the first area to burn.

The evaporated fuel was calculated according to the following equation:

$$\frac{dm_{ev}}{dt} = \text{Const.}\left(\begin{matrix}\text{turbulence}\\ \text{factor}\end{matrix}\right) m_f^{1/3} (m_f - m_{ev})^{2/3} \left(\frac{m_a}{m_a + m_f}\right)^{0.4} \tag{2.26}$$

The ignition delay was calculated according to:

$$\int_0^{\sigma_i} \frac{dt}{\sigma(p,\ T_z)} = 1,$$

where

$$\sigma(p,\ T_z) = \text{Const.}\ p^{-0.757}\ .\ \exp\left(\frac{5500}{T_z}\right) \tag{2.27}$$

The burning rate equations were as follows:

For zones with ϕ larger than unity:

$$\frac{dm_b}{dt} = \text{Const.}\ p^{0.757}(m_a\ .\ \phi_s - m_b).\ \exp\left(-\frac{5500}{T_z}\right) \tag{2.28}$$

For zones with ϕ less than unity:

$$\frac{dm_b}{dt} = \text{Const.}\ p^{0.757}(m_{ev} - m_b).\ \exp\left(-\frac{5500}{T_z}\right) \tag{2.29}$$

ϕ being the ratio of unburnt fuel vapour to unburnt air (suffix s means stoichiometric).

b) The Shahed model

This model, directed at NO_x formation and heat release studies, was presented in two parts. The spray mixing model was published by Chiu et al (1976). The NO_x formation and the heat release results, together with a general description of the model but excluding the spray mixing details had already been published by Shahed et al

(1975). A combination of the two models will be described here.

The spray was treated as a gaseous jet assuming very rapid evaporation of the fuel. Model calculations began at 'incipient ignition'. The compression pressure at ignition and the trapped mass were either supplied or obtained from a simulation of the intake and compression processes. A spray tip penetration correlation was obtained experimentally. The experiments involved a specially designed chamber charged with high pressure-temperature gas (with controlled swirl decaying with time). At a pre-selected swirl level, a single shot injection of fuel was achieved under a desired injection pressure. Shadowgraph pictures and Schlieren films supplied the necessary information on the history of spray movement and evaporation.

The zone subdivision map can be seen in Fig. (2.12). Each outer zone completely envelopes an inner zone and extends from the jet-back to the jet-front. Only the zone which is furtherst out directly entrains a fresh charge from the non-burning surrounding. Only the innermost zone is considered too rich to contain reacted fuel. All the intermediate zones have fuel in a burnt state dictated by chemical equilibrium conditions. From any inner zone to an outer zone the fuel/air ratio reduces, thus implying a different equilibrium state for the products of combustion. The moment the fuel crosses the innermost zone boundaries, it changes by a step function from a raw, unburnt phase to a phase of partial oxidation (dictated by the state of equilibrium of the combustion products). From then onwards

it is a matter of shifting equilibrium, determined by the local equivalence ratio.

However, the assumption of chemical equilibrium, while reasonable during the later stages of combustion, does not necessarily satisfy the conditions of premixed burning at the earlier stages.

Calculation of mixture properties was based on the local temperature, fuel/air ratio and chemical equilibrium, as programmed by Olikara and Borman (1975), using absolute internal energy, Powel (1957).

The jet-mixing model can be summarised as follows.

Experimental correlations were obtained for the spray tip penetration and the spray trajectory in swirling air. In the absence of experimental data, an equation was assumed for the motion of the jet-back. An attempt was made to represent the shape of the deflected cross-section by two half ellipses but this was abandoned due to lack of test data in the vertical direction and also due to the complexity of computation of the mass in the spray. A circular cross-section, larger than that of a straight jet, was used instead.

A concentration profile, c/c_m (Abramovich - 1963) was assumed, together with a hyperbolic decay of the centre-line concentration. A time-dependent coefficient, $\alpha(t)$, was introduced in the concentration equation to take account of the concentration variation with time. This coefficient was computed by the conservation of the injected fuel mass. Before the jet detached from the nozzle (end of injection), the boundaries shifted with time from

one concentration contour to another, forming a new zone. No more zones were formed after the end of injection.

The conservation of the injected fuel within the spray boundaries was expressed by:

$$\left.\begin{aligned} \int_o^t m_f \, dt &= 2\pi \int_{x_b}^{x_f} \int_o^R c \cdot \rho \cdot r \cdot dr \cdot dx \\ c/c_m &= 1 - (r/R)^{1.5} \\ c_m &= \frac{1}{\alpha(t) \cdot x + 1} \end{aligned}\right\} \quad (2.30)$$

where $\alpha(t)$ was the coefficient to be determined from the mass conservation integral.

Once (α) was calculated, the amount of prepared mixture, which was the fresh mixture crossing the rich limit of combustion, could be determined by calculating the mass of fuel in the layer adjacent to the rich limit contour. This was done through the following integrals for the fuel prepared ($\dot{m}_{fp}$) and the air (oxygen) prepared ($\dot{m}_{op}$) respectively:

$$\begin{aligned} \dot{m}_{fp} &= 2\pi \int_{x_b}^{x_f} \int_{r(\phi_j)}^{r(\phi_{j+1})} c \cdot \rho \cdot r \cdot dr \cdot dx \\ \dot{m}_{op} &= 2\pi \int_{x_b}^{x_f} \int_{r(\phi_j)}^{r(\phi_{j+1})} (1 - c) \cdot \rho \cdot r \cdot dr \cdot dx \end{aligned} \quad (2.31)$$

The position of the jet front ($\dot{x}_f$), as explained before, was given by the following empirical relation:

$$x_f = F \cdot t^{0.6} \quad (2.32)$$

As usual, (F) was related to the injection pressure, $(P)_{inj}$ the nozzle hole diameter (d) and the charge density (ρ_a). The reduction in jet front penetration in the presence of swirl ($x_f - x_{fs}$) was expressed by the following relation:

$$\frac{x_f - x_{fs}}{x_f} = 0.35\left(\frac{x_{fs}}{d} \cdot \lambda^2\right)^{0.44} \tag{2.33}$$

where λ^2 was the ratio of the momenta of air and the fuel jet. The swirl velocity (u_s) was given by solid body rotation ($u_s = x_{fs} \cdot w$), i.e.:

$$\lambda = \frac{x_{fs} \cdot w}{u_o} \left(\frac{\rho_a}{\rho_f}\right)^{\frac{1}{2}} \tag{2.34}$$

The tangential displacement (y_s) of the spray along the direction of air swirl was also given in terms of λ:

$$\frac{y_s}{d} = \lambda^2 \left(\frac{x}{d}\right)^{2.217} \tag{2.35}$$

The motion of the jet-back was given by the following relation:

$$x_b = 0.5\ F(t - \Delta t)^{1.6} \tag{2.36}$$

where F was the same as in equation (2.32) and Δt was the injection duration.

c) The Hiroyasu model

A model which predicted the rate of heat release

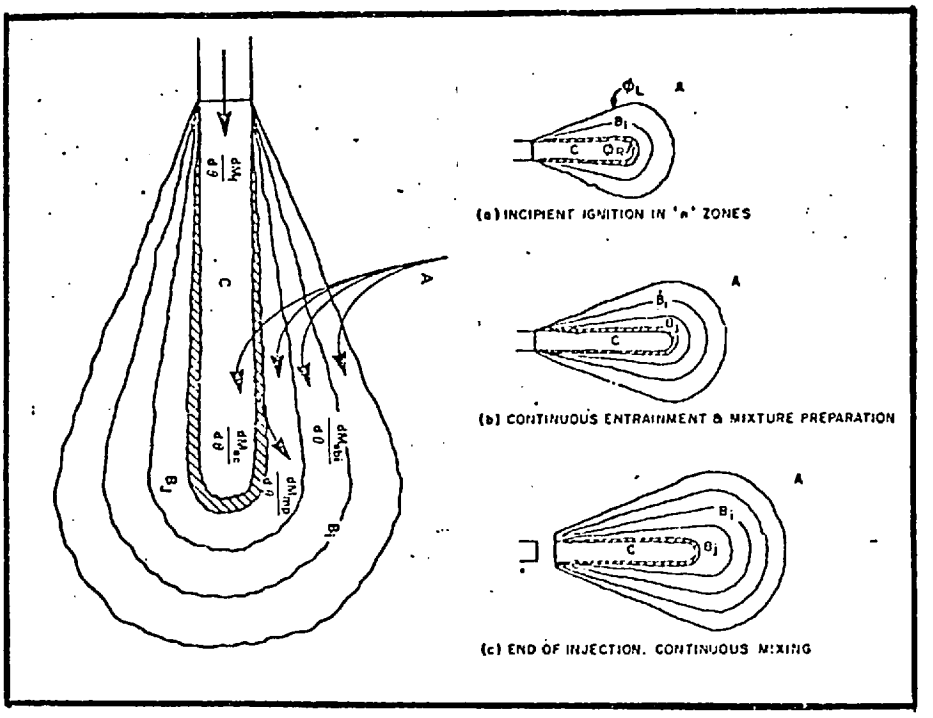

Fig. 2.12. Progressive evolution of combustion zones.
SHAHED - (1975)

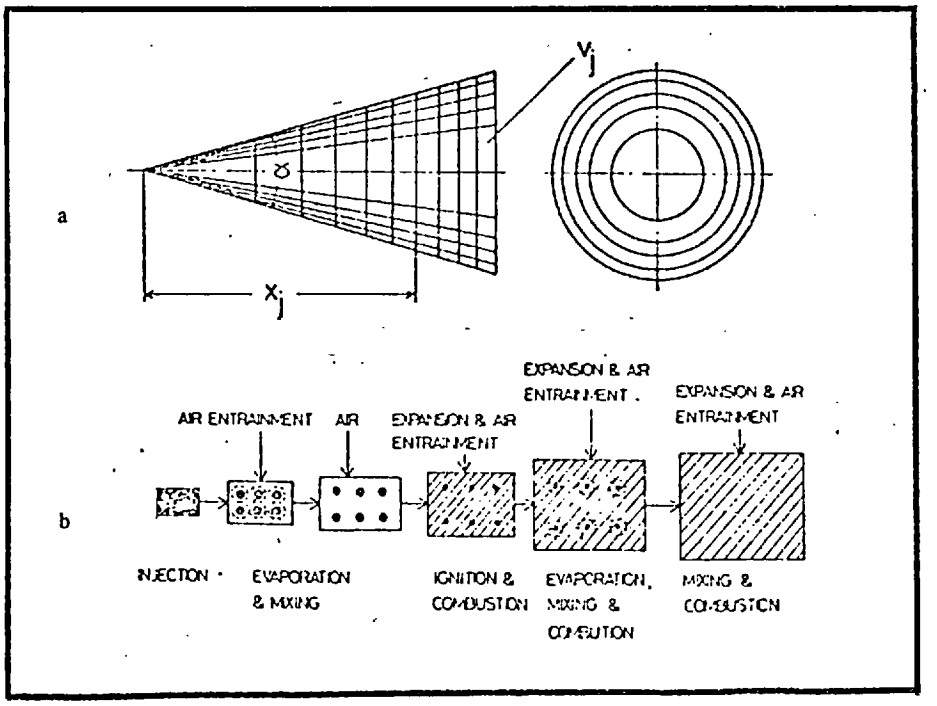

Fig. 2.13. a: Diagram of divided package of the spray
b: Schematic diagram of the spray combustion
HIROYASU - (1976)

for the purpose of nitric oxide and soot formation computations was presented by Hiroyasu and Kadota (1976). It consisted of a series of programmes for spray formation, droplet evaporation, ignition delay, heat release and emission formation respectively.

The spray formation programme considered zone sub-divisions in a conical axi-symmetric spray. Cross sections perpendicular to the jet axis formed the axial divisions and were assumed to separate the fuel injected during different intervals. Radial divisions were chosen to equalise the solid angle of a cone with the vertex located at the nozzle orifice. The injected fuel was therefore shared between small packages as shown in Fig. (2.13). The mass of air in each package was then determined and no mass transfer was considered between packages.

The jet front was assumed to be flat and its penetration was calculated from an empirical relation proposed by the same authors (1975) in the following form:

$$x_f = F \cdot t^{0.5} \qquad (2.37)$$

where F was related to variables such as the air density (ρ_a), the nozzle orifice diameter (d), the pump plunger diameter (d_p), the pump rack position (r_p), and the pump speed (n_p):

$$F = \text{Const.}\ n_p^{0.15} \cdot r_p^{0.1} \cdot d_p^{0.4} \cdot d^{0.25} \cdot \rho_a^{-0.5} \qquad (2.38)$$

Penetration of all the packages was assumed to be alike and the position of the cross sections shown in Fig. (2.13) was given by:

$$x_j = F \cdot (t - j \cdot \Delta t)^{0.5} \tag{2.39}$$

where j was an integer and Δt was the fixed time-step.

The volume between two consecutive sections was computed as:

$$V_j = \frac{\pi}{3} \tan^2 a \cdot (x_{j+1}^3 - x_j^3) \tag{2.40}$$

In the droplet evaporation programme, the rate of fuel evaporation was computed according to single droplet evaporation equations with a Sauter Mean Diameter calculated for each individual package from an empirical relation given by Hiroyasu (1974). A droplet size distribution was taken into account and thus each package had its own number of droplets (n) of initial diameter (D_o). The evaporated mass (m_{ev}) was then related to the instantaneous droplet diameter (D) and density (ρ) in the following simplified form:

$$m_{ev} = \frac{\pi}{6}(\rho_o D_o - \rho D)n \tag{2.41}$$

In this way the instantaneous values of ϕ_{ev} (the equivalence ratio of vaporised fuel to air) was known for each package.

In the ignition delay programme, the varying delay concept was used together with a Wolfer type formula

$$\int_{o}^{\sigma_i} \frac{dt}{\sigma(p,\ T_z,\ \phi_{ev})} = 1 \qquad (2.42)$$

$$\sigma = 0.01 \cdot p^{-2.5} \cdot \phi_{ev}^{-1.04} \cdot \exp\left(\frac{6000}{T_z}\right) \qquad (2.43)$$

where σ_i was the ignition delay for the package (in s) and P was the cylinder pressure (in MPa). ϕ_{ev} and T_z (^{o}K) referred to the instantaneous conditions for each package.

In the heat release programme, the information from the above calculations was used to predict the fuel burning rate and consequently both the cylinder pressure diagram and the individual package temperature history. The evaporated fuel was assumed to start burning immediately after the ignition delay as determined by the available entrained air. Although the fuel evaporation was calculated from single droplet theories, the burning rate was not considered in single droplet mode (diffusion flame to surround the droplet). Instead, the total amount of evaporated fuel and the entrained air were considered to support the flame (flame surrounds a group of droplets). Thus the incremental fuel burnt was either dictated by the air shortage ($\phi_{ev} > 1.$), or it was equal to the evaporated amount ($\phi_{ev} < 1.$). The heat release rate was then equal to this burning rate multiplied by the calorific value.

The energy equation was applied to the whole cylinder contents rather than to individual packages. The cylinder pressure calculation was based on the overall instantaneous heat released minus heat lost ($\frac{dQ}{d\theta}$ = net heat addition):

$$\frac{dP}{d\theta} = \frac{1}{V}\{(\gamma - 1)\ \frac{dQ}{d\theta} - \gamma\ p\frac{dV}{d\theta}\} \qquad (2.44)$$

where (V) was the cylinder volume and (γ) was the ratio of specific heats at constant pressure and constant volume.

Individual package temperatures were then calculated assuming adiabatic compression or expansion depending on $P(\theta)$, after package combustion. Thus, $T_z(\theta)$ which was needed for the pollution formation programme, was given in terms of the package temperature at combustion $T_z(\theta_c)$, i.e.:

$$T_z(\theta) = T_z(\theta_c)\{\frac{P(\theta)}{P(\theta_c)}\}^{\frac{\gamma-1}{\gamma}} \qquad (2.45)$$

where θ_c was the crank angle at combustion for the package.

The air entrainment was calculated from the volume of an individual package in the following way:

$$\Delta m_a = c_w \cdot c_{sa} \cdot \frac{\pi}{3} \cdot \rho_a \cdot \tan^2 a \cdot (x_{j+1}^3 - x_j^3)$$

where (a), the jet half cone angle was determined from photographs. From ignition to end of evaporation $a = (8 + \theta/5)$, and from end of evaporation to end of combustion $a = (4 + \theta/10)$ were used.

c_w and c_{sa} represented the effect of the impinging spray on the wall and the effect of the air swirl respectively. The numerical values of these constants were not stated.

2.3 Discussion

The above literature survey has dealt with models involving evaporation ignition delay, reaction rates, jet

penetration air entrainment, etc., treated in various theoretical or experimental manners.

Separate studies on jet tip penetration alone, have been reported by Schweitzer (1937), Lyshevskiy (1956), Wakuri (1960), Rusinov (1963), Sitkei (1964), Parks et al (1966), Ogasawara and Sami (1966), Oz (1969), Burt and Troth (1969), Taylor and Walsham (1970) and Dent (1971). A comparison of their results can be seen in an extensive survey carried out by Hay and Jones (1972). Further correlations for jet tip penetration were reported by Whitehouse and Sareen (1974), Chiu et al (1976) and Hiroyasu and Kadota (1976).

A survey relating to combustion of liquid droplets was presented by Williams (1973). His survey is of general interest but some points related to diesel engine combustion are mentioned, basically implying that diesel engine combustion modelling today does not benefit directly from droplet combustion theories. Evidently the theories of single and multiple droplet evaporation and burning are not complete enough to take into account the effect of a limited mass of air surrounding the droplet. Moreover, at supercritical conditions droplet evaporation may well follow quite a different pattern than that suggested by a classic film theory. Experimental evidence of Savery and Borman (1970) supports this view. The behaviour of a liquid jet near the thermodynamic critical region is discussed by Newman and Brzustowski (1971). They describe an experimental analysis in which a liquid jet issues into a gas where the pressure and temperature are close to or exceed the liquid critical conditions. They present also

a theoretical analysis in which the two phase spray is treated as a turbulent submerged jet. The application was primarily for rockets where high thrust levels impose the necessity of a pressure in the combustion chamber in excess of the fuel critical pressure. This situation may well apply to diesel engine running conditions.

Williams (1973) also reports that in the combustion of dense fuel sprays, the assumption that a burning droplet is immersed in an infinite quantity of gaseous oxidiser may no longer be valid and the process may be controlled by a different mechanism. He emphasizes that more information is needed in connection with entrainment of air and recirculated gases, and in particular a more accurate analysis of the process should consider finite reaction rates.

It has been seen that Lyn, as early as 1960-62, suggested that air-entrainment effects should be included in his model. Shipinski and others have discussed shortcomings in their models arising from lack of proper air-entrainment calculations and excessive relience on droplet evaporation dominated combustion.

Hence any new model which could successfully include the air-entrainment effect may well prove to be a useful advance. While the contemporary models do attempt to do this, at times they include droplet evaporation considerations which would not be required if due regard was paid to the mixing process during ignition delay.

In the early stages of this project, results obtained using the C.A.V. model suggested that an approach

based on jet-mixing theories may well be fruitful and thus a multi-zone model based on this concept has been developed herein.

CHAPTER 3

MIXTURE FORMATION

3.1 Introduction

In the previous chapter, it was noted that a realistic mixture formation model is an essential pre-requisite of any fundamental treatment of the heat release process in diesel engines. This chapter is devoted to explaining all the steps taken in formulating this part of the analysis.

3.2 The free jet

The simplest form of a fuel spray can be modelled by the equations of a circular free jet. The object will be to establish relations for the jet growth, velocity and concentration distribution with respect to the issuing velocity, nozzle hole diameter and surrounding medium density.

3.2.1 Definitions

The basic variables of a free jet shown in Fig. (3.1) are the nozzle hole diameter (d_o), the issuing fluid velocity (u_o) and density (ρ_o), the surrounding medium density (ρ_a) and the jet potential core and transition zone length (measured from the nozzle exit) denoted by x_c and x_t respectively.

The following relations describe the velocity and concentration profiles along a nondimensional radius (y)

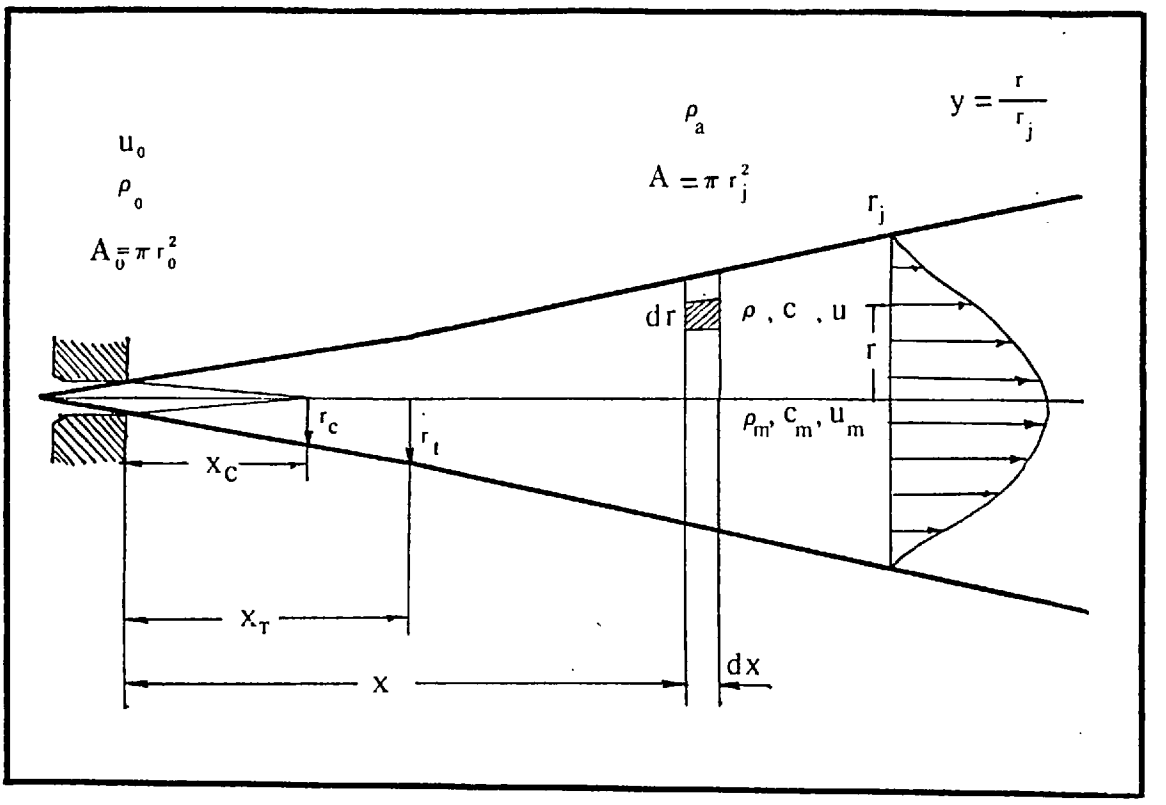

Fig. 3.1. Schematic diagram of the free jet.

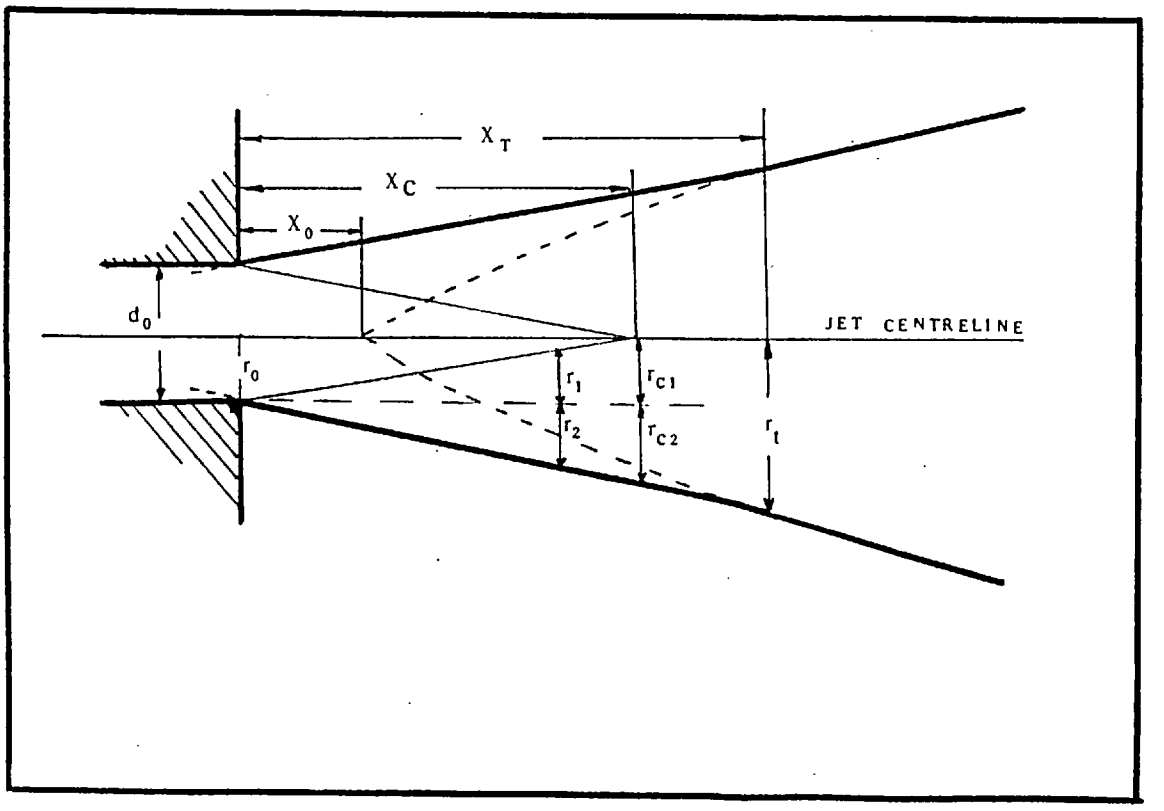

Fig. 3.2. Sketch of the initial jet region

for any cross section at $x > x_t$ (Abramovich, 1963).

$$\frac{u}{u_m} = (1 - y^{1.5})^2 \qquad (3.1)$$

$$\frac{c}{c_m} = (1 - y^{1.5}) \qquad (3.2)$$

(y, r, see Fig. 3.1).

These relations are based on experimental evidence and are convenient to use due to the fact that they define a boundary for the jet at y = 1, where the axial velocity (u) and the jet fluid concentration (c) become zero. (Other relations give an asymptotic distribution extending to infinity).

3.2.2 Momentum conservation

The conservation of momentum at various cross sections of the jet is given in the following manner:

Momentum at nozzle exit = $\rho_o A_o u_o^2$

Momentum at any cross section = $\int_o^A \rho u^2 \, d A$

In a small volume (v) containing air (m_a) and fuel (m_f) (fuel in the form of vapour m_v and/or liquid m_l), the mixture density (ρ) can be expressed in terms of c (by definition $c = \frac{m_f}{m_a}$):

$$\rho = \frac{m_l + m_v + m_a}{v}$$

$$\rho = \frac{m_a}{v} (1 + c)$$

$$\rho = \rho_a (1 + c) \qquad (3.3)$$

$$\rho_o A_o u_o^2 = \rho_a \int_o^A (1 + c) u^2 \, d A \qquad (3.4)$$

or by considering equations (3.1) and (3.2):

$$\rho_o A_o u_o^2 = \rho_a u_m^2 \{ \int_o^A (\frac{u}{u_m})^2 \, dA + c_m \int_o^A (\frac{c}{c_m}) (\frac{u}{u_m})^2 \, dA \}$$

$$\rho_o A_o u_o^2 = 2\pi r_j^2 \rho_a u_m^2 \{ \int_o^1 (1 - y^{1.5})^4 \, y dy + \int_o^1 (1-y^{1.6})^5 y dy \}$$

$$\rho_o A_o u_o^2 = \rho_a A u_m^2 \{ I_{f4} (1.) + c_m \cdot I_{f5}(1.) \}$$

The above integrals are evaluated in appendix (A) leading to the following form of the momentum equation:

$$\rho_o A_o u_o^2 = \rho_a A u_m^2 (0.134 + 0.108 c_m) \qquad (3.5)$$

3.2.3 Mass conservation

With a similar approach the fuel mass flow balance can be written:

$$\rho_o A_o u_o = \rho_a \int_o^A c \cdot u \cdot dA \qquad (3.6)$$

Following the same sequence of substitutions, the final form of mass balance is given by equation (3.7).

$$\rho_o A_o u_o = \rho_a \cdot A \cdot u_m \cdot c_m \int_o^1 2 \cdot (1 - y^{1.5})^3 \, y \, dy$$

$$\rho_o A_o u_o = \rho_a \cdot A \cdot u_m \cdot c_m \{ I_{f3}(1.) \}$$

$$\rho_o A_o u_o = 0.18 \rho_a A u_m c_m \qquad (3.7)$$

3.2.4 Velocity and concentration decay

It is customary to employ a suitable law for the growth of the mixing layer to establish a relation between the jet cross-sectional area (A) and the axial distance (x). Alternatively it is possible to do this after deriving equations for the centreline velocity and concentration decay. This means that it is possible to express the centre-line velocity (u_m) and centreline concentration (c_m) in terms of the jet diameter (d_j).

First, a relation between u_m and c_m is established by combining equations (3.5) and (3.7):

$$\frac{u_o}{u_m} = \frac{0.75}{c_m} + 0.6 \qquad (3.8)$$

Substituting (3.8) in (3.7) gives:

$$\rho_o A_o \left(\frac{0.75}{c_m} + 0.6\right) = 0.18 \rho_a A c_m \qquad (3.9)$$

The equivalent air jet diameter (d') is defined by the following relation:

$$d' = d_o \sqrt{\rho_o / \rho_a} \qquad (3.10)$$

$$A_o = \pi \frac{d_o^2}{4} = \frac{\pi}{4} \frac{d'^2}{\rho_o / \rho_a}$$

$$A = \pi \frac{d_j^2}{4}$$

$$\frac{\rho_o A_o}{\rho_a A} = \left(\frac{d_j}{d'}\right)^2$$

Rearranging (3.9) gives:

$$\left(\frac{1}{c_m}\right)^2 + 0.8 \left(\frac{1}{c_m}\right) - 0.24\left(\frac{d_j}{d'}\right)^2 = 0$$

Solution of this quadratic equation gives the centreline concentration (c_m):

$$\frac{1}{c_m} = - 0.4 + \{0.16 + 0.24(d_j/d')^2\}^{\frac{1}{2}} \qquad (3.11)$$

Substitution of (3.11) in (3.10) gives a similar expression for the velocity decay:

$$\frac{u_o}{u_m} = 0.3 + \{0.09 + 0.134(d_j/d')^2\}^{\frac{1}{2}} \qquad (3.12)$$

These exact relations can be written in simpler form by introducing the nondimensional jet diameter (d_j').

$$d_j' = \frac{d_j}{d'} \qquad (3.13)$$

$$\frac{1}{c_m} = 0.4(\sqrt{1 + 1.5\ d_j'^2} - 1) \qquad (3.14)$$

$$\frac{u_o}{u_m} = 0.3(\sqrt{1 + 1.5\ d_j'^2} + 1) \qquad (3.15)$$

At the transition cross section ($u_o = u_m$) the following relations hold:

$$d'_{jt} = 1.73$$

$$d_{jt} = 1.73\ d_o\ \frac{\rho_o}{\rho_a} \tag{3.16}$$

$$c_{mt} = 1.87$$

3.2.5 Growth of the mixing layer

The growth of the mixing layer is given in terms of jet centreline density (ρ_m), the surrounding media density (ρ_a) and an experimental constant determined by Abramovich (1963), i.e. 0.22 for the developed part and 0.27 for the initial region of the jet.

$$\frac{dr_j}{dx} = (\text{Const.})\ \frac{\rho_a + \rho_m}{2\rho_m} \tag{3.17}$$

For the developed part of the jet, writing ρ_m in terms of c_m from (3.3) gives:

$$\frac{dr_j}{dx} = 0.22\ \frac{1 + 0.5\ c_m}{1 + c_m} \tag{3.18}$$

Combining (3.18) and (3.14):

$$0.44.d\left(\frac{x}{d'}\right) = \left(1 + \frac{1.25}{1+1.5d'^{2}_{j}+0.25}\right).d(d'_j) \tag{3.19}$$

Integration of (3.19) gives a relation between the nondimensional jet diameter and the axial distance (the jet growth):

$$0.44\left(\frac{x}{d'} - \frac{x_o}{d'}\right) = d_j' + \ln\left(1.22\, d_j' + \sqrt{1 + 1.5 d_j'^2}\right)$$

$$- 0.25 \arctan\left(1.28 d_j' \frac{\sqrt{1 + 1.5\, d_j'^2} - 0.24}{\sqrt{1 + 1.5 d_j'^2} + 0.31\, d_j'^2}\right) \quad (3.20)$$

3.2.6 Initial region of the jet

The relationship between the length of the potential core (x_c) and the transition region (x_t) is simply derived from the geometry shown in Fig. (3.2):

$$\frac{x_t}{x_c} = \left(\frac{r_{jt}}{r_o} - 1\right)\frac{r_{1c}}{r_{2c}}$$

According to Abramovich (1963), $\frac{r_{1c}}{r_{2c}}$ is 0.45 and x_c is $24r_o$, therefore:

$$\frac{x_t}{r_o} = 10.7\left(\frac{r_t}{r_o} - 1\right) \quad (3.21)$$

From equation (3.16) and (3.20), xt/d' can be calculated:

$$\frac{x_t}{d'} = \frac{x_o}{d'} + 6.8 \quad (3.22)$$

Also from equations (3.16) and (3.21)

$$\frac{x_t}{x_c} = 0.45\left(1.73\sqrt{\rho_o/\rho_a} - 1\right)$$

$$\frac{x_t}{d'} = 5.35\left(1.73 - \sqrt{\rho_a/\rho_o}\right) \quad (3.23)$$

(For an air jet in air $x_t \approx 1.5x_c$)

Now (x_o/d'), (the constant of integration in equation 3.19), which is the position of the virtual origin measured from the nozzle exit, can be determined from equations (3.22) and (3.23):

$$\frac{x_o}{d'} = 2.4555 - 5.35 \sqrt{\rho_a/\rho_o} \qquad (3.24)$$

The effect of the air density on variables such as the transition length, position of the virtual origin and the jet radius at transition, are shown in the following table (fuel density assumed 0.83):

$\sqrt{\frac{\rho_a}{\rho_o}}$	$\frac{1}{10}$	$\frac{1}{9}$	$\frac{1}{8}$	$\frac{1}{7}$	$\frac{1}{6}$	$\frac{1}{5}$	$\frac{1}{4}$
$\frac{x_o}{d'}$	1.92	1.86	1.78	1.69	1.56	1.38	1.12
$\frac{x_t}{d'}$	8.72	8.66	8.58	8.49	8.36	8.18	7.9
x_t	36.	32.	28.	24	20	17.5	13
r_{jt}	3.6	3.2	2.84	2.48	2.12	1.8	1.4

In equation (3.24) the term $- 5.35 \sqrt{\rho_a/\rho_o}$ is denoted by $\frac{x_h}{d'}$.

Now that the constant of integration in equation (3.20) is determined, the centreline velocity and concentration can be expressed in terms of $\frac{x}{d'}$ by substituting (3.20)

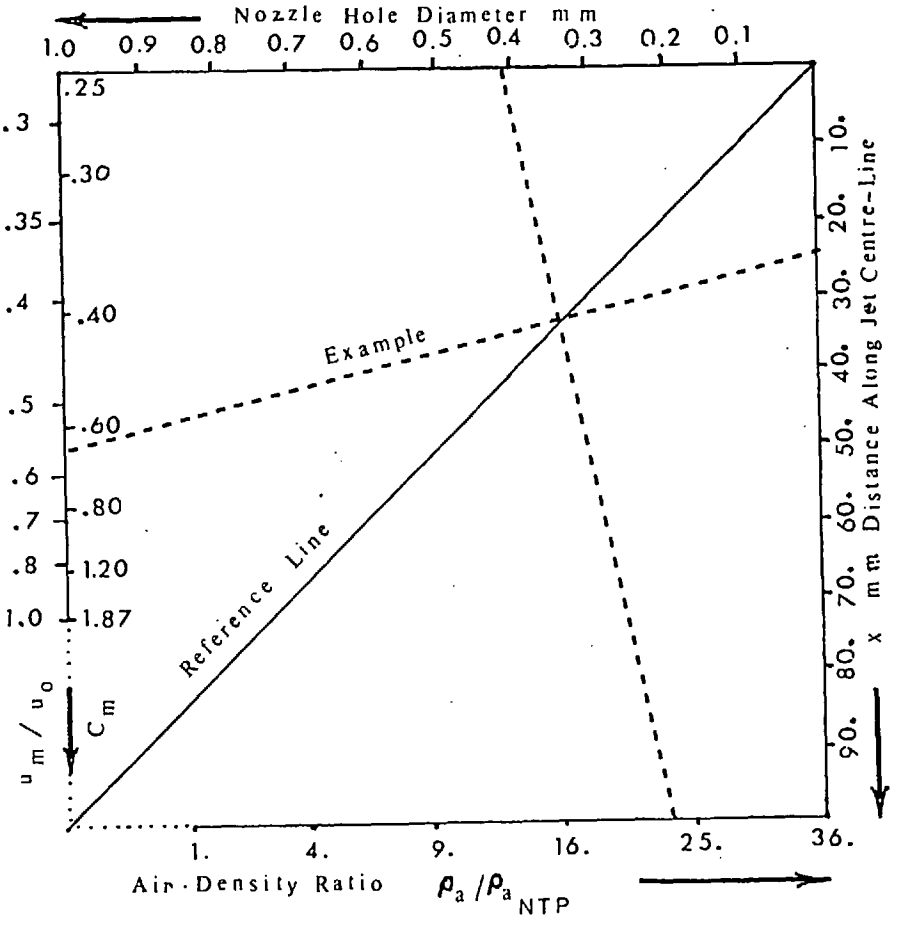

Fig. 3.3. The relationship between jet variables.

in (3.14) and (3.15).

This results in a lengthy analytical expression which is solved numerically. The following approximate expressions are derived by simplification ($\sqrt{1.5\ d_j'^2} \simeq 0.539\frac{x}{d'}$), i.e.:

$$\frac{l}{c_m} = 0.22\ \frac{x}{d'} \tag{3.25}$$

$$\frac{u_o}{u_m} = 0.16\ \frac{x}{d'} \tag{3.26}$$

Equation (3.26) agrees exactly with the following relationship given by Albertson et al (1963) (for an air jet in air)

$$6.2\ \frac{u_o}{u_m} = \frac{x}{d_o}$$

In equation (3.26) d' can be replaced by d_o whenever the density ratio is unity (equation 3.10). The relationship of the main jet variables is demonstrated in a double N nomogram, Fig. (3.3).

3.2.7 Fuel and air flow

The fuel and air mass flow rates at various parts of the free jet can be calculated with the aid of the $I_{f3}(y)$ and $I_{f2}(y)$ integrals respectively (Appendix A).

$$\dot{m}_f(y) = \rho_a\ A\ \ u_m\ \ c_m\ .\ I_{f3}(y) \tag{3.27}$$

$$\dot{m}_f(1) = 0.18\ \ _a\ .\ A\ .\ u_m\ .\ c_m$$

similarly:

$$\dot{m}_a(y) = \rho_a A u_m I_{f2}(y)$$

$$\dot{m}_a(1) = 0.257 \rho_a A u_m \tag{3.28}$$

The fuel and air mass deposited in a narrow strip of length dx will be needed when determining jet penetration:

Fuel: $$dm_f(y) = \rho_a A c_m(y^2 - \frac{4}{7} y^{3.5})dx$$

$$dm_f(1) = 0.43 \rho_a A u_m c_m dx \tag{3.29}$$

Air: $$dm_a(y) = \rho_a A y^2 dx$$

$$dm_a(1) = \rho_a A dx \tag{3.30}$$

Air entrainment is also calculated from the above information for a free jet.

3.3 The wall jet

If a free jet hits the wall perpendicularly, it will spread along radial directions forming a wall jet. In this section the equations governing a wall jet emerging from a free jet are described.

3.3.1 Definitions

Fig. (3.4) shows the cross section of a wall jet, assuming that it is generated by a free jet of radius r_i

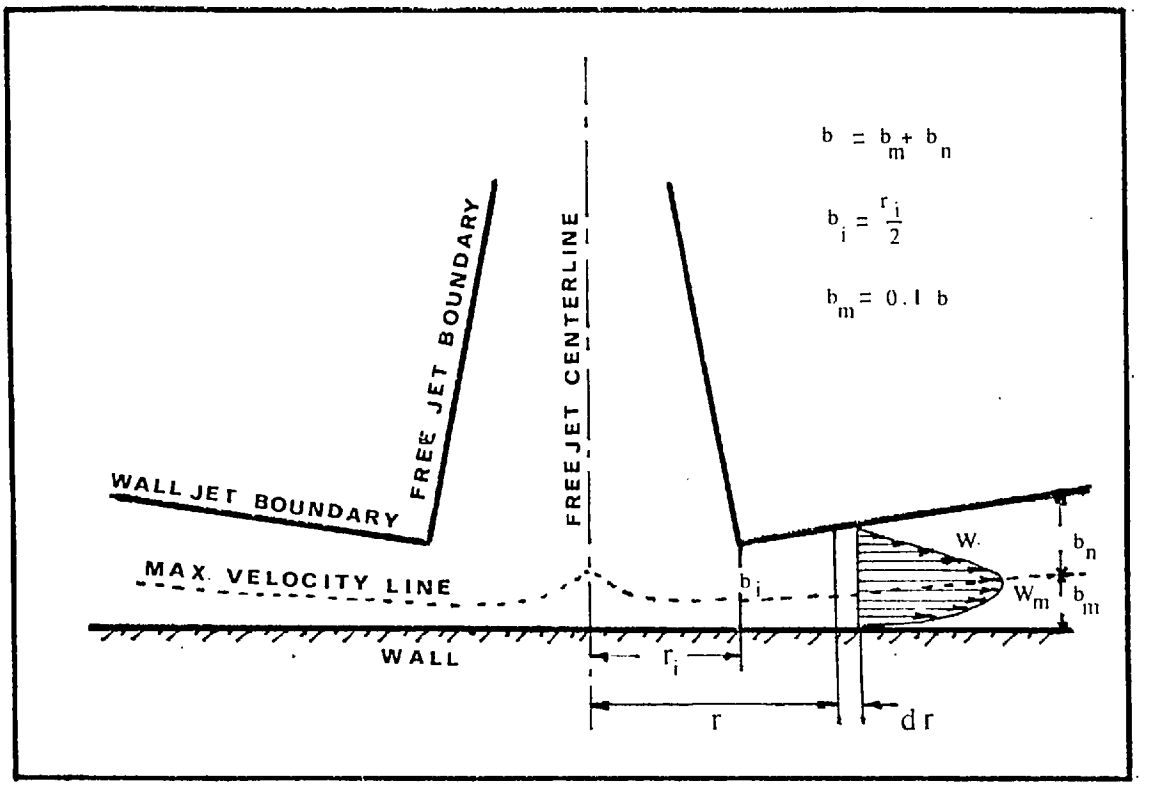

Fig. 3.4. Schematic diagram of the wall jet

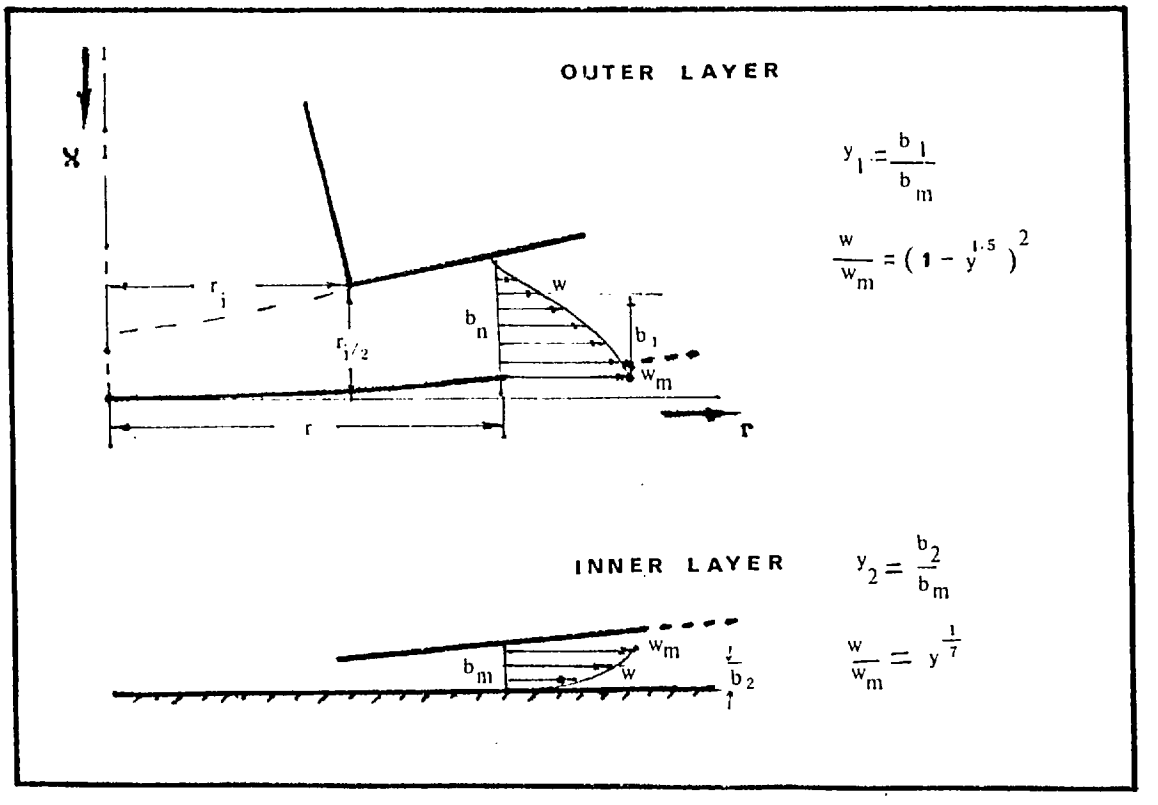

Fig. 3.5. Inner and outer layers of the wall jet

when hitting the wall. The maximum velocity line divides the jet into two layers of width b_m and b_n such that $b_w = b_m + b_n$.

The following equations are based on the work of Abramovich (1963) and Glauert (1956).

In the inner layer (with $y = \frac{b1}{b_m}$), the velocity profile is given by:

$$\frac{w}{w_m} = y^{1/7} \tag{3.31}$$

In the outer layer (with $y = \frac{b2}{b_n}$), the velocity profile is the same as that of a free jet.

$$\frac{w}{w_m} = (1 - y^{1.5})^2 \tag{3.32}$$

b_w is the wall jet thickness at a radius r and b_i is the initial thickness at a radius r_i.

3.3.2 Wall jet variables related to a free jet

At transition from a free to a wall jet, it is assumed that the change in cross-sectional area, and the change in density are negligible. Therefore:

$$\pi r_i^2 = 2\pi\ r_i b_i$$

$$b_i = r_i/2 \tag{3.33}$$

Since the air flow at the initial cross section of the wall jet should also be equal to that of a free jet (at

the impingement area), the following equation can be written:

$$\dot{m}_{awi} = 0.257\ \rho_a\ A_i\ u_{mi} \tag{3.34}$$

The same applies to the fuel flow:

$(\dot{m}_f = 0.18\ \rho_a\ A\ u_m\ c_m)$, i.e.:

$$\rho_o\ A_o\ u_o = \int_o^{A_w} \rho_a \left(\frac{w}{w_m}\right)\left(\frac{c}{c_m}\right)\ .\ w_m\ .\ c_{mw}\ .\ dA \tag{3.35}$$

3.3.3 Wall jet fuel and air flow

With a procedure similar to that of a free jet, the fuel and air flow in the wall jet are calculated.

$$\dot{m}_{aw} = 0.407\ \rho_a\ .\ A\ .\ w_m \tag{3.36}$$

$$\dot{m}_{fw} = 0.416\ \rho_a\ .\ A\ .\ w_m\ c_{mw} \tag{3.37}$$

The integral on the right hand side of equation (3.35) was calculated in two stages (for the inner and outer layers separately). Had the inner layer been neglected the constants in equation (3.36) and (3.37) would have been $I_{w2}(1)$ and $I_{w3}(1)$ respectively (given in Appendix A).

Equations (3.36) and (3.37) are solved to obtain the ratio of free and wall jet maximum velocities at impingement.

$$\frac{w_{mi}}{u_{mi}} = 0.63 \tag{3.38}$$

Similarly, combining (3.35), (3.37) and (3.38):

$$\frac{c_{mwi}}{c_{mi}} = 0.68 \tag{3.39}$$

The fuel and air deposited in a narrow strip of width dr along the wall jet radius can be calculated similarly to that of a free jet, for later use. For simplicity, the distribution in the outer layer, is assumed to apply to the whole width (Appendix A).

Fuel: $$dm_f(y) = \rho_a \cdot A \cdot c_{mw}(y - \frac{2}{5} y^{2.5})dr$$

$$dm_f(1) = 0.6\ \rho_a \cdot A \cdot c_{mw} \cdot dr \tag{3.40}$$

Air: $$dm_a(y) = \rho_a \cdot Ay\ dr$$

$$dm_a(1) = \rho_a \cdot A \cdot dr \tag{3.41}$$

3.3.4 The wall jet growth, velocity and concentration decay

In the C.A.V. model the wall jet was treated by the following relations based on the theoretical solution of Glauert (1956).

The velocity variation with radius was given by:

$$\frac{w_m}{wm_i} = (\frac{r_i}{r})^{1.06} \tag{3.42}$$

The growth of the mixing layer was given by:

$$\frac{b}{b_i} = \left(\frac{r}{r_i}\right)^{1.006} \tag{3.43}$$

For small distances of jet travel, the results will not vary a great deal if the powers on the right hand side of (3.42) and (3.43) are taken as unity. Consequently, the following convenient relations can be established:

$$\frac{A_w}{A_i} = \frac{2\pi rb}{2\pi r_i b_i} = \left(\frac{r}{r_i}\right)^2 \tag{3.44}$$

and from (3.37)

$$A_w \cdot c_m \cdot w_m = A_i \, c_{mi} \, w_{mi}$$

$$\frac{c_m}{c_{mi}} = \frac{w_m}{w_{mi}} = \frac{r_i}{r} \tag{3.45}$$

The relations describe the maximum velocity and concentration decay and the wall jet growth.

3.4 The starting jet

In the preceding sections of this chapter, equations were derived to describe the motion, medium entrainment and the distribution of jet fluid within free and wall jets. It was assumed that the cross sections dealt with were sufficiently far behind the jet front and had reached steady state conditions.

The term "starting jet" here applies to a free or a wall jet which includes the developing jet front. For a free jet, this has been observed to be of mushroom shape and is often assumed to have the shape of the velocity

profile. It is sometimes named "the bell" or "the cap". Similarly, for a wall jet, it can be assumed to be of a toroidal shape with a cross-section resembling the appropriate velocity profile.

3.4.1 Definitions

The "starting jet" before and after impingement, is shown in Fig. (3.6). The surface of "the cap" is known as the jet front. Studies to explain this type of jet in diesel engine sprays, date back to the classic work of Schweitzer (1937). Whitehouse (1973), quoting Schweitzer, followed the reasonable assumption that (x_s) denotes the steady state attainment front. This means that at the bell shaped cap the injected fluid meets the resistance of the medium, slows down and is pushed aside to form the steady jet boundaries. In fact, the motion of a vortex ring is associated with this part of a starting plume, and has been studied by Turner (1962) and Morton (1973) amongst others.

The jet tip penetrates with a velocity (u_f) and the steady state front trails behind with a velocity (u_s). These velocities are obviously less than the steady jet centreline velocities at corresponding positions. (Borman and Johnson, 1960). This is the reason why the penetration calculated on the basis of steady jet velocities, has to be reduced by a factor (the impulsive jet factor). In other words, this factor, which is experimentally shown to be in the order of 0.6 to 0.7, is the ratio of the actual jet penetration to that of a hypothetical jet front moving with the steady jet centreline velocity.

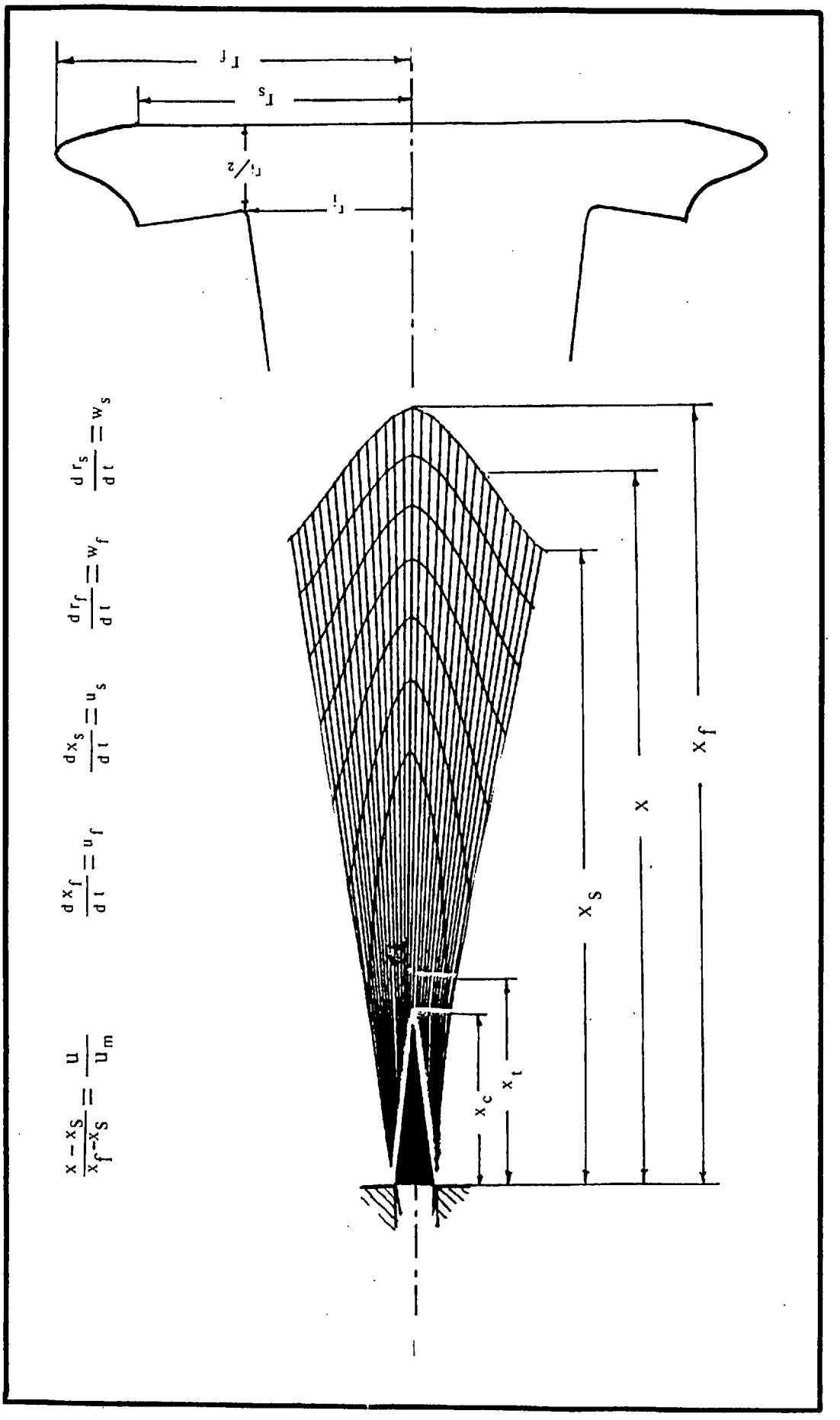

Fig. 3.6. The developing jet.

3.4.2 The free jet penetration

It is proposed here to derive an equation for the jet penetration by calculating the impulsive jet factor. This method will also make it possible to calculate the penetration of a wall jet (no experimental correlation has been reported for a starting wall jet).

Let us first calculate $x_m(t)$, the distance travelled by a point along the steady jet centreline:

$$\frac{dx_m}{dt} = u_m$$

substituting for u_m from equation (3.26)

$$dx_m = 6.2\frac{d'u_o}{x_m}\,dt$$

integrating from 0 to $x_m(t)$:

$$(\frac{x_m}{d'})^2 = 12.4(\frac{u_o t}{d'}) \qquad (3.46)$$

It is generally agreed that the theoretical form of the penetration equation should be as follows: (Dent, 1971).

$$\frac{x_f}{d'} = k(\frac{u_o t}{d'})^{\frac{1}{2}} \qquad (3.47)$$

where k is determined experimentally and $(\frac{k}{\sqrt{12.4}})$ is the impulsive jet factor.

Let us now determine k by equating the mass of fuel injected and fuel deposited in the jet at an interval dt. (equation 3.27):

$$\rho_o A_o u_o dt = 0.43 \rho_a A c_m dx_f$$

$$\rho_o A_o u_o = 0.43 \rho_a A c_m u_f \tag{3.48}$$

Comparison of equations (3.48) and(3.7) shows that,

$$u_f = u_m/2.4 \tag{3.49}$$

This means that the penetration velocity is less than the steady jet velocity by a factor of $(\frac{1}{2.4})$. It is also possible to show that the penetration velocity is equal to the jet half-radius velocity at the corresponding cross-section:

$$u_{\frac{1}{2}} = u_m(1 - 0.5^{1.5})^2 = \frac{u_m}{2.4} = u_f$$

Now recalling equation 3.26 and writing $u_f = \frac{dx_f}{dt}$

$$2.4\, x_f \cdot dx_f = 6.2\, d'\, u_o\, dt$$

$$(\frac{x_f}{d'})^2 = 5.2\ (\frac{u_o t}{d'}) \tag{3.50}$$

comparison of equation (3.46) and (3.50) gives the value of the impulsive jet factor, (x_f/x_m):

$$\frac{x_f}{x_m} = 0.65 \tag{3.51}$$

This is in general agreement with experimental values, so the final form of the penetration equation can be written as follows:

$$\frac{x}{d'} = 2.28\left(\frac{u_o t}{d'}\right)^{\frac{1}{2}} \qquad (3.52)$$

3.4.3 The wall jet penetration

With a similar procedure an approximate relation is obtained for the motion of the wall jet front.

First, the motion of a hypotetical particle on the steady wall jet maximum velocity line, is considered:

$$w_m = \frac{dr}{dt}$$

$$r \cdot dr = w_{mi}\, r_i\, dt \qquad \text{(equation 3.45)}$$

Integrating both sides and defining a non-dimensional wall jet radius (r/d'), (d', in terms of the issuing free jet nozzle diameter as before) results in:

$$\left(\frac{r}{d'}\right)^2 - \left(\frac{r_i}{d'}\right)^2 = 2\,\frac{r_i}{d'}\left\{\frac{w_{mi}(t - t_i)}{d'}\right\}$$

where t is measured from the commencement of injection and t_i is the time taken for the free jet to hit the wall, consequently:

$$\frac{r - r_i}{r_i} = 1.41\left\{\frac{w_{mi}(t - t_i)}{r_i}\right\}^{\frac{1}{2}} \qquad (3.53)$$

Equation (3.53) is the penetration equation for a particle on the maximum velocity line of a steady wall jet. The actual penetration can be obtained by considering equation (3.40):

$$\rho_o A_o u_o\, dt = 0.6\, \rho_a A\, c_m\, dr_f$$

or,

$$\rho_o A_o u_o dt = 0.416 \rho_a A c_m w_m dt$$

$$0.6 \, dr_f/dt = 0.416 \, w_m$$

$$\frac{w_m}{w_f} = 1.44 \tag{3.54}$$

where w_f is the wall jet penetration velocity and w_m is the maximum velocity of a steady wall jet at the corresponding cross-section ($w_m = w_{mi} \frac{r_i}{r_f}$).

$$\frac{dr_f}{dt} = 0.7 \, w_{mi} \frac{r_i}{r_f}$$

i.e.:

$$(\frac{r_f}{d'})^2 - (\frac{r_i}{d'})^2 = 1.4 \frac{r_i}{d'} \{\frac{w_{mi}(t - t_i)}{d'}\}$$

This equation, written in the form of equation (3.53), gives the wall jet penetration:

$$\frac{r_f - r_i}{d'} = 1.18 \{\frac{w_{mi}(t - t_i)}{r_i}\}^{\frac{1}{2}} \tag{3.55}$$

The theoretical impulsive wall jet factor, therefore will be $\frac{r_f - r_i}{r - r_i} = 0.83$.

3.4.4 The development time

The next parameter to characterize a starting jet, is the development time, which also determines the length of the cap. As described earlier, the base of the cap is

considered to be the steady state attainment front, and trails behind the jet tip by a time lag (t_o). Whitehouse (1973) reported this lag to be 1/3 ms for most of the sprays encountered in the diesel engines examined by spray photography. Theoretically, the following relations are derived to relate (t_o) to the cap length, the injection velocity and the charge density.

Consider the free jet penetration equation in the following form:

$$(\frac{x_f}{d'})^2 = k^2 \frac{u_o t}{d'} \tag{3.56}$$

The position of the steady front (x_s), (trailing behind by t_o), can then be given in the following form:

$$(\frac{x_s}{d'})^2 = k^2 \frac{u_o (t - t_o)}{d'} \tag{3.57}$$

Writing (3.56) and (3.57) in differential form and substituting for k from (3.50):

$$2x_f \cdot dx_f/dt = k^2 u_o d' = 2x_s \cdot dx_s/dt$$

$$x_f \cdot u_f = x_s \cdot u_s = 2.6 u_o d' \tag{3.58}$$

On the other hand, subtracting (3.57) from (3.56) gives:

$$(\frac{x_f}{d'})^2 - (\frac{x_s}{d'})^2 = 5.2(\frac{u_o t_o}{d'}) \tag{3.59}$$

$$(x_f - x_s)(x_f + x_s)/2 = 2.6 u_o t_o d'$$

By this equation it is shown that the cap length $(x_f - x_s)$ is inversely proportional to the position of its centre $(x_f + x_s)/2$. This means that as the cap moves away from the nozzle its length becomes shorter (the jet front flattens).

In practice, the length of the cap will obviously depend on the charge resistance, so an exact calculation could be difficult. Here, to be consistant with the above approach, a simplified calculation will suffice.

For $t < t_o$, the steady front does not exist. At $t = t_o$ when $x_s = 0$, the initial cap length $x_{fo} = u_o t_o$, is substituted in equation (3.59) and gives:

$$t_o = \frac{5.2\ d'}{u_o} \tag{3.60}$$

This means that t_o depends on the injection velocity, nozzle hole diameter and the charge density.

The initial cap length, therefore, depends on the nozzle diameter and charge density, given by:

$$x_{fo} = 5.2\ d' \tag{3.61}$$

Also, combining euqations (3.59) and (3.60):

$$(x_f - x_s)(x_f + x_s) = (5.2\ d')^2 \tag{3.62}$$

This determines the cap length according to the position of the jet front.

Two examples of the spray development before impingement, are demonstrated in Fig. (3.7) and (3.8) using the data of Chapter 4 and assuming stagnant surroundings for the spray. The jet front is shown at equal time inter-

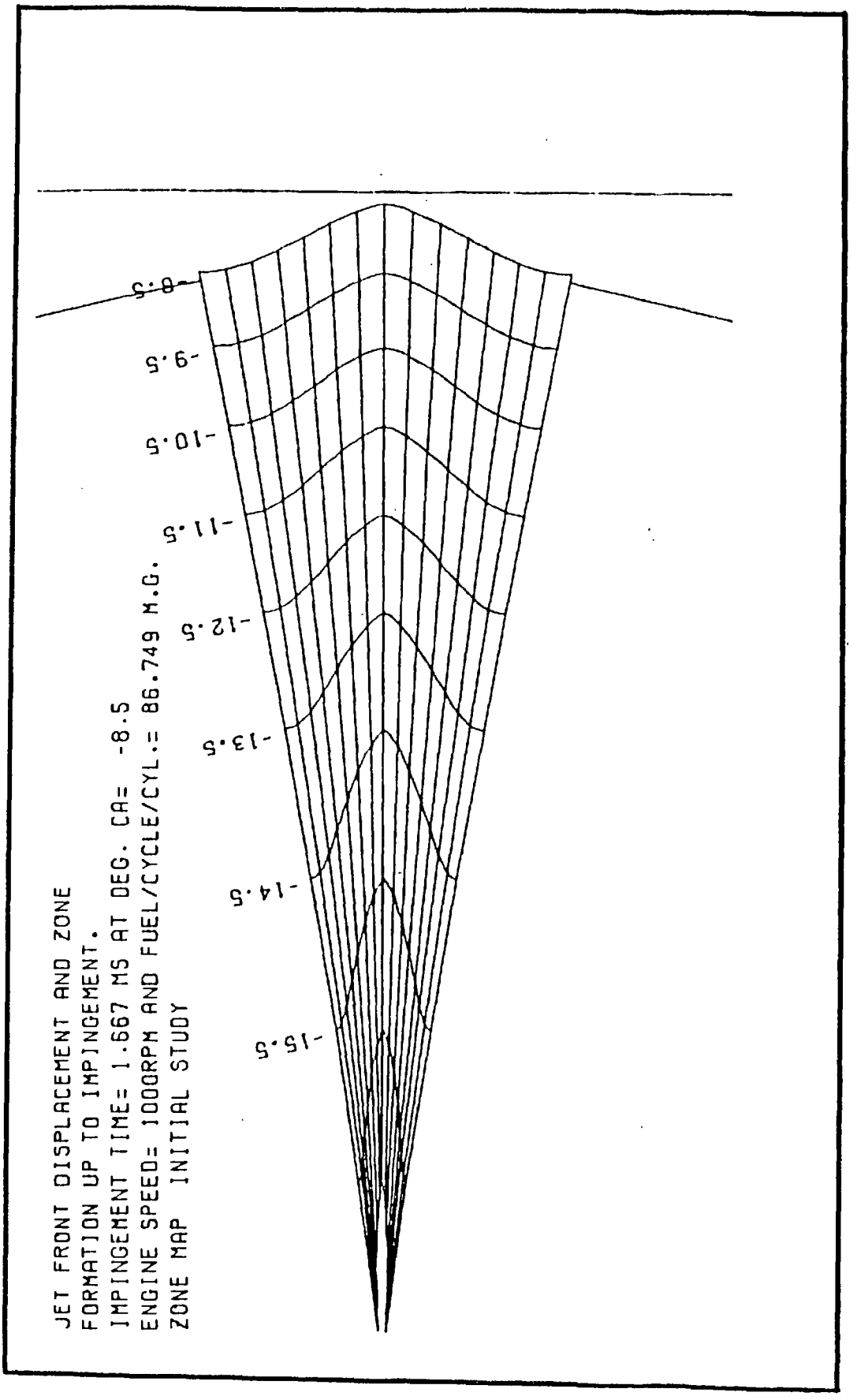

Fig. 3.7. Jet development and zone-division initial study (example 1)

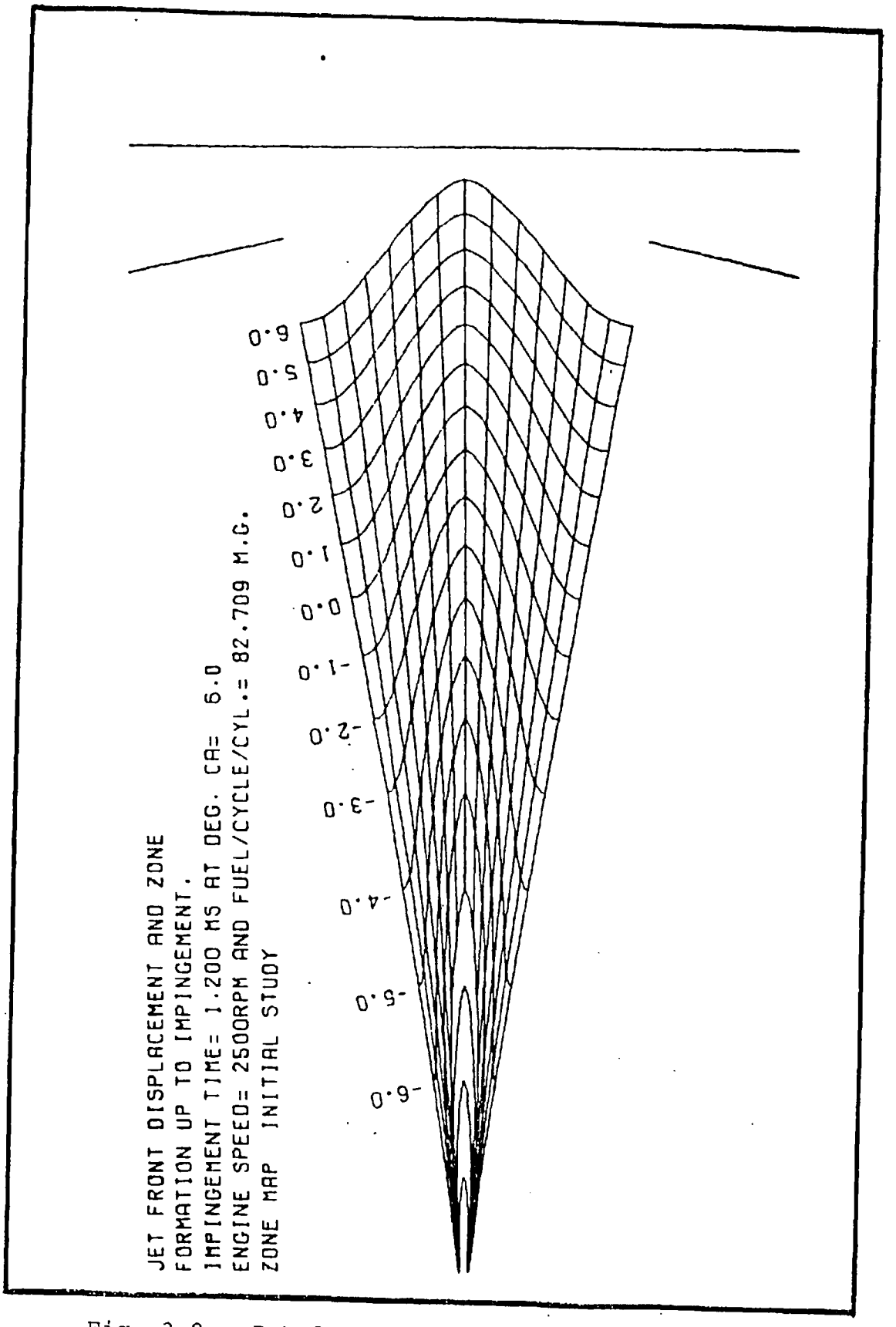

Fig. 3.8. Jet development and zone-division initial study (example 2)

vals marked by the engine crank angle. The lines dividing the jet radius are drawn to investigate a possible pattern of dividing the spray into a number of zones suitable for studying combustion problems. This will be explained in the next section.

3.5 A multizone spray model

In this model the intention is to divide the spray into a number of zones such that each zone represents the motion of the same fuel element (entraining air only). At the same time, it is necessary to trace which zone exactly replaces another during each fixed time increment.

The advantages of such a zone subdivision will be explained in Chapter 5. Here it is enough to say that once such a pattern is established, the remaining computations for predicting heat release will be simplified.

3.5.1 Moving zones of equal fuel mass

The fuel injected is divided and directed to (KR) concentric layers such that by choosing the appropriate layer thickness for each, and by further subdivisions in the axial direction, zones of equal fuel mass are formed.

It will be shown that the contours of the bell shaped jet-front, at equal time intervals (Δt), together with an unequal layer thickness (thinner near the half-velocity line) are capable of producing the pattern described.

The fuel mass in each zone is intended to be:

$$m_{fz} = \frac{\dot{m}_f \cdot \Delta t}{(KR)} = \frac{\rho_o \cdot A_o \cdot u_o \cdot \Delta t}{(KR)} \qquad (3.63)$$

The zone volume and zone air are then calculated accordingly:

$$m_{az} = \frac{\rho_o \cdot A_o \cdot u_o \cdot \Delta t}{KR \cdot c} \qquad (3.64)$$

$$V_z = \frac{\rho_o \cdot A_o \cdot u_o \cdot \Delta t}{\rho_a \cdot KR \cdot c} \qquad (3.65)$$

The zone volume can alternatively be written in terms of the zone length and width:

$$V_z = 2\pi \cdot r \cdot \Delta r \cdot \Delta l \qquad (3.66)$$

The zone 'residence time' is defined as the time taken for the point mass centre of the zone to travel a distance equal to the zone length. i.e.:

$$\Delta t_r = \frac{\Delta l}{u} \qquad (3.67)$$

One would be inclined to choose a pattern of zone division that gives a constant residence time for all zones, so that at fixed intervals each zone is replaced by the one immediately behind it (in the same layer). The only advantage of such a pattern would be in the convenience of labelling the zones and tracing their motion. Yet the pattern would have severe disadvantages. It would necessitate a sophisticated mass transfer calculation between zones of adjacent layers (both in fuel and air). Moreover, it would result in very large values of zone length for the inner

zones (i.e. nearer the jet centreline). The reason for this is that the zone length would have been proportional to velocity. All these aspects could create difficulties in further numerical computations.

Alternatively the following zone division pattern was devised.

In the radial direction, unequal thicknesses were considered for (KR) number of concentric layers such that the number could be selected arbitrarily and the non-dimensional thickness of each layer (Δy_K) could be calculated accordingly.

In the axial direction, each layer was further divided by the jet front contours at equal intervals; thus the number of zones in each layer (LX) increases while injection continues but is fixed by a number (LMAX) after the end of injection.

The following calculations show how this pattern satisfies the condition of maintaining equal fuel mass in all zones.

Combining euqations (3.65) and (3.66):

$$2\pi \cdot c \cdot \rho_a \cdot r \cdot \Delta r \cdot \Delta l = \frac{\rho_o A_o u_o \Delta t}{KR} = \text{const.} \tag{3.68}$$

writing the l.h.s. in terms of y, c_m and A:

$$2c_m \rho_a A(1 - y^{1.5})y \cdot \Delta y \cdot \Delta l = \frac{\rho_o A_o u_o \Delta t}{KR}$$

replacing $(\rho_o A_o u_o)$ by $\{I_{f3}(l) \rho_a A u_m c_m\}$ from equation (3.7):

$$2(1 - y^{1.5})y\ \Delta y\ \Delta l = \frac{I_{f3}(1)\ .\ u_m\ .\ \Delta t}{KR} \qquad (3.69)$$

The axial divisions are intended to be marked by the jet front at equal intervals (Δt). Therefore, the zone length (Δl) is chosen proportional to the tip velocity:

$$\Delta l = u_f\ .\ \Delta t = \frac{u_m}{2.4}\ \Delta l = \frac{I_{f3}(1)}{I_{f1}(1)}\ u_m\ \Delta t \qquad (3.70)$$

Substituting Δl in equation (3.69):

$$(1 - y^{1.5})y\ .\ \Delta y = \frac{I_{f1}(1)}{2\ .\ KR} = \text{const.} \qquad (3.71)$$

To satisfy this equation, the zone width (Δy) must be a function of y. It is noted that, when y is small (jet centreline), Δy must be large; similarly when y approaches unity (jet boundary), $(1 - y^{1.5})$ becomes small and again Δy must be large.

Choosing any number of layers (KR), then the position (y_K) and the corresponding non-dimensional thickness (Δy_K) for each layer, from KI = 1. to KI = KR are calculated such that:

$$\int_o^{y_K}(1 - y^{1.5})\ y\ dy = \frac{2KI - 1}{KR}\ .\ \frac{I_{f1}(1)}{2}$$

The value of the l.h.s. integral is given in Appendix A. Thus:

$$I_{f1}(y_K) = y_K^2(1 - \frac{4}{7}\ y_K^{1.5}) = \frac{2KI - 1}{2KR}\ I_{f1}(1) \qquad (3.72)$$

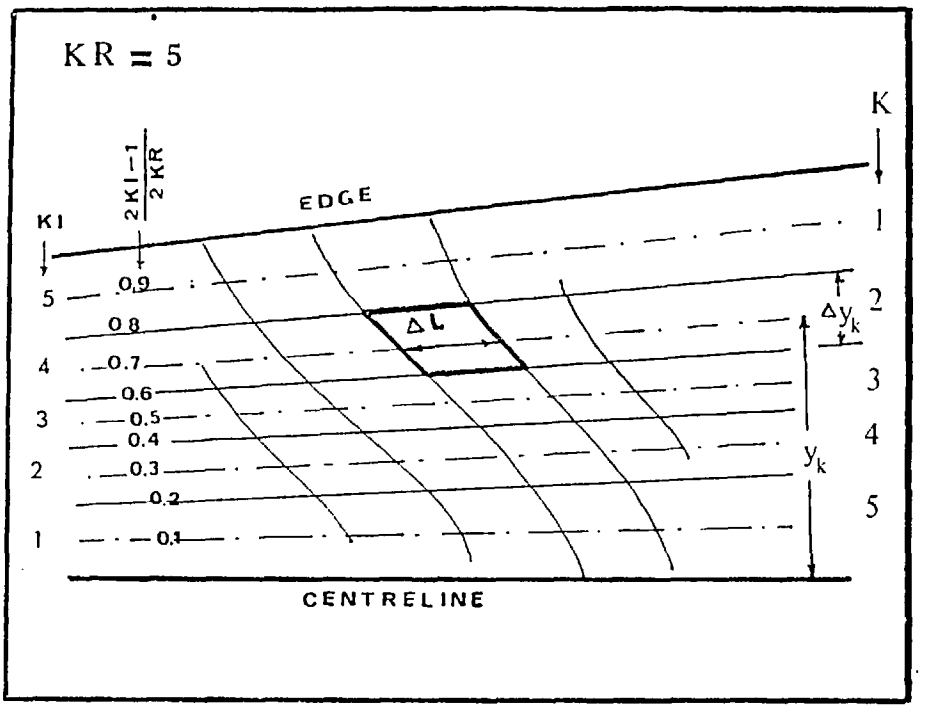

Fig. 3.9. Variables of a zone division pattern with unequal layer width.

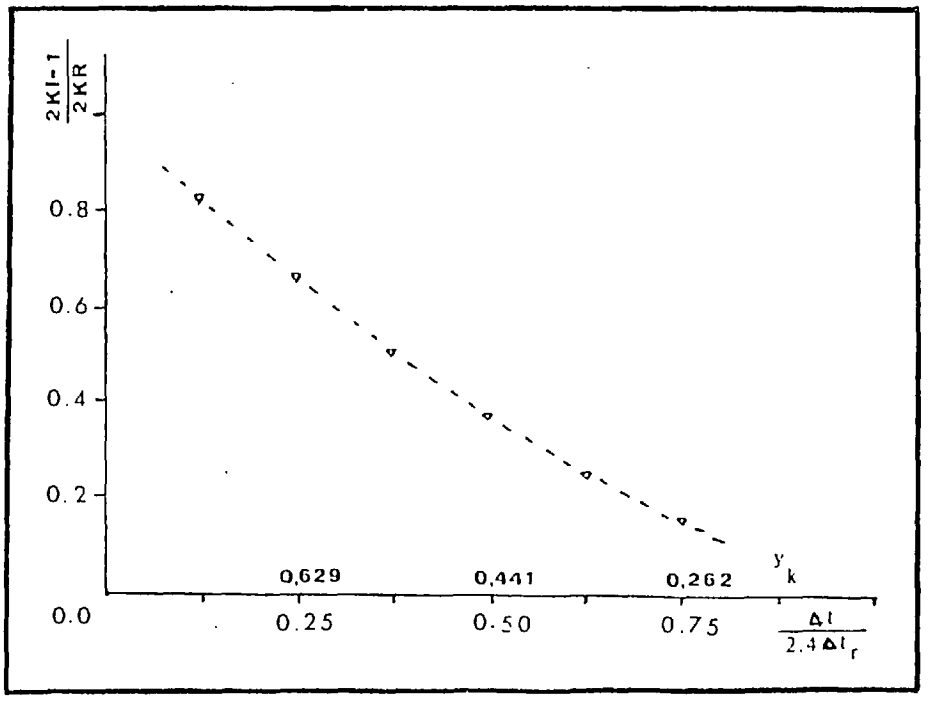

Fig. 3.10. Relationship between zone residence time and layer number.

In this way, the condition of maintaining equal fuel mass in each zone is satisfied and at the same time the contours of the jet front give the axial position of the zones. It should be noted that no attempt was made to calculate this pattern for the initial region of the jet. To avoid a complicated calculation of the exact width and length of the zones in the initial region, it is argued that the relative reduction in zone length will be compensated by the increase in fuel concentration for the outer zones (due to the change in concentration distribution in the initial region of the jet).

Therefore, it is assumed that the jet front contours in the initial jet region also provide the axial divisions for the layers mentioned, thus allowing longer inner tubes compared to the outer ones. This shows that near the nozzle, approximately equal volumes are considered for all layers, which again means that the condition of equal fuel mass is satisfied.

To complete the zone-division pattern, the velocity distribution is recalled from equation (3.1). At the same time combining (3.67) and (3.70) gives:

$$\Delta l = u \cdot \Delta t_r = \frac{u_m}{2} \Delta t$$

$$\frac{\Delta t}{\Delta t_r} = 2.4(1 - y_K^{1.5})^2 \qquad (3.73)$$

Equation (3.73) shows that the residence time (Δt_r) for a zone near the jet boundary is larger than for those near the centreline. It is also shown that (Δt_r) is a function

of y only:

$$\Delta t_r(x, y) = \frac{\Delta l(x, y)}{u(x, y)} = \frac{u_m(x) \cdot \Delta t}{2.4\ u(x, y)} = \frac{\Delta t}{2.4(1 - y^{1.5})^2}$$

Since in the axial direction the zone length is proportional to the velocity, the residence time is not a function of axial distance and is a function of the non-dimensional radius y_K only.

Once the number of layers (KR) is chosen, (y_K) for each layer is calculated from equation (3.72) and is substituted in equation (3.73) to determine $\Delta t_r(K)$. Obviously at the jet half-radius ($y_K = 0.5$), the residence time is equal to the time step (i.e. $\Delta t_r = \Delta t$). In section 3.4.2 it was shown that the jet front moves with a velocity equal to the jet half-radius velocity. Thus the zones in the outer layers ($\Delta t_r > \Delta t$) lag behind, and the zones in the inner layers ($\Delta t_r < \Delta t$) try to overtake the half-radius zones.

To express the residence time (Δt_r) and the velocity (u_K) in terms of the layer number (KI), the position (y_K) is calculated from equation (3.73) and is substituted in equation (3.72) after defining δ_K as follows:

$$\delta_K = \left(\frac{u_K}{u_m}\right)^{\frac{1}{2}} = (1 - y_K^{1.5}) = \left(\frac{\Delta t}{2.4\ \Delta t_r}\right)^{\frac{1}{2}}$$

$$y_K = (1 - \delta_K)^{2/3}$$

$$(1 - \delta_K)^{4/3} \cdot (1 + \frac{4}{3}\ \delta_K) = \frac{2KI - 1}{2KR} \qquad (3.74)$$

Equation (3.74) in effect demonstrates the relationship between the velocity and the layer number. For example,

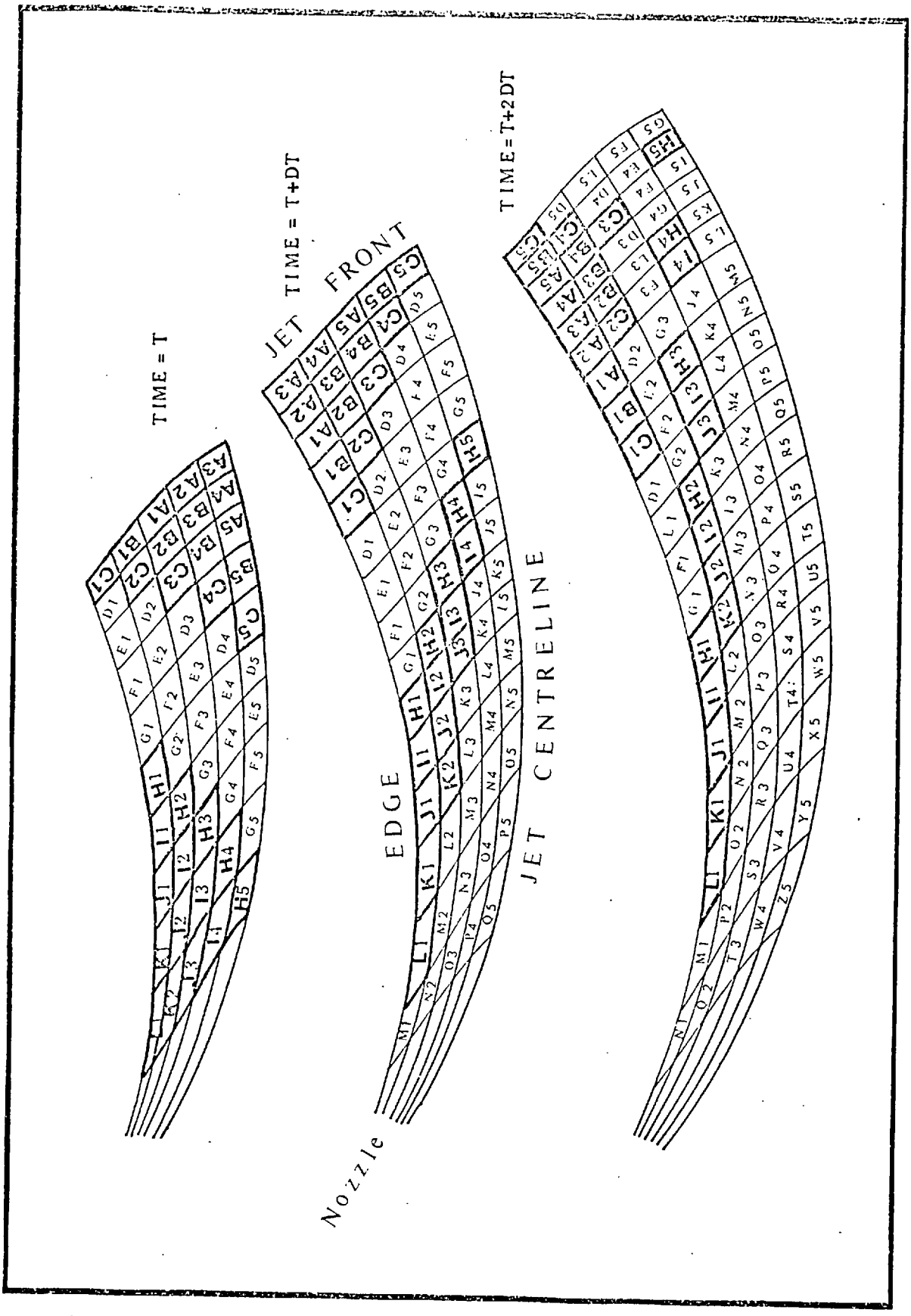

Fig. 3.11. Development of individual zones with time.

if KR = 5 then $(\frac{u_K}{u_m})^2$ is 0.24 and 0.9 for the first and the last layers respectively. The equation is presented in graphical form in Fig. (3.10). Except for the two extreme ends (which will only come into effect for very large values of KR) an approximately linear relationship is noticed. Thus $\frac{1}{\Delta t_r} \propto \frac{2KI - 1}{2KR}$ and $u_K \propto 2\ KI - 1$.

The constant of proportionality is negative, therefore, to have u_K increasing with the layer number, layers are numbered in the opposite direction (from edge to centreline). i.e. K is defined as follows:

$$K = KR - KI + 1$$

The above argument shows that if in the first layer $u_K = u_1$, then in the kth layer $u_K = (2K - 1)u_1$ and so on.

Preference was given to expressing equations in terms of residence time $\Delta t_r(K)$ instead of velocity (u_K) because the residence time is a function of y_K only whereas velocity is a function of both y_K and x. The reason for this is that u_m is a function of x but Δt is constant.

3.5.2 Zones in intermittent jets

The zone formation pattern described does not consider a finite injection duration. To simulate intermittent sprays this is now taken into account by including the effect of a developing jet-front (as in section 3.4) and a truncating jet-back (as in the C.A.V. model, section 2.2 c)). The following approximate pattern is proposed for the motion of the zones.

During each time increment (Δt) a total of KR x KR

zones are allowed to be accommodated in their new places created by the movement of the jet-front. This is done while each layer supplies (2K - 1) zones.

The same number, i.e. (KR^2) zones are created at the nozzle end during each step while injection continues. After the end of injection it is assumed that the movement of the jet-back truncates the spaces occupied by the last $(KR)^2$ zones during each step.

The sum of a series of consecutive odd numbers (starting from unity) is always an exact square, i.e.:

$$\sum_{K=1}^{K=KR} (2K - 1) \equiv (KR)^2$$

The velocities calculated for (KR) layers (with the particular layer thicknesses chosen in the previous section) were proportional to (2K - 1). Therefore the $(KR)^2$ new spaces created by the movement of the jet-front consist of (2K - 1) zones from each layer. This necessitates a change of layer for the zones supplied by the high velocity layers (i.e. layers below the half-radius). The pattern is demonstrated in Fig. (3.11). It can be seen that in effect a rotation about the half-radius is allowed for the zones reaching the front during each interval. The jet is shown at the beginning and the end of two consecutive intervals (three states) and the zones are labelled by a combination of letters and numbers for illustration purposes.

Obviously this pattern does not truly represent the complicated vortices that exist behind the jet-front. In

general, however, it is believed that the zones at the jet front do not stay at the front but move to the sides to form the jet boundaries. This is allowed for by the above pattern in an approximate manner. It should also be noted that the derivations are based on the following assumptions. The concentration values of a developed jet are used throughout the computations. Zone velocities along the layers are approximated by the axial velocities of a developed jet at corresponding positions.

The pattern is further explained in the following package written for use in a computer programme. It shows how the zones are labelled (using numbers only) to relate them to one another at the beginning and end of each step (Fig. 3.12).

Each zone is labelled by the two parameters K and L which are related to K1 and L1, denoting a previous state. K and K1 represent the layer number and L and L1 represent positions along the layer. LX represents the number of zones in a layer (LX = KR x number of steps), reaches LMAX at the end of injection and does not increase subsequently. For example if the jet is divided into 4 layers (KR = 4) and if the injection duration is divided into 10 steps then during each step 16 zones will be created (4 in each layer), LX will take values equal to multiples of 4 reaching LMAX = 40 and there will be a total of 160 zones. During each step zones in layers K = 1, 2, 3, 4 will travel distances equivalent to 2K - 1 = 1, 3, 5, 7 zone-lengths and there will be changes of layer as imposed by the jet-front and the jet-back. (K = 1 near the edge,

K = KR near the centreline and L = 1 at the jet-front, L = LX at the nozzle and, i.e. L = LMAX at the jet-back). These are calculated by the following package for each step:

```
DO 111   L = 1, LX
L1 = L
DO 101   K = 1, KR
K1 = K
LK = L + K
IF (LK . LE . KR)    K1 = KR + 1 - L
IF (LK . GT . LMAX)    K1 = LMAX + 1 - L
L1 = LK + K1 - KR - 1
101 Continue
111 Continue
```

All the zone variables can be calculated within this package, and can be stored until the end of computations for the next step. For example, the zone position x_{z2} and concentration c_{z2} at the end of a current step are stored in the locations XP(K, L) and CONS2(K, L) respectively. At the next step these values are addressable by XP(K1, L1) and CONS2(K1, L1) for the same zone. Since the concentrations at the beginning and end of the step are needed in the same loop of the programme, separate storage locations are used for them (i.e. CONS2(K, L) = c_{z2} and CONS1(K, L) = c_{z1}, where: CONS1(K, L) = CONS2(K1, L1)).

Similarly any other property of the zone can be related to a previous value for the same zone via this labelling code.

injection duration = 10.Δt

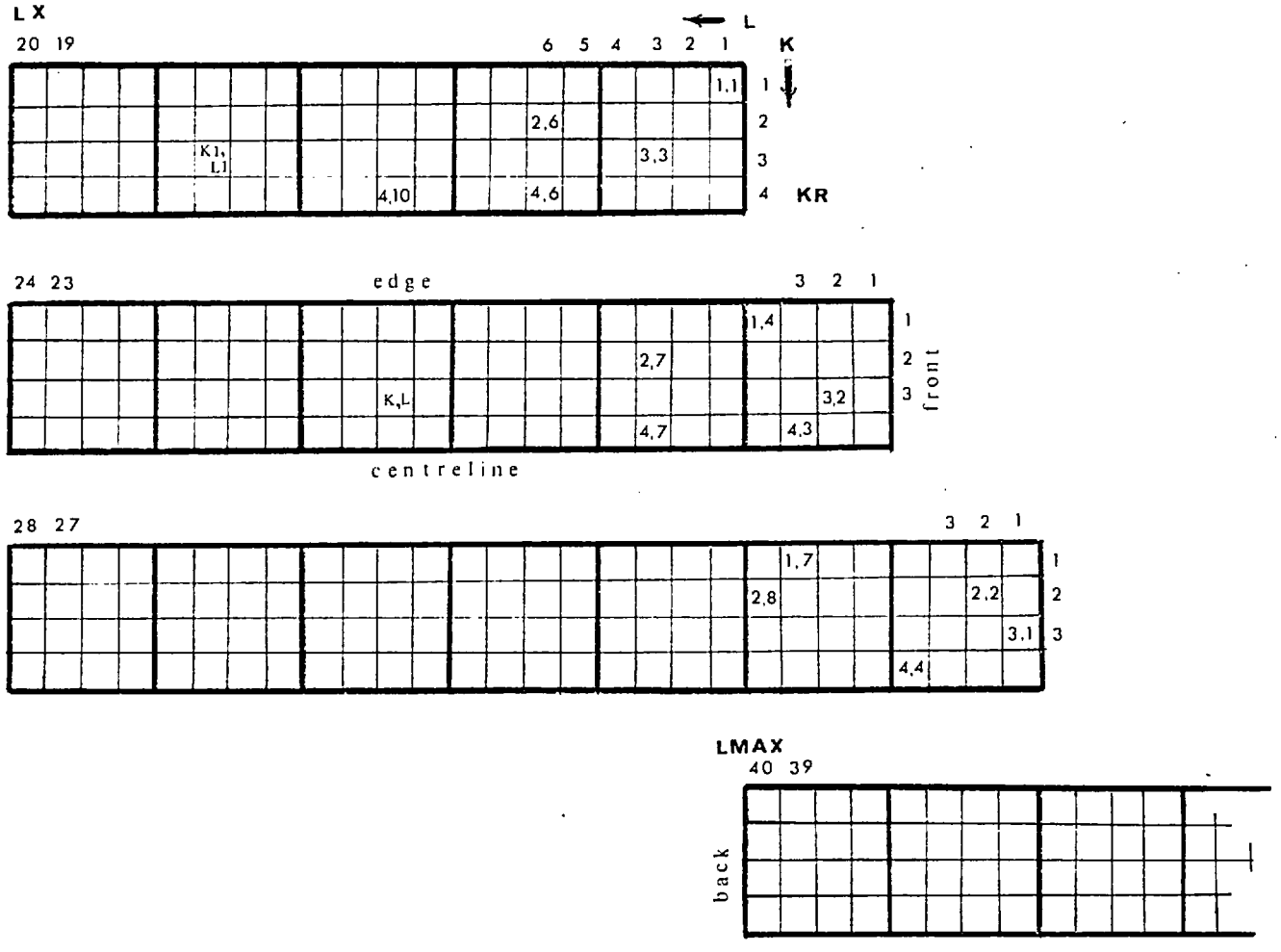

Fig. 3.12. Zone labeling code

3.5.3 Air swirl

Air swirl in the combustion chamber of a diesel engine is assumed to be present in the form of solid body rotation about the point of injection. (Centrally located nozzle). The jets are therefore confronted with a cross flow and are deflected accordingly. Zones of constant concentration will no longer be circular (contrary to what was considered in previous sections). Only a three dimensional treatment of the jet, can provide the necessary solution to describe the shape of such zones. This is beyond the limits of the present study. However, experimental correlations which describe the jet in air swirl make it possible to relate the variables to those of a straight jet.

The angular velocity of the air motion in engines is usually given in terms of the swirl ratio (SR). By definition, (SR) is the equivalent solid body RPM of the air motion, divided by the engine RPM.

$$SR = \frac{\text{RPM (swirl)}}{\text{RPM (engine)}} = \frac{w_s}{2\pi(\text{RPM})} \tag{3.75}$$

The tangential velocity (u_s) and the cross flow momentum ($\rho_a\ u_s^2$) are given in terms of swirl angular velocity (w_s)

$$u_s = x_s \cdot w_s \tag{3.76}$$

Jet deflection parameter (λ) is also widely used. This is defined as the square root of the ratio of cross flow and jet momenta:

$$\lambda^2 = \frac{\rho_a u_s^2}{\rho_o u_o^2} \tag{3.77}$$

The parameter (λ) is used in correlations to describe jet deflection and concentration change compared to a straight jet. Abramovich (1963), Shandorof (1966) and Jordinson (1956), amongst others, have studied jets in cross flow. Patrick(1965) presented his results on jets in cross flow for a range of $0 < \lambda < 0.152$. This range is adequate for diesel engine conditions. The following analytical relations are based on Patrick's results:

$$\frac{x_{sl}}{d'} = \lambda^{-0.85} \left(\frac{y_{sl}}{d'}\right)^{0.34} \tag{3.78}$$

This is the equation of the jet centreline which gives the tangential displacement (y_{sl}) along the swirl direction, in terms of (x_{sl}) the radial distance in the original direction of injection. Fig. (3.13).

The concentration decay in terms of (s), which is the distance along the curved centreline, is given by the following equation:

$$\frac{1}{c_{sm}} = \left\{\frac{s}{d'} \cdot e^{(7.8\lambda - 1.85)}\right\}^{1.18} \tag{3.79}$$

It is noted that as λ increases, c_{sm} becomes smaller. This means that for higher swirl ratios the centreline concentration (for the same arc distance) reduces (higher rate of air entrainment). To complete the model, the concentration distribution in the plain perpendicular to the centreline is needed. Obviously this depends on the angle (θ) relative to the direction of cross flow. Usually,

experimental results give a set of concentration values measured in a plane which divides the jet into two identical halves. The direction of swirl is parallel to this plane which embodies the jet centreline and the two curves denoting the jet boundaries. The jet centreline is nearer to the leading edge than to the trailing edge. In general the jet cross section has a kidney shape with two counter rotating vortices towards the trailing edge. It is this that makes a three dimensional treatment difficult. The sketches in Fig. (3.14) and (3.15) are for the purpose of flow visualisation only and no attempt has been made to calculate the shape of such zones. Instead, it is assumed that for each zone in the straight jet there exists a corresponding zone in the deflected jet as shown in Fig. (3.13). The concentration reduction due to swirl is then calculated for each zone assuming a proportionality factor which is a function of the corresponding centreline concentrations. i.e.:

$$c_{sz}(K, L) = \frac{c_{sm}(L)}{c_{m}(L)} \cdot c_{z}(K, L) \qquad (3.80)$$

Equation (3.78) is used for the calculation of the deflected jet centreline (Fig. 3.13). y_{sl} is measured along the direction of swirl (circular are distances) and x_{sl} in the direction of radii.

The centreline concentrations $c_{sm}(L)$ are calculated from equation (3.79). Zone air entrainment and zone volume are then calculated knowing the zone concentration from equation (3.80).

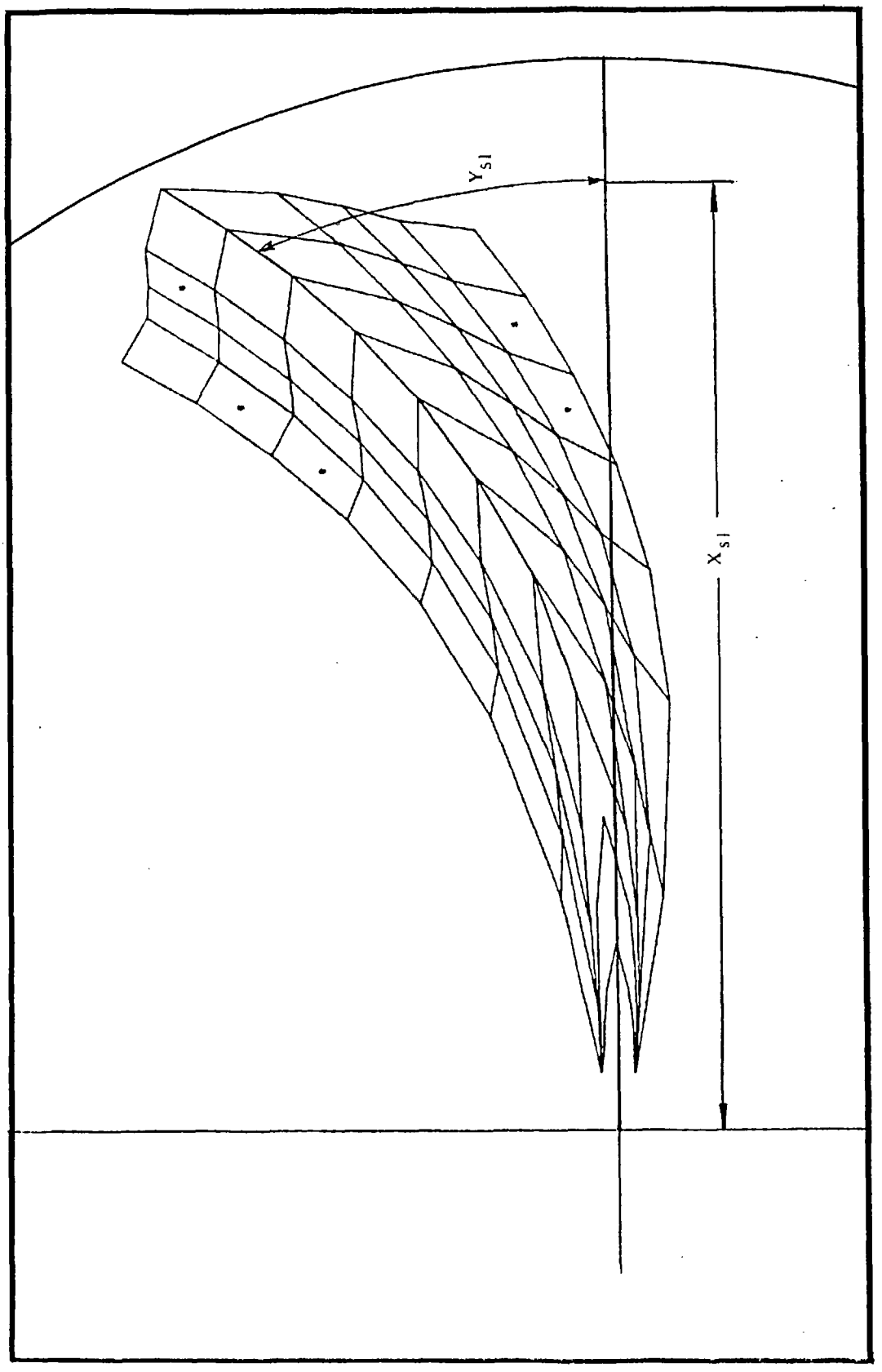

Fig. 3.13. The deflected jet in swirling cross-flow

3.5.4 Zones after impingement

In sections 3.3 and 3.4.3 it was explained that a free jet forms a radial wall jet after impingement. Now it is intended to extend the free jet zone formation model to describe what happens to the zones after entering the wall jet region. Obviously the transition region is extremely complex and may involve large irregular eddies. However, the flow settles to form a regular wall jet which, as explained before, consists of an outer layer and an inner layer. The outer layer has a velocity profile the same as that of a free jet and occupies 90% of the total width. To make some sort of a zone division model possible, the inner layer was neglected. This means that the maximum velocity line was assumed to be very near the wall. Thus, it was possible to establish continuity for the motion of the zones approaching the wall. Fig. (3.15) shows that the zones can follow exactly the same pattern of flow, becoming thinner in width and length and assuming a diameter which grows larger as they move along the wall. Zones at the wall jet-front are treated in the same manner as the free jet-front. This means that fast-moving zones of the high velocity region move sideways and become slow-moving zones. Had the inner layer been taken into account, a similar pattern would be considered allowing zones to move and settle to zero velocity on the wall (a much finer mesh would have been necessary due to the small width of the inner layer). This approach also has the advantage of being convenient for the computer programme which will be presented in Chapter 5.

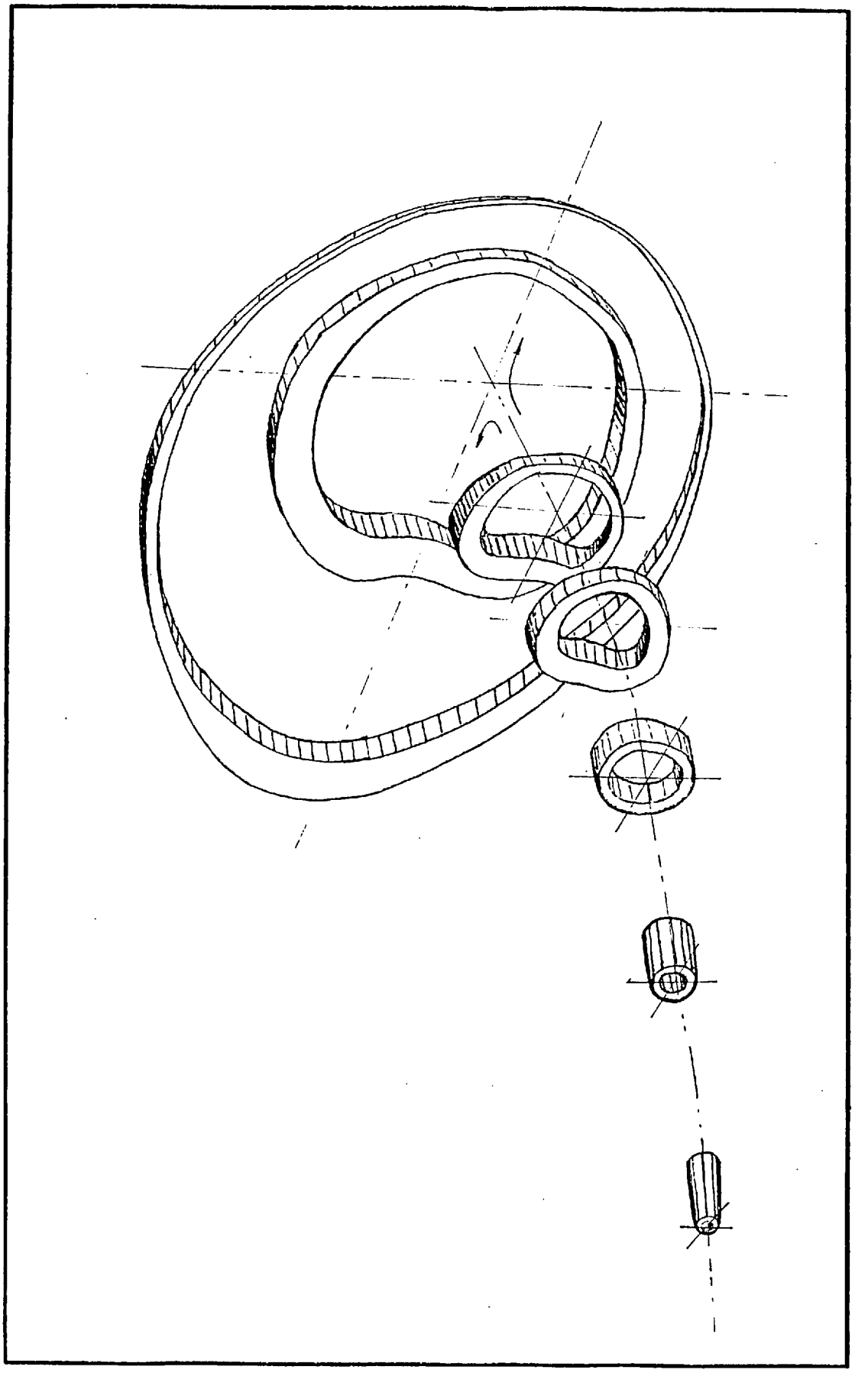

Fig. 3.14. Visualisation of zone growth

Fig. (3.15) shows how the zones are treated after impingement. Rows and layers can be numbered in the same way as for the free jet. No change is caused in the general pattern of zone-division. In other words zones are formed by the contours of the wall jet-front. However the narrow inner layer which would have resulted in very small zones moving inwards and settling on the wall, is neglected.

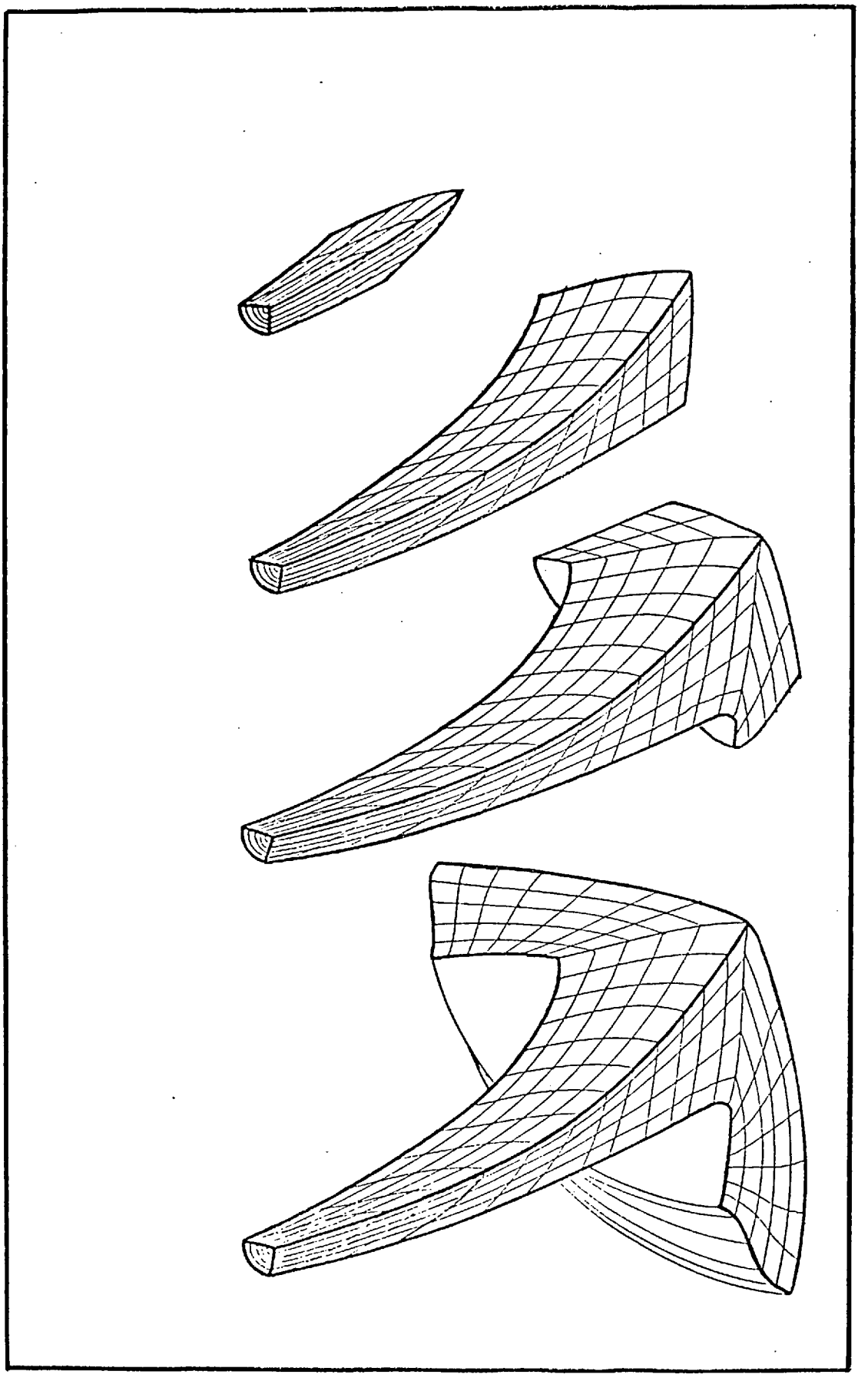

Fig. 3.15. Zone motion with deflection and impingement

CHAPTER 4

EXPERIMENTAL WORK

4.1 Introduction

As mentioned before, two types of experimental data were needed to satisfy the requirements of the present work.

a) data to provide initial conditions for the prediction model,

b) data to be compared with the theoretical results.

The theoretical model was devised in such a way that the initial conditions could be reduced to a minimum number of variables. This was required to make the computer programme as versatile as possible in the future applications. In fact, in the absence of measured data an estimate of the trapped conditions and the injection rate will be sufficient to run the prediction programme. However for evaluating the predicted results, accurate experimental data are needed.

A Leyland 520 series turbocharged engine was instrumented to supply data under direct computer control. This will be described in the next two sections. A separate section is devoted to the injector details. The data logging system is explained by Marzouk (1976). The method of applying the data to the prediction model is explained in the last section of this chapter.

4.2 Test facility

The test facility consisted of an all digital control and data logging system.

A PDP-15 computer and the engine test bed were housed in a two level laboratory. The computer and associated electronics were mounted on a mezzanine gallery overlooking the test bed, thus allowing the shortest possible cable runs.

The complex package of electronics which transfers information between the computer and the engine, handling various forms of signals, is known as the interface.

The computer configuration was a 16 K core store, 18 bit word length, 0.8 μs cycle time, 256 K word disc, three small magnetic tape transports, paper tape input and output facilities and teletype input and output.

Engine power was absorbed by an eddy-current dynamometer which had a low interia rotor and a thyristor drive unit for rapid overall response. The manual control of the brake torque was possible via a ten-turn potentiometer. Alternatively, the computer issued a ten-bit word to one of the interface digital buffers, to represent the required torque. This word was passed through a digital to analogue converter and into a three-term controller which operated the thyristor drive unit, accurately setting the eddy field current for the required torque. The dynamometer embodied a high accuracy strain-gauged torsional load cell to provide continuous read-out of brake torque.

A moire fringe optical incremental shaft encoder was mounted on the engine crankshaft for engine speed measurement and various timing functions. Two types of output tracks were provided, one giving a single output pulse once each revolution (gate pulse), the other giving pulses at

regular rotations of a fraction of degree. The engine speed was continuously available to the computer in the form of the reciprocal of a measured interval. A 12-bit counter registered the number of pulses, from a 25 kHz crystal clock, between successive crankshaft revolution marker pulses. This method of speed measurement did not suffer from errors common to conventional techniques which involve analogue to digital conversion of a speed meter reading.

For visual speed checks, a 60 tooth gear wheel and a magnetic pick-up on the dynamometer were used together with a conventional speed meter.

The turbocharger speed was measured in much the same manner as engine speed, but with a 500 kHz clock frequency. A magnetic nut on the compressor end of the turbocharger shaft generated the necessary signal. Logic circuitry, including a digital buffer to store the counter contents following the arrival of a new marker pulse, eliminated the possibility of the computer reading an incomplete interval. To check the synchronisation of data logging with the engine firing revolution, a digital counter incremented by the marker pulses was employed to count the number of crankshaft revolutions (twice the number of engine cycles) following any specified instant.

A digital stepping motor was mounted on the engine and linked to the governor lever, for automatic control of the desired fuel input. Command words from the computer were issued to the stepping motor drive unit via a digital buffer. Each word was programmed to contain two instructions, the required number of steps and the direction of motor rotation. This was transferred to a binary downcounter

where the logic circuitry determined the operational mode. Stepping pulses going to the motor were also fed back to the down counter to record the number of steps executed. When the counter was cleared, an electronic flag informed the computer that the instructed operation was completed (i.e. the governor set point was changed).

The computer was available exclusively for engine tests when required. The control instructions were fed in via the teletype before or during a test. Operations were performed by loading and executing the required software modules which were programmes written in Macro (a low level language).

It was possible to perform operations such as bringing the engine to a required condition, settling to a certain stability criteria, data sampling, sequencing test events, data processing and output of results. On line computations, e.g. averaging fifty cycles, were also performed.

The data loggers were analog to digital converters (A D C), which converted (- 5 to + 5 or 0 to + 10 Volt) analogue signals into (10 bit) binary digits, capable of servicing up to 32 channels. Logic circuitry including multiplexing facilities, sample and hold amplifiers, various selectors and convertors in addition to an extra 8K word memory, made various manipulations possible.

4.3 Test bed equipment

Engine

A Leyland 520 series engine was provided by British Leyland Ltd. Smith (1973) discusses the particular features

of this engine. The following information was used in the prediction model:

No. of cylinders: 6 in line

Type: 4 stroke, compression ignition

Combustion chamber: open type, direct injection

Bore: 0.118 m

Stroke: 0.125 m

Compression ratio: 15.1:1

Full load speed range: 800-2600 RPM

Valve timing: ATDC (Firing)	Open	Close
Inlet	35^{o}	59^{o}
Exhaust	134^{o}	374^{o}

Static injection timing: 24^{o} BTDC

Firing order: 1, 5, 3, 6, 2, 4

Swept volume: 8.2 litres

Con. rod length: 0.2182 m

Injection: Multi-element mechanically governed pump and four-hole injectors.

Turbocharger:

The engine was pulse turbocharged up to a delivery pressure of 2.1:1 by a Holset 4LE turbocharger. This consisted of a centrifugal compressor and a dual entry radial turbine. One exhaust manifold was connected to cylinders 1, 2, 3 and another to 4, 5, 6. The engine was equipped with a boost sensing fuel control to limit smoke, but this was not used in these tests.

A magnetised nut was fitted at the compressor end of the turbocharger shaft and a Cussons-Ricardo magnetic pick

up was used to obtain the turbocharger speed signal.

Dynamometer

A vibrometer eddy current dynamometer (type 3WB/25), capable of a maximum torque of 1520 NM at 1800 rev/min was selected and installed. The stator coils were supplied with a highly stable d.c. current via a thyristor-controlled exitation unit. The power was dissipated by cooling water from the stator jacket. A thermal safety switch intervened in cases of insuffficient cooling. Calibration was achieved statically using torque arms and weights.

Flexible coupling

Appropriate linking of the engine and dynamometer was achieved by selecting a Silentblock (type O No. C-358-S, Cushion-Drive) flexible coupling. A plate and a keyed shaft were designed and built to couple it to the engine flywheel.

Frames and mounting

A frame structure was designed for rigid mounting of the engine and the dynamometer. This was then supported on a concrete foundation via six antivibration mountings (Metalastic-Cushifoot, Sandwich Type, B3 series 17/213).

Temperature control

Engine cooling water and lubricating oil were both passed through external heat exchangers. Each one was provided with a diversion by-pass fitted with a Sarco TW3 temperature sensing flow control valve. The temperature

sensors commanded the valves via oil-filled capillary tubing to choose the right porportion of flow to be cooled so that the temperature was maintained at a set value ($\pm 1^{o}C$).

Stepping motor

A Sigma 3437-D200-F075 permanent magnet digital stepping motor was rigidly mounted on the engine and linked to the governor control. It was capable of rotating at two step sizes of 1.8 and 0.9 degrees up to a speed of 3850 steps/sec. Governor set point resolution of 1/2000 (full range) was possible with a gear reduction selection of 56.25:1 which allowed a quick change in engine speed.

Optical shaft encoder

A Ferranti Heavy Duty shaft encoder (type 28H2/M4) was used for angular displacement measurements. It comprised of a Moire-fringed glass disc with a solid state light source and a light-sensitive pick up. The sinusoidal output was transformed via processing logic to a square wave (digitiser pulse) every quarter of a degree with an additional track of one pulse per revolution for absolute position indication. This was compared to the dynamic position of the T.D.C. by running cyl.(1) motored.

A bearing was designed and built together with an appropriate framesuch that the digitiser could be directly coupled to the engine crankshaft via axially (but not torsionally) flexible couplings.

Cylinder pressure transducer

An AVL 12Q500C water-cooled piezoelectric trans-

ducer was used for cylinder pressure measurement. To overcome the problem of thermal shock, it was recessed into the head by a distance of 4 mm. Calibration was achieved statically using a dead weight tester.

A Kistler E568 high impedence charge amplifier was used with this transducer and a 0-10V output, compatible with the data logger range was obtained. Sufficient positive offset was provided to prevent momentary negative values.

Fuel and air flow meters

Fuel consumption at steady states was measured by a conventional mass balance system. Equal length delivery pipes were fitted for all the six injectors. A check was made by collecting the injected fuel from each injector into a measuring vessel to see the difference in fuel delivery to various cylinders. This was done under steady state engine running conditions, checking one injector at a time. The variation was found to be within 1.5%.

Air consumption was measured using a hot-wire anemometer. A short intake pipe with a venturi (B.S. 726/1957), a flow straightener and the hot-wire probe were fitted at the compressor inlet. The venturi meter was used for calibration. A large damping chamber preceeding the intake pipe was used during the calibration tests.

Manifold pressure transducers

Philips (PR 9370 series) water-cooled strain gauge transducers were used to measure pressure in the inlet and

exhaust manifolds. They consisted of a water-cooled pressure diaphragm and a 4-arm bridge rosette type strain gauge, giving a bridge unbalance signal proportional to the pressure applied.

Bryans Southern Instruments (type MO 4/900) bridge amplifiers were used with all Philips transducers applying a 4 Volt excitation voltage. The transducers had a range of 0-5 bars and a natural frequency of 7 kHz. For static calibration a dead weight tester was used.

4.4 The injector instrumentation

The instrumentation of the Leyland N.85 Injector (Fig. 4.9) involved difficult design and machining. The effort was directed towards installing the needle lift transducer as close to the needle as possible. The purpose was to avoid altering the original interia of the needle. A long pin attached to the needle would have increased the inertia and thus would affect its movement. The position of the transducer is shown in Fig. (4.9) and various pieces are numbered to explain the details.

A long hole was drilled in the central spindle (1) such that the transducer body (3) could be mounted in it and held with a thin stainless steel tube (2). The transducer wires were passed through this tube leading to pinned connections outside the injector for easy dismantling.

Parts (10) and (11) were originally one piece. To drill a hole and allow the pin (4) through it, the bottom part had to be replaced by (11) so that it was of a slightly larger diameter. The original diameter was too small to have sufficient surface area after drilling the hole.

Similarly (9) was replaced so that it had a larger diameter at the top. This was drilled and tapped accurately to hold the transducer pin straight. The length of the pin was adjusted such that it reached a specified position inside the transducer body.

In this way the tranducer operated successfully inside the injector as close to the needle as possible. Checks were made to ensure that the values of the nozzle opening pressure and the full lift did not alter due to these modifications.

The miniature fuel line pressure transducer (6) can also be seen in Fig. (4.9). A hole was drilled at the side of the injector fuel gallery and the transducer (6) was secured in it using a nut (7). A copper washer (8) provided the necessary sealing.

The injector and transducer particulars are given below:

Injector:

Make and type	Leyland N.85
No. of spray holes	4
Diameter of spray holes	0.41 mm
Needle valve seat angle	63^{o}-30'
Nozzle seat angle	63^{o}
Needle valve lift	0.48 mm
Spring free length	28.017 mm
Relative angle of spray holes	140^{o}
Needle diameter	5.08 mm
Discharge pressure	215 bars
Nozzle details	see Fig. (4.10)

Some of the equipment can be seen in photo graphs (Figures 4.1 to 4.8) as listed below:

1. Engine
2. Dynamometer
3. Coupling
4. Optical shaft encoder linkage
5. Stepping motor connection to engine governor
6. Fuel pump and rack position transducer
7. The instrumented injector
8. Cylinder pressure transducer
9. Air inlet orifice
10. Turbocharger speed pick-up
11. Compressor
12. Turbine
13. Visual check instruments
14. Amplifier (cylinder pressure signal)
15. Amplifier (needle lift signal)
16. Amplifiers (manifold pressure signals)
17. Bridge excitation voltage monitor
18. Amplifier (fuel line pressure signal)
19. Oil cooler
20. Oil temperature control valve
21. Cooling water heat exchanger
22. Cooling water temperature control valve
23. Transducer feed water supply
24. Optical shaft encoder
25. Bearing (shaft encoder mounting)
26. Couplings (shaft encoder linkage)

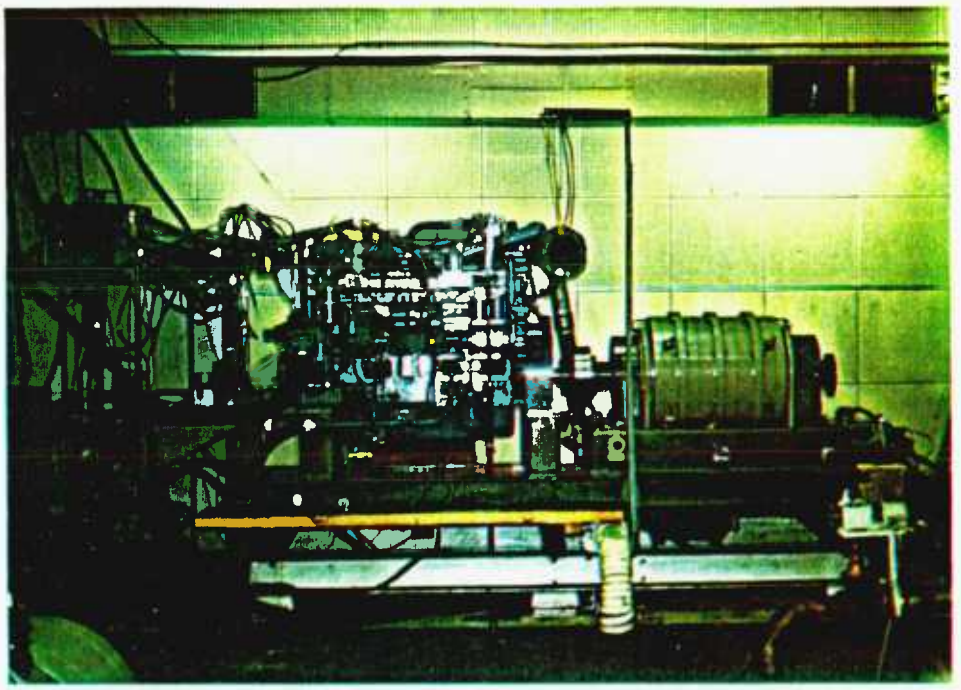

Fig. 4.1 General view of the test-bed.

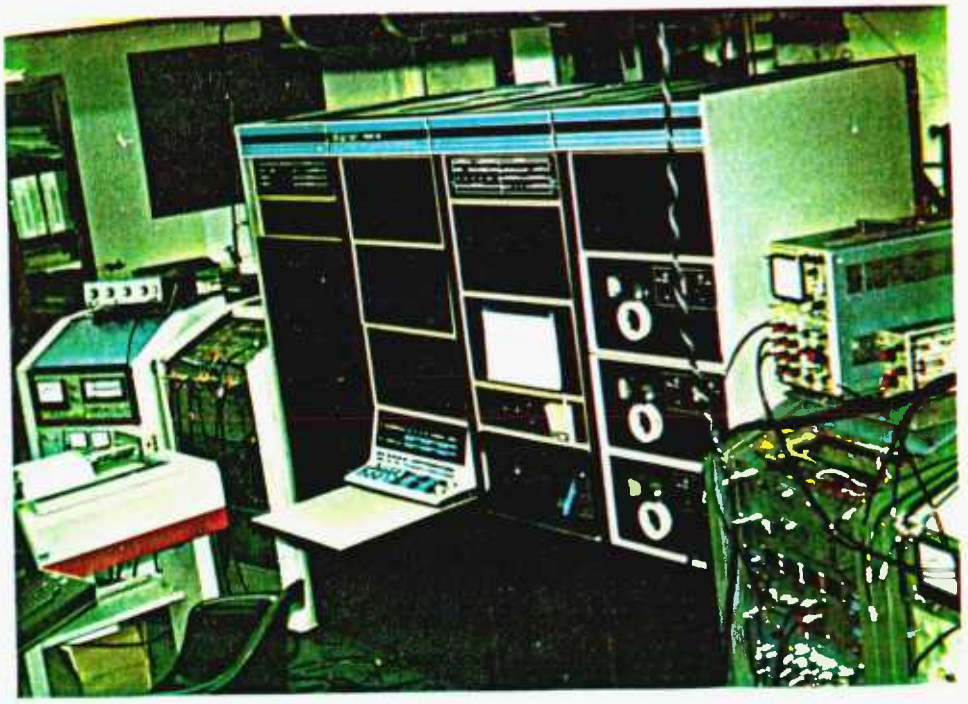

Fig. 4.2 PDP 15 computer and peripherals.

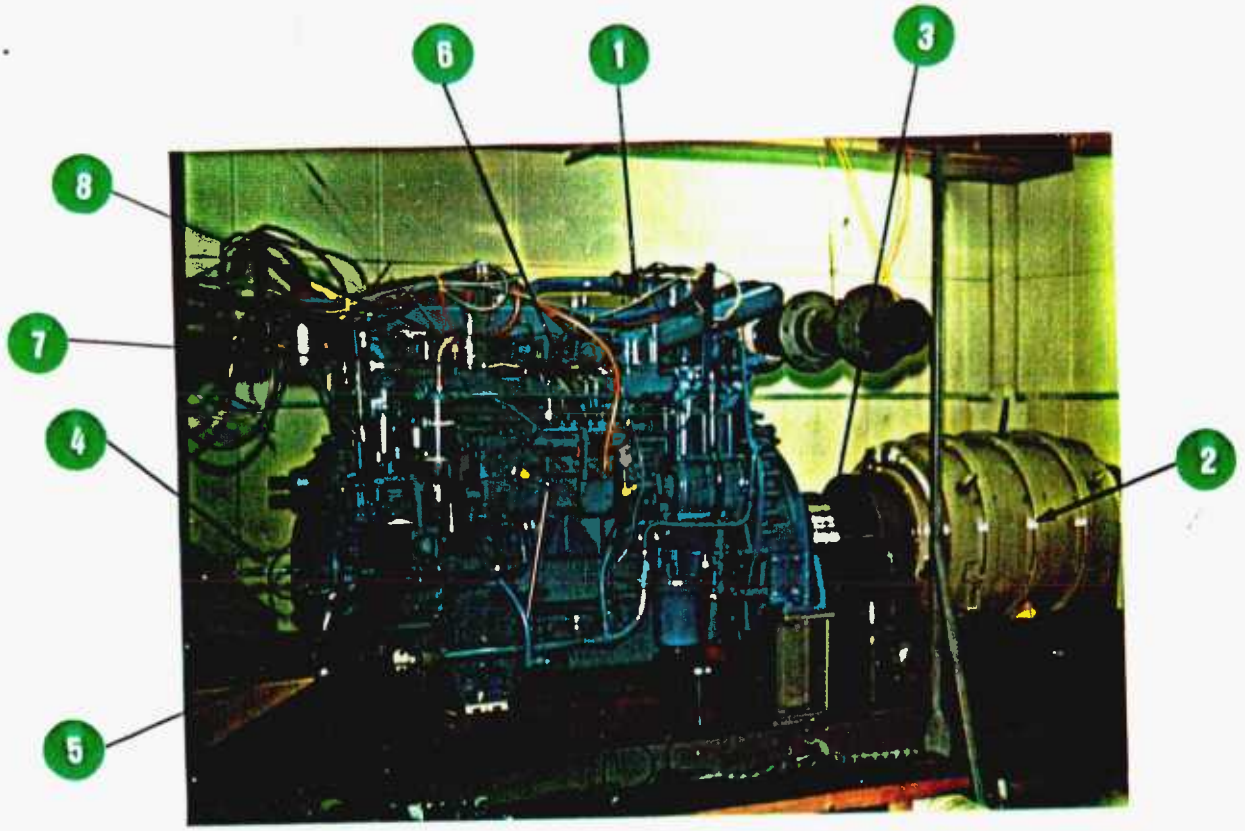

Fig. 4.3 The Leyland 520 engine.

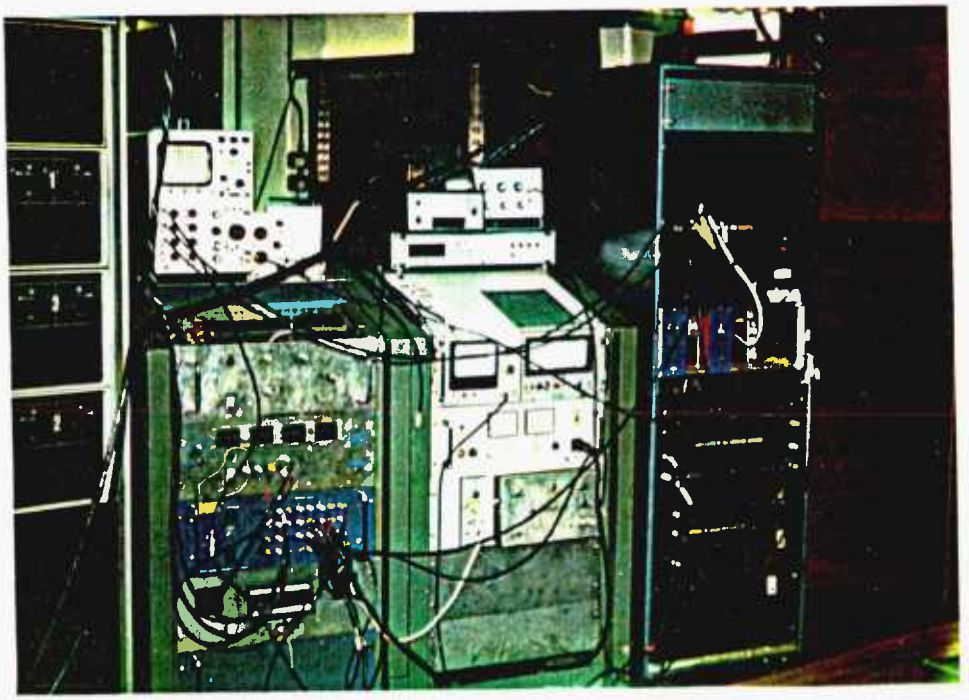

Fig. 4.4 The data logging interface.

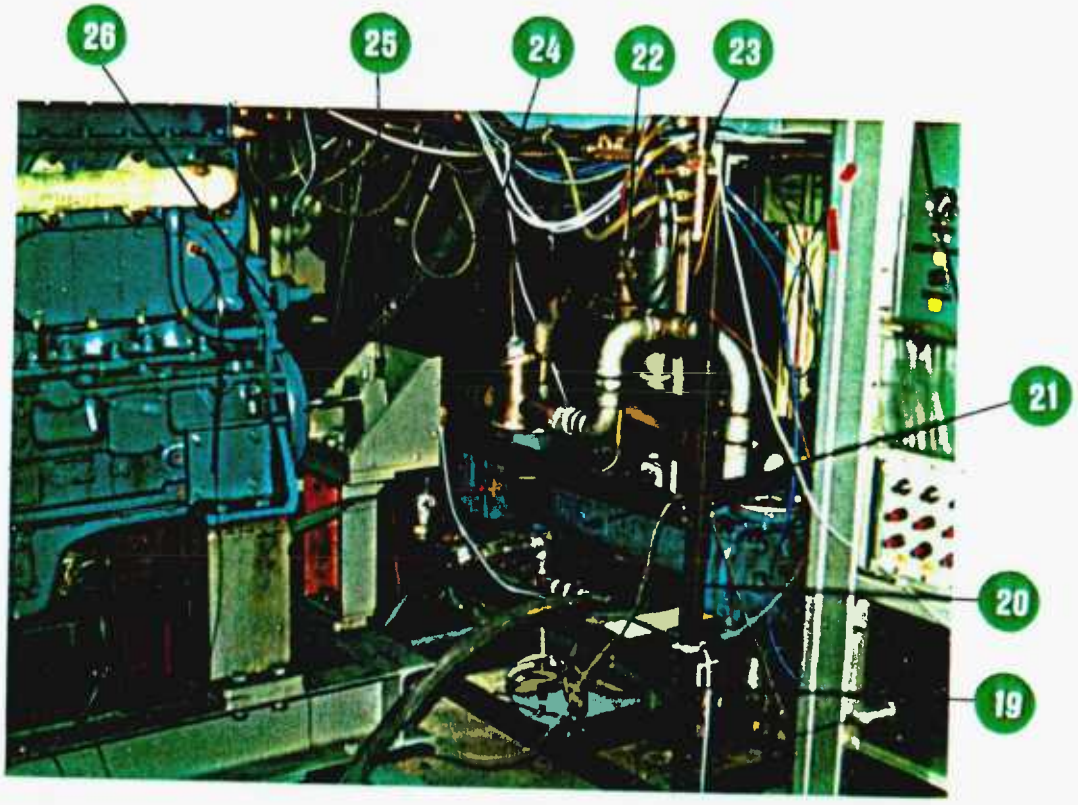

Fig. 4.5 Auxilliary equipment tower.

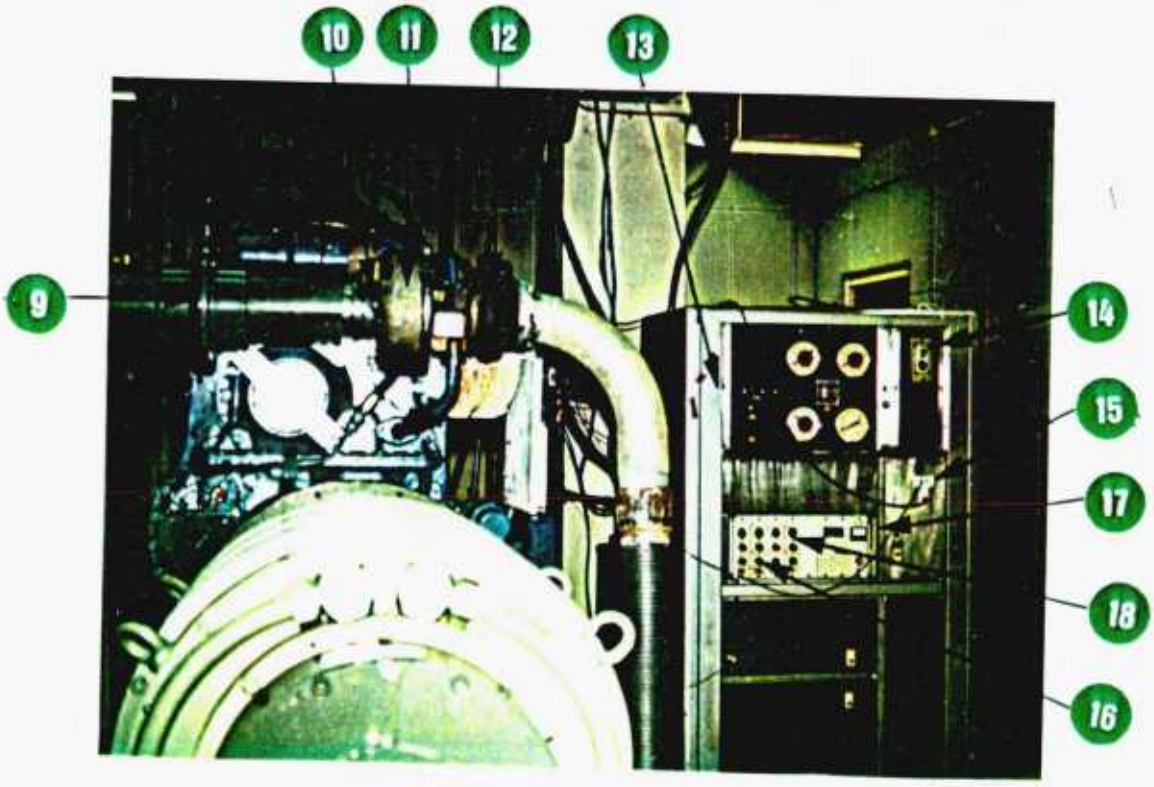

Fig. 4.6 Test-bed instrumentation panel.

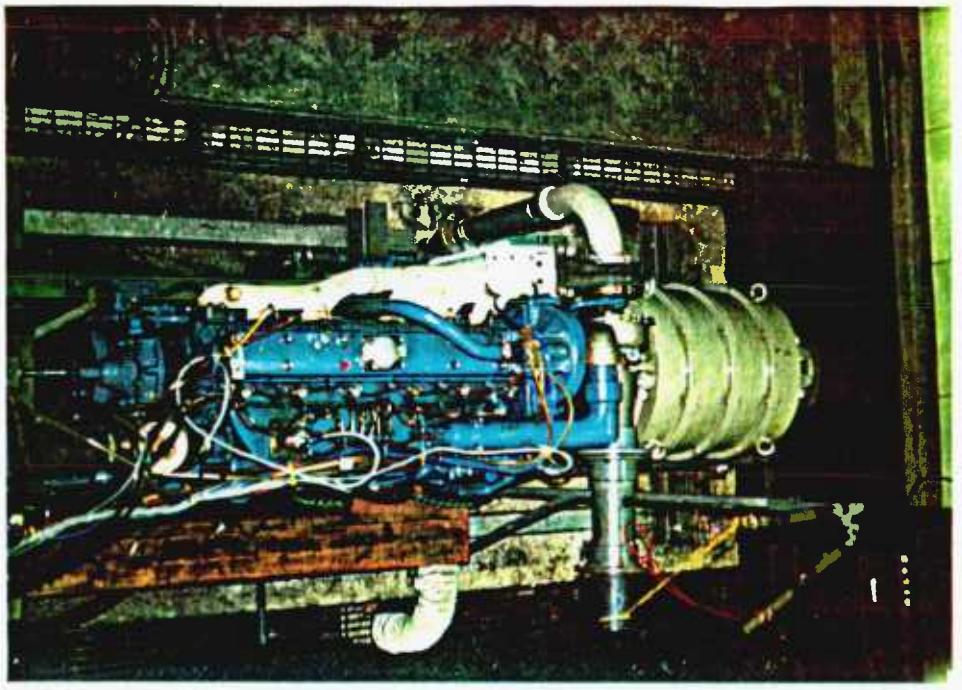

Fig. 4.7 Top view of the test-bed

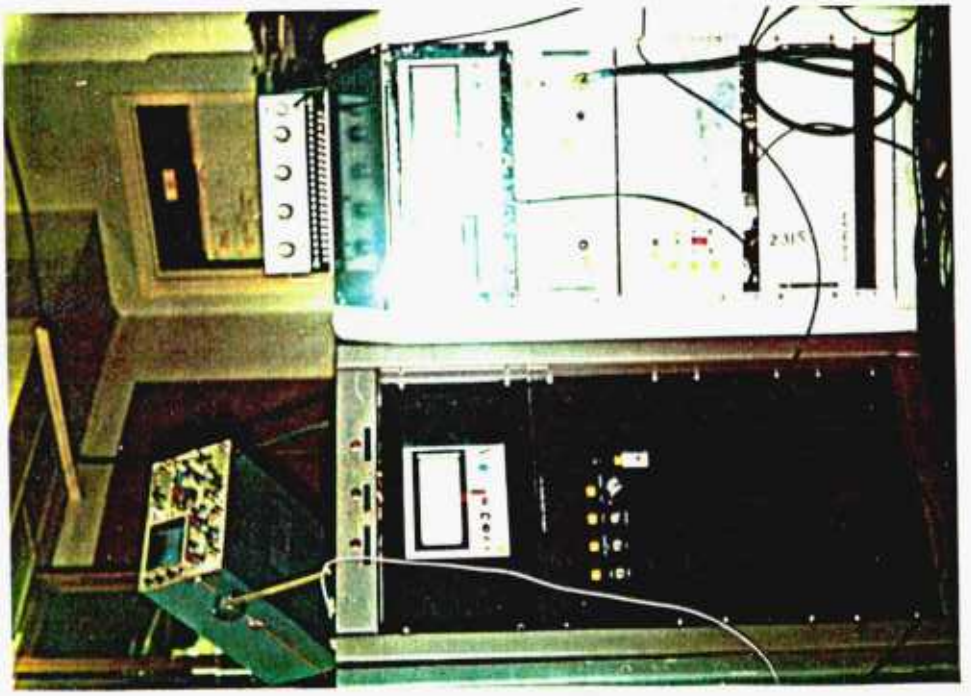

Fig. 4.8 Engine control and monitoring units.

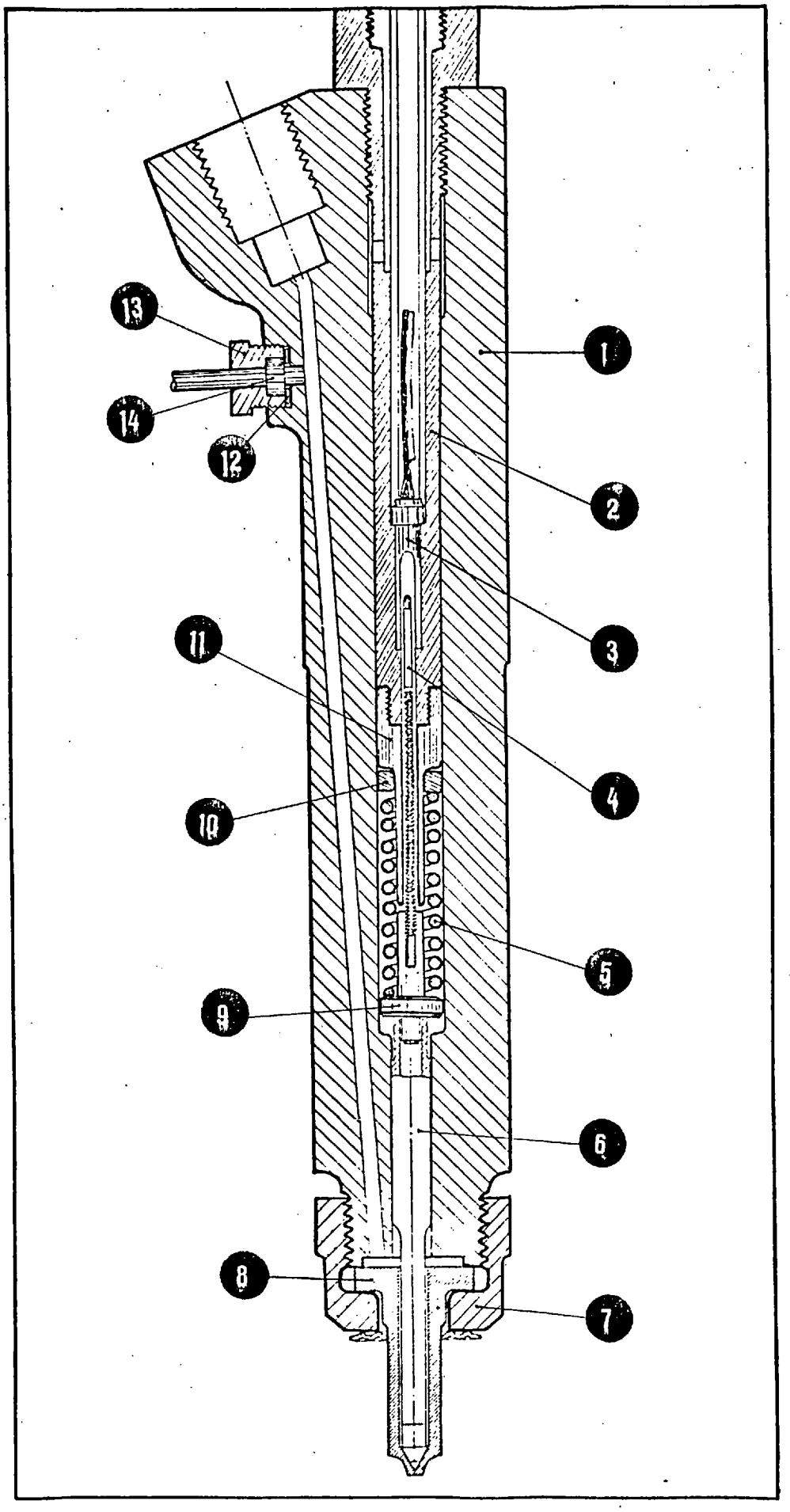

Fig. 4.9. Cross sectional drawing of the instrumented injector.

Needle lift transducer

Vibrometer (type NM1 - 100/B) inductive displacement transducer was used. As explained, this consisted of a pin having a high parmeability metal core moving inside an inductive coil. The coil formed part of a.c, bridge network in conjuction with a carrier amplifier.

An AVL (type 100-TR1/A) carrier amplifier with a carrier frequency of 100 kHz was used together with an operational amplifier to obtain a 0-10V range of output for the needle lift signal (0.018 in. full lift). The calibration was carried out statically using a micrometer.

Fuel line pressure transducers

Apart from a standard AVL strain gauge transducer (type 31DP500 E.2) which was installed at the point of entry to the injector, a tiny Intersonde VT series strain gauge transducer was inserted in the injector body as shown in Fig. (4.9). This was flush mounted to the 2 mm delivery gallery inside the injector with the intention of recording readings closer to the actual injector sac. Unfortunately this transducer failed after a short time, so the fuel line pressure data was only available through the AVL transducer. The amplifier was the same as those used for the inlet and exhaust manifold transducers. The transducer was calibrated using a dead weight tester.

Coefficients of discharge

Coefficients of discharge (c_d) were calculated from measured steady fuel flow rates (Fig. 4.12). It was intended

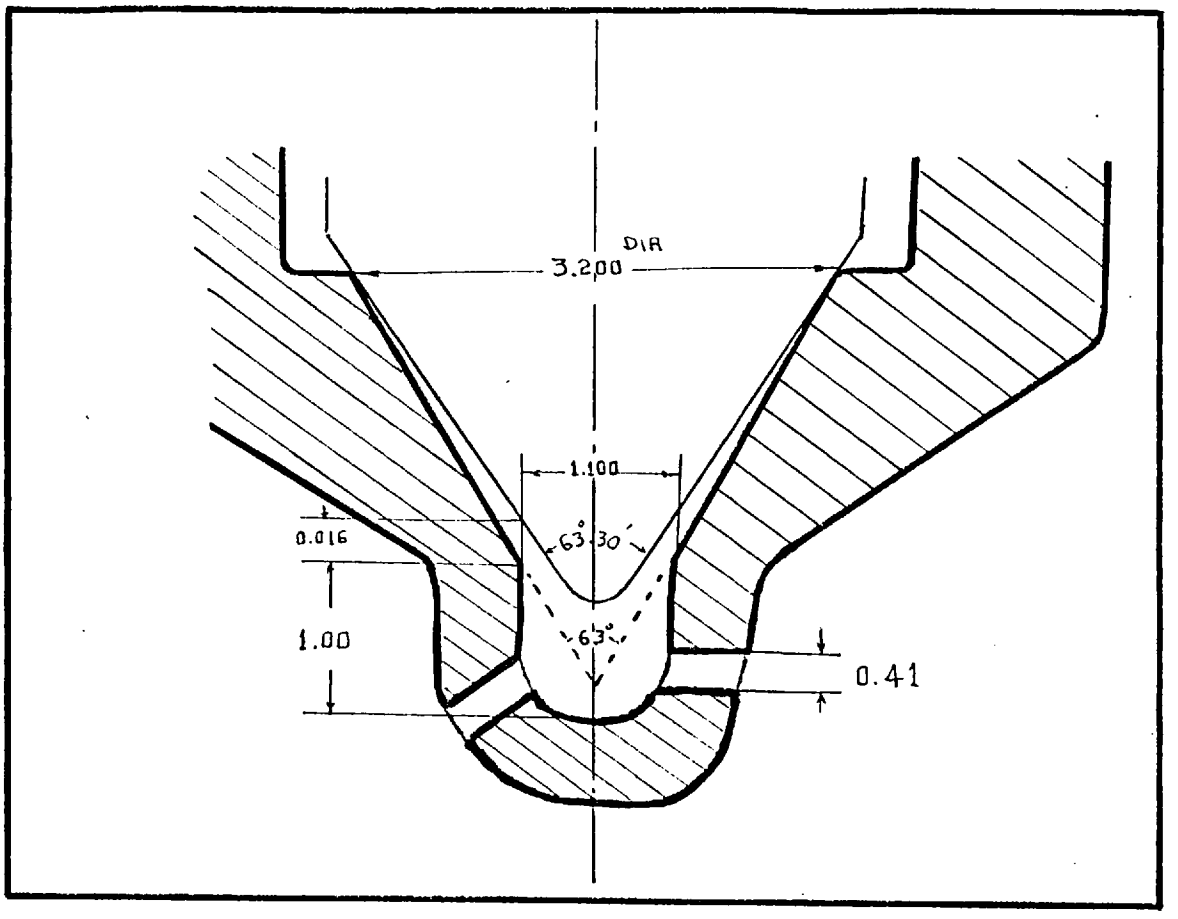

Fig. 4.10. Injector nozzle geometry

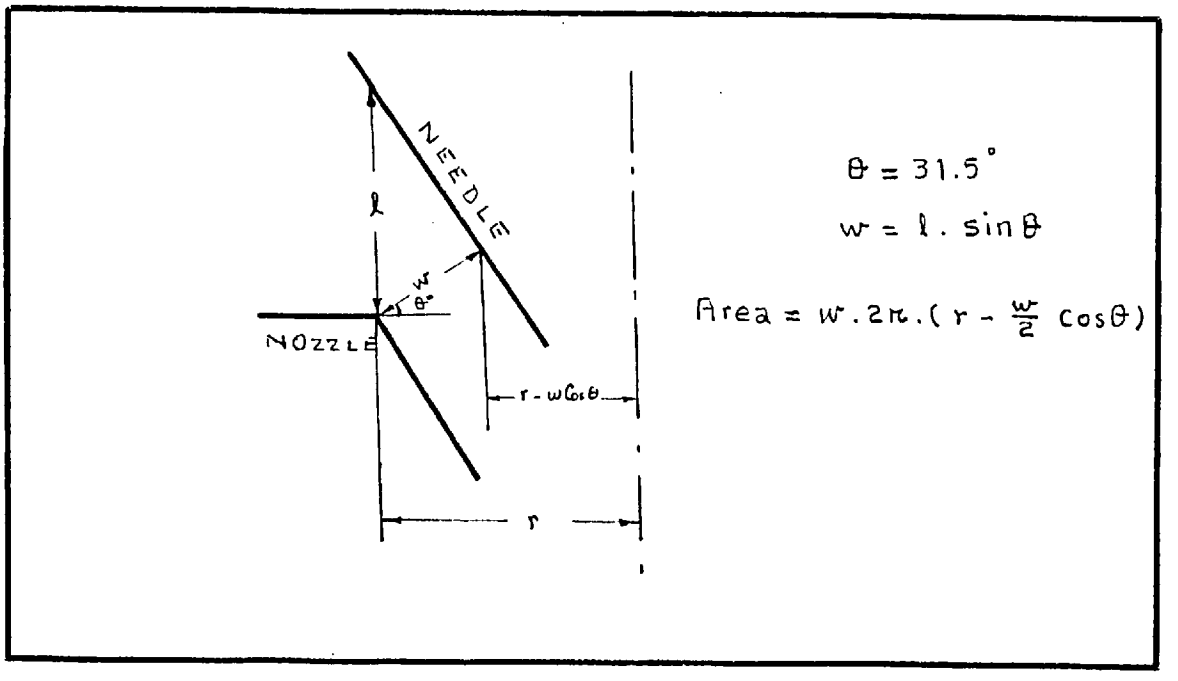

Fig. 4.11. The flow area at needle lift

to calculate instantaneous fuel flow rates based on these coefficients. The fuel line pressures very near the nozzle seat were needed for this purpose. Unfortunately this method of calculation was abandoned due to the failure of the injector gallery transducer and due to complexities arising in the theoretical model by considering the effects of variations in injection velocity. Average injection rates were calculated instead by dividing the total injected fuel to the measured injection duration.

The following method of calculating instantaneous fuel flow rates is recommended for future use:

$$\dot{m}_f = 15.5\ \rho_o\ c_d\ .\ A_{eff}\ .\ \sqrt{\Delta P}\quad (gm/s)$$

where ρ_o (gm/cm^3) is the fuel density and ΔP(bar) is the overall pressure drop across the nozzle. The effective area (mm^2) is considered on the basis of two restrictions in series. i.e.:

$$A_{eff} = \frac{1}{(1/A + 1/Al)^{\frac{1}{2}}}$$

A is the variable flow area during needle lift (area perpendicular to the direction of flow at the smallest diameter of the nozzle seat). Al is the sum of the nozzle hole areas (Al = number of holes x A_o). A is calculated from the nozzle geometry shown in Fig. (4.10) and (4.11):

$$A = w\ .\ 2\pi(r - \frac{w}{2}\cos\theta)$$

$$A = 0.638\ \pi l(l. - 0.453\ l)$$

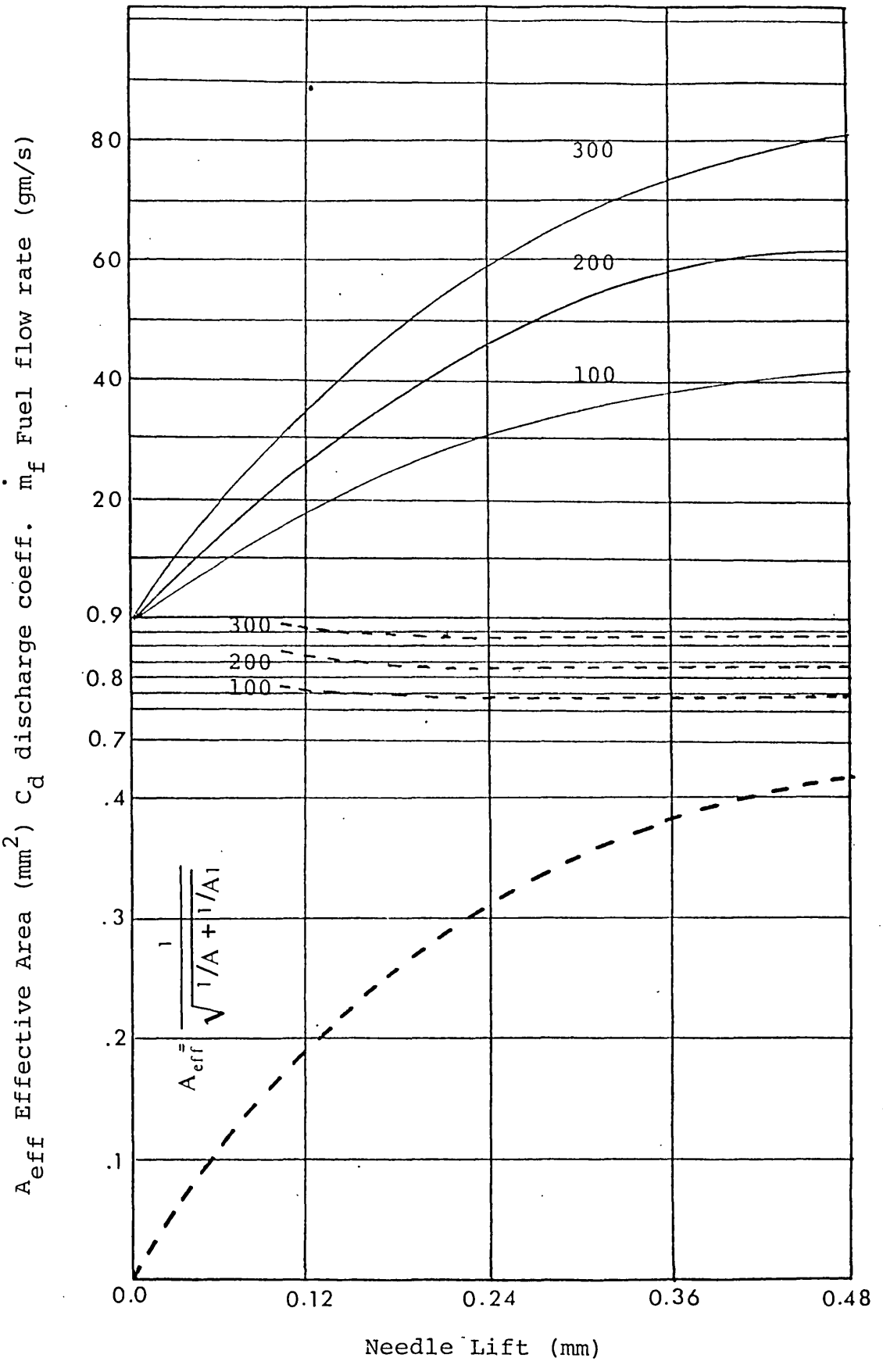

Fig. 4.12. Injection rate and nozzle discharge coeff. vs. needle lift. (Injection pressure diff. 100, 200, 300 bar).

Effective areas in terms of needle lift (l) and the consequent fuel flow rates are shown in Fig. (4.12).

4.5 Data

Selected data necessary to run the prediction model is shown in Table 4.1 for five loads at four engine speeds. The beginning and end of injection (in degrees crank angle relative to T.D.C.) given in columns 6 and 7 were extracted from digitized needle-lift diagrams. These together with values of injected fuel mass (column 3) constitute the simplest form of fuel input data required to run the prediction programme. Alternatively the use of nozzle geometry, fuel line pressure and needle lift data will determine the injection rate (in which case fuel consumption will be calculated automatically).

The injection duration (Δt_{inj}), fuel per cycle per cylinder (FCC) and average injection rates ($\dot{m}_f$) versus engine speed and load are shown in Fig. (4.14), (4.15) and (4.17) respectively. The numbers 1, 2, 3, 4 and 5 refer to the consequtive values of engine load (i.e. bmep = 0.0, 225.0, 450.0, 675.0 and 900.0 kN/m^2 respectively). The values of overall fuel to air equivalence ratio ($FCC/m_{at}/c_s$) and the trapped mass (m_{at}) are shown in Fig. (4.13) and (4.16).

The cylinder pressure at injection (column 5) was extracted from the cylinder pressure diagrams and was supplied to the model as initial condition. In cases where the cylinder pressure diagram was also supplied to the program (for comparisons) the initial condition (i.e. the cylinder pressure at injection) was selected automatically by the program.

Load	Engine speed rev/min	BMEP kN/m2	F/c/c mgm.	Trapped air gm.	P cyl. bar	°CA Inj. start	°CA Inj. end	ρ_{air} kg/m3	T cyl. °K	Turbocharger speed (rev/min)	P Boost kN/m2
1	1000	0.0	10.56	1.539	23.18	-18.5	-14.5	10.823	764.5	10336.68	100.0
2	1000	224.62	25.64	1.561	24.03	-18.5	-13.0	10.982	781.5	13856.36	102.0
3	1000	450.00	42.44	1.567	26.10	-18.5	-11.5	11.025	845.5	18957.24	107.0
4	1000	668.61	60.44	1.600	27.56	-18.5	-8.5	11.257	874.4	24231.16	113.0
5	1000	901.50	86.50	1.613	27.99	-18.5	-6.0	11.348	880.9	30620.62	121.3
1	1500	0.0	12.29	1.468	25.51	-16.0	-11.0	11.218	812.1	18120.78	100.0
2	1500	225.38	26.43	1.479	26.91	-15.5	-8.5	11.483	837.0	19752.14	101.0
3	1500	453.76	42.05	1.535	29.07	-15.5	-7.0	11.918	871.1	26076.02	109.9
4	1500	691.15	59.13	1.674	31.63	-16.0	-6.0	12.585	897.6	33931.74	122.3
5	1500	909.01	78.75	1.801	36.12	-16.0	0.0	13.762	937.4	41524.34	133.5
1	2000	0.0	15.08	1.400	29.14	-12.5	-5.0	11.891	875.2	24426.26	100.4
2	2000	225.38	28.04	1.472	30.79	-13.0	-5.5	12.327	892.0	28615.64	106.9
3	2000	450.75	43.71	1.599	36.38	-12.0	-1.5	13.771	943.5	37753.46	122.2
4	2000	676.13	60.09	1.772	41.05	-12.5	-1.0	15.051	974.0	45154.34	139.0
5	2000	901.50	77.01	1.946	45.84	-13.0	0.5	16.296	1004.6	53134.70	158.8
1	2500	0.0	18.26	1.350	31.76	-10.5	1.5	12.093	937.9	31470.50	102.3
2	2500	214.85	31.75	1.466	35.69	-10.5	1.0	13.132	970.6	38466.08	115.1
3	2500	450.75	48.56	1.756	43.15	-11.5	2.0	15.329	1005.3	49849.88	129.9
4	2500	676.17	64.94	1.998	51.41	-11.5	3.5	17.441	1052.7	58486.00	164.5
5	2500	901.50	82.64	2.128	56.05	-12.0	6.5	18.323	1092.3	66356.66	195.3

Table 4.1. Selected Data

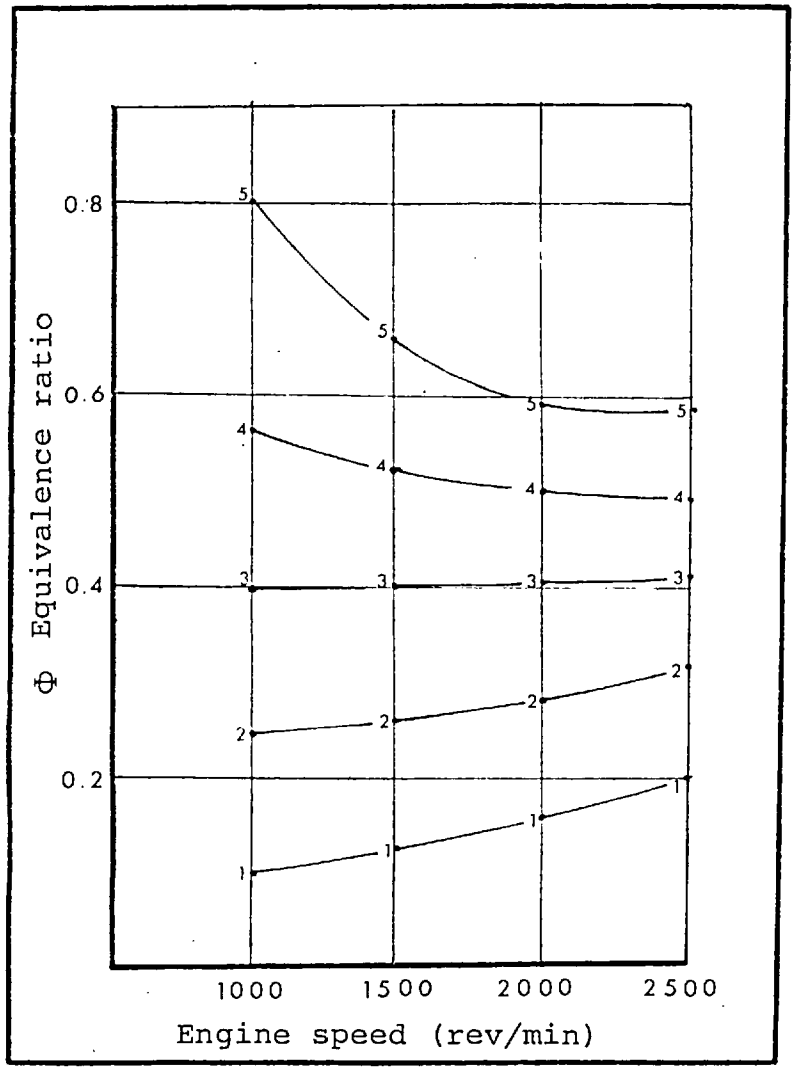

Fig. 4.13. Variation of fuel to air equivalence ratio with speed and load.

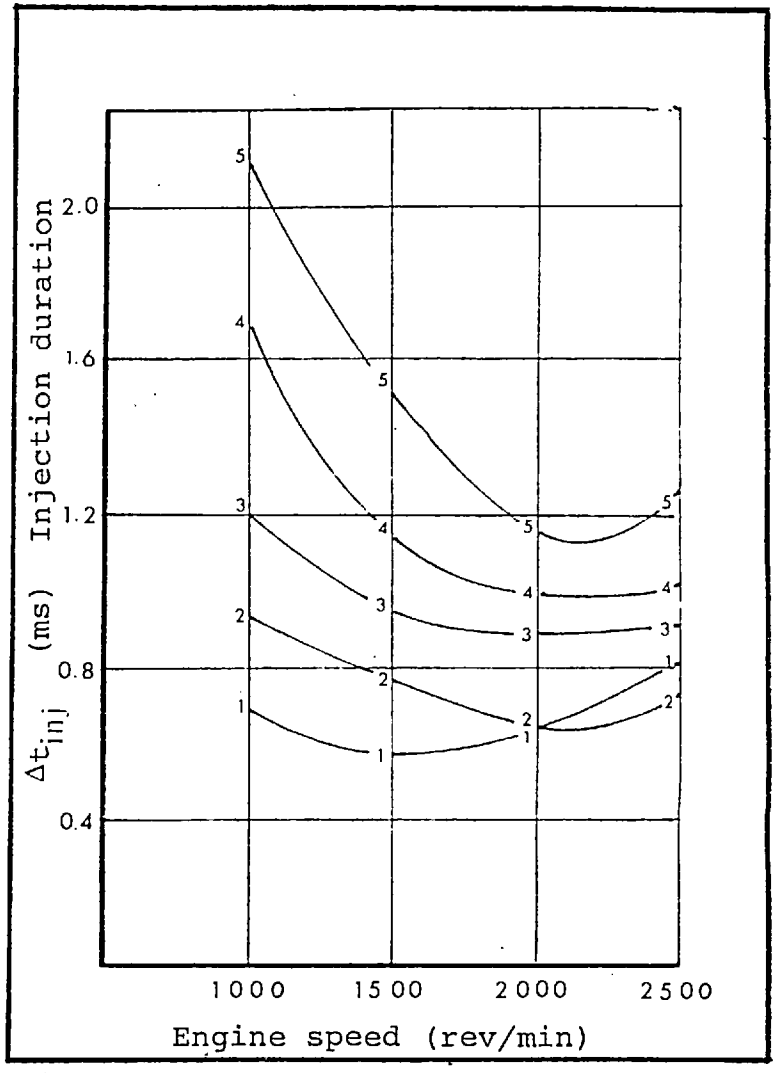

Fig. 4.14. Variation of injection duration with engine speed and load.

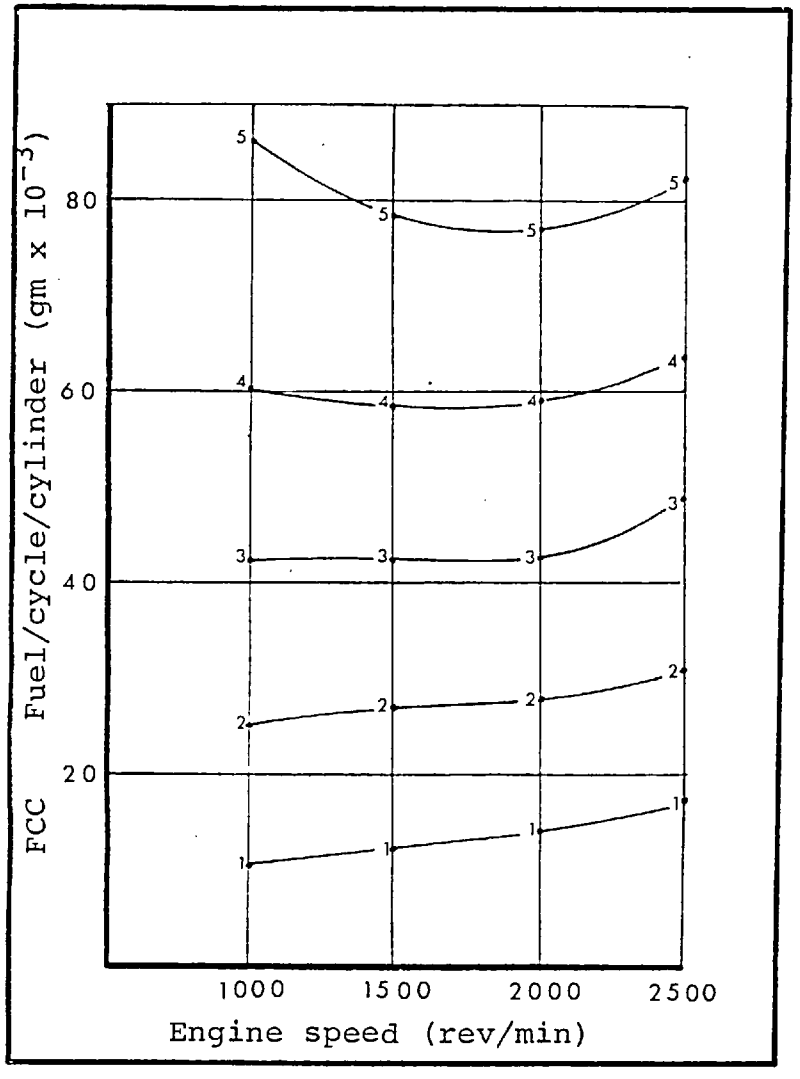

Fig. 4.15. Variation of fuel/cycle/cylinder with engine speed and load.

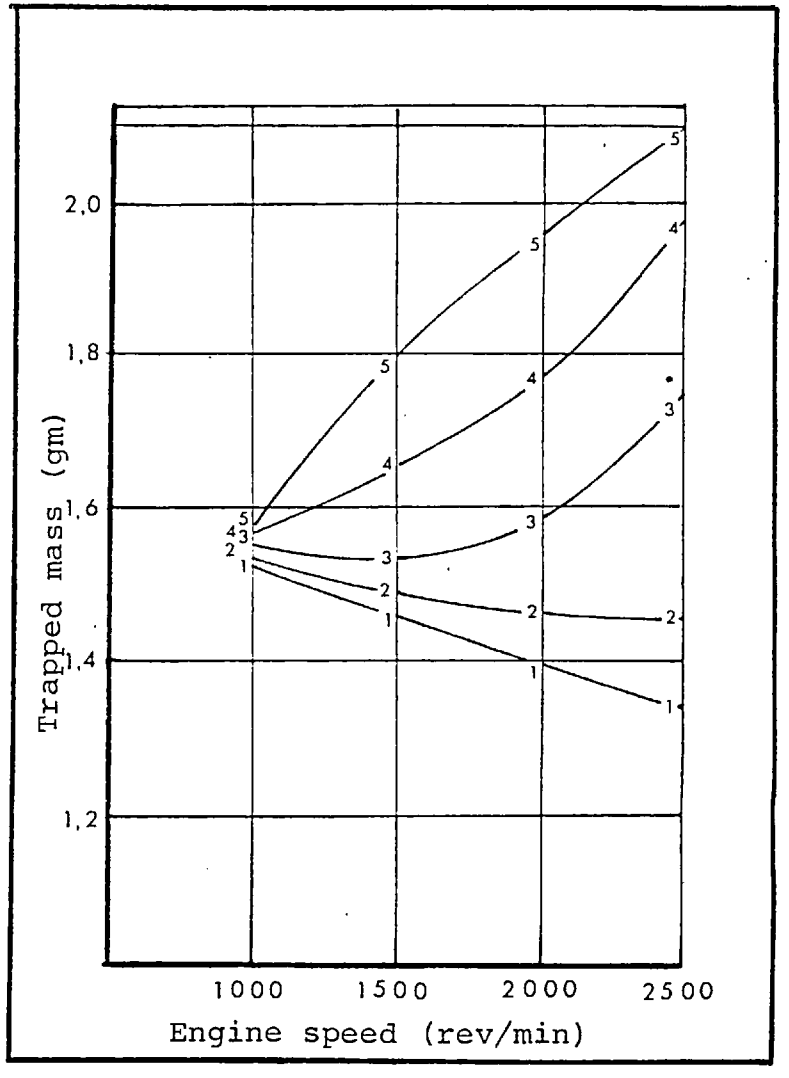

Fig. 4.16. Variation of trapped mass with engine speed and load.

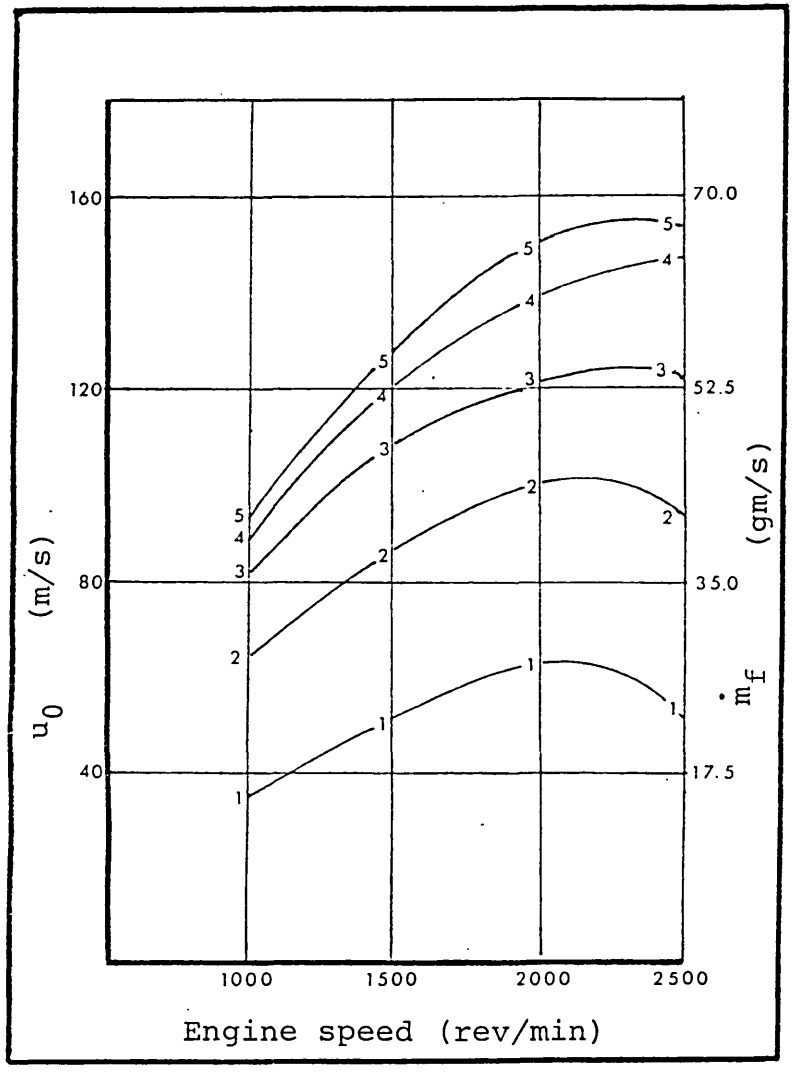

Fig. 4.17. Average injection velocity and injection rate versus engine speed and load.

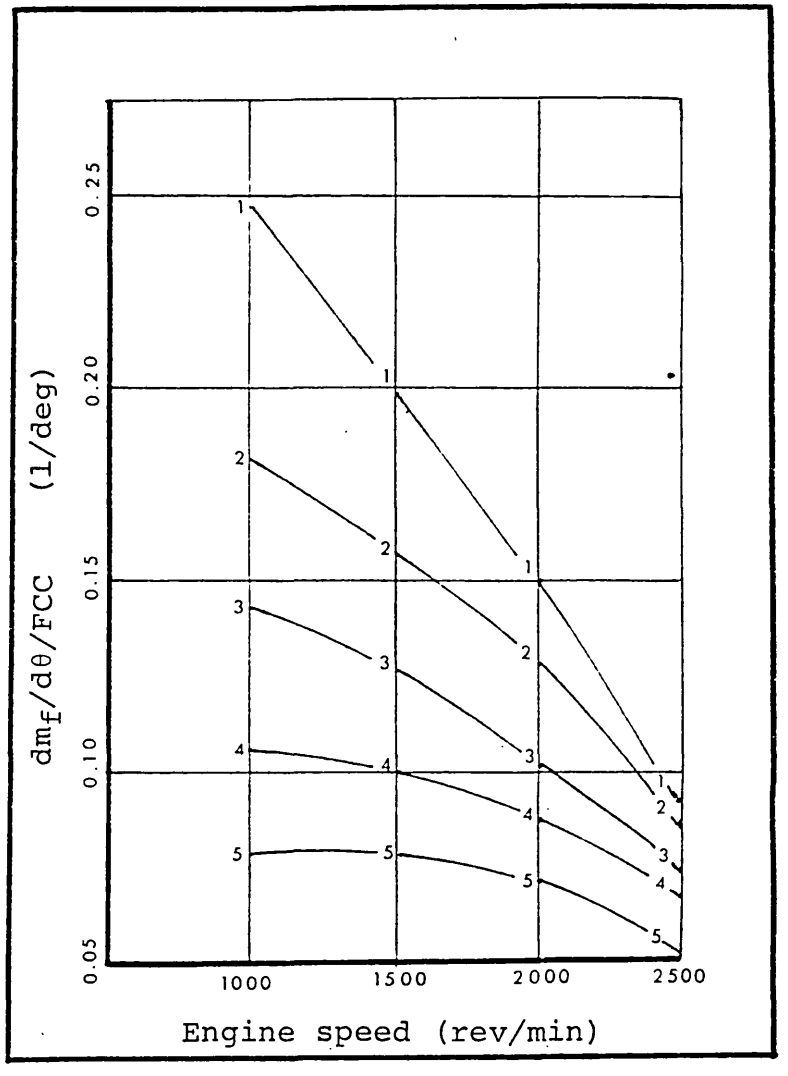

Fig. 4.18. Fuel/degree/FCC versus engine speed and load.

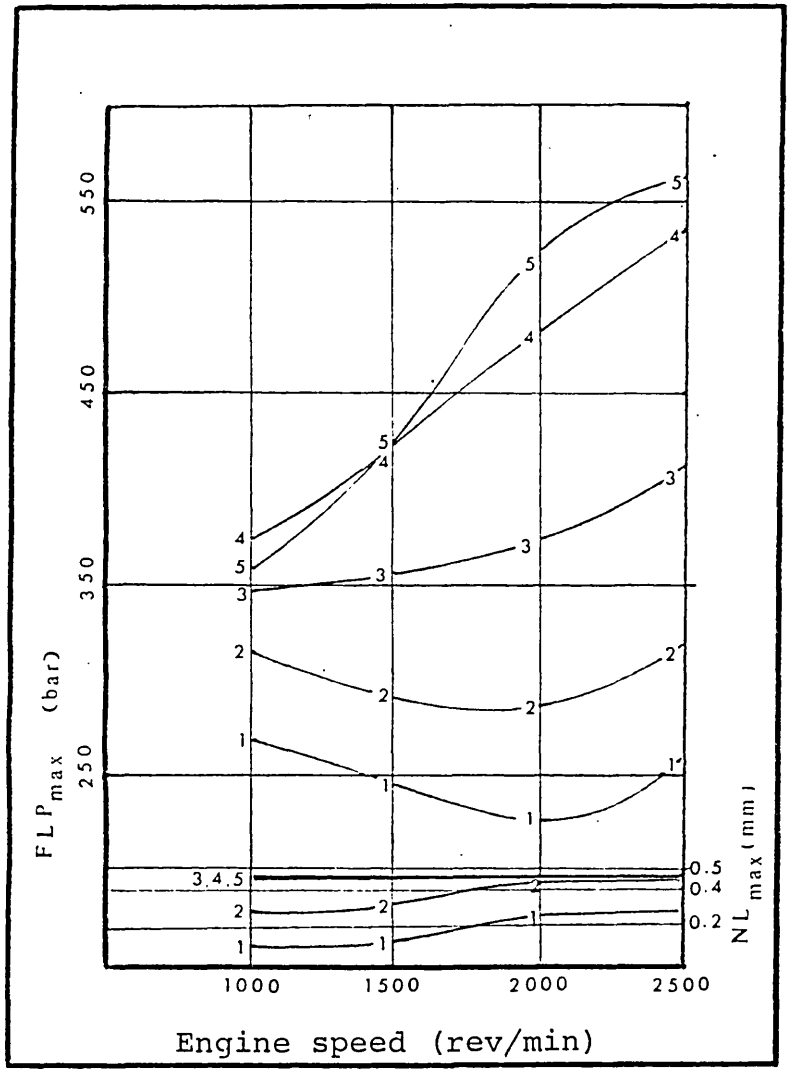

Fig. 4.19. Variation of maximum fuel line pressure and needle lift with speed and load.

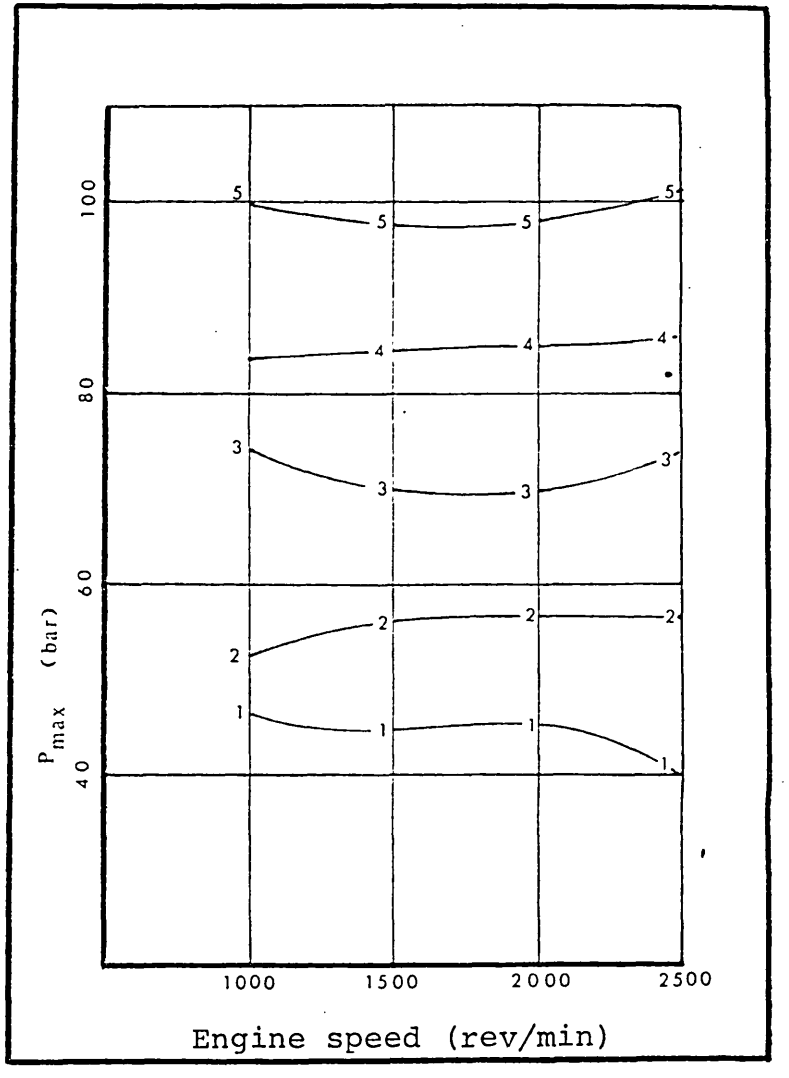

Fig. 4.20. Variation of maximum cylinder pressure with engine speed and load.

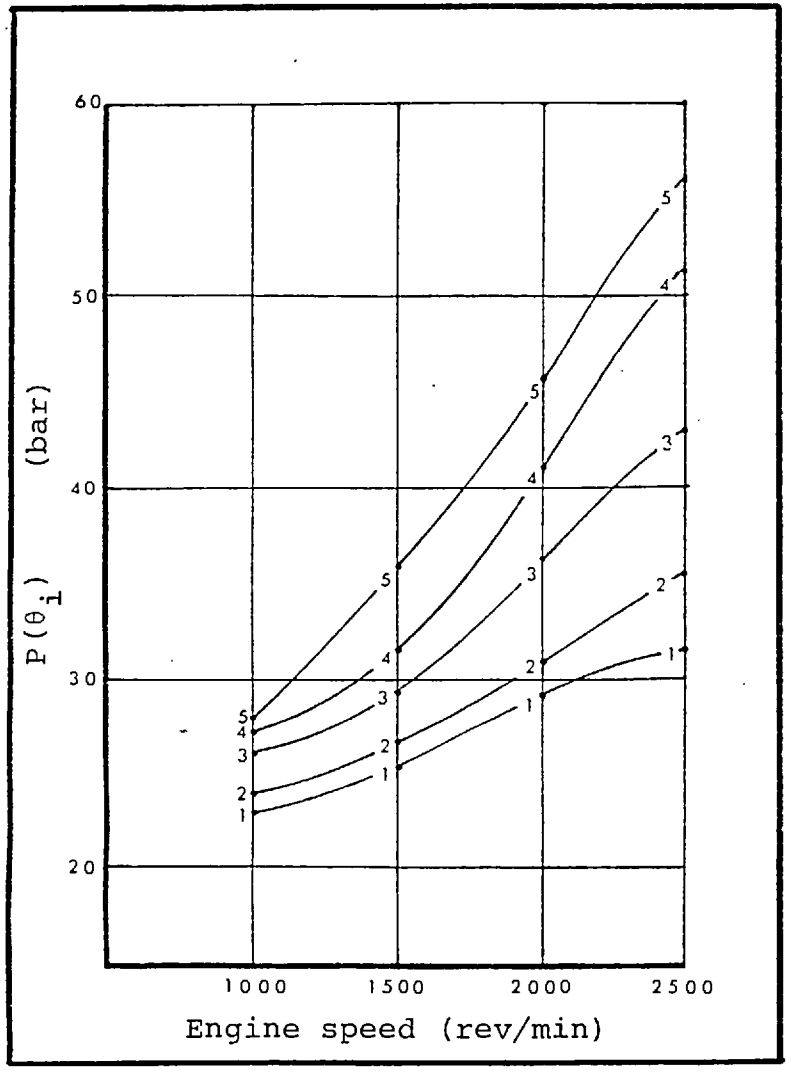

Fig. 4.21. Cylinder pressure at injection versus engine speed and load.

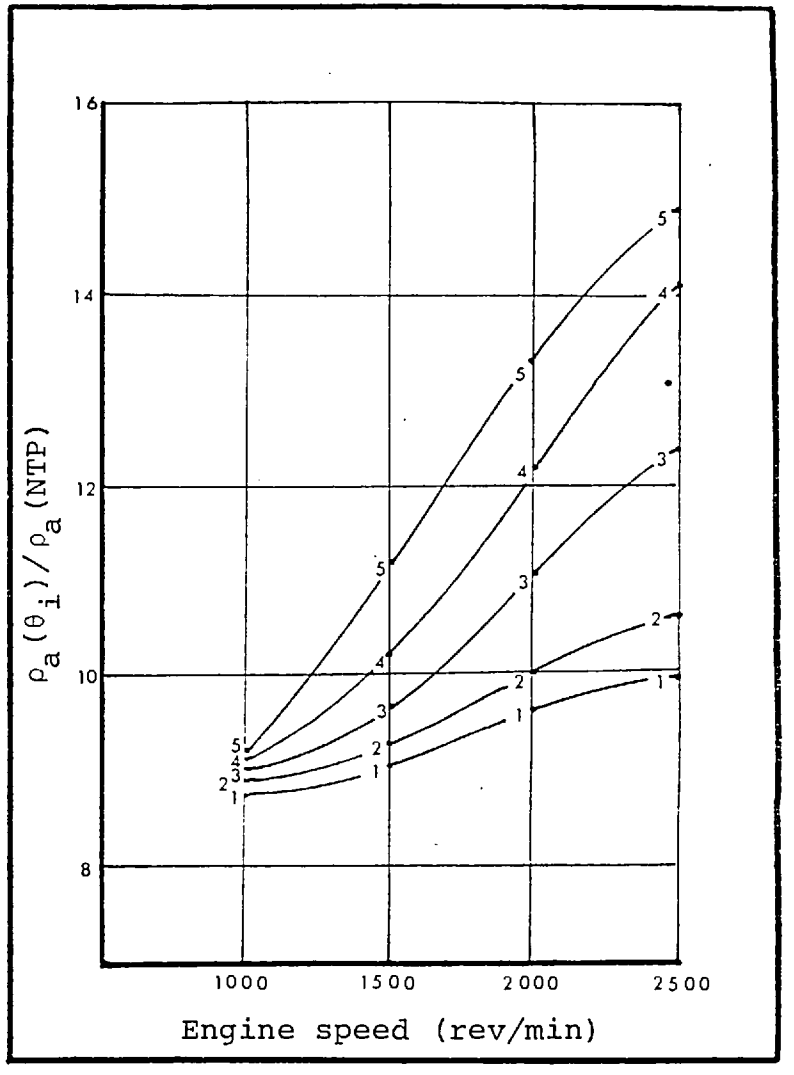

Fig. 4.22. Air density ratio at injection versus engine speed and load.

CHAPTER 5

Heat Release Prediction

5.1 Introduction

In this chapter the details of the heat release prediction model are explained. The model is based on a multizone analysis of the cylinder contents. The zone division pattern of chapter three provides the essential structure. The number of zones within each jet depends on the injection schedule and the time step chosen for a step-by-step computation. The remainder of the cylinder contents are considered as one zone. This is termed the non-burning zone while all other zones are termed burning zones as soon as they are formed. Burning rates are considered to be based on activated collisions within each zone. Equations are set up to describe zone thermodynamics. Heat release, heat transfer, pressure change and work done are calculated. Each zone has its own temperature history but pressure is assumed to be the same for all zones. A computer program has been written to perform all the computations for the model. The data input instructions are explained for the type of data given in the previous chapter.

5.2 The heat release model

It has already been stated that the exact nature of processes occurring during the heat release period is rather uncertain. The model described here, therefore, is

essentially based on those phenomena which are believed to be dominant.

A careful choice of variables and a suitable method of formulation and solution has reduced the complexity of the problem. A number of assumptions have been necessary.

Consider what happens during a small time step of cycle calculations. The piston moves and the cylinder volume changes. The calculation of cylinder volume and heat transfer area (according to engine geometry) are given in Appendix B. As a result of fuel injection, moving zones of fuel-air mixture are formed. This was explained in chapter three. The point of interest now is how to compute the zone thermodynamics.

In chapter two it was explained how, in the C.A.V. model, the Arrhenius equation was applied to the whole cylinder contents. This equation is now applied to individual zones. In the same manner, the first law of thermodynamics is applied to individual zones. Thus, during each time step every zone undergoes a process of mixing, burning and temperature change.

It is assumed that the change in pressure is equal for all zones. The thermodynamic state equation is applied to individual zones assuming a homogeneous perfect gas mixture in each zone. This means that the volume occupied by liquid fuel is neglected. This assumption will be explained when evaporation is discussed. Zone volume is expressed in terms of zone density and mass. Zone mass is expressed in terms of fuel mass and fuel to air ratio.

Computations start by estimating a pressure for the whole cylinder contents at the end of the step. Heat

transfer is computed according to Eichelberg's equation for the whole cylinder contents during the step. It is assumed that total heat transfer is shared between zones according to their mass and temperature. This means that heat transfer between zones has not been specifically modelled and is considered to be inherent in the above pattern. The particular zone division pattern devised in chapter three is for the following purpose. No mass transfer between zones is considered, except for supply of unburnt air from the nonburning zone to each zone. In other words, since the pattern is devised to allow the fuel in each zone to stay in that zone, it is assumed that burnt fuel, in the form of products of combustion, also stays in that zone. Recall also the advantage of having equal fuel mass in all zones. In this manner two variables for each zone namely the fuel to air ratio and the fraction of burnt fuel are sufficient to monitor the burning rate. It is assumed that if the zone fuel/air concentration is within the inflammability limits, reaction occurs according to the Arrhenius equation. Thus if the zone temperature is low, the rate of burning is insignificant (even though the concentration is within inflammability limits). Thus no specific criterion is given for ignition. In particular, it is not assumed to be dominated by droplet evaporation laws. Interaction of variables in the Arrhenius equation decides when ignition should occur in the zone. At high temperatures the burning rate is limited either by shortage of unburnt air or unburnt fuel in the zone.

Thus the zone burning rate, heat release and heat transfer are determined and the energy equation is applied

to find the zone temperature at the end of the step. This simply means that the change in internal energy of the zone should be equal to the net heat added to the zone plus flow of enthalpy into the zone minus work done by the zone. The same applies to non-burning zones, except that there is no heat release in those zones. At the same time, the volume for each zone is calculated applying the state equation to each zone.

The volume constraint for the end of the step decides whether the estimated pressure is true or not. If not, a new estimate is made and the calculations are repeated for the same step. This iterative process is continued until all equations are satisfied. The numerical techniques employed will be explained separately.

5.2.1 Assumptions

Before setting up the governing equations, the following assumptions should be stated.

1) All gases in the cylinder are assumed to be perfect in the range of conditions encountered.

2) The pressure is constant throughout the cylinder at any time.

3) Each zone is homogeneous in composition and uniform in temperature.

4) Fuel mass burning rate is assumed to be governed by a second order reaction given by the Arrhenius equation for all zones from rich to lean limits of inflammability.

5) The constants in the Arrhenius equation do not change throughout the computations.

6) Thermodynamic equilibrium is reached at the end

of each small time step.

7) All the sprays from various holes of the injector nozzle are identical.

5.2.2. Governing equations

As explained, the general approach used here is to write the first law of thermodynamics, the equation of state and the burning rate equation for each zone. The zone formation pattern is assumed to explicitly supply the necessary information on the fuel and air mass in the zones. In addition, the sum of the volumes of all zones is equal to the instantaneous cylinder volume at any time. These equations, together with the assumption that pressure is equal in all zones, are solved numerically to obtain the pressure variation and the heat release rate.

The energy equation is written in the following form:

$$\frac{d(m_z U_z)}{dt} = -p \frac{dV_z}{dt} + \frac{dq_z}{dt} + h_a \frac{dm_z}{dt} \qquad (5.1)$$

This means that the zone is considered as an open system and the first law of thermodynamics is applied to it, taking into account the mass change in the zone. Let us recall that the zones in the spray are chosen such that the change in mass $(\frac{dm_z}{dt})$ is only due to the additional air entrained into the zone. Thus $(h_a \frac{dm_z}{dt})$ is the flow of enthalpy into a zone in the spray. The same applies to the non-burning zone where $(\frac{dm_z}{dt})$ is negative (mass flow out of the zone).

The rate of net heat addition to the zone is denoted by $(\frac{dm_z}{dt})$. In the case of a burning zone this represents heat release minus heat transfer.

The internal energy (U_z) is the specific value per unit mass at a temperature (T_z). (By definition U_z is the sensible heat at $T_z\,^{o}K$ above that at $0^{o}K$).

The state equation is written as:

$$p.V_z = m_z.R.T_z \qquad (5.2)$$

This equation is assumed to apply to each individual zone including the whole of the non-burning zone. It must be stated that for a 4-hole nozzle, 4 identical sprays and non-burning zones are assumed and calculations are performed accordingly.

For any burning zone, the Arrhenius equation is written in terms of instantaneous values of temperature and available fuel and air.

The variable (b) is defined as the ratio of fuel burnt (m_{fb}) over fuel burnt plus unburnt (m_f). This variable is sometimes named "reactedness" or "burnt fraction".

$$b = \frac{m_{fb}}{m_f}$$

With a suitable grouping of variables, (b) and (ϕ) are employed to represent the concentration terms in the equation. ϕ is the fuel to air equivalence ratio, i.e.:

$$\phi = \frac{c}{c_{st}} \qquad (c = \frac{m_f}{m_a})$$

Thus if N_a and N_f are the concentrations of unburnt air and unburnt fuel per unit volume respectively, then:

$$N_f.N_a = \left(\frac{m_{fu}}{V}\right)\left(\frac{m_{au}}{V}\right) = \left(\frac{m_f - m_{fb}}{V}\right)\left(\frac{m_a - m_{fb}/c_{st}}{V}\right)$$

$$= \frac{m_f}{V}(1 - b)\frac{m_a}{V}(1 - b.\phi)$$

$$= c.\rho_a^2(1 - b)(1 - b.\phi)$$

Now the Arrhenius equation is written in the following form:

$$\frac{\dot{m}_{fb}}{V}(Kg/s/m^3) = K\ (m^3/Kg/s).N\ (Kg/m^2).N\ (Kg/m^3).e^{-\frac{E}{RT}}$$

E is the activation energy and k_s is the steric factor.

Substituting for $N_f.N_a$, the final form of the equation can be written for a zone:

$$\frac{db_z}{dt} = k_s.\rho_{az}.(1 - b_z).(1 - \phi_z b_z).\ \exp(-E/RT_z) \qquad (5.3)$$

In this way the burning rate is considered to be dependent on concentrations of both fuel and air at any time. This of course makes the solution procedure more difficult in a multizone model, but is considered essential since there are cases where the effect of either concentration can not be neglected.

5.2.3. Further information

a) Heat transfer

The following method due to Eichelberg (1939) is employed in its original form to compute heat transfer rates from the engine cylinder contents. The heat transfer coefficient (h_c) is defined and expressed in terms of the mean piston speed (u cm/s) and instantaneous values of average cylinder temperature ($T^{\circ}K$) and cylinder pressure (p bar):

$$h_c = 0.283(p.T)^{\frac{1}{2}}(u_p)^{\frac{1}{3}} \quad W/m^2/^{\circ}K \qquad (5.4)$$

On this basis, the instantaneous rate of heat transfer is given in terms of the heat transfer area (A) and the mean wall temperature (T_w):

$$\dot{q}_w = h_c A \ (T - T_w) \qquad (5.5)$$

The heat transfer area (A) includes the piston crown, the cylinder head, the valves and the exposed surface of the cylinder liner. T_w is estimated by considering different temperatures for these areas, i.e.:

$$T_w = \frac{\Sigma \ A_i \ . \ T_{wi}}{\Sigma \ A_i}$$

As mentioned before, it is assumed that this heat loss is shared among various zones according to their mass and temperature as follows:

$$\dot{q}_{wz} = \frac{m_z . T_z}{m_a T_a + \Sigma m_z T_z} \cdot \dot{q}_w \qquad (5.6)$$

The validity of applying this method of heat transfer calculation to the present heat release model needs further investigation.

b) Evaporation

The simplest way to include the effect of fuel evaporation in the model is to express it in terms of droplet lifetime, Williams (1976). The method allows the available fuel concentration to be calculated on the basis of a predetermined droplet lifetime as follows:

The rate of droplet evaporation is written in terms of droplet diameter (D):

$$\frac{dm}{dt} = - k.D \qquad \text{where } \left(m = \frac{\pi D^3}{6}\right)$$

$$dm = \frac{\pi D^2}{2} dD = - kDdt \qquad (5.7)$$

i.e.
$$\int_{D_0}^{D} \frac{\pi}{2} D \, . \, dD = \int_{0}^{D} - kdt$$

$$\frac{\pi D_0^2}{4} = k \, . \, t_\ell$$

$$k = \frac{\pi D_0^2}{4 \, . \, t_\ell}$$

The droplet diameter can now be written in terms of the droplet lifetime:

$$D = D_0 \ (1. - t/t_\ell)^{\frac{1}{2}}$$

If the ratio of fuel vapor to total fuel mass is denoted by (τ), the following relation can be written:

$$\tau = 1. - (1. - t/t_\ell)^{3/2} \qquad \text{for } t < t_\ell \qquad (5.8)$$

Thus in equation (5.3), available unburnt fuel (1-b) can be replaced by available unburnt vapor (τ - b) i.e.:

$$\frac{db}{dt} = K_s \ \rho_a(\tau - b)(1 - b \ . \ \phi) \ \exp \ (-E/RT) \qquad (5.9)$$

or:

$$\frac{db_z}{dt} = K_s \rho_{az} \left| 1 - \left(1 - \frac{t_z}{t_\ell}\right)^{3/2} - b_z \right| (1 - b_z\phi_z) \exp(-E/RT_z)$$

This provision is built into the model to apply in cases where the fuel has not completely evaporated even though the mixture is within the inflammability limits. Obviously in cases where the cylinder pressure at injection is in excess of the critical pressure, fuel droplet lifetime is much shorter that the time taken for a zone to entrain enough air to start burning. In such a case the term (τ - b) would have automatically changed to (1 - b) anyway. (Values of τ are computed for $t < t_\ell$ only. After that, τ is automatically set to unity). The approach is particularly useful

for such cases as low cylinder pressure where droplet life-time could have values up to 0.4 ms or more.

c) Numerical constants

The following values for the activation energy and the steric factor of the Arrhenius equation were used throughout the computations for any running condition of the engine, (Grigg and Syed, 1969):

$E = 30000$ (kcal/kg mole) $= 1.254 \times 10^8$ (J/mole)

$K_s = 5 \times 10^7$ (m^3/kg/s)

This value of E is used in conjunction with the universal gas constant ($\bar{R} = 1.986$ kcal.kg mole$^{\circ}$K) and results in the following relation:

$$K_s \cdot \rho_{az} \exp\left(-\frac{E}{RT_z}\right) = 0.5\ \rho_{az} \cdot \exp\left(18.4208 - \frac{15000}{T_z}\right)$$

ρ_{az} is always computed in (gm/cm^3) so that the non-dimensional fuel burning rate $(\frac{db}{dt})$ is in $(\frac{1}{ms})$.

This together with the zone fuel mass (m_{fz}) and a calorific value $q_v = 41800$ J/gm (10000 kcal/kg) results in the zone heat release $(\frac{dq}{dt})$ as follows:

$$\frac{dq}{dt} = q_v \cdot m_f \cdot \frac{db}{dt} \qquad (5.10)$$

$$\frac{dq}{dt} = 41.8\ m_f \cdot \rho_a\ (1 - b)(1 - b\phi)\ 0.5 \exp\left(18.4208 - \frac{15000}{T}\right)$$

The rich and lean limits of inflammability are considered to be $c_r = 0.3$ and $c_\ell = 0.025$ respectively (Shahed-1975). The value of stoichiometric fuel to air ratio used throughout the computations is $c_{st} = 0.066$ (therefore $\phi_r = 4.5$ and $\phi_\ell = 0.375$).

Fuel specifications are given in Appendix (C). Fuel vapor density is calculated from vapor pressure and temperature ($\rho_v = \frac{P_v}{R_v T}$) where R_v is the ratio of the universal gas constant and the fuel molecular weight ($M_v = 200$).

Thus the ratio of fuel vapor and air gas constants is given as follows:

$$\frac{R_v}{R_a} = \frac{(\bar{R}/M_v)}{(\bar{R}/M)} = \frac{200}{29} = 6.9$$

The ratio of the fuel and air partial pressures can also be written in terms of molecular weight and fuel to air concentration:

$$\frac{P_v}{P_a} = \frac{m_v \cdot M_a}{m_a \cdot M_v} = \frac{c}{6.9}$$

The zone air density can now be expressed in terms of the total pressure ($p = p_v + p_a$)

$$\rho_{az} = \frac{1}{(1 + c_z/6.9)} \cdot \frac{p}{R_a T_z} \qquad (5.11)$$

The term ($\frac{c}{6.9}$) becomes very small compared to unity as c decreases. Therefore, it can be neglected provided the burning rate equation is not applied to the zone during the initial period of high fuel concentration (i.e. low air). By the time the zone crosses the inflammability limit ($c = c_r$), the term (c/6.9) becomes already too small compared to unity (i.e. $\frac{0.3}{6.9} = 0.00435 << 1.$).

d) Zone fuel and air mass

So far the mass of fuel or air did not enter the calculations directly. By the particular grouping of

variables, they appeared in the form of density, concentration or equivalence ratio. This was done deliberately to reduce the number of variables which require storage locations in the computer program. Although the computation time increases slightly with this method, the approach is believed to be beneficial because a user in general is more likely to be confronted with limited storage facilities rather than limited computing time.

In chapter three it was explained that for an injection duration equal to NI steps, there will be NI x $(KR)^2$ zones per spray. (eg. 6^o crank angle in $\frac{1}{2}^o$ steps gives N = 12, so if KR = 3 then the number of zones per spray will be NZ = 108). These zones will have equal fuel mass, which is calculated by dividing the mass of fuel injected into the cylinder per cycle (FCC) to the number of (sprays) injector holes and to the number of zones per spray (NZ).

$$m_{fz} = FCC/HOLES/NZ \tag{5.12}$$

Since m_{fz} is constant, it is calculated once only in the beginning of the program and thereafter it is used in conjuction with c_z (the zone fuel to air ratio) to give the zone air mass as many times as required.

$$m_{az} = m_{fz}/c_z \tag{5.13}$$

The new and old concentrations referring to the beginning and end of a step are both used for the computation of the air added to the zone, i.e.:

$$\Delta m_{az} = m_{fz}\left(\frac{1}{cz_2} \quad \frac{1}{cz_2}\right) \tag{5.14}$$

In high temperature regions of the jet, Δm_{az} can be the limiting factor determining the reaction rate in the zone. This is of course in cases where there is still sufficient fuel left to burn in the zone. These aspects will be discussed in the next chapter. It is also noted that the assumptions leading to the basic structure of the model are such that no change is considered in the individual zone air entrainment pattern after combustion. However, the zone volume obviously alters due to expansion at high flame temperatures. A complication also arises at the jet-back when fast moving zones at inner layers are replaced by slow moving zones from outer layers. Since the concentration distribution of a developed jet shows higher values at corresponding positions, it is assumed that the zone concentration does not alter at the jet-back until the zone reaches a position corresponding to a lower concentration region in the developed jet.

Another complication arises when the air surrounding the jet is depleted. This obviously does not happen in reality. To overcome this difficulty, in the model, a condition is imposed to make the air entrainment of individual zones depend on the availability of the surrounding air in the confined space of the combustion chamber. i.e.:

$$\Delta' m_{az} = \Delta m_{az} \times \frac{m_{an}}{m_{at}} \qquad (5.15)$$

As the mass of the non-burning zone (m_{an}) reduces, this condition becomes more effective such that when m_{an} is a small fraction of the trapped mass (m_{at}), the effective entrainment ($\Delta' m_{az}$ becomes small compared to that

calculated previously (Δm_{az}). In this way m_{an} never becomes zero (or negative). Without this condition, even before depletion of air, numerical instability would arise in the solution procedure, and thus the model would not be able to cope with possible sets of data having a rich overall fuel to air ratio. (For the test data examined in this thesis, air depletion would not occur until well after the end of combustion. However, it is important to consider equation (15) if the calculations are to be performed up to exhaust valve opening).

e) Zone Specific Heats

Temperature dependent specific heats are used for the mixture in each zone according to equivalence ratio. For air, the following fifth order polynomical proposed by Edson (1960) gives the variation of constant pressure specific heat with temperature ($T^* = T/1000$, T in ^oK and CPA in $KJ/^oK/kg$):

$$CPA(T^*) = 0.88311 + 0.372(T^*) - 0.15\ (T^*)^2 + 0.03135\ (T^*)^3 - 0.003524\ (T^*)^4 + 0.0016235\ (T^*)^5$$

To obtain a similar analytic function for mixture properties, the data on stoichiometric combustion products ($\phi_b = 1$) was curve fitted and it was found that by adding a fourth order polynomial to CPA(T^*), the misture specific heat can be calculated (CPM(T^*), $KJ/^oK/kg$ original air) as follows:

$$CPM\ (T^*) = CPA(T^*) + \phi_b \left|0.085757 + 0.01463\ (T^*) + 0.11683\ (T^*)^2 - 0.1336\ (T^*)^3 + 0.0451\ (T^*)^4\right|$$

Thus the products of stoichiometric combustion will have the following constant pressure specific heat:

$$CPP\ (T^*) = 0.968867 + 0.38663\ (T^*) - 0.03317\ (T^*)^2 - 0.10225\ (T^*)^3 + 0.041576\ (T^*)^4 + 0.0016235\ (T^*)^5$$

It follows that CPM (T*) is considered on the basis of the mass fractions of air and products of stoichiometric combustion, i.e.

$$m \cdot CPM = m_a \cdot CPA + m_p \cdot CPP$$

or

$$CPM = (1 - \phi_b)\ CPA + \phi_b\ CPP$$

ϕ_b is the ratio of burnt fuel mass to that of original air divided by stoichiometric fuel to air ratio.

Similarly, the constant volume specific heat CVM(T*) is computed from the following relation:

$$CVM\ (T^*) = CPM\ (T^*) - R$$

Alternatively values obtained from the more time consuming Olikara subroutines (1975) can be used neglecting the effect of pressure. A comparison with lean mixture combustion products for 800 psi is shown in Fig. (5.1). It is noted that only the stoichiometric combustion products were used for curve fitting.

f) Calculation of the swirl ratio

Calculation of zone air entrainment requires determination of the deflection parameter (λ) and therefore the

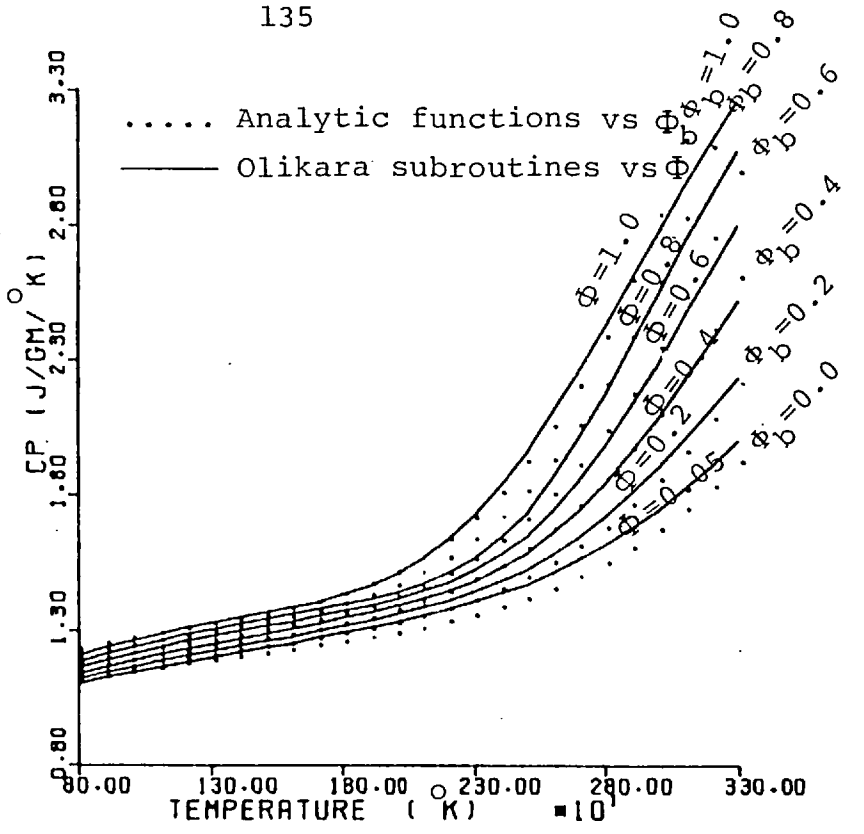

Fig. 5.1. Constant pressure specific heat vs. mixture temperature

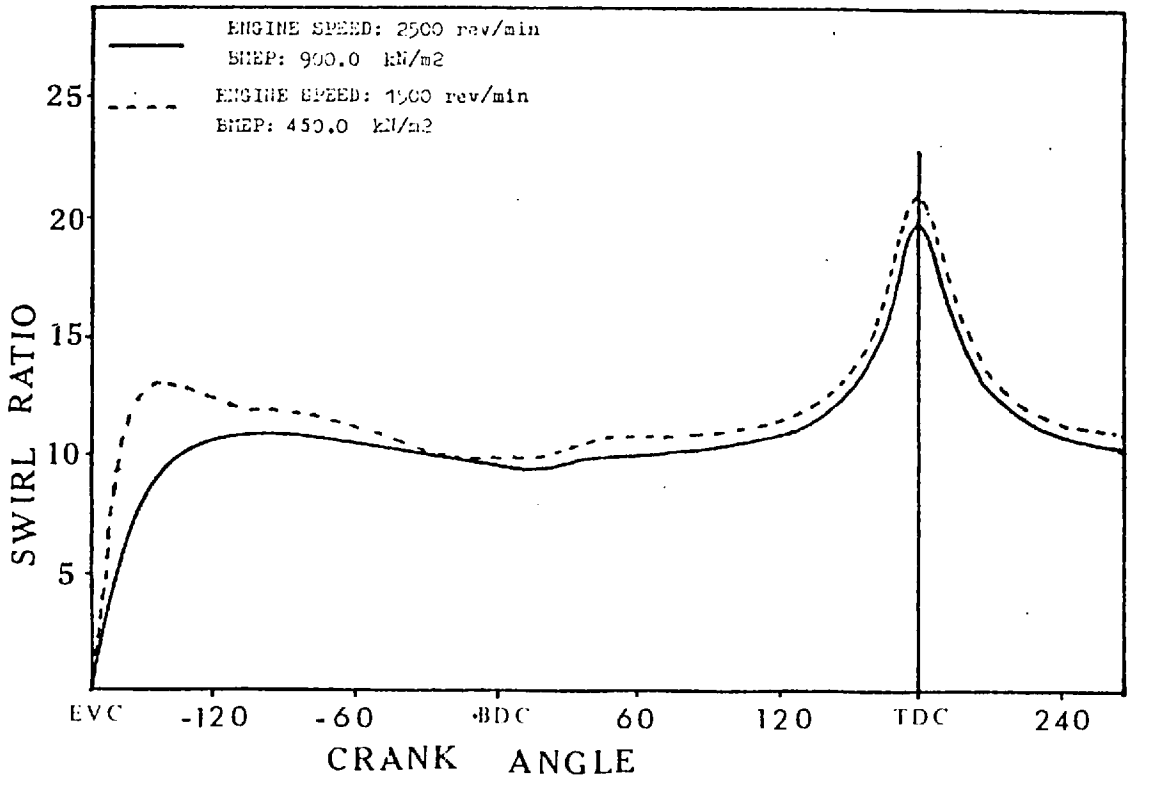

Fig. 5.2. Variation of swirl ratio with crank angle

swirl ratio (section 3.5.3). A method proposed by Dent (1973) was adopted and the swirl ratio was calculated for various running conditions of the direct-injection engine data analysed in this thesis. Basically this method is based on the assumption that during the induction period the moment of momentum of air entering through the inlet valve is equal to the rate of change of angular momentum of the cylinder contents. This gives the swirl angular velocity (ω) during the induction period:

$$\omega(t) = \left(\frac{8}{B^2}\right) \frac{\int_0^t \dot{m} \cdot u^* \cdot r_v \cdot dt}{\int_0^t \dot{m} \cdot dt}$$

Where u* is the component of inlet velocity in the direction of swirl and r_v is the distance of valve centre from cylinder centre.

During compression the swirl velocity is further increased due to reduction in the inertia of the cylinder contents. In other words as the piston moves towards T.D.C., the piston bowl contains a higher proportion of the cylinder contents. This has the effect of increasing the angular velocity during compression which is calculated (neglecting the effect of friction) as follows:

$$\frac{d}{dt}(I_c \omega_c) = 0$$

I_c is the inertia of the cylinder contents and is calculated in terms of the volume occupied by the piston bowl (V_b) and that of the remainder of the combustion

chamber ($V_0(\theta)$), as well as the ratio of piston bowl diameter to cylinder bore (D_b/B).

$$I_c = \frac{m}{2} \left| \frac{V_0(\theta) + V_b(D_b/B)^2}{V_0(\theta) + V_b} \right|$$

$V_0(\theta)$ is computed by multiplying the piston area by the distance of the piston crown from the cylinder head ($V_0(\theta) = A_p \cdot S(\theta)$). At T.D.C., V_0 is the same as the clearance volume minus the bowl volume. Thus I_c is minimum at T.D.C. and therefore ω is maximum.

The computed variation of swirl ratio with crank angle is shown in Fig. 5.2 for two running conditions. Values at other conditions lie between these two curves. It appears that the maximum swirl ratio is nearly constant for various running conditions and therefore the swirl velocity is proportional to the engine speed.

The interest in the present model is in the swirl ratio from the time of fuel injection to T.D.C., which was found to vary between SR = 17 to SR = 21 depending on engine running condition. A value of 18 was therefore used for all running conditions. The constants used in the computations are: D_b = 7.1 cm, V_b = 79 cm^3, r_v = 2.76 cm and $u^* = \sqrt{2}\, u_a/2$ (where u_a is the instantaneous velocity of the air entering the cylinder).

The computer program for the present heat release model is written for part of the engine cycle where both valves are closed. Therefore the swirl ratio calculation was performed within the complete cycle simulation program of Marzouk (1976). However, if the heat release program

is used in conjuction with a cycle simulation program that includes the induction period, the computations can be performed simultaneously.

It is noted that in any case the heat release model requires a mean value for the swirl ratio during the fuel injection period. As explained above a value of 18 was found to be a reasonable estimate for this engine according to Dent's model. This resulted in various values for cross flow momentum, air velocity and deflection parameter at different running conditions according to engine speed, charge density and injection velocity. This in turn made it possible to calculate individual zone concentrations which were ultimately needed for the solution of equations in the heat release model.

5.3 Solution procedure

An iterative procedure is employed for simultaneous solution of the differential equations. There are n burning zones and one non-burning zone at any time (n reaches n_{max} at the end of injection and does not increase subsequently). There are 2n + 2 equations for zone energy balance (15) and thermodynamic state (16) and there are n equations for zone burning rates (17). There is a further single equation for the volume constraint (bringing the total number of equations to 3n + 3). The same number of unknown variables are T_z (n + 1), V_z(n + 1), b_z (n) and p.

For every step the computations start by estimating the cylinder pressure for the end of the step (p_{i+1}). The first estimate (arbitrarily) is made by the following

relation:

$$p^0_{i+1} = p_i \frac{V_i}{V_{i+1}}$$

The cylinder volume V_i (at the beginning of the step) and V_{i+1} (at the end of the step) are calculated from engine geometry and p_i is known from the previous step. Then $b_{z,\,i+1}$ $(z = 1, n)$ and $T_{z,\,i+1}$, $V_{z,\,i+1}$ $(z = 1, n+1)$ are calculated as follows:

$$b_{z,\,i+1} = b_{z,\,i} + K_s \cdot \rho_{az,\,i} (1 - b_{z,\,i+1})(1 - \phi_{z,\,i+1}$$

$$b_{z,\,i+1}) e^{-\frac{E}{R \cdot T_{z,\,i}}} \cdot \Delta t$$

This equation is a quadratic in $b_{z,\,i+1}$ such that one of its roots (the smaller) is always acceptable ($b_{z,\,i} \leq b_{z,\,i+1} \leq 1/\phi_{z,\,i+1}$ for rich mixtures $\phi \geq 1$ and $b_{z,\,i} \leq b_{z,\,i+1} \leq 1$ for lean mixtures $\phi \leq 1$).

With this value of $b_{z,\,i+1}$, zone heat release and heat transfer are calculated from equations (5.10) and (5.6) respectively and therefore the net heat added to the zone (Δq_z) at an interval Δt is obtained.

Next, $U_{z,\,i+1}$ and $T_{z,\,i+1}$ are calculated by integrating the energy equation over the step as follows:

$$m_{z,\,i+1} U_{z,\,i+1} = m_{z,\,i} U_{z,\,i} + \frac{\Delta t}{2} \left|\frac{d(m_z U_z)}{dt}\right|_i$$

$$+ \left.\frac{d(m_z U_z)}{dt}\right|_{i+1}$$

In general this equation represents a second order predictor-corrector method and requires successive iterations to obtain $U_{z,\ i+1}$ after substituting the slopes at beginning and end of the step. i.e.:

$$\frac{d(m_z U_z)}{dt}\Big|_i = - p_i \frac{dv}{dt}\Big|_i + \frac{dq}{dt}\Big|_i + h_a \frac{dm}{dt}\Big|_i$$

$$\frac{d(m_z U_z)}{dt}\Big|_{i+1} = - p_{i+1} \frac{dv}{dt}\Big|_{i+1} + \frac{dq}{dt}\Big|_{i+1}$$

$$+ ha \frac{dm}{dt}\Big|_{i+1}$$

However this can be avoided by replacing $\frac{dv}{dt}$, $\frac{dq}{dt}$ and $\frac{dm}{dt}$ in both equations by $(V_{z,\ i+1} - V_{z,\ i})/\Delta t$,and $\Delta q_z/\Delta t$ and $(m_{z,\ i+1} - m_{z,\ i})/\Delta t$ respectively, i.e.:

$$m_{z,\ i+1}\ U_{z,\ i+1} = m_{z,\ i}\ U_{z,\ i} - \left(\frac{P_{i+1} + P_i}{2}\right)(V_{z,\ i+1}$$

$$- V_{z,\ i}) + \Delta q_z + ha_i (m_{z,\ i+1} - m_{z,\ i})$$

This equation is solved together with the state equation to calculate the zone volume and temperature at the end of the step:

$$V_{z,\ i+1} = \frac{m_{z,\ i+1} \cdot R \cdot T_{z,\ i+1}}{P_{i+1}}$$

So far calculations are performed on the basis of the first estimated value of cylinder pressure (p^0_{i+1}). To correct this pressure through successive iterations, the Secant method (a modified Newton's method) is employed in updating the estimated values and repeating the computations until the volume constraint equation is satisfied, i.e.

First correction

$$p^1_{i+1} = p^0_{i+1} \frac{\sum_{z=1}^{z=n+1} V^0_{z,\,i+1}}{V_{i+1}}$$

With p^1_{i+1} the process is repeated and the following values are calculated:

$$V^1_{z,\,i+1},\ T^1_{z,\,i+1},\ \sum_{z=1}^{z=n+1} V^1_{z,\,i+1} \text{ and}$$

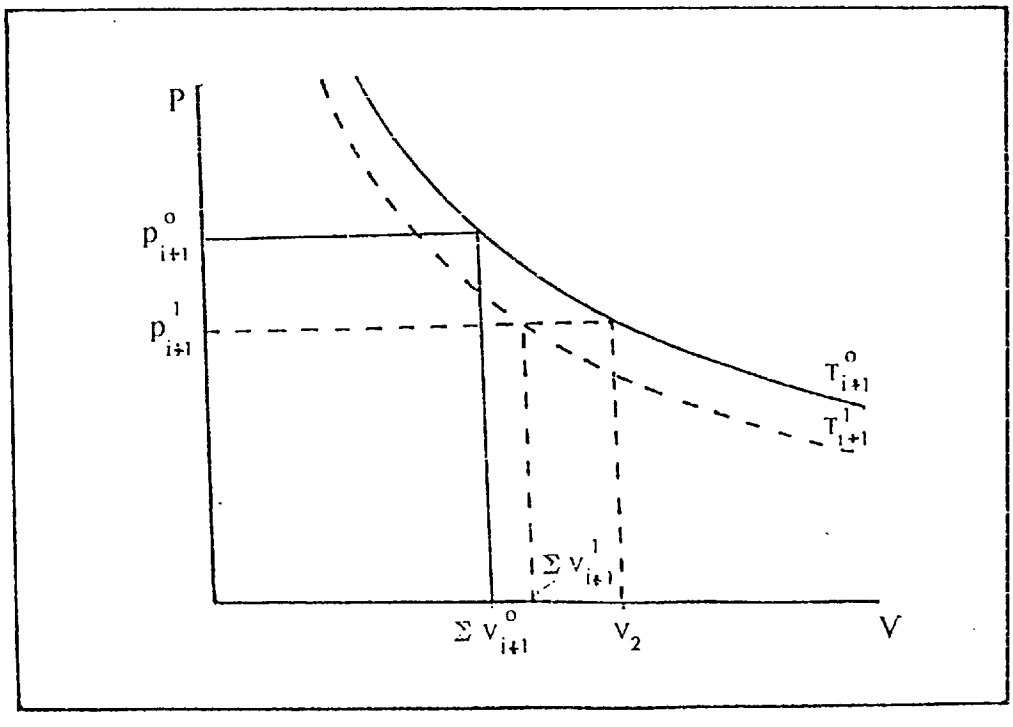

Fig. 5.3. P-V diagram to illustrate the iteration procedure

$$\left.\frac{\partial \Sigma V_z}{\partial p}\right|_{i+1}^{1} = \frac{\Sigma V_{z,\,i+1}^{0} - \Sigma V_{z,\,i+1}^{1}}{p_{i+1}^{0} - p_{i+1}^{1}}$$

Successive corrections:

$$p_{i+1}^{j+1} = p_{i+1}^{j} - \frac{\Sigma V_{z,\,i+1}^{j} - V_{i+1}}{\left.\frac{\partial \Sigma V}{\partial p}\right|_{i+1}^{j}}$$

This method provides a relatively fast convergence of the iteration to satisfy the following criterion:

$$\frac{p_{i+1}^{j+1} - p_{i+1}^{j}}{p_{i+1}^{j}} \leq 0.001$$

This criterion is usually satisfied in two or three iterations. At certain steps, however, the number of iterations increases. These are at conditions where there is an abrupt change in the rate of cylinder pressure rise. Similarly at some stage during the expansion stroke, where the cylinder pressure has started to decrease but the average cylinder temperature is still increasing, the number of iterations might increase. In any case this number does not exceed 6 or 7 for the value of 0.001 chosen as the convergence criterion. The method does not suffer from instability and convergence is guaranteed with the present solution procedure.

Fig. 5.3 shows a possible direction in which the iteration may proceed. In general, however, the rate of pressure change can be positive or negative combined with either an increase or a decrease in the cylinder volume. Usually a step size smaller than 1° CA does not alter the accuracy of the solution. This means that a time step of 1/6 to 1/15 ms is used at engine speeds of 1000 to 2500 rev/min. The number of layers can be reduced to a minimum of KR = 2 without affecting the accuracy of the solution. (i.e. a minimum number of zones).

5.4 The computer program

The computer program was developed concurrent with formulation of the model. In this way a structure for the model which was suitable for programming was found. The main effort was directed at keeping the program short, easy to use, with as little computation time and storage requirements as possible. The idea was to keep it in a form suitable for future use in a larger complete cycle simulation program. Proper choice of variables (or particular grouping of variables) was the main key. The number of storage locations was mainly dependent on the number of steps during injection of fuel (i.e. dependent on injection duration and the chosen time step).

The flow diagram is shown in Fig. 5.4 and the following is an explanation of its various sections:

1. Input variables

The following groups of variables are listed in DATA statements in the beginning of the program:

1a) Engine geometry:

These include cylinder bore, stroke, connecting rod length, clearance volume, minimum heat transfer area, piston bowl radius, swirl ratio, nozzle hole diameter and the number of nozzle holes.

1b) Fuel properties and related variables:

These include the fuel density, calorific value, rich and lean limits of inflammability, activation energy and the steric factor.

1c) Initial conditions

These include the injection rate and timing, trapped mass and cylinder pressure at the commencement of injection.

1d) Variables to be chosen by the user.

These include the computation step size, total number of steps, number of layers in spray for zone-division and input-output option switching integers.

2. Statement functions

A number of statement functions are supplied for frequent computation of the following variables:

2a) Specific heats of air and combustion products are supplied as a function of temperature.

2b) Fraction of stroke travelled by the piston is supplied as a function of crank angle to evaluate instantaneous cylinder volume and heat transfer area.

2c) Instantaneous cylinder volume is supplied as a function of the fraction of stroke denoting piston position.

2d) A function is supplied to assist the calculation of the relative layer width for the zone division pattern.

3. Optional data.

Experimental data may be supplied for comparison with the predictions. A "READ" statement is provided to accept the digitised cylinder pressure diagram with a certain format. The crank angle position of the first data value relative to T.D.C. should be stated for deciding the number of data values to be discarded before reaching the one corresponding to the dynamic injection timing.

4. Preliminary calculations.

This section is placed prior to the main step count loop to calculate various constants and to perform any possible arithmetic outside the main loop to shorten the overall computing time.

5. First stage of the main loop

The crank angle step counter is increased by one (indicating end of step). Cylinder volume, total heat transfer, etc. are calculated. Subsequently any computations not relating to individual zones are performed.

The step-count indicator is examined with respect to the number of injection steps to decide on zone formation for the fuel entering the cylinder. If there is fuel injection during the step, two sets of imaginary initial zones are labelled and numbered from which, a set (KR^2 zones) is to be added to the cylinder contents.

Jet penetration as well as positions of the most advanced zones are calculated deciding whether impingement has taken place. (If it is not the first step of injection, the positions of all other zones is automatically determined

by knowing which zone replaces another through the zone labelling code).

6. First zone-count double-loop

Each zone is labelled by two integers K and L denoting positions along and across the jet and is related to its previous address (K1, L1) where all previous values for the same zone are stored. New values of air entrainment and concentration is calculated and the fuel burning rate equation is integrated over the step to give the heat release for each zone. Some of the calculations concerning individual zones are performed, and necessary values are stored; thus preparing for the final computation of all the zone variables in a further loop with successive updating of the cylinder pressure.

7. Cylinder pressure iteration loop

This section includes all those computations which depend on successive estimates of the cylinder pressure. Therefore it embodies a second zone-count double loop as well as the computations related to the non-burning zone. The total entrained air is already known from the first zone-count loop which is executed only once for each step. Thus the non-burning zone mass is known and by satisfying the energy equation and the state equation, zone temperature and volume are calculated according to the estimated cylinder pressure. This pressure is updated by applying the volume constraint equation after executing the second zone-count double-loop.

8. Second zone-count double-loop

This is placed within the cylinder pressure iteration loop to compute the unknown variables of all burning zones as many times as required. Therefore it is considered to be the most time consuming part of the whole program. It is useful to note for future development of this program that any additional statement which is not relevant to the pressure iteration can be placed in the first or the third zone-count loops which are executed only once for each step.

9. Output options within the main loop

General computations for the step are completed and variables not concerning individual zones (such as the total rate of heat release, cylinder pressure, work done, rate of pressure rise, etc.) are stored against the crank angle. These can be presented in the form of written or graphical output outside the step count loop. Individual zone variables, on the other hand, are only stored at the beginning and end of one step at any time. Thus they may be written in matrix form as separate records for successive crank angle steps consecutively on an output file. In this way there is no need for a large number of storage locations in the program just for the sake of output. Alternatively one large matrix is provided for storing a single variable for all zones against crank angle. In this case the usual label of each zone (K, L) is replaced by a single integer. For zones which have not yet been formed at a certain crank angle the value of the variable is ficticiously put to zero to keep the matrix in tact. This matrix as well as each of the matrices noted before, may be plotted in a three dimensional form.

10. Third zone-count double-loop.

At the end of the computations for each step, this loop serves the purpose of placing the existing zone variables in the stores assigned to save them for use in the next step. It is noted that two storage locations are used for each variable at any time to denote its value at the baginning and end of each step. Their addresses are related to one another through the zone labelling code. At this stage in the program both stores contain the same value. Therefore one is free for use during the next step.

11. Program end

The program ends after completing the computations for the required number of steps and after executing the final output instructions.

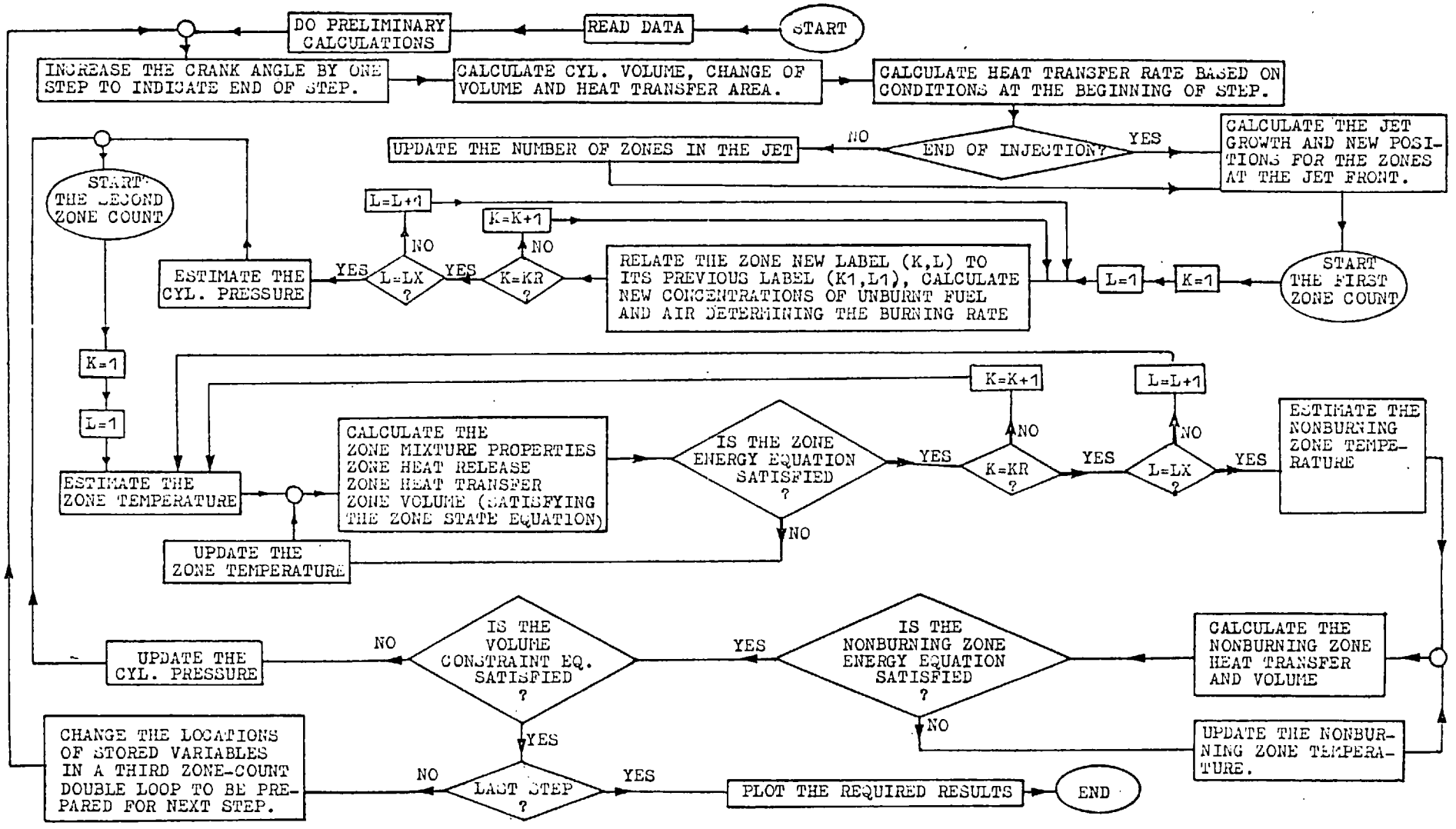

Fig.5.4. Flow diagram of the computer program.

CHAPTER 6

Discussion and Evaluation of Results

6.1 Introduction

In this chapter the predictive capabilities of the full model are presented and discussed. Experimental verification of the model is achieved by comparing predicted and measured cylinder pressure diagrams for the engine running conditions mentioned in chapter four. At the same time, the merits and shortcomings of the general structure of the model and the validity of various assumptions are discussed.

Predicted and measured cylinder pressure diagrams are compared and the rate of pressure rise and the rate of heat release for eight running conditions are presented.

The response of the model to variations in certain parameter is investigated.

Predicted temporal and spatial distributions of zone variables such as temperature, buring rate, etc. are demonstrated and described.

The general structure of the model and the interaction of parameters and their influence on various phenomena occuring during combustion are discussed.

6.2 Comparison of model predictions with experimental data

The diagrams presented in this section represent the graphical output of the computer program. Cylinder pressure is computed step by step, using a step size of one degree CA. Measured (dotted lines) and predicted (full lines)

cylinder pressure and rate of pressure rise are compared in Fig. 6.1 to 6.8. Cases 1,3,5,7 are at 450.0 kN/m^2 bmep and engine speeds of 1000, 1500, 2000 and 2500 rev/min respectively (Fig. 6.1, 6.3, and 6.7). Cases 2, 4, 6 and 8 are at 900.00 kN/m^2 bmep and same engine speeds as above (Fig. 6.2, 6.4, 6.6 and 6.8).

The diagrams show a fairly close agreement between the predicted and measured rates of pressure rise in most of these running conditions. The predicted moment of ignition is however earlier than that measured. The reasons for this will be discussed when the burning pattern of the individual zones is presented (section 6.4). Obviously a shorter ignition delay period results in a smaller initial rate of pressure rise. This is the reason why the predicted peak pressure is smaller than that measured. It should be noted that the initial rate of pressure rise and therefore the cylinder pressure diagram is very sensitive to changes in the ignition delay period. As mentioned before, ignition in this model is predicted through the same equations as those employed during the remainder of the combustion period. Improvements in the accuracy of ignition prediction therefore can only be achieved by improving the model in general.

The predicted rates of heat release (full lines) are also in reasonable agreement with those computed from cylinder pressure diagrams (dotted lines). Here, an exact agreement is not expected, however, for the following reason: The computation of the rate of heat release from cylinder pressure diagrams requires the assumption of a homogeneous mixture and a uniform temperature for the whole cylinder contents at any one time. (Whitehouse - 1961). This

assumption conflicts both with reality and with the basic nature of the present model which involves heterogeneous mixtures and a non-uniform temperature distribution due to its multi-zone structure.

In other words, if the heat release rate diagrams predicted by the present model were employed in a single-zone model (based on mass averaged temperatures), the resulting cylinder pressure diagrams would not be the same as those predicted using the present model. For the same heat release, in a single zone model, predicted pressures would be higher. Therefore, heat release rates predicted using the present model are expected to be higher than those obtained (on the basis of mass averaged temperatures) from measured cylinder pressure even when the predicted and measured cylinder pressures are exactly the same.

Thus the cylinder pressure and rate of pressure rise diagrams provide a better basis for comparison than heat release diagrams. However, the latter serves as a good guideline in various assessments concerned with model predictive capabilities.

For example, it is observed that correct prediction of the first peak is important. Closer agreement between measured and predicted maximum cylinder pressure is observed only in cases where there is a reasonably good prediction of the first peak in the rate of heat release diagram. Cases 1 and 3 are two good examples of such a condition.

In nearly all cases examined herein, the predicted ignition delay is shorter than that measured. Obviously this is the main reason for the disparity between the predicted and measured results. In cases where the predicted

moment of ignition is markedly different, the initial rate of pressure rise and the maximum pressure also distinctly differ from those measured.

In a discussion of the reasons for this shortcoming of the model, it is noted that ignition is predicted on the basis of two phenomena, namely, the jet mixing process and temperature dependent reaction rates.

The jet mixing process has been explained in chapter three. The dominant variables in determining air entrainment are the injection velocity, swirl ratio and air density. The effects of these variables may be combined in the deflection parameter (λ). When λ increases, the overall air fuel ratio increases. Thus the possibility increases that in a short time favorable mixture conditions for ignition will be established. On the other hand an increase in injection velocity causes an increase in jet penetration and therefore has a similar effect on air entrainment.

Temperatures also have a marked effect on ignition delay. The Arrhenius equation(eq. 5.14), employed in this model, dictates that at low temperatures burning rates are insignificant even though sufficient air may be available in a zone. The exponential temperature dependent term in this equation reveals that a significant rise in the burning rate may be expected at temperatures between 800 to 1000^{o}K depending on the air pressure (i.e. density). In fact, at a fixed air density, the burning rate at 700^{o}K is about one order of magnitude lower than that at 800^{o}K. The same applies to the temperature rise resulting from the subsequent heat liberated in a zone. For example at 700^{o}K, low burning rates may produce only a 5^{o}K temperature rise whereas at

800°K, high burning rates may cause a temperature rise of about 50°K or more. In the present model this is calculated on a zone-to-zone basis and the results will be shown and discussed in section 6.4.

Other models which use experimental correlations to calculate ignition delay, employ a mass averaged temperature and an overall density for the cylinder contents. In such models the physical and chemical aspects of ignition delay are not separated. This is the reason why constants replacing the activation energy and the steric factor in these correlations are usually different from those of the Arrhenius equation employed herein.

It is appropriate to mention here that even in multi-zone models the fact that the constants mentioned above are not within their universally accepted range, may be due to the following reason: if these constants are used in an Arrhenius type equation and show a slower reaction than that expected from a certain mixture strength of a particular fuel and air, then there is reason to believe that the physical aspects of the reaction, such as the mixing pattern, have been miscalculated in advance.

In such cases the constant replacing the activation energy may take any value and so would the pre-exponential constant. Therefore the Arrhenius type equation would not solely represent the chemical reaction concerned; it would be an equation representing a part of the physical mixing pattern plus the chemical reaction rate. In the present model such an approach has been avoided.

The above discussion suggests that the present model has the following advantages. The physical and chemical

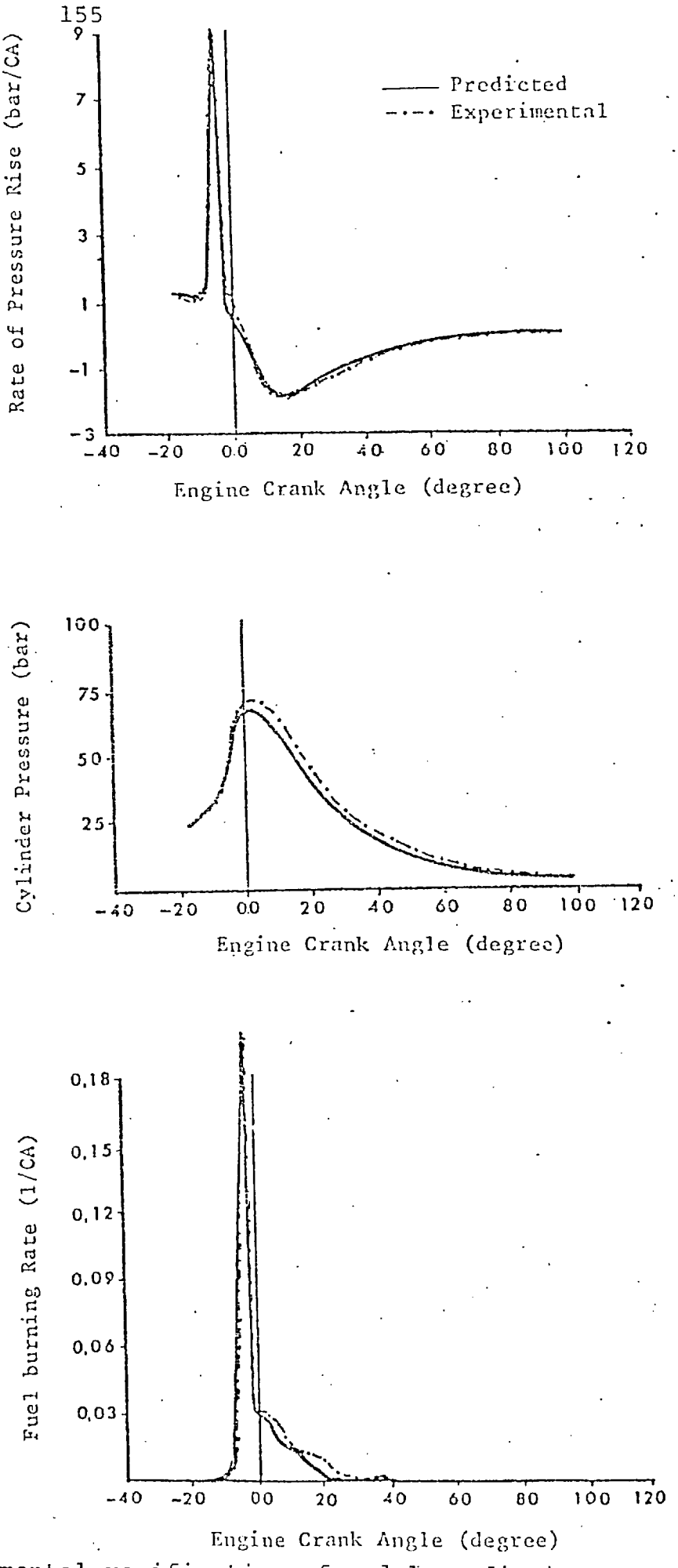

Fig. 6.1. Experimental verification of model predictions (case 1). Engine speed 1000 rev/min, bmep 450 kN/m2

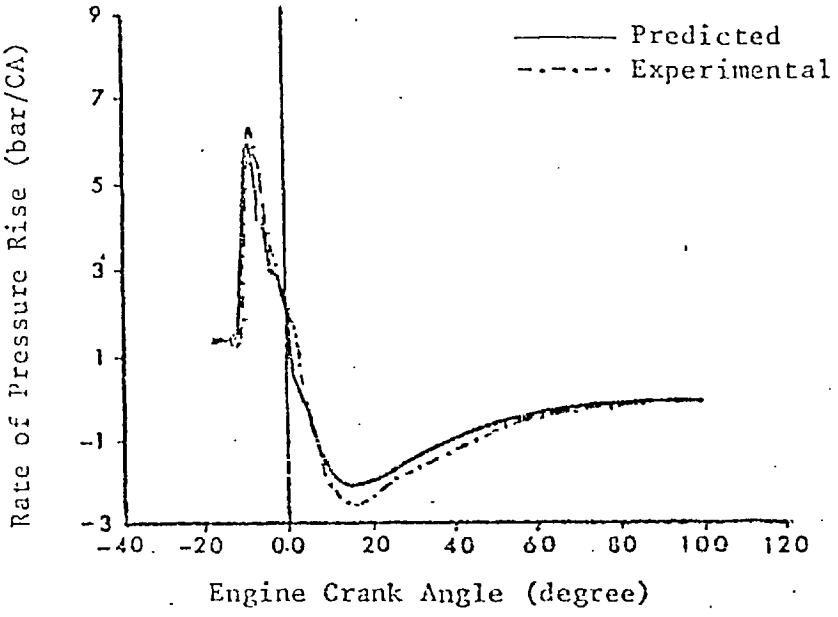

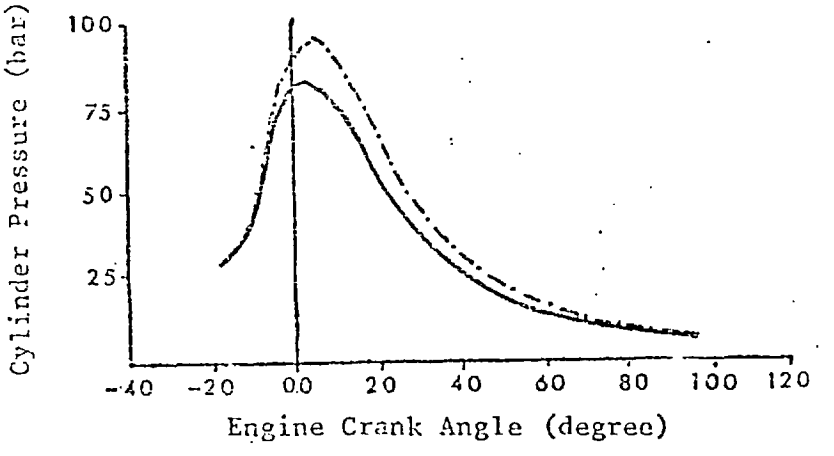

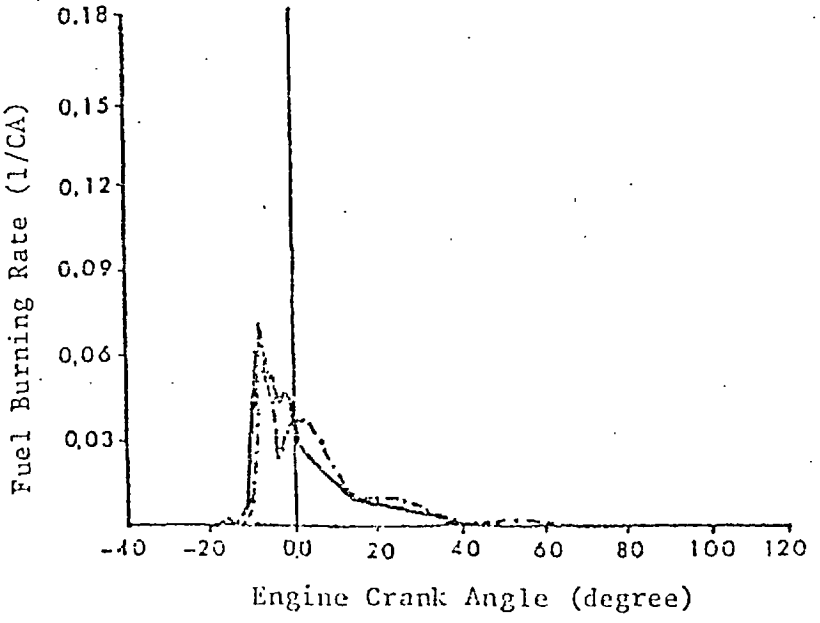

Fig. 6.2. Experimental verification of model predictions (case 2). Engine speed 1000 rev/min, bmep 900 kN/m2

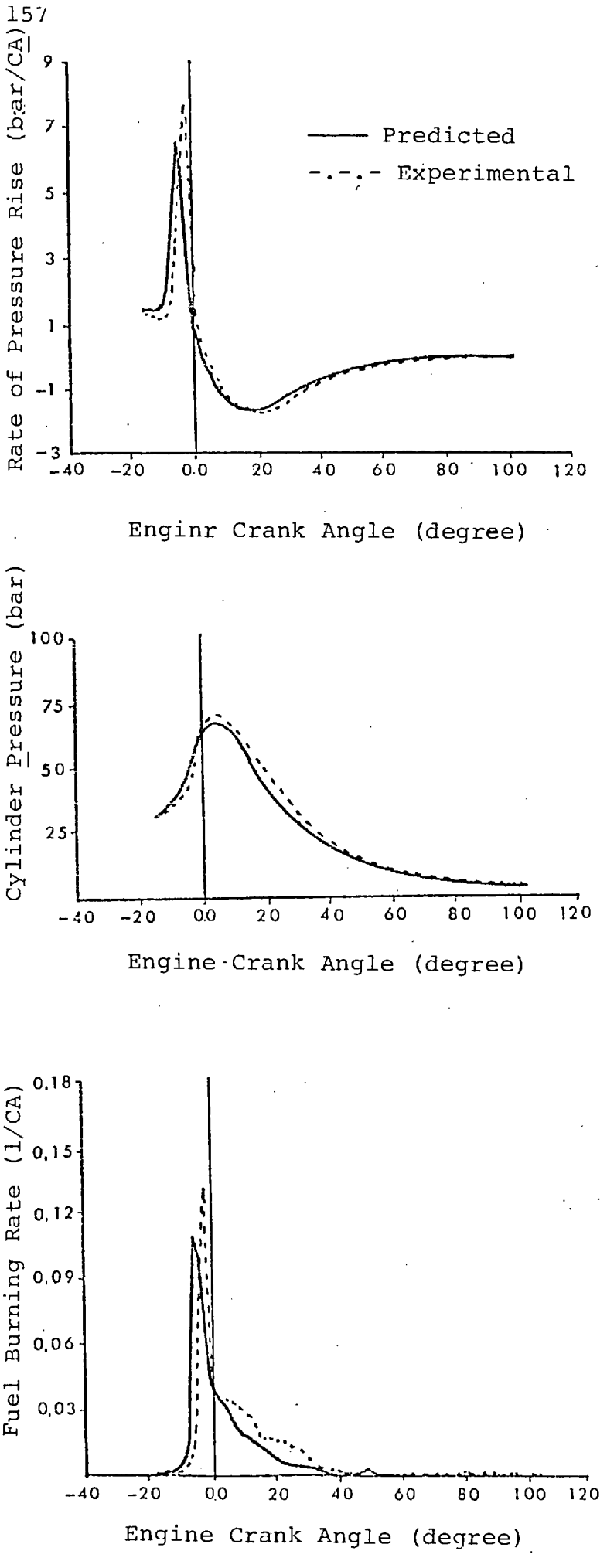

Fig. 6.3. Experimental verification of model predictions (case 3). Engine speed 1500 rev/min, bmep 450 kN/m2

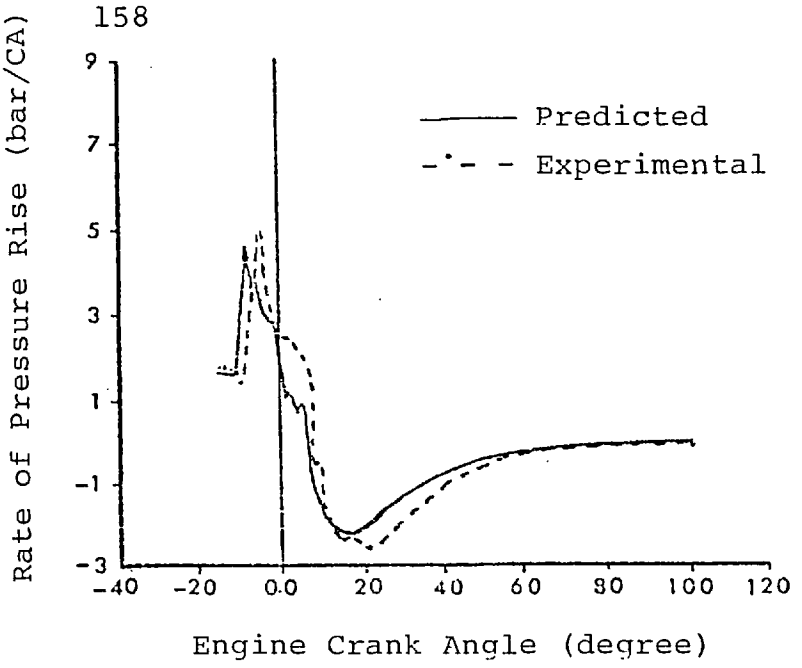

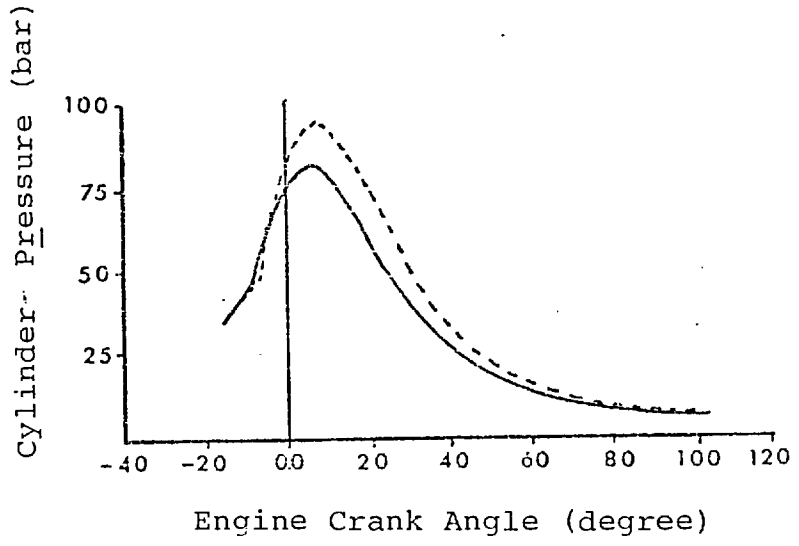

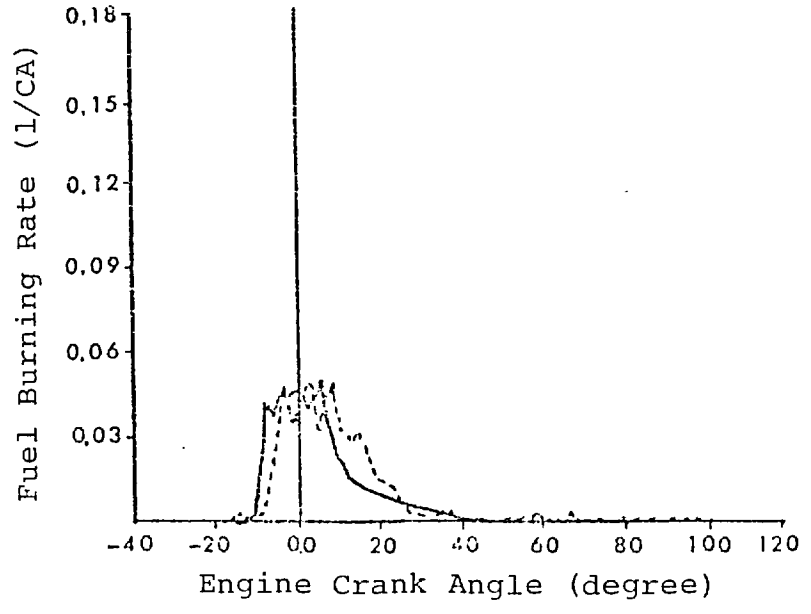

Fig. 6.4. Experimental verification of model predictions (case 4). Engine speed 1500 rev/min, bmep 900 kN/m2

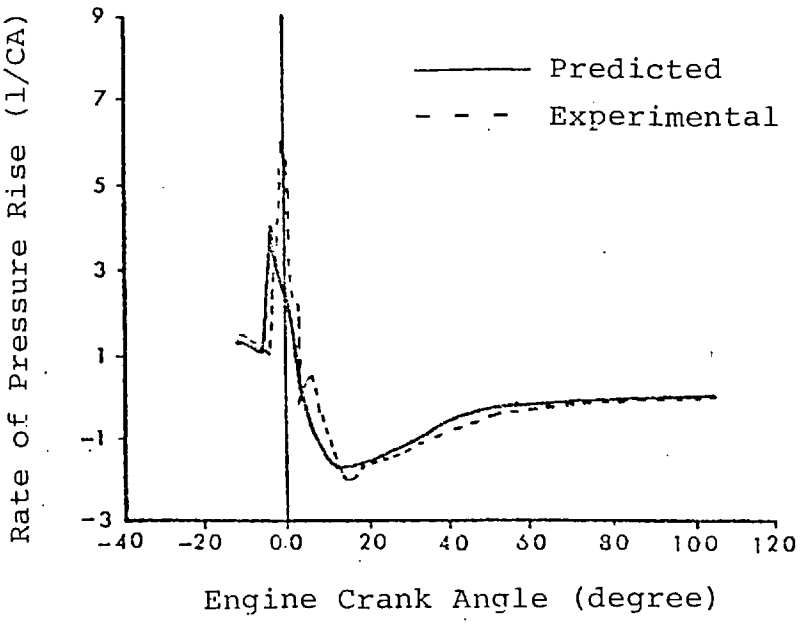

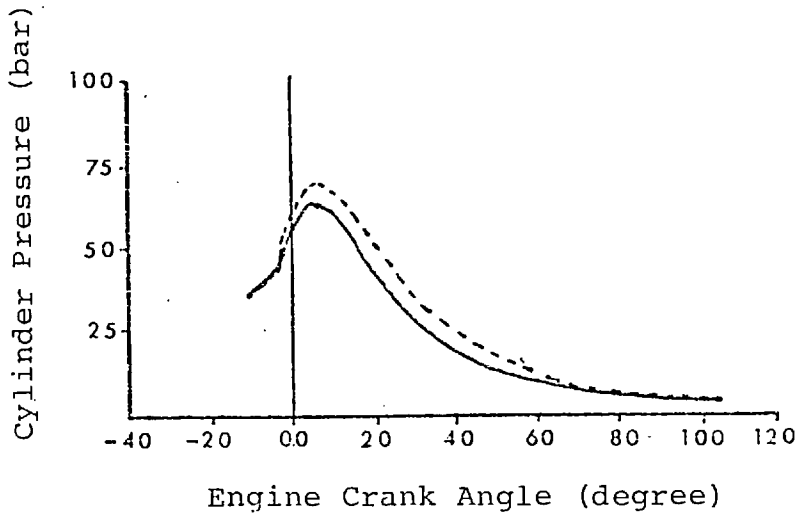

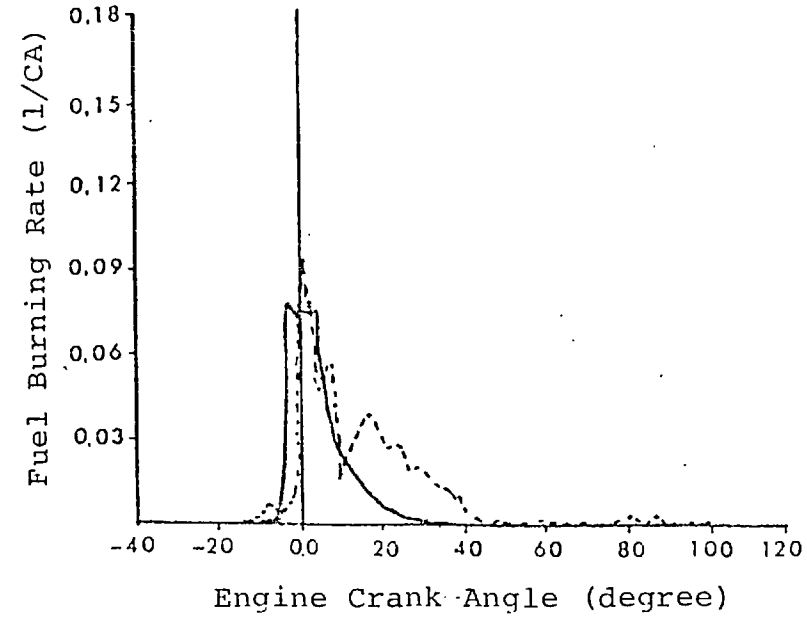

Fig. 6.5. Experimental verification of model predictions (case 5). Engine speed 2000 rev/min, bmep 450 kN/m2

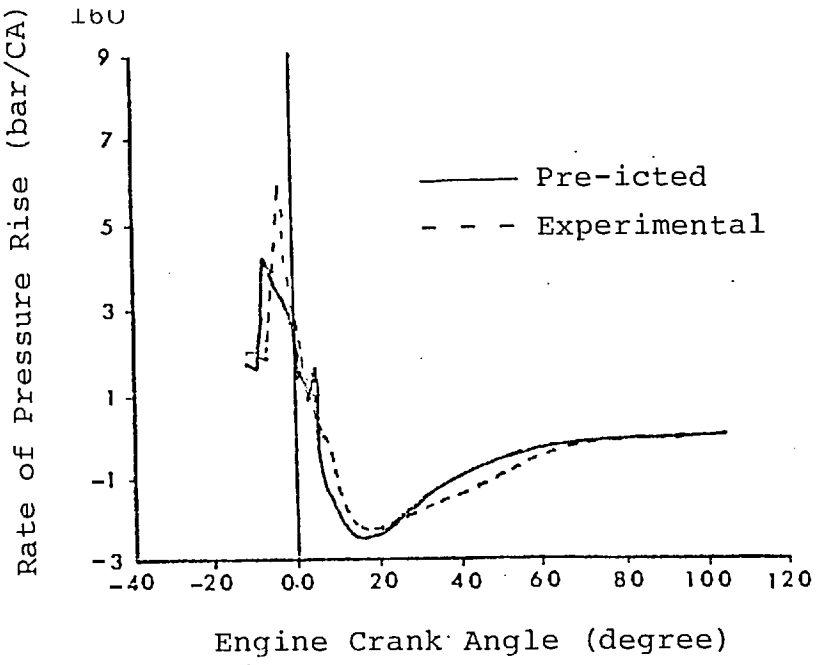

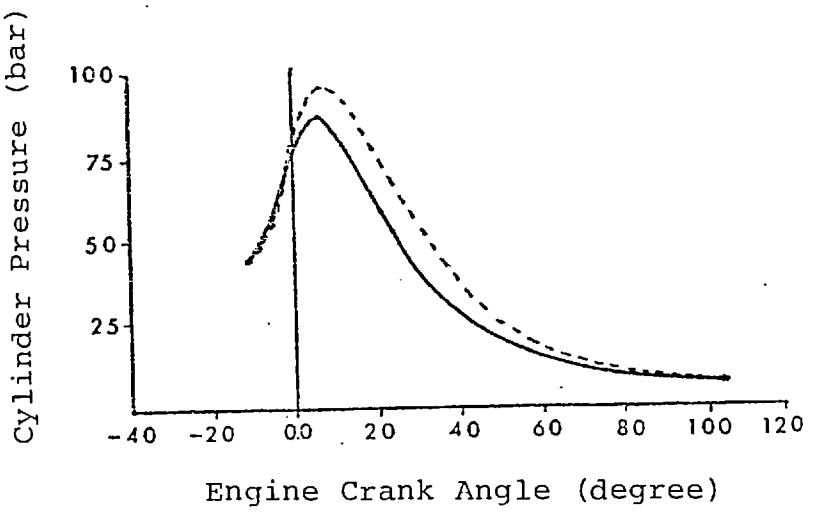

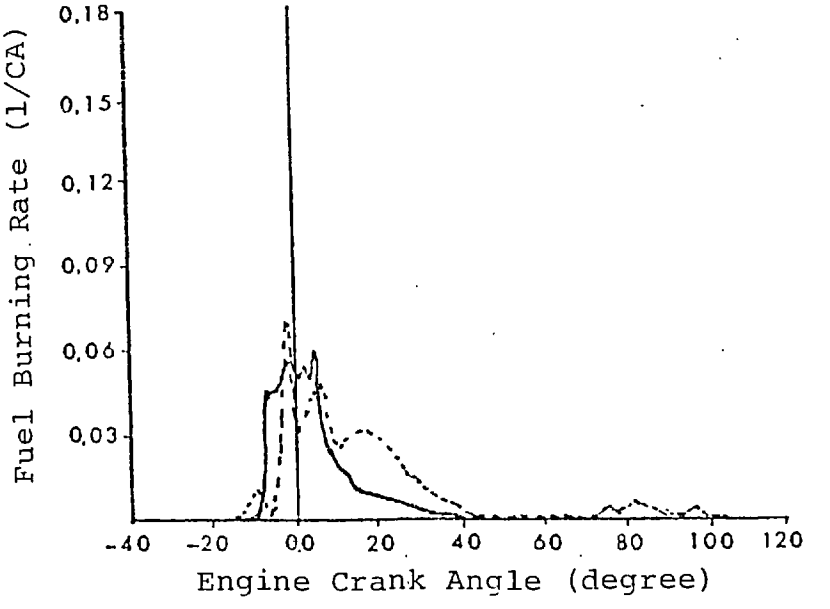

Fig. 6.6. Experimental verification of model predictions (case 6). Engine speed 2000 rev/min, bmep 900 kN/m2

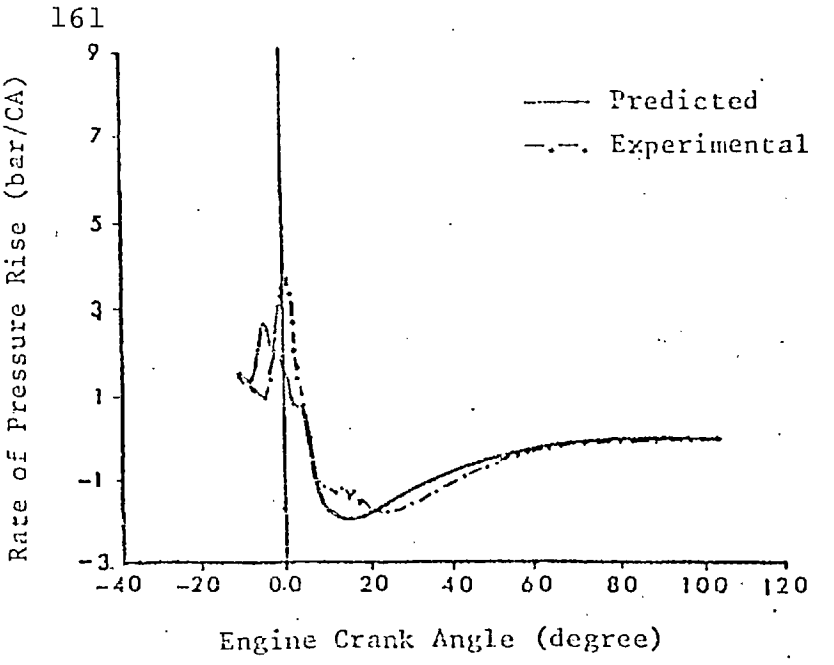

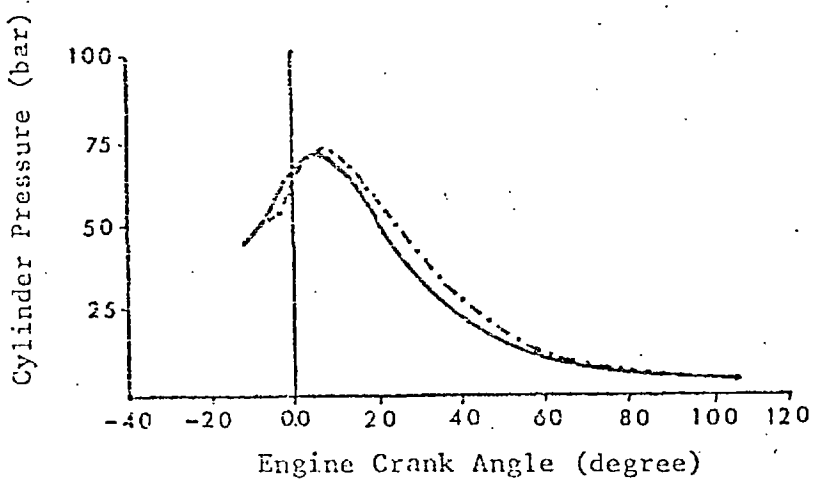

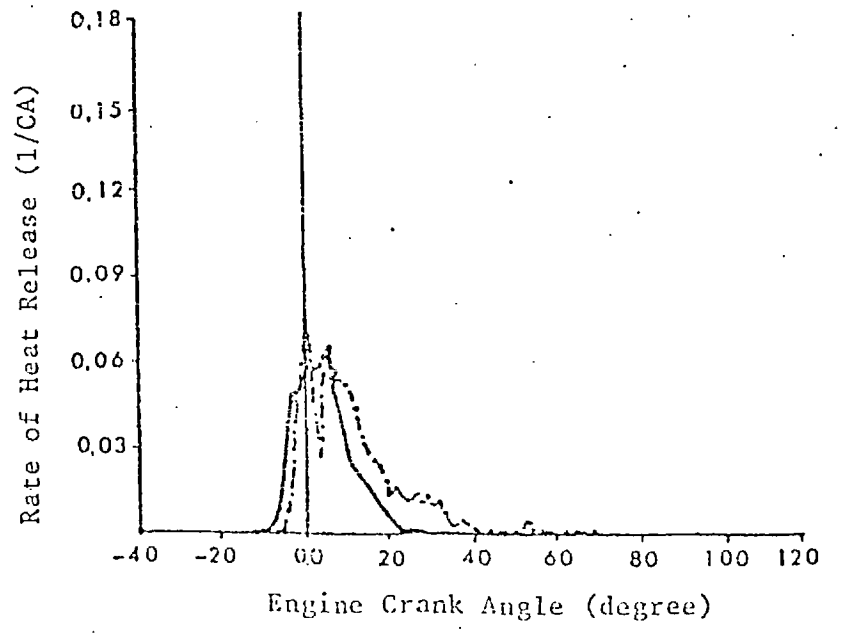

Fig. 6.7. Experimental verification of model predictions (case 7). Engine speed 2500 rev/min, bmep 450 kN/m2

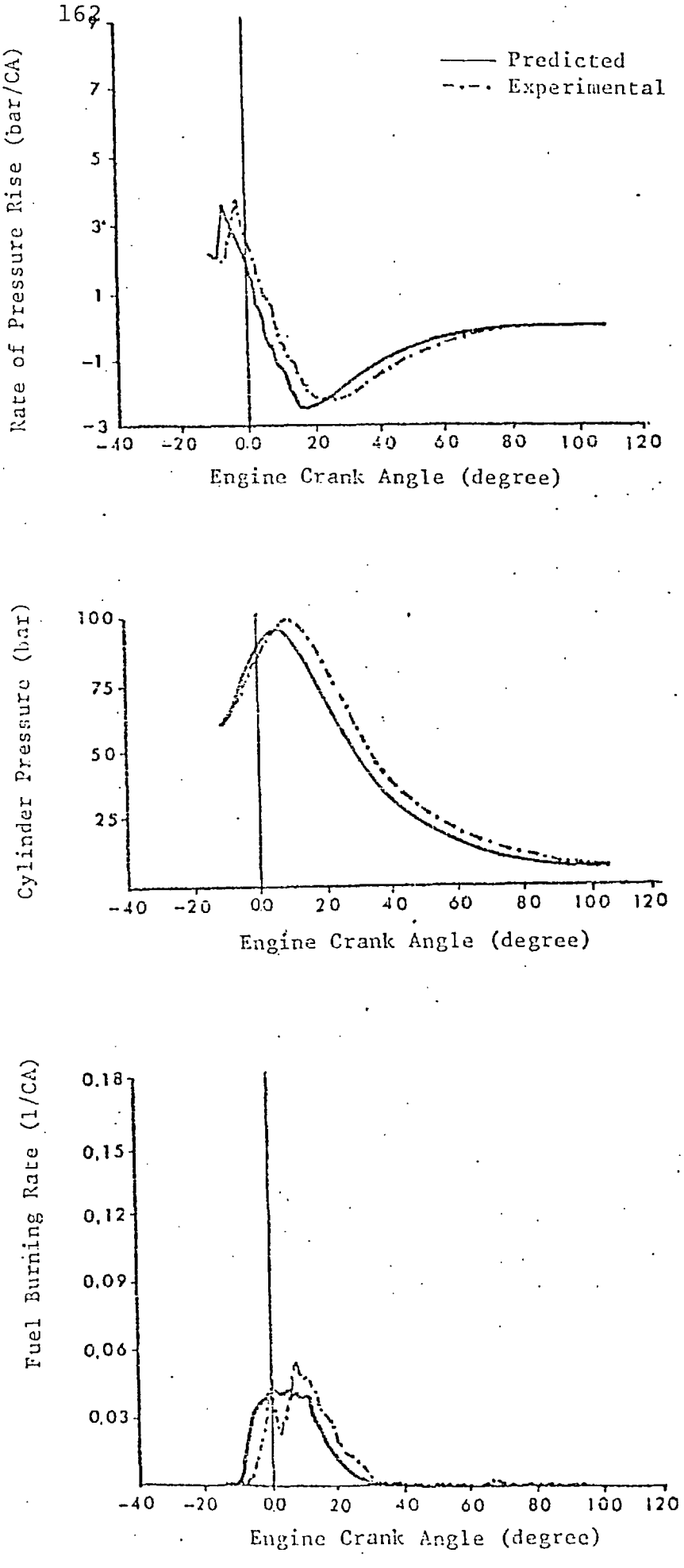

Fig. 6.8. Experimental verification of model predictions (case 8). Engine speed 2500 rev/min, bmep 900 kN/m2

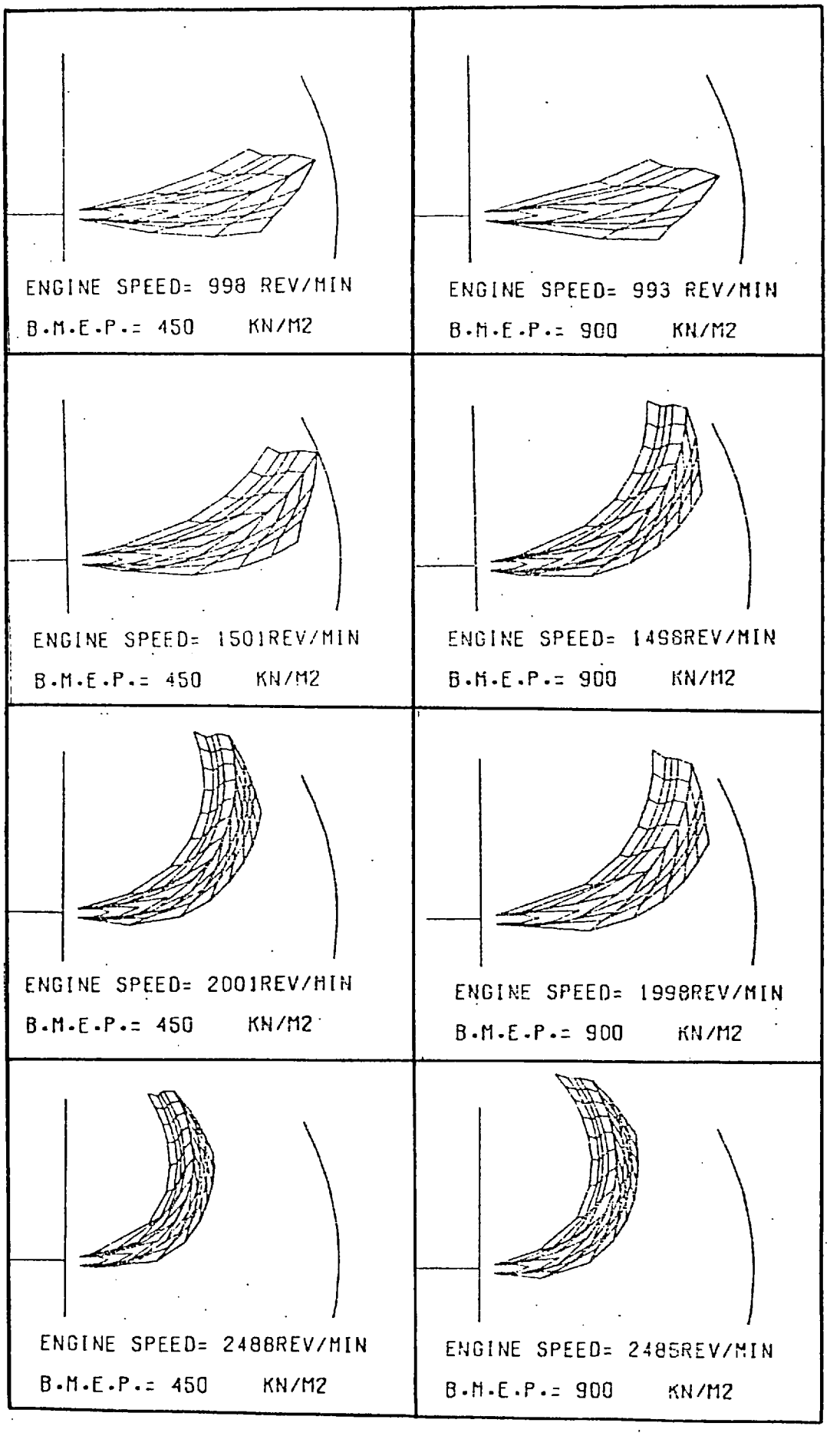

Fig. 6.9. Jet-front displacement every degree crank angle before wall impingement (cases 1 to 8).

phenomena affecting the reaction have been separated. In this way it is easier to subject the model to further improvement if changes in the mixing pattern are required. Furthermore, if the chemical aspect of the reaction is correct and at the same time predicted heat release and cylinder pressures agree with measured data, then it follows that the physical aspects of the mixing pattern must have been correct.

Another advantage in the proper separation of the physical and chemical aspects of the burning process in diesel engines is that at the later stages of combustion the reaction is completely dominated by physical factors. This is because high temperatures dictate very fast reaction rates which are far greater than those allowed by the mixing pattern. This will directly affect the prediction of the rate of heat release during the later stages of diesel engine combustion.

In this model the chemical aspect of the process has been treated in a straightforward manner. The assumptions concerning this part of the problem and the constants employed reveal that the Arrhenius type equation used here deals with the chemical reaction only, such that physical factors are not included in this equation. This does not mean, however, that there is no scope for improvements in the formulation of the chemical aspect of the present model. This simply means that there is more scope in improving the physical aspects, namely, the mixing pattern in this model.

Fig. 6.9 shows the two dimensional jet-front displacement every degree crank angle before wall impingement for cases 1 to 8. It is seen that the calculated path of the jet varies according to engine speed and load. The

effect of engine speed on jet deflection is greater than the effect of load. This is because the increase in injection velocity is less than the increase in swirl velocity with increasing engine speed. The distance of the wall (piston bowl) from the nozzle hole is 35 mm and jet deflection is shown as calculated by equation 3.78 according to injection velocity, swirl velocity and charge density in each case.

Division across the jet indicates that four layers have been considered in the zone division pattern for each case. In chapter five it was explained that the number of layers in the jet (KR) is optional. In fact the accuracy of the results does not change when the computer program is run using the value of 2 or 6 for KR. The same applies to the time step (1 degree crank angle in obtaining the present diagrams, i.e. 0.133, 0.111, 0.083 and 0.066 ms at engine speeds of 1000, 1500, 2000 and 2500 rev/min respectively). Thus a crank angle step of 1 degree is adequate for all the computations in this model.

This gives a relatively large number of zones which is believed to be beneficial if the model is used for predicting the formation of various pollutants in different parts of the spray.

Divisions along the jet indicate jet front positions every degree crank angle. It should be remembered that more divisions along the jet (KR times as many) are necessary to show the zone division pattern. Small divisions inside the jet contours for the first three steps also have not been shown (Fig. 6.9).

It is seen that at part load and low speed (case 1) the jet hits the wall after 6 degrees CA with low deflection, whereas at high load and speed (case 8) the jet deflection is high and wall impingement occurs after 12 degrees CA (measured from commencement of injection).

In section 6.4 each zone will be indicated by one point on a rectangular mesh with zone variables shown on a vertical axis (three dimensional plots). Zone positions can also be presented in the same manner by three dimensional plots. However, it is believed that Fig. 6.9 provides better means of showing zone positions for quick reference. Thus these diagrams are included in the output of the computer program to provide some information on jet development, deflection and zone growth together with the cylinder pressure and heat release predictions shown in Figs. 6.1 to 6.8.

6.3 Effects of varying certain parameters on model predictions

The ability of the present model to predict engine performance during the heat release period was verified experimentally in the previous section. The response of the model to changes in some parameters will be discussed in this section.

Injection timing, swirl ratio, trapped mass and injection rate are altered one by one and the predicted cylinder pressure, rate of pressure rise and rate of heat release curves are presented under each of these conditions (Fig. 6.10 to 6.13).

The predictions at standard conditions for case 3 serve as baseline (bmep = 450 kN/m^2, engine speed = 1500 rev/min, dynamic injection timing = -15.5^{o} BTDC, swirl ratio = 18, fuel/cycle/cylinder = 42.05 mgm, trapped mass = 1.535 gm, injection duration = 8^{o} CA).

The response of the model to changes in injection timing (baseline, 7^{o} advanced and 7^{o} retarded) is shown in Fig. 6.10. Advancing injection results in a longer ignition delay period, largely due to the influence of temperature in the Arrhenius equation (eq. 5.3). Consequently a more rapid initial pressure rise is predicted together with a higher peak cylinder pressure compared to the standard timing. The present model provides the opportunity of studying this phenomenon on a zone-to-zone basis. With advanced timing, when ignition does begin in one zone, there are more zones with favourable mixture concentrations than would be the case with standard timing. Hence initially more fuel burns, resulting in a higher rate of pressure rise. Retarded timing has the opposite effect.

It is also noted that as injection is retarded, the decline in the rate of pressure rise becomes influenced more by piston movement, than by changes in the peak heat release rate. In other words usually a more significant change in the peak heat release rate is associated with an advance rather than a retard in injection timing, whereas the same does not apply to changes in the peak rate of cylinder pressure rise. To discuss the reasons behind this phenomenon the rate of cylinder pressure rise

caused solely due to piston motion (e.g. for a motored engine) should be remembered. Obviously, as the piston moves towards T.D.C., the rate of pressure rise reduces (in absence of ignition or prior to ignition). Thus even if the change in the rate of pressure rise due to ignition were the same for two different injection timings, the peak rate of pressure rise would still be lower for the retarded timing. The peak heat release rate is not affected much, simply because at retarded timings ignition delay is less temperature sensitive (because of high temperatures).

For example the predictions shown in Fig. 6.10 reveal that a 7^{o} advance, increases the peak rate of heat release from 0.11 to 0.17 whereas a 7^{o} retard reduces it only by a small fraction. Nevertheless the change in the peak rate of pressure rise is significant in both cases (i.e. a peak of 6 bar/CA at standard injection timing is changed to 8 bar/CA at 7^{o} advance and to 4 bar/CA at 7^{o} retard).

The effect of changing the swirl ratio is predicted in Fig. 6.11. Obviously a higher swirl ratio in general increases air entrainment. When this is studied on a zone-to-zone basis, it is noted that an increase in the swirl ratio causes an increase in the air mass of all zones. Thus at the moment when the mixture first ignites in one zone all other zones approaching their self-ignition temperature contain more air. Increased swirl therefore results in an increase in the initial combustion rate since more fuel in each zone will be able to burn at this instant. Reducing the quantity of air in these zones by reducing swirl, results in a lower initial rate of pressure rise. It is interesting

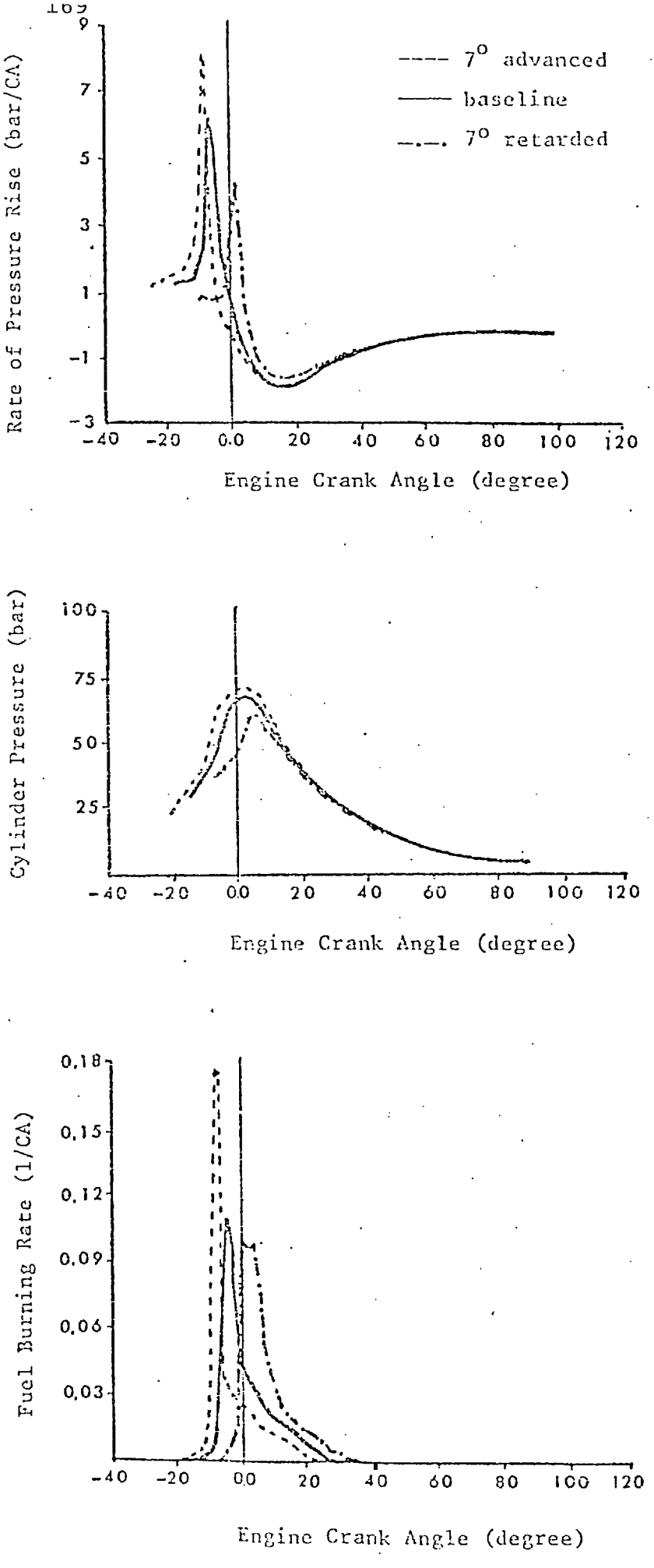

Fig. 6.10. Predicted effect of injection timing (case 3)

to note that ignition delay is hardly effected. Thus the change in the peak rate of pressure rise due to a change in swirl is very similar to the change in the peak heat release rate.

The two variables mentioned above, namely the injection timing and the swirl ratio, may have the same effect on the cylinder pressure but in two different ways.

In the former case advancing the injection timing increases the number of zones that are ready for premixed burning due to a delayed ignition. In the latter case an increased swirl, increases the amount of air in all the zones ready for premixed burning rather than the number of zones. Either way results in an increased initial rate of pressure rise and consequently an increased peak cylinder pressure is obtained.

This discussion shows that increased swirl may increase the peak heat release rate even in cases where the ignition delay is reduced. Such a condition is expected to occur at high loads or at retarded injection timings where ignition is dominated by physical factors. In the present situation (case 3 - Fig. 6.11), temperature appears to be the dominating factor on ignition and thus a % 20 increase or decrease in swirl alters the peak heat release rate without having much effect on ignition delay.

An example in which cylinder temperature has a marked effect on the rate of heat release can be seen in Fig. 6.12. Here a decreased temperature combined with an increased trapped mass, for example due to more effective intercooling on a turbocharged engine, lengthens the ignition delay period.

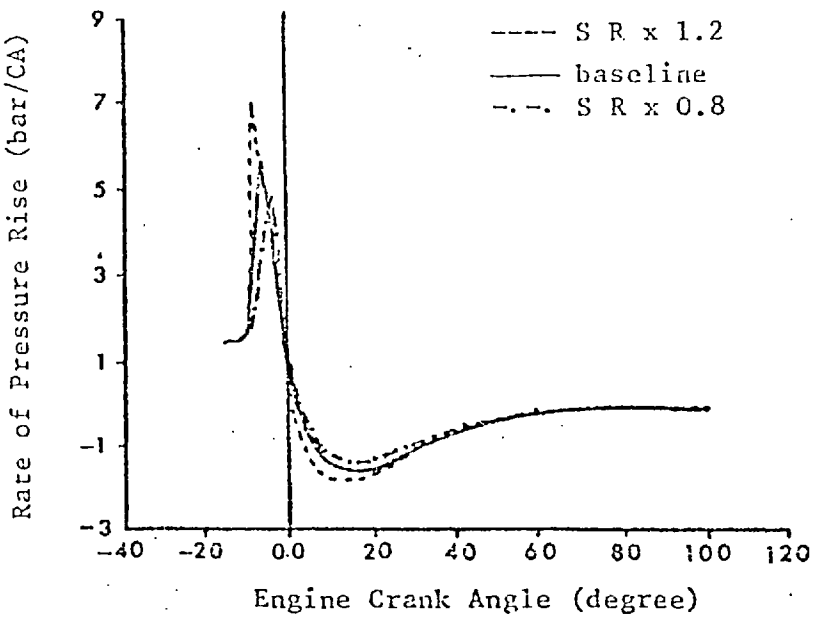

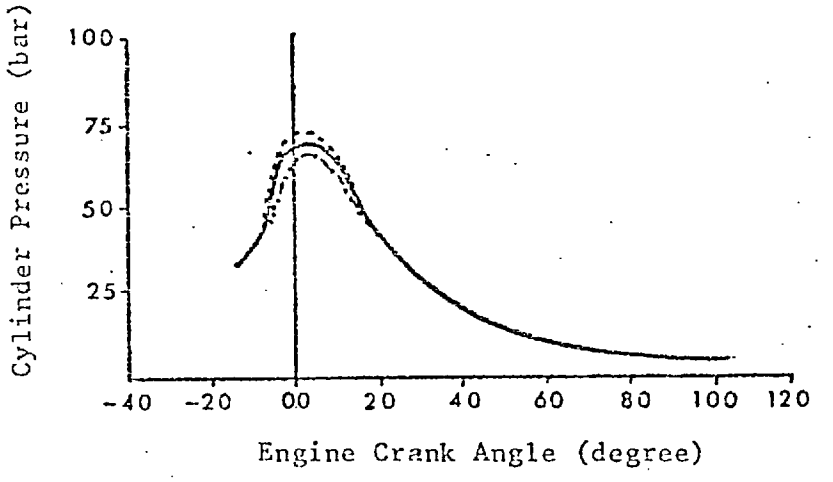

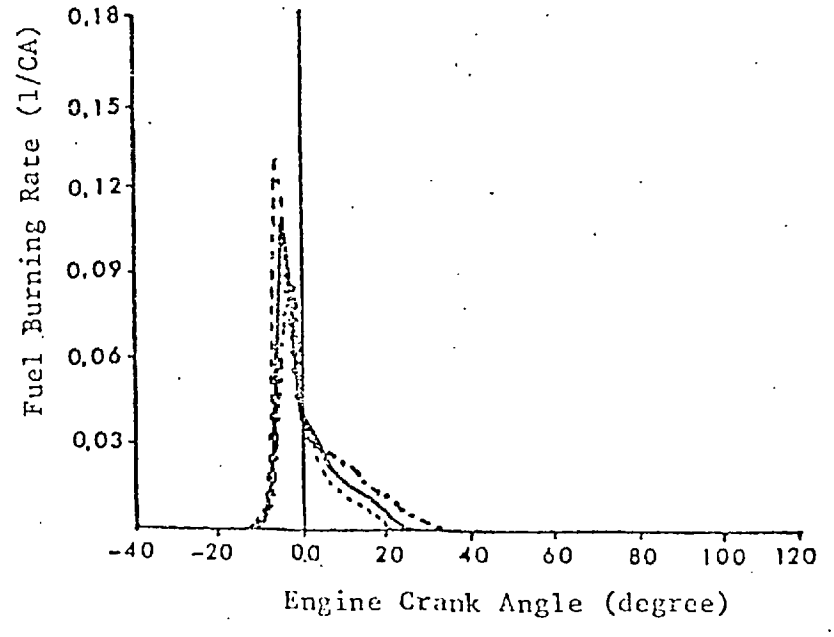

Fig. 6.11. Predicted effect of swirl ratio (case 3).

Swirl momentum and air entrainment are increased. A very rapid initial pressure rise results together with high peak cylinder pressure. With the initial pressure kept constant, initial temperature is very sensitive to the trapped mass. Thus, to investigate this case, the standard conditions for case 3 are compared with two cases where the trapped mass is either increased or decreased by % 5 (i.e. initial temperature is altered by % 5). The result is a substantial change in the peak rate of heat release and in the peak rate of pressure rise in each case (Fig. 6.12). Clearly the main cause here, is the change in the ignition delay period and thus the chemical kinetic aspect of the problem is emphasised.

The effect of varying the injection rate is demonstrated in Fig. 6.13. Here (again for case 3) the injection duration is kept constant and injection rate is altered (% 10 high and % 10 low). Therefore the fuel/cycle/cylinder is also altered (in proportion to the injection rate).

It should be remembered that the heat release rate diagrams are non-dimensional (i.e. fuel burning rate is divided by fuel/cycle/cylinder). Thus to obtain the absolute values, the heat release rate in any of the diagrams presented herein should be multiplied by the fuel/cycle/cylinder.

It is seen that in this case also the response of the model is realistic because higher cylinder pressures are predicted with higher injection rates. The increase in the peak rate of pressure rise is not due to ignition delay. The absolute values of the peak heat release rate are increased due to an increase in the injection rate.

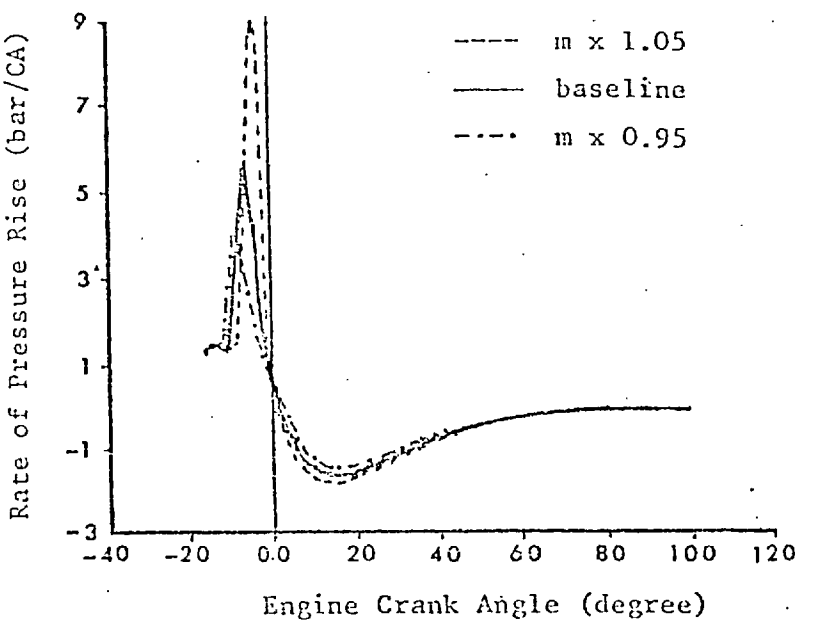

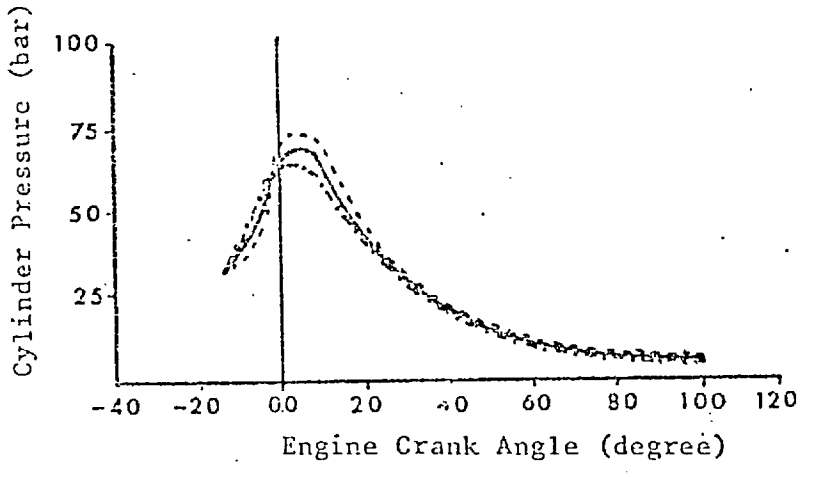

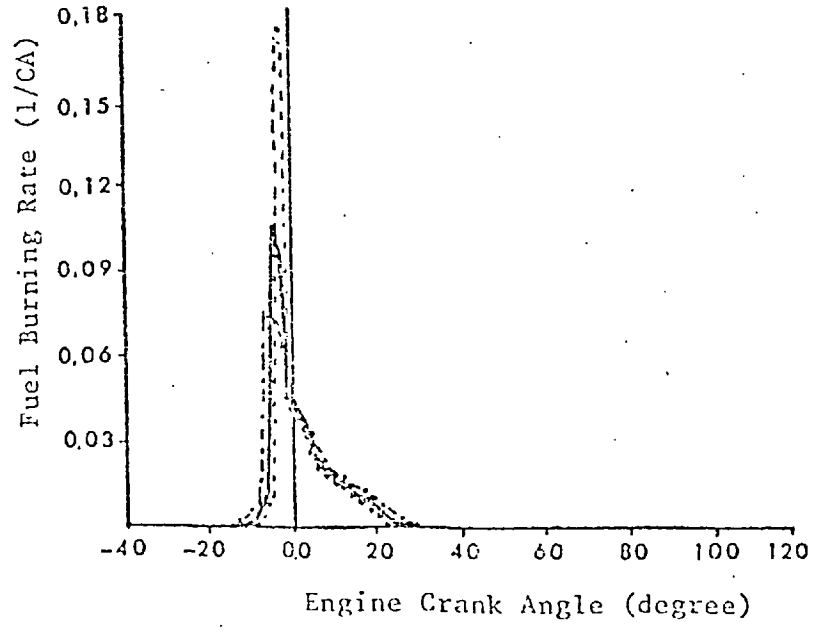

Fig. 6.12. Predicted effect of trapped mass (case 3). Initial pressure is constant, i.e. initial temperature changes.

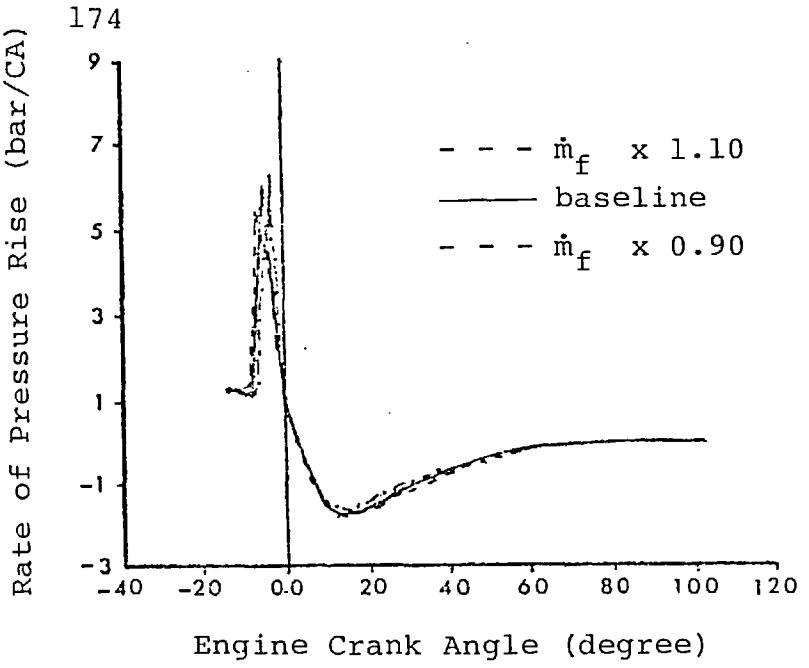

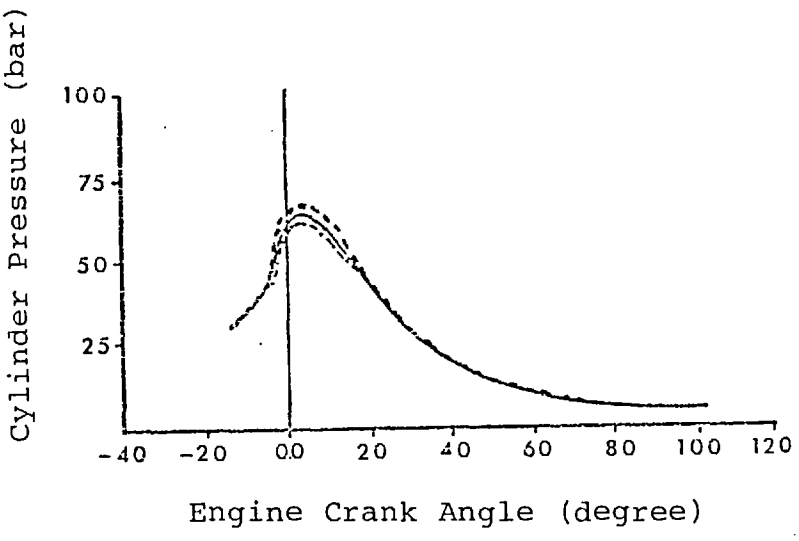

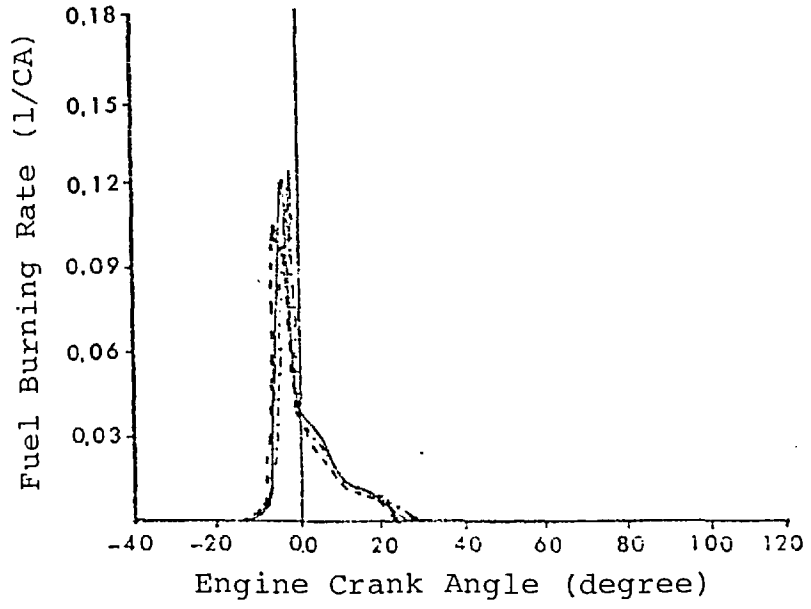

Fig. 6.13. Predicted effect of injection rate _case 3).

An increase in the injection velocity causes an increase in the mass of fuel in each zone combined with an increase in air entrainment. (Note: higher air entrainment in this case does not mean higher air/fuel ratio per zone; it simply means more air and more fuel in each zone). This results in a higher rate of energy release and consequently a higher peak pressure is obtained compared to the standard case. Reduced injection rate has the opposite effect.

Obviously in each of the cases of parametric variation examined above, changes in both chemical and physical factors are involved. But only the effects of the dominant variables have been emphasised in discussing each individual case.

6.4 Investigation of the history and distribution of the predicted zone variables

Case 3 (at part load, 1500 rev/min) and case 8 (at high load, 2500 rev/min) were chosen for investigation of the temporal and spacial distribution of zone variables. This is an interesting feature of the multizone structure of the present model. Apart from providing useful information on various phenomena occurring during combustion, this study demonstrates the merits of the model so far as future polutant formation predictive capabilities are concerned.

Figs. 6.14 and 6.15 show the initiation and development of combustion within a fuel spray, expressed as the percentage of fuel burnt in each individual zone.

A uniform rectangular mesh is used for convenience. Thus each point of the mesh represents a zone and each diagram indicates zone conditions at one degree crank angle interval.

In this case, the first diagram is at 7^{o} after the commencement of injection. A total of 8 diagrams are constructed to demonstrate the individual zone history and distribution for each variable (b_z in this case). Thus the last diagram is at 14^{o} after commencement of injection (i.e. 6 degrees after the end of injection).

It is seen that six layers are considered in the zone division pattern. Therefore at the end of injection there are 8 x 6 x 6 i.e. 288 zones in a diagram. From then onwards no more zones are created and the existing zones continue their motion within the moving jet bounderies according to the pattern explained before (chapter 3).

Zones at the jet front, centreline, jet back and jet fringe constitute the four sides of the rectangular mesh (centreline being shown towards the front of the figure).

On the vertical axis in this case b_z is shown, taking values between zero (i.e. no fuel burnt in the zone) and unity (complete combustion).

Combustion is seen to start in a zone behind the jet front but near its edge, and rapidly spreads towards zones at the jet-front, back and centreline. Thus substantial premixed burning occurs at this particular test condition (part load).

14^{o} after the commencement of injection, only some of the zones at the edge of the fuel spray have received sufficient air to burn completely. More transverse zones will be required to reveal an area at the jet fringe that is too weak to burn.

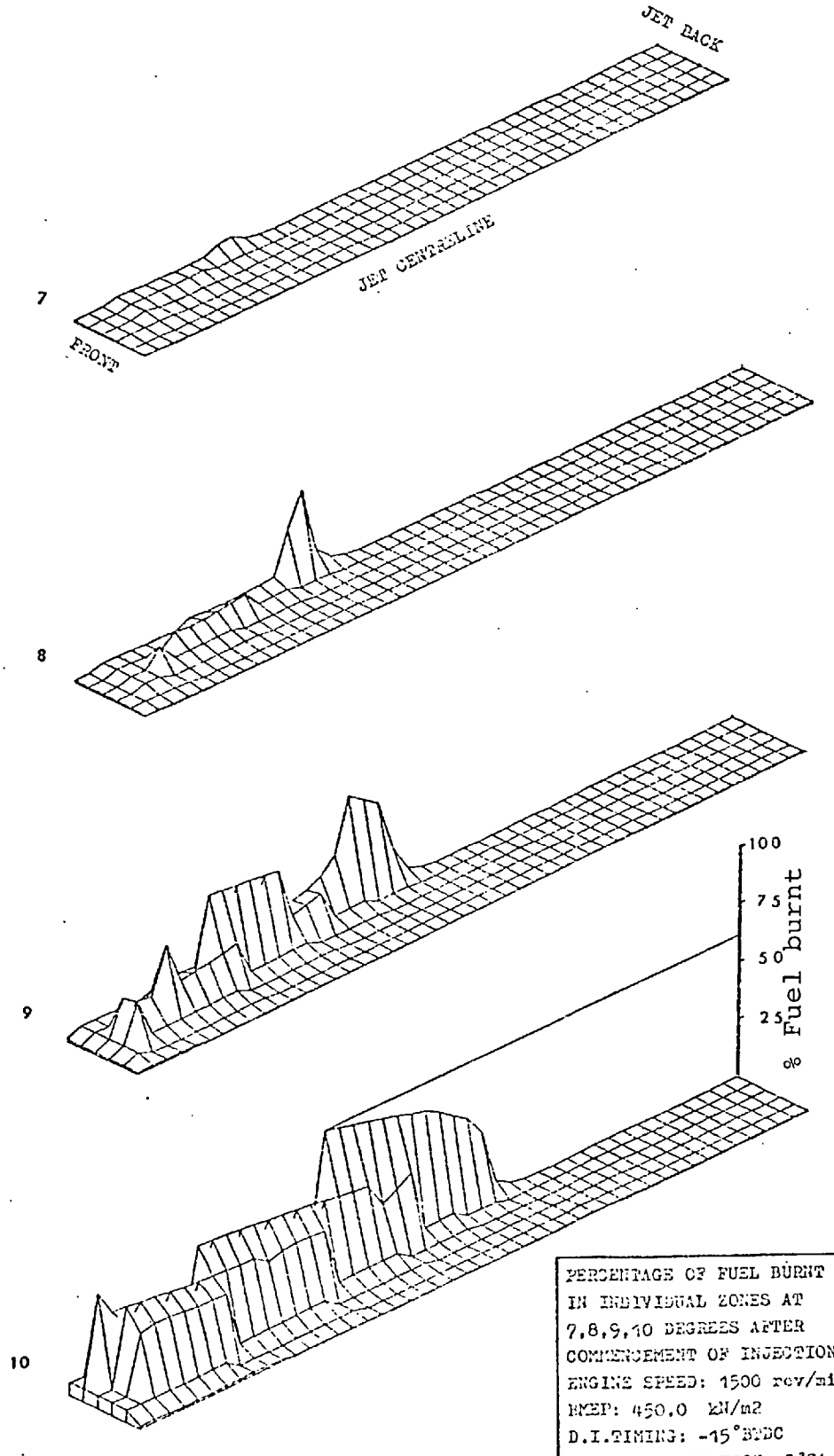

PERCENTAGE OF FUEL BURNT IN INDIVIDUAL ZONES AT 7,8,9,10 DEGREES AFTER COMMENCEMENT OF INJECTION.
ENGINE SPEED: 1500 rev/min
BMEP: 450.0 kN/m2
D.I.TIMING: -15°BTDC
INJECTION DURATION: 8°CA

Fig. 6.14.

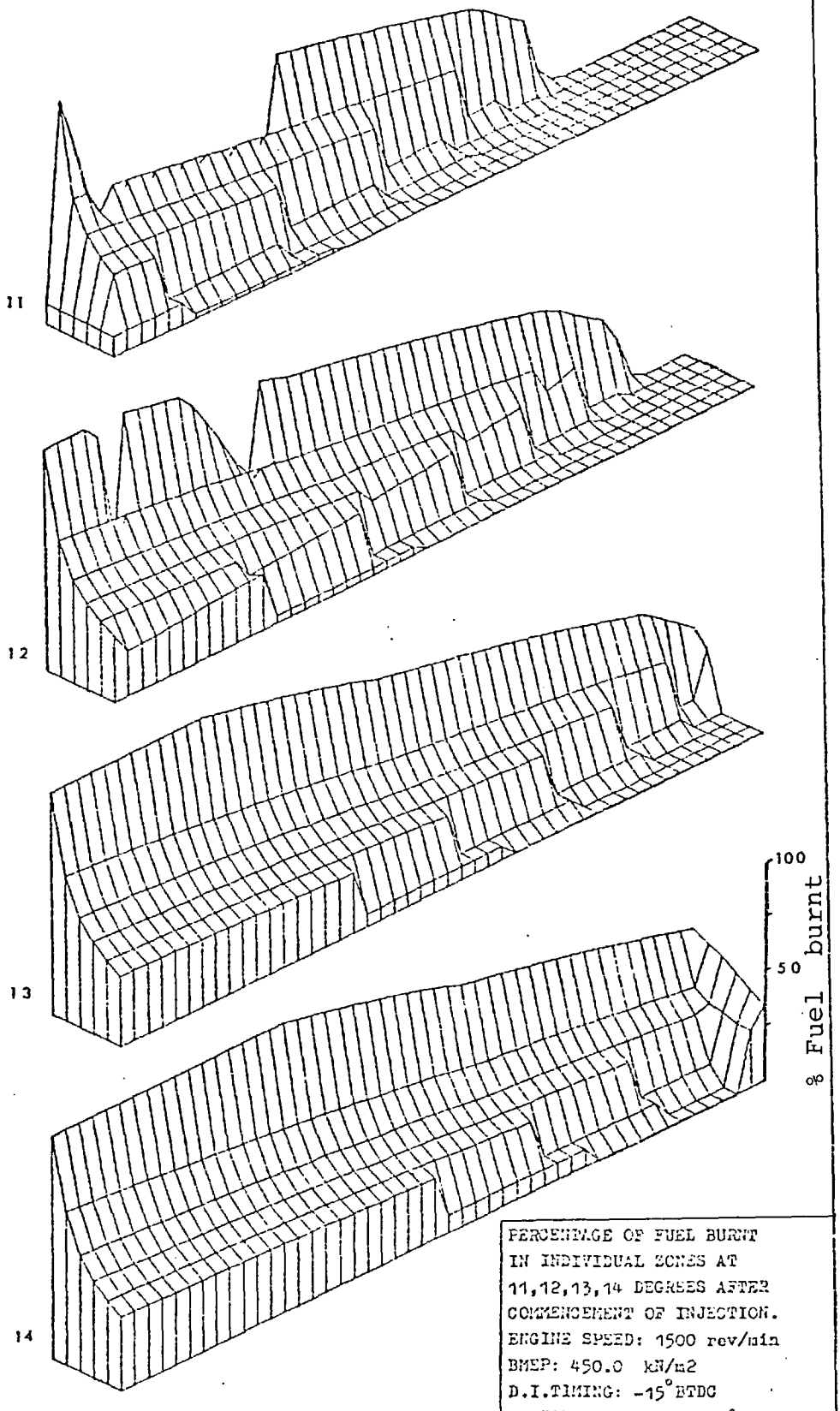

PERCENTAGE OF FUEL BURNT
IN INDIVIDUAL ZONES AT
11,12,13,14 DEGREES AFTER
COMMENCEMENT OF INJECTION.
ENGINE SPEED: 1500 rev/min
BMEP: 450.0 kN/m2
D.I.TIMING: -15° BTDC
INJECTION DURATION: 8°CA

Fig. 6.15.

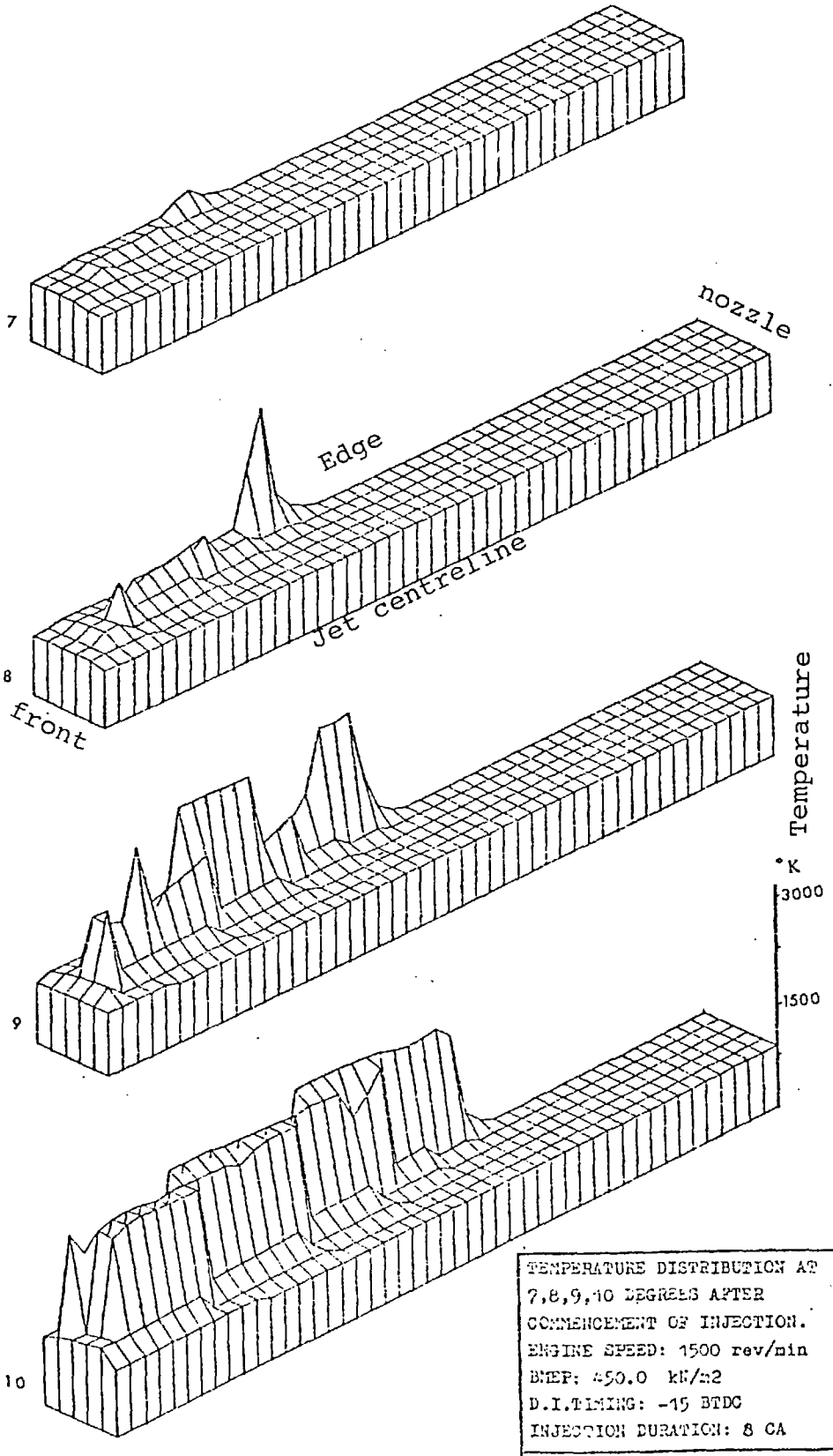

TEMPERATURE DISTRIBUTION AT 7,8,9,10 DEGREES AFTER COMMENCEMENT OF INJECTION.
ENGINE SPEED: 1500 rev/min
BMEP: 450.0 kN/m2
D.I.TIMING: -15 BTDC
INJECTION DURATION: 8 CA

Fig. 6.16.

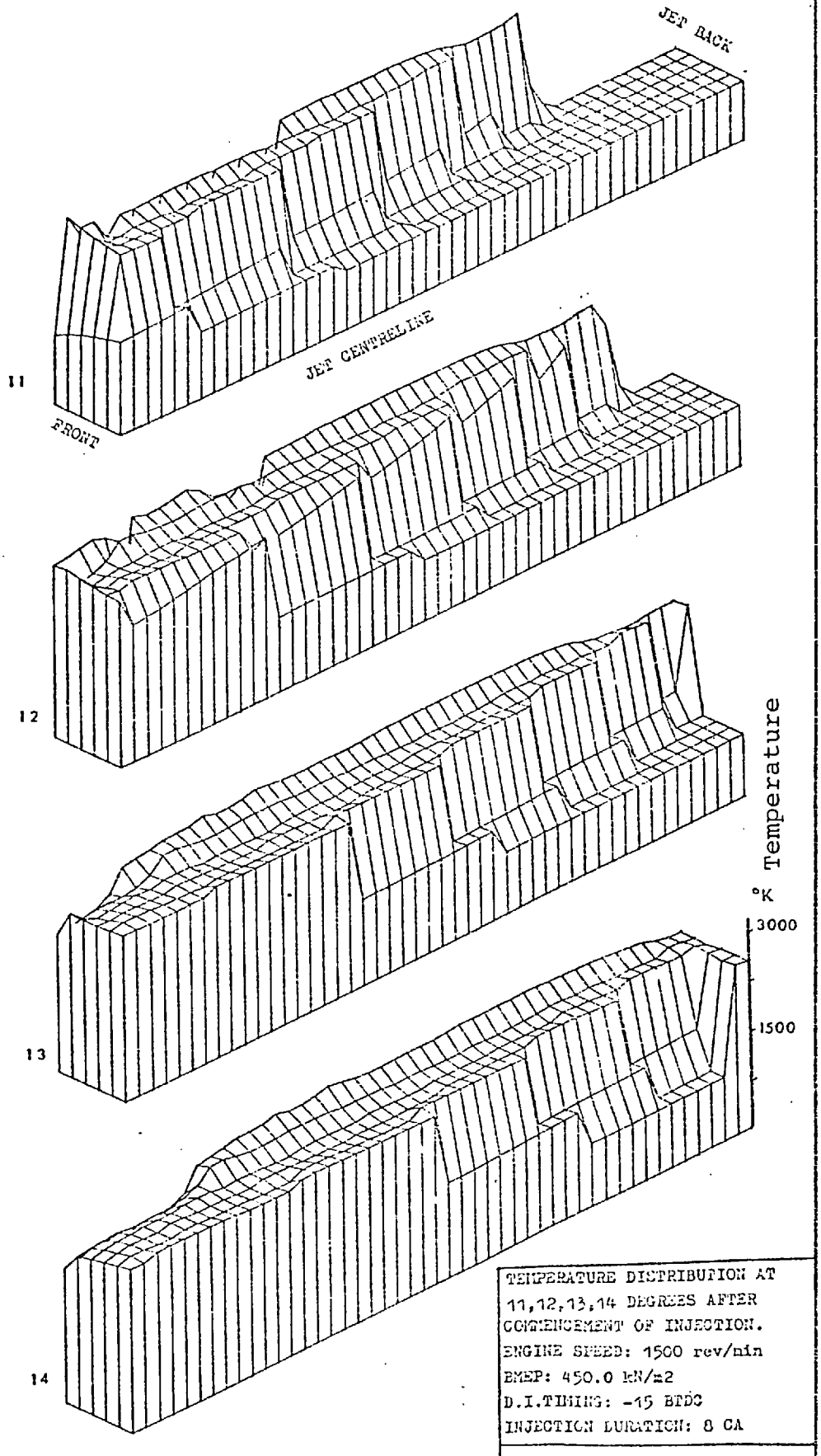

TEMPERATURE DISTRIBUTION AT 11,12,13,14 DEGREES AFTER COMMENCEMENT OF INJECTION.
ENGINE SPEED: 1500 rev/min
BMEP: 450.0 kN/m2
D.I.TIMING: -15 BTDC
INJECTION DURATION: 8 CA

Fig. 6.17.

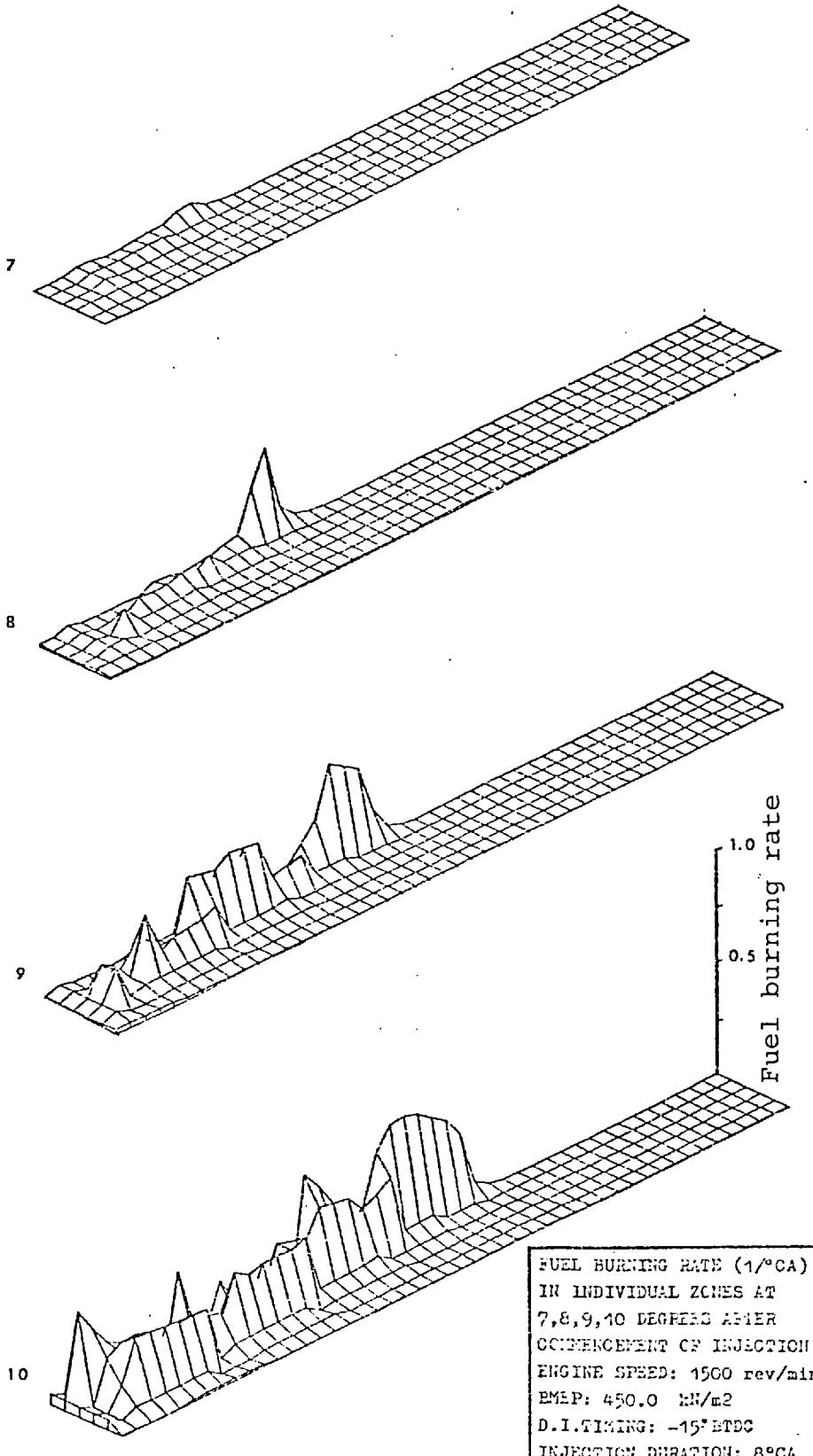

FUEL BURNING RATE (1/°CA)
IN INDIVIDUAL ZONES AT
7,8,9,10 DEGREES AFTER
COMMENCEMENT OF INJECTION.
ENGINE SPEED: 1500 rev/min
BMEP: 450.0 KN/m2
D.I.TIMING: -15° BTDC
INJECTION DURATION: 8°CA

Fig. 6.18.

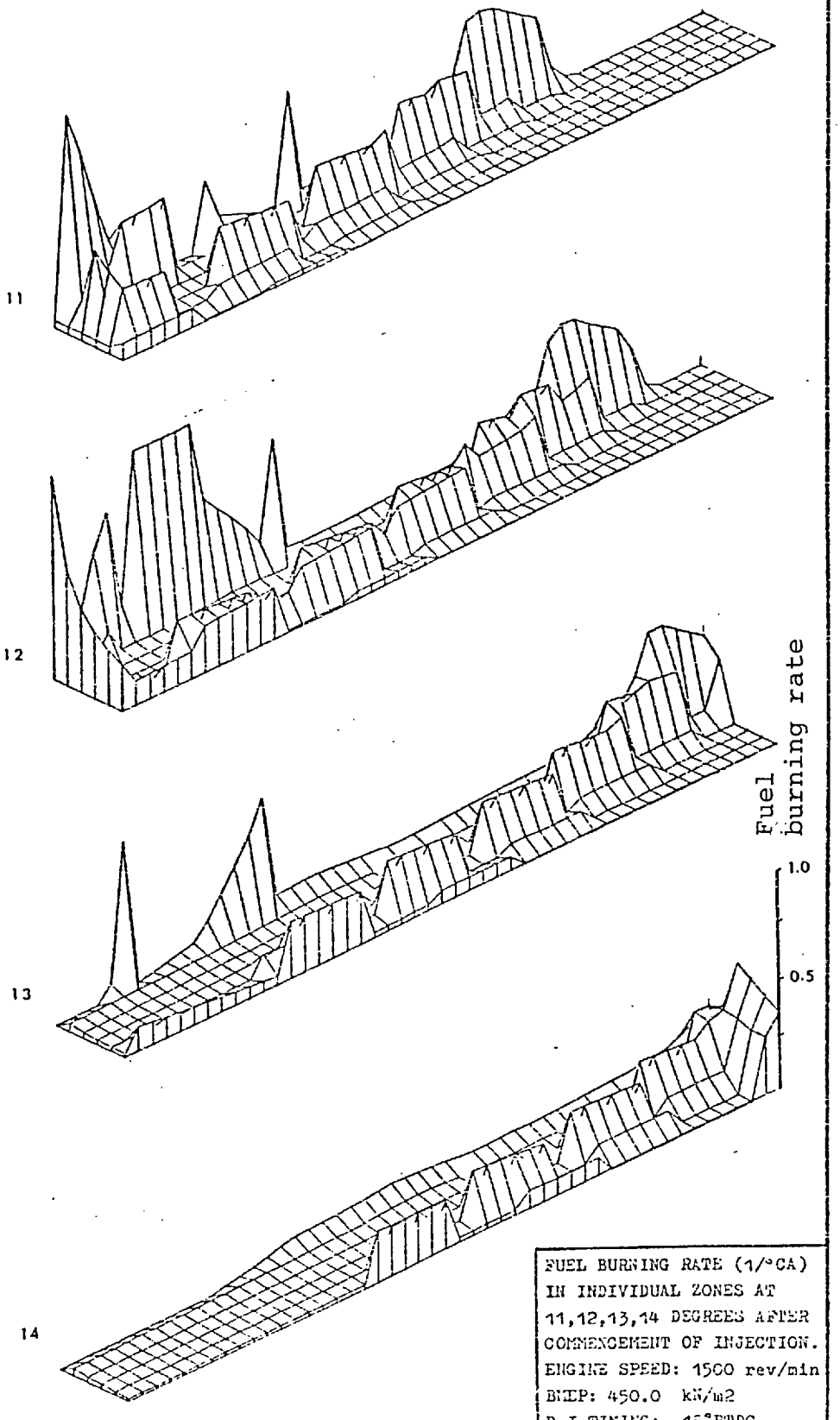

FUEL BURNING RATE (1/°CA)
IN INDIVIDUAL ZONES AT
11,12,13,14 DEGREES AFTER
COMMENCEMENT OF INJECTION.
ENGINE SPEED: 1500 rev/min
BMEP: 450.0 kN/m2
D.I.TIMING: -15°BTDC
INJECTION DURATION: 8°CA

Fig. 6.19.

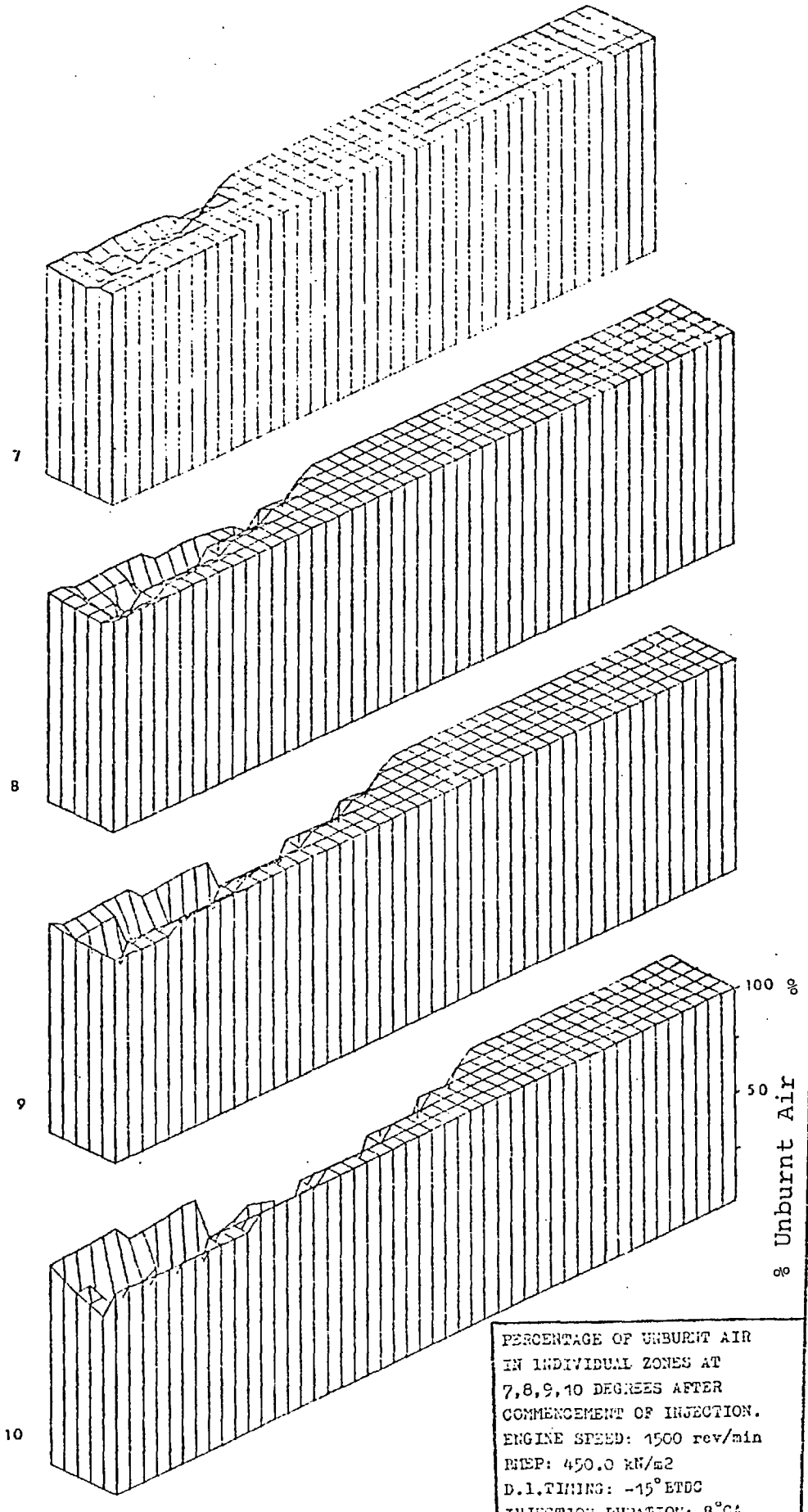

PERCENTAGE OF UNBURNT AIR IN INDIVIDUAL ZONES AT 7,8,9,10 DEGREES AFTER COMMENCEMENT OF INJECTION.
ENGINE SPEED: 1500 rev/min
BMEP: 450.0 kN/m2
D.I.TIMING: -15°ETDC
INJECTION DURATION: 8°CA

Fig. 6.20.

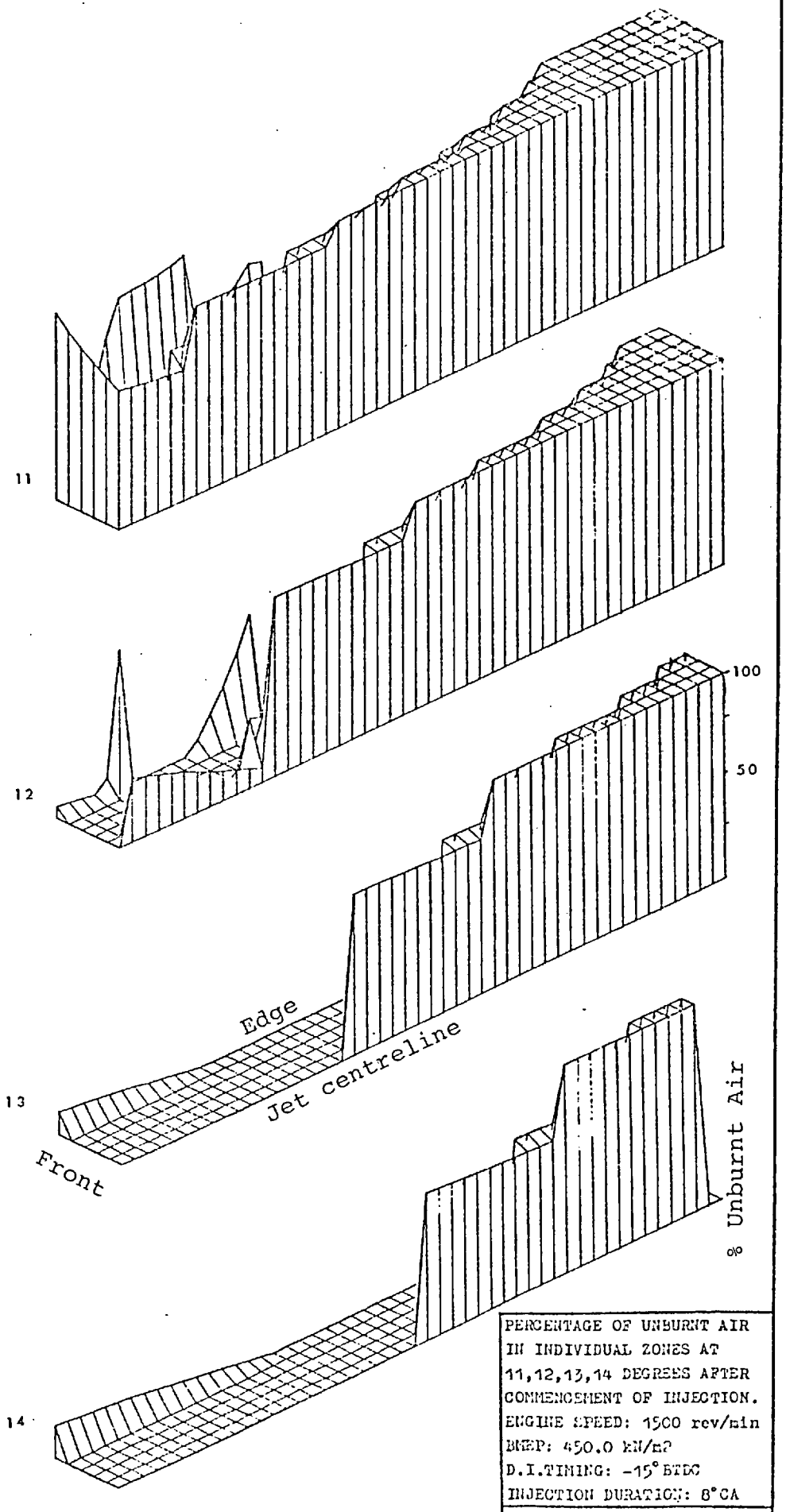

PERCENTAGE OF UNBURNT AIR IN INDIVIDUAL ZONES AT 11,12,13,14 DEGREES AFTER COMMENCEMENT OF INJECTION.
ENGINE SPEED: 1500 rev/min
BMEP: 450.0 kN/m²
D.I.TIMING: -15° BTDC
INJECTION DURATION: 8°CA

Fig. 6.21.

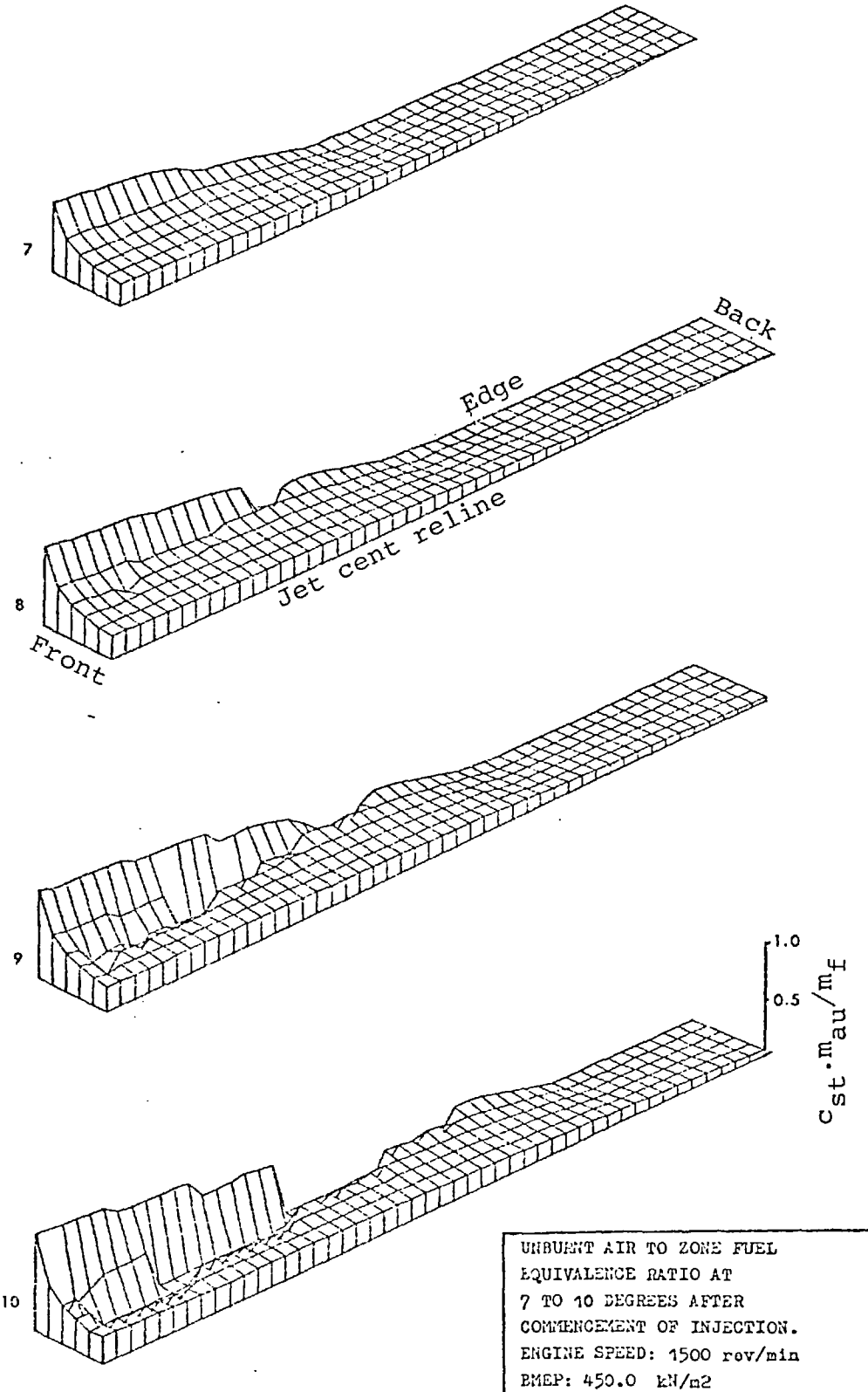

UNBURNT AIR TO ZONE FUEL EQUIVALENCE RATIO AT 7 TO 10 DEGREES AFTER COMMENCEMENT OF INJECTION.
ENGINE SPEED: 1500 rev/min
BMEP: 450.0 kN/m2
D.I.TIMING: -15°BTDC
INJECTION DURATION: 8°CA

Fig. 6.22.

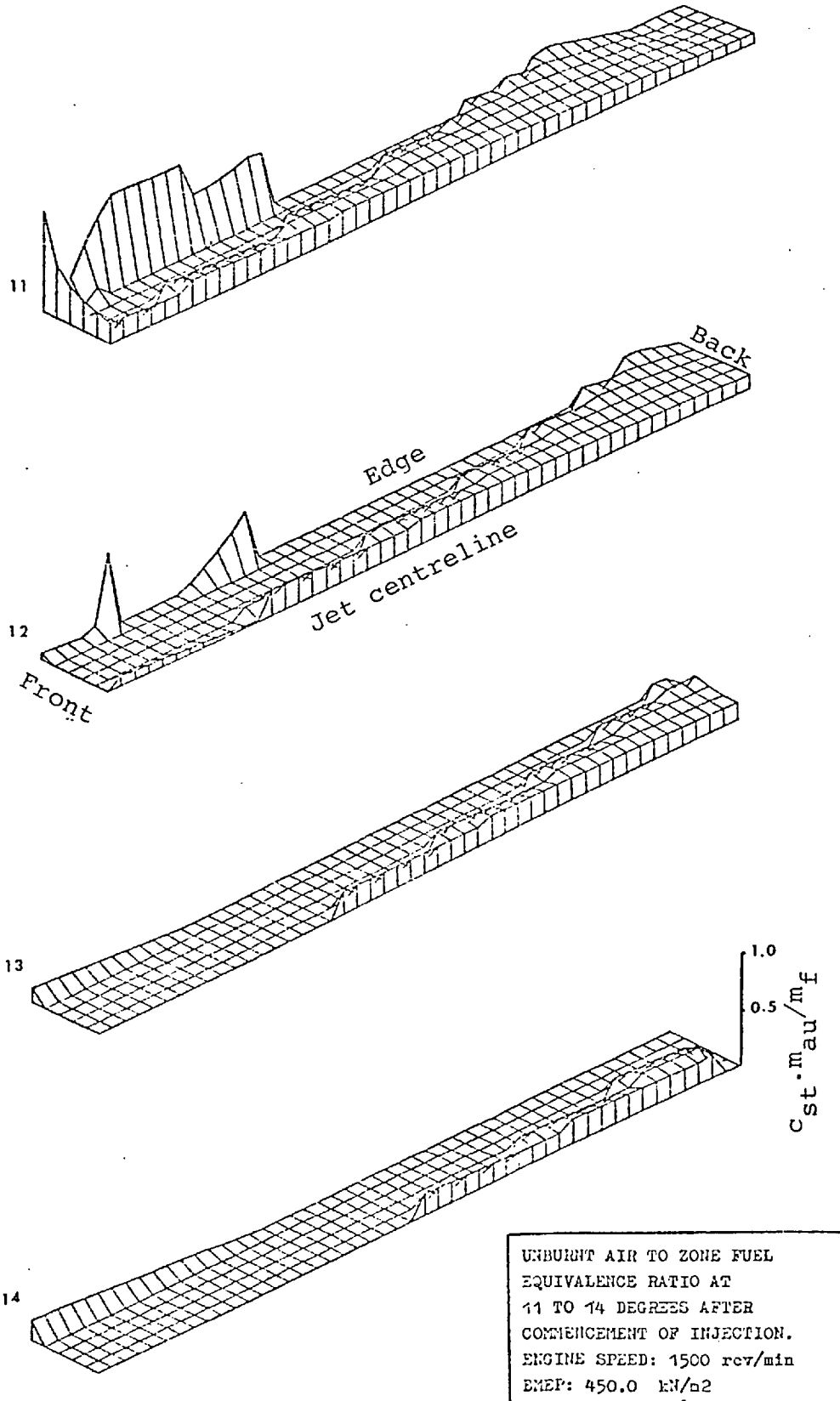

UNBURNT AIR TO ZONE FUEL EQUIVALENCE RATIO AT 11 TO 14 DEGREES AFTER COMMENCEMENT OF INJECTION.
ENGINE SPEED: 1500 rev/min
BMEP: 450.0 kN/m2
D.I.TIMING: -15°BTDC
INJECTION DURATION: 8°CA

Fig. 6.23.

The pattern of temperature distribution (Fig. 6.16 and 6.17) is similar to that of burnt fuel, except where further air enters a zone in which combustion is complete. This reduces the temperature for example at the front corner zones 13^{o} to 14^{o} after the beginning of injection.

The fuel burning rate distribution diagrams (Fig. 6.18 and 6.19 show that at 14^{o} after the start of injection, there is evidence of very low burning rates in most zones of the fuel spray (e.g. on the centre line towards the jet front). However. Fig. 6.14 and 6.15 reveal that a large amount of fuel remains to be burnt in these zones. Insufficient air is available. Thus these areas of low burning rate are diffusion controlled and it is the large number of these zones in total that contribute to the significant total heat release rate by diffusion burning, according to the assumptions of the model.

Fig. 6.20 and 6.21 show the history and distribution of unburnt air expressed as percentage of total air in the zone (total air is the unburnt air plus that present in the products of a locally stoichiometric combustion). The initiation of combustion is marked in these diagrams by the appearance of a pit (in diagram 7) behind the jet front, indicating that some air in these zones has taken part in the reaction. These diagrams provide information on the state of zones affected by air-limited combustion. For example diagrams 13 and 14 contain a large number of zones in which all the available air has burnt. A look at the same diagram numbers in Figures 6.14 and 6.15 reveals that there is still some unburnt fuel in these zones. At the

same time the burning rate diagrams (Fig. 6.18 and 6.19) show that some burning (however small) is taking place in these zones. Thus the burning in each of these zones is controlled by the small amount of air entering the zones during each step (i.e. at this stage of the zone the air takes part in the reaction as it enters the zone).

Further diagrams may be constructed to demonstrate any other property of the zones such as position or equivalence ratio. A set of useful diagrams for example are those shown in Fig. 6.22 and 6.23. These are constructed for the purpose of showing the difference in the burnt equivalence ratio of the zones at various parts of the jet. It is noted that the available unburnt air is divided by the total mass of the zone fuel (burnt plus unburnt) and is further divided by the stoichiometric air fuel ratio ($m_{au} \cdot c_{st}/m_f$). These diagrams show that the zones at the front and edge of the spray contain more air than the zones at the back and centreline. Consequently it becomes clear why the percentage of burnt fuel is different in two zones which may have the same percentage of burnt air (something which is not readily demonstrated in the previous diagrams).

Similarly, the same sets of diagrams are constructed in Fig. 6.24 to 6.33 for engine running conditions at high speed and load (case 8: bmep = 900 kN/m^2, engine speed = 2500 rev/min, dynamic injection timing = -12^o BTDC, swirl ratio = 18, fuel/cycle cylinder = 82.64 mgm, trapped mass = 2.128 gm and injection duration = 18^o CA).

At this test condition the turbochanger develops high inlet manifold pressure and temperature. Hence the

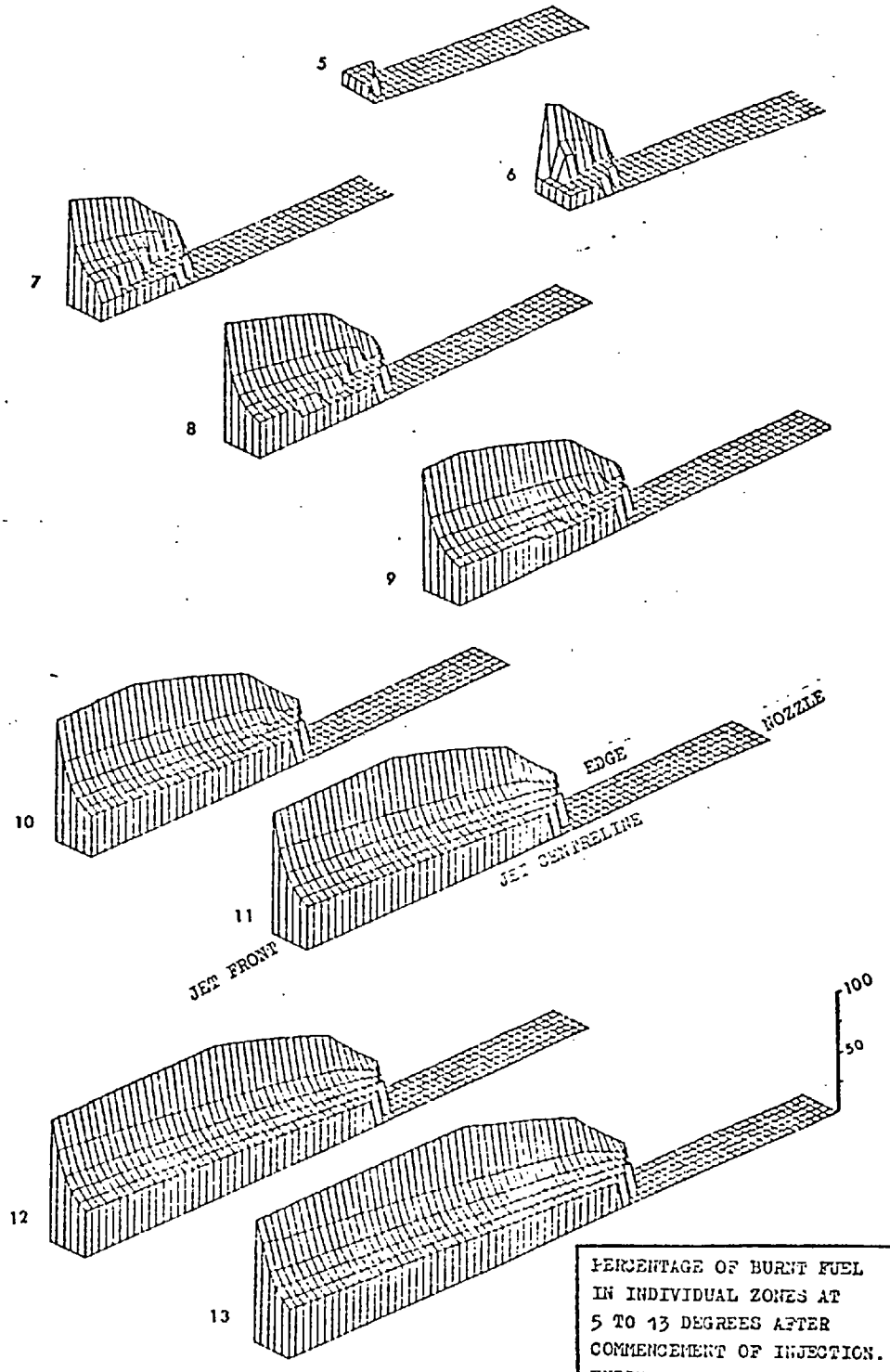

PERCENTAGE OF BURNT FUEL
IN INDIVIDUAL ZONES AT
5 TO 13 DEGREES AFTER
COMMENCEMENT OF INJECTION.
ENGINE SPEED: 2500 rev/min
BMEP: 900.0 kN/m2
D.I.TIMING: -12°BTDC
INJECTION DURATION: 18°CA

Fig. 6.24.

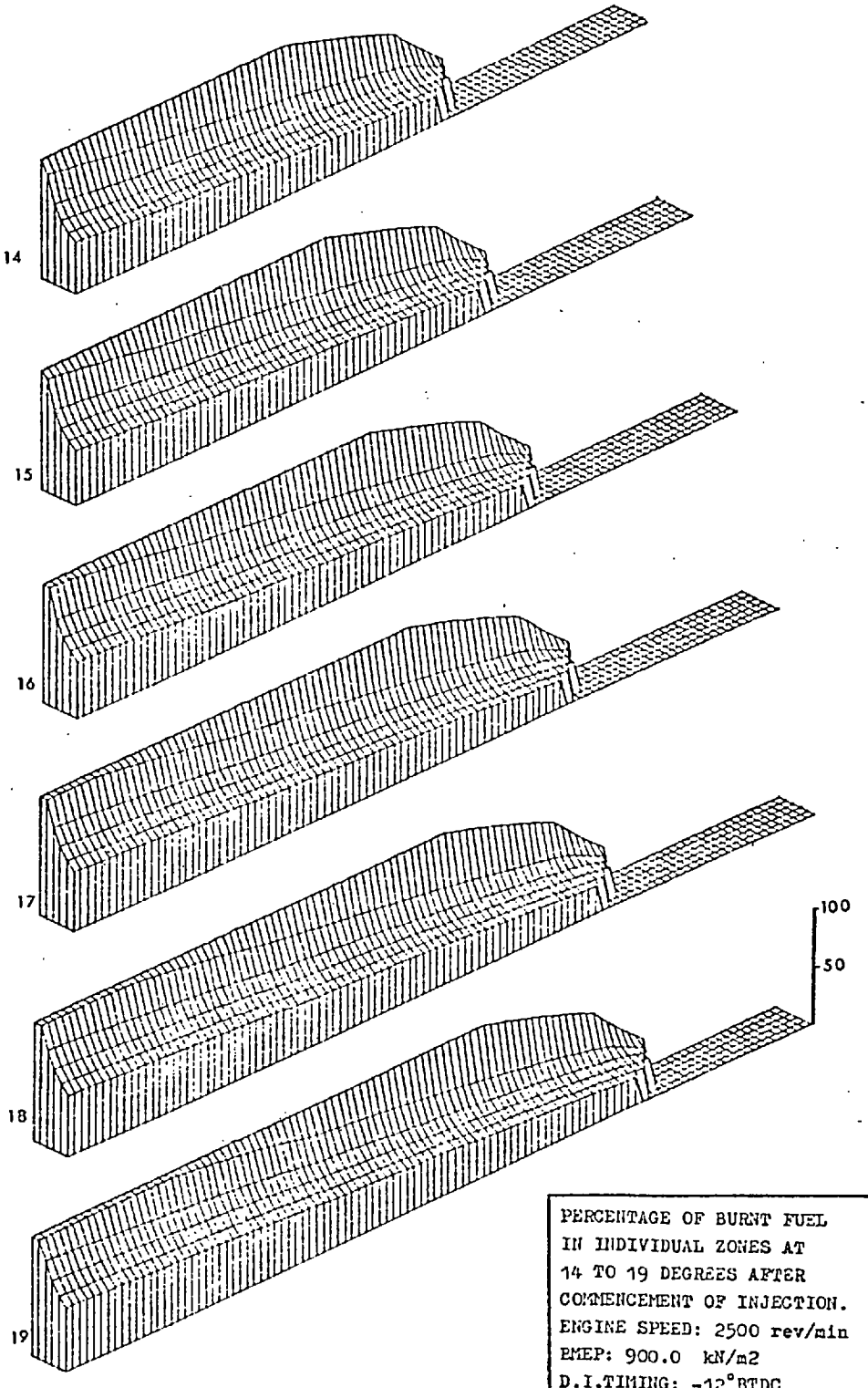

PERCENTAGE OF BURNT FUEL
IN INDIVIDUAL ZONES AT
14 TO 19 DEGREES AFTER
COMMENCEMENT OF INJECTION.
ENGINE SPEED: 2500 rev/min
EMEP: 900.0 kN/m2
D.I.TIMING: -12°BTDC
INJECTION DURATION: 18°CA

Fig. 6.25.

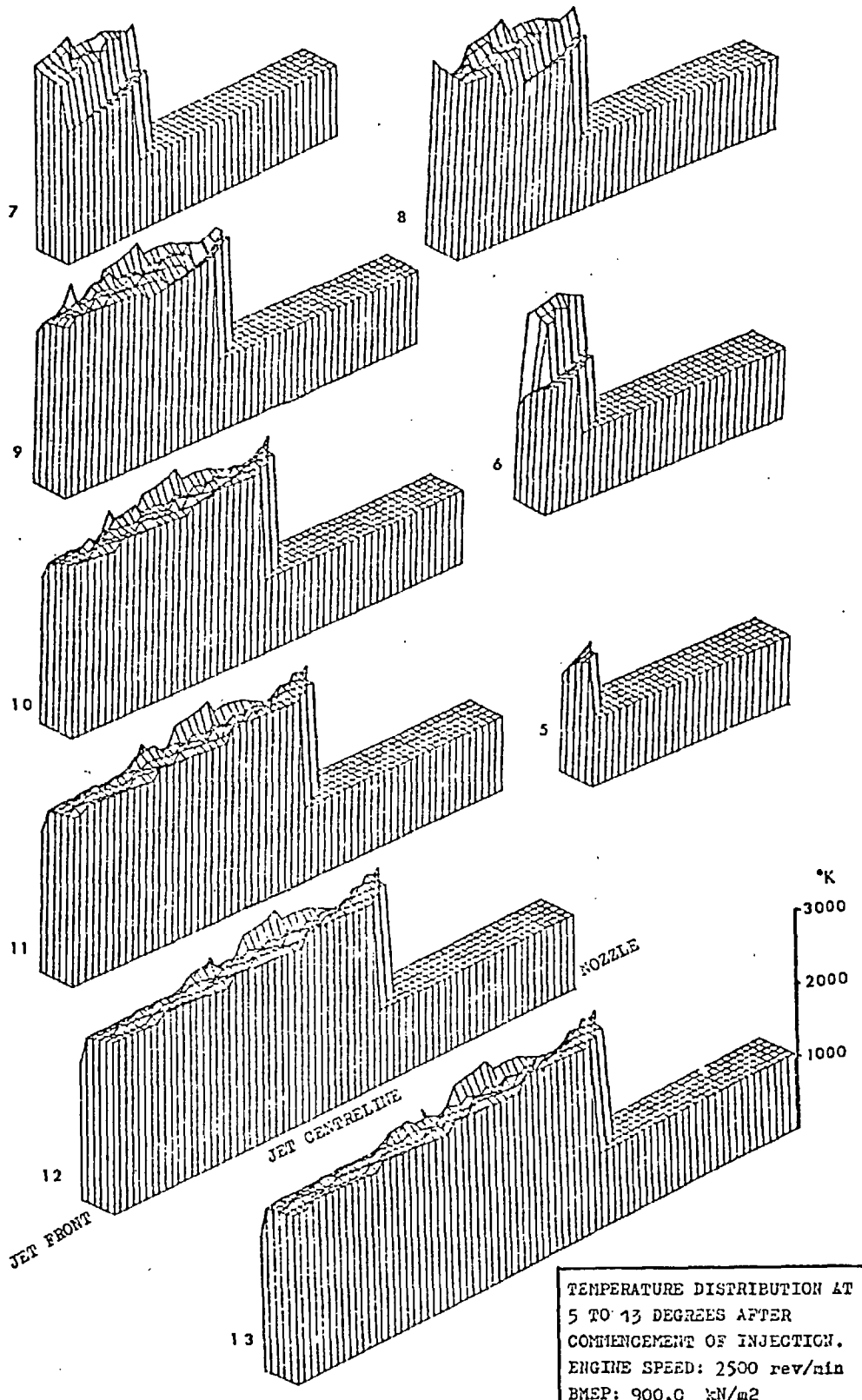

TEMPERATURE DISTRIBUTION AT
5 TO 13 DEGREES AFTER
COMMENCEMENT OF INJECTION.
ENGINE SPEED: 2500 rev/min
BMEP: 900.0 kN/m2
D.I.TIMING: -12°BTDC
INJECTION DURATION: 18°CA

Fig. 6.26.

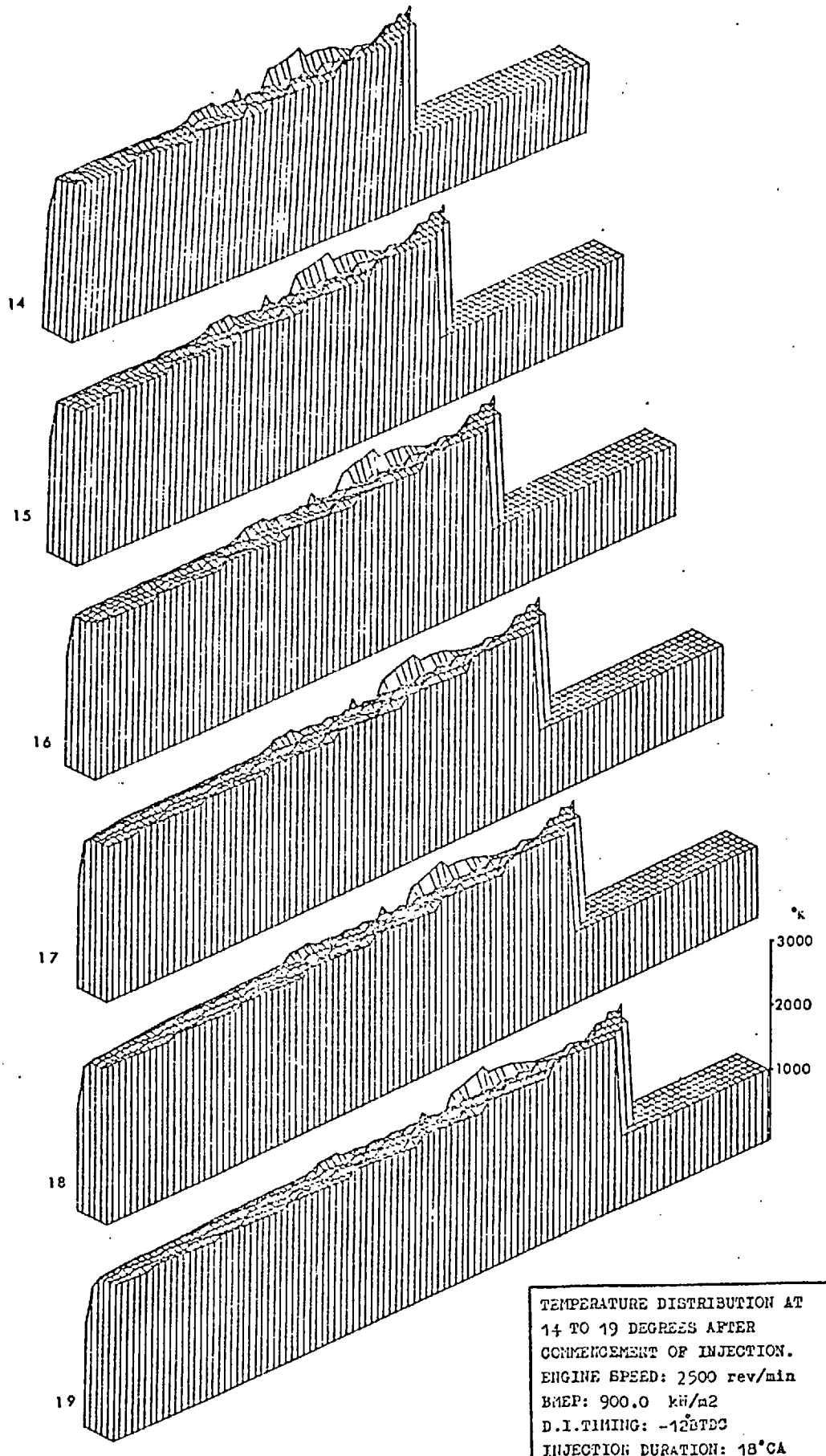

TEMPERATURE DISTRIBUTION AT 14 TO 19 DEGREES AFTER COMMENCEMENT OF INJECTION.
ENGINE SPEED: 2500 rev/min
BMEP: 900.0 kN/m2
D.I.TIMING: -12°BTDC
INJECTION DURATION: 18°CA

Fig. 6.27.

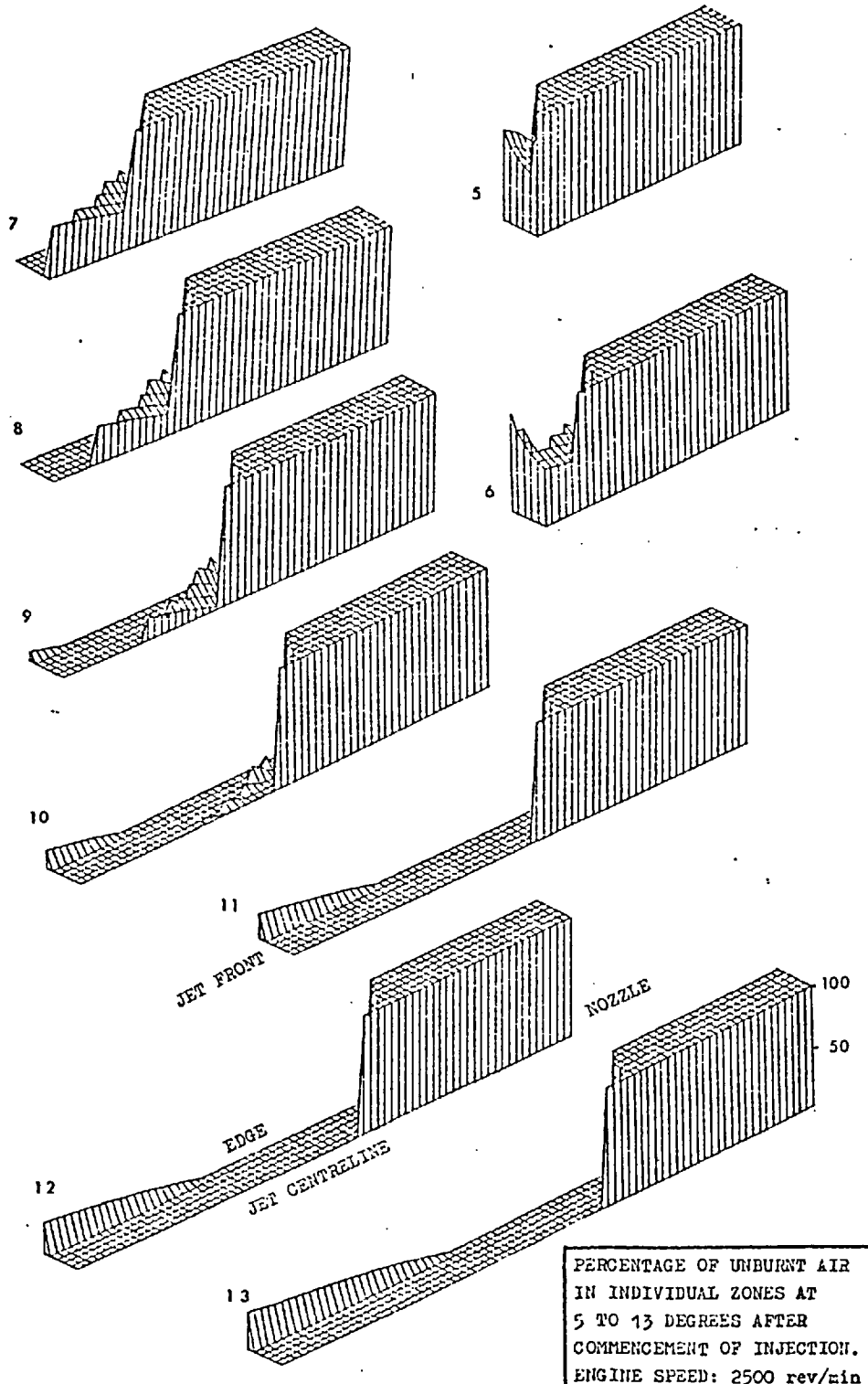

PERCENTAGE OF UNBURNT AIR
IN INDIVIDUAL ZONES AT
5 TO 13 DEGREES AFTER
COMMENCEMENT OF INJECTION.
ENGINE SPEED: 2500 rev/min
BMEP: 900.0 kN/m2
D.I.TIMING: -12°BTDC
INJECTION DURATION: 18°CA

Fig. 6.28.

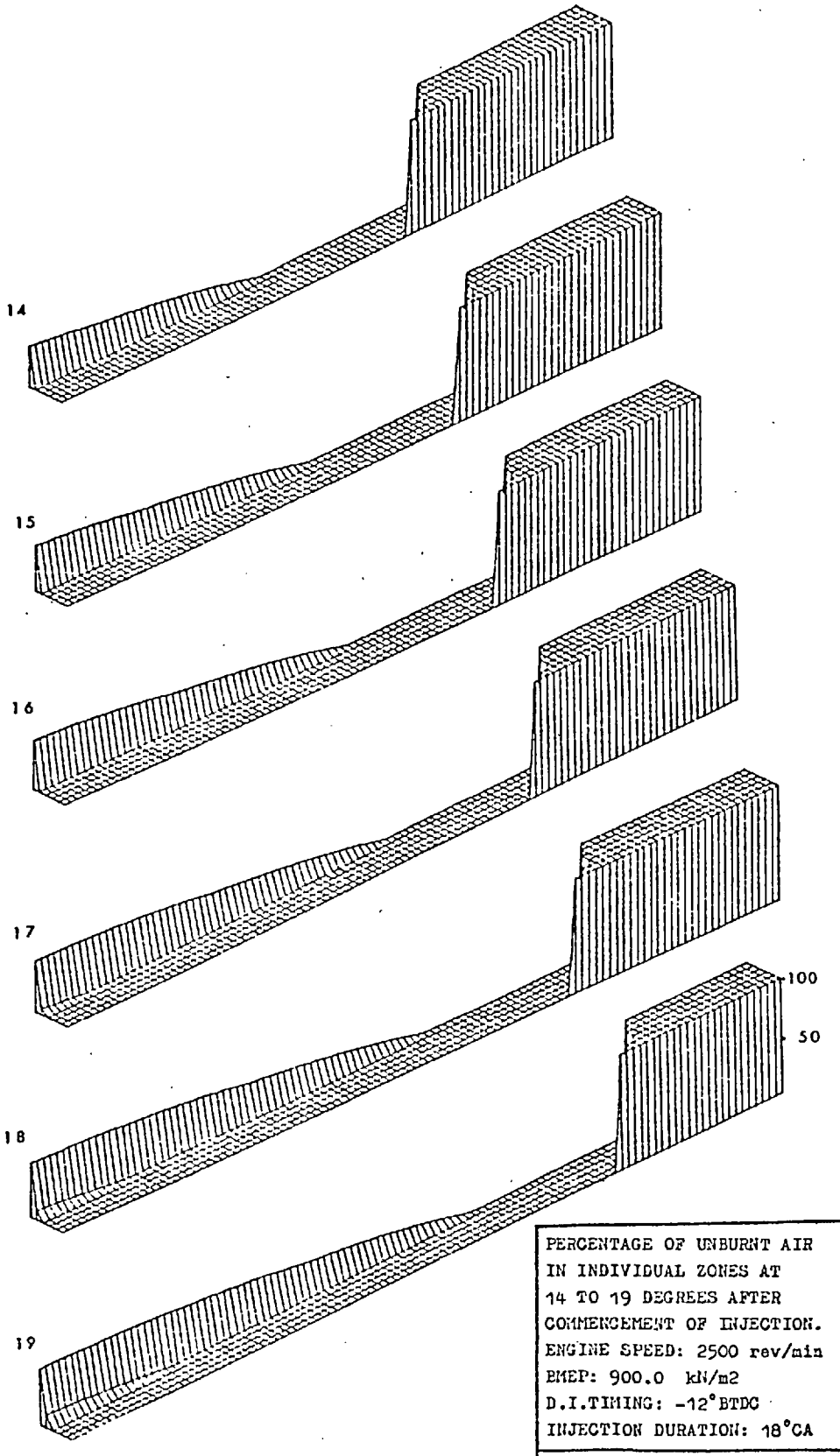

PERCENTAGE OF UNBURNT AIR
IN INDIVIDUAL ZONES AT
14 TO 19 DEGREES AFTER
COMMENCEMENT OF INJECTION.
ENGINE SPEED: 2500 rev/min
BMEP: 900.0 kN/m2
D.I.TIMING: -12°BTDC
INJECTION DURATION: 18°CA

Fig. 6.29.

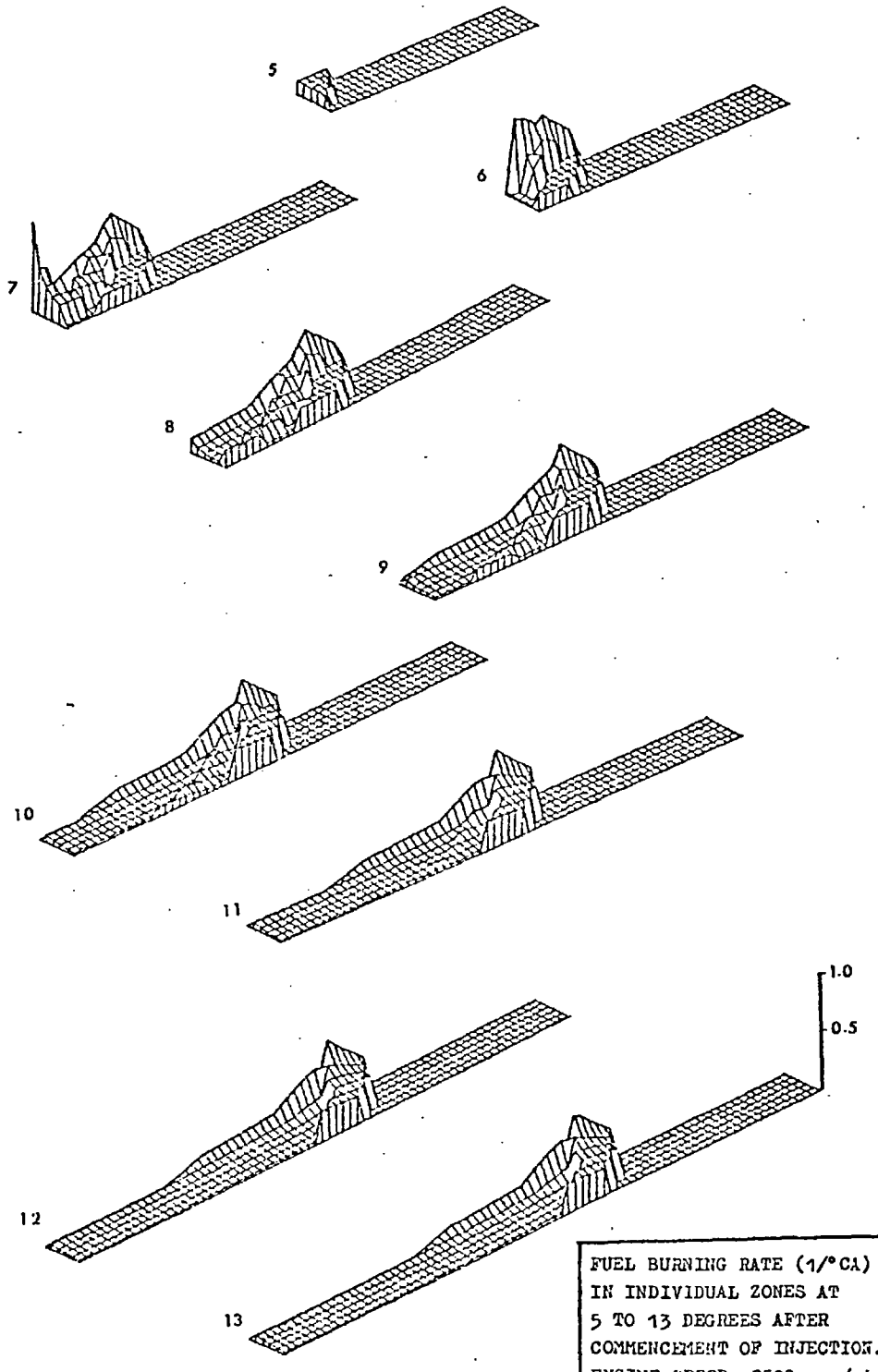

FUEL BURNING RATE (1/°CA)
IN INDIVIDUAL ZONES AT
5 TO 13 DEGREES AFTER
COMMENCEMENT OF INJECTION.
ENGINE SPEED: 2500 rev/min
BMEP: 900.0 kN/m2
D.I.TIMING: -12°BTDC
INJECTION DURATION: 18°CA

Fig. 6.30.

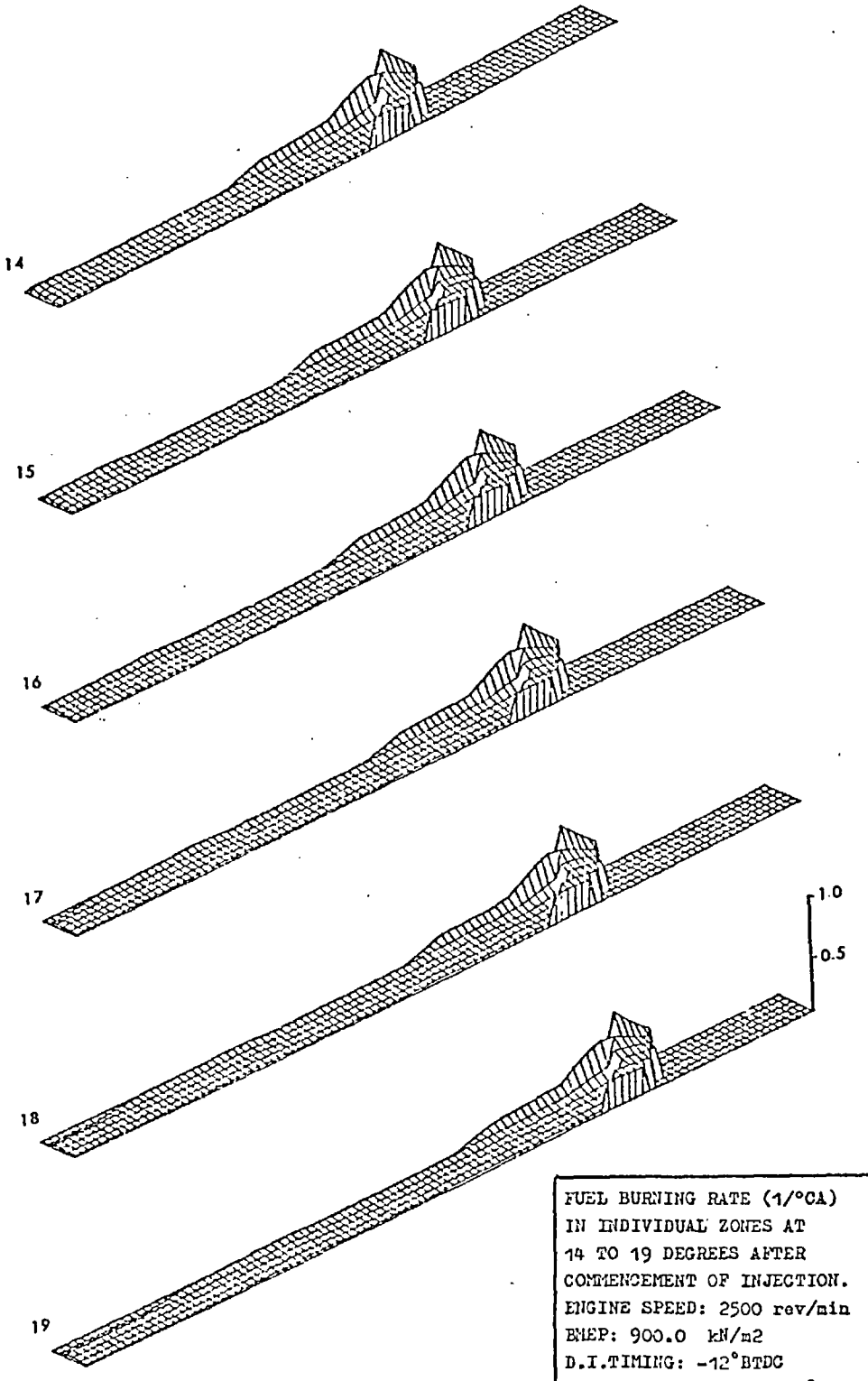

FUEL BURNING RATE (1/°CA)
IN INDIVIDUAL ZONES AT
14 TO 19 DEGREES AFTER
COMMENCEMENT OF INJECTION.
ENGINE SPEED: 2500 rev/min
BMEP: 900.0 kN/m2
D.I.TIMING: -12°BTDC
INJECTION DURATION: 18°CA

Fig. 6.31.

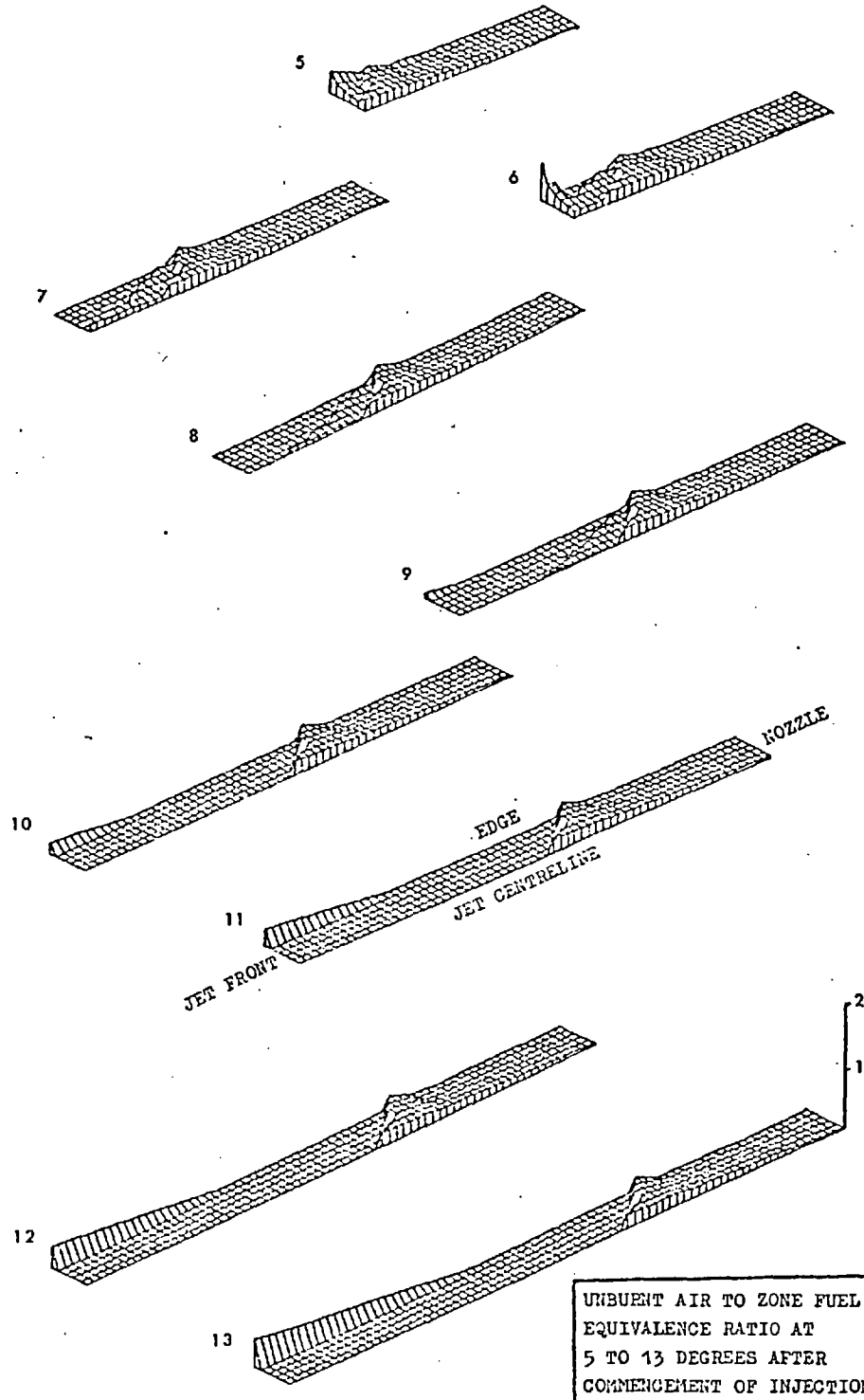

UNBURNT AIR TO ZONE FUEL EQUIVALENCE RATIO AT 5 TO 13 DEGREES AFTER COMMENCEMENT OF INJECTION.
ENGINE SPEED: 2500 rev/min
BMEP: 900.0 kN/m2
D.I.TIMING: -12°BTDC
INJECTION DURATION: 18°CA

Fig. 6.32.

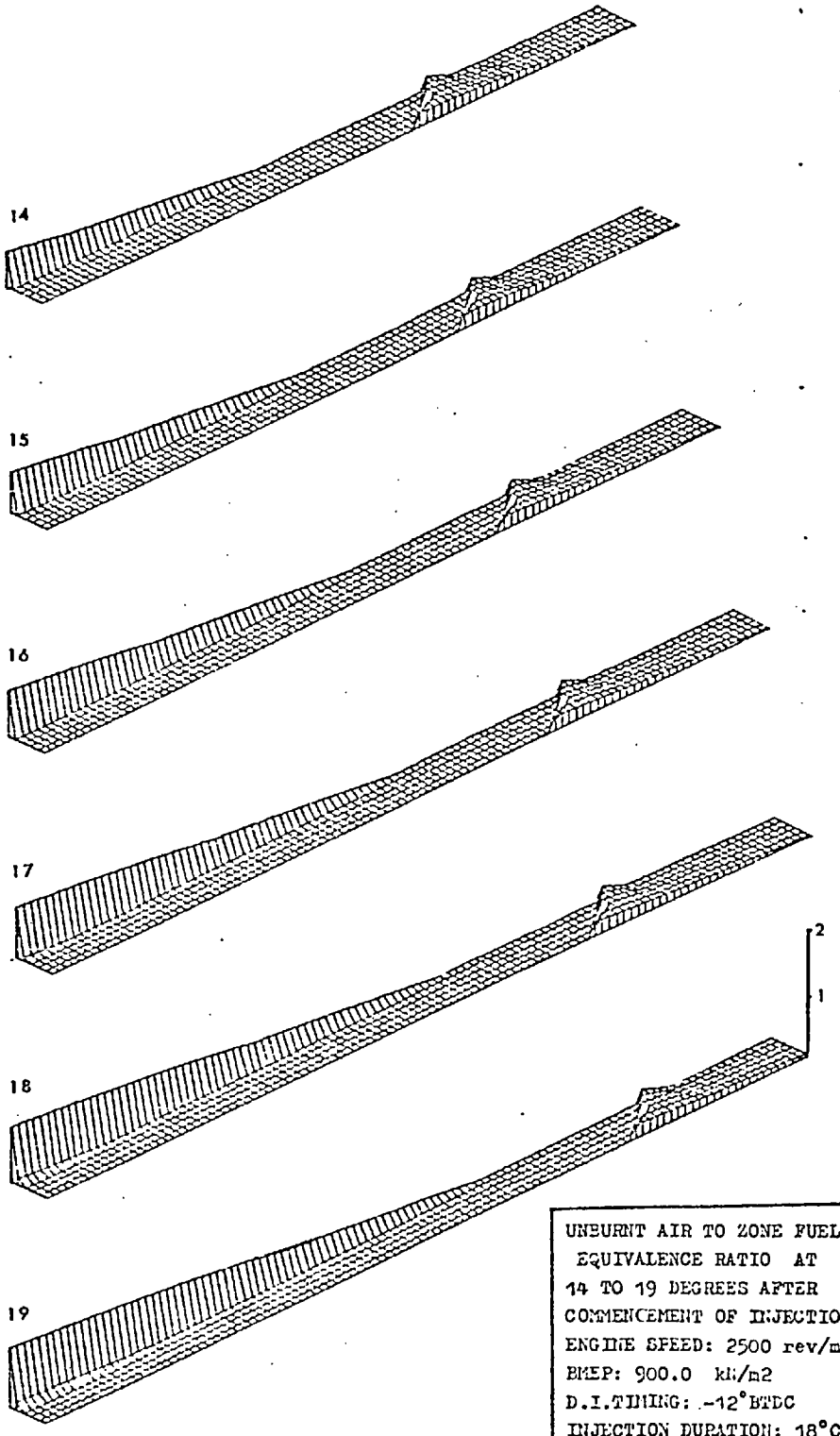

UNBURNT AIR TO ZONE FUEL EQUIVALENCE RATIO AT 14 TO 19 DEGREES AFTER COMMENCEMENT OF INJECTION.
ENGINE SPEED: 2500 rev/min
BMEP: 900.0 kN/m2
D.I.TIMING: -12°BTDC
INJECTION DURATION: 18°CA

Fig. 6.33.

temperature and pressure at injection are significantly above those of the previous case. Predicted ignition delay is shorter; combustion commencing 0.33 ms (5 degrees) after injection (c.f. 0.77 ms, 7 degrees in the previous case). Also in contrast to the previous case, ignition takes place as soon as a small group of zones are within the inflammability limits (temperatures are high enough). However, when this happens, there are not very many other zones ready for premixed burning. This is why a noticeable first peak does not appear in the overall fuel burning rate curve (Fig. 6.8). Thus within only two degrees after ignition, a fairly regular flame is established (Fig. 6.24). This flame is supported by further zones that cross the rich limit in turn, undergo premixed burning followed by gradual diffusion burning as they move along (Fig. 6.25). The injection duration is relatively long (18 degrees) during which the number of zones undergoing diffusion burning gradually increases. Eventually every zone will either be in a diffusion burning mode or will have attained complete combustion. The fairly uniform burning pattern predicted in this test condition is compatible with the experimental burning rate curve (Fig. 6.8).

If the distribution of the zone variables along and across the jet are not required, the time history of a variable for all zones can be accommodated in one (or two) diagrams only. Figures 6.34 to 6.37 show four such diagrams for the percentage of fuel burnt in each of the two cases examined before (cases 3 and 8). In fact the two diagrams of Fig. 6.34 and 6.35 have replaced all the diagrams of

Fig. 6.14 and 6.15 and give the history of this variable for a longer duration (24 deg. CA).

Moreover, in the previous diagrams, it is difficult to follow the history of individual zones because of the complexity of the zone motion within the spray. Here, each zone has been given a number which makes it possible to construct a three dimensional diagram for any variable against zone number and crank angle.

Initially the value of the variable is set to zero for all those zones that have not been created. The numbering of the zones is compatible with the order in which they are created (i.e. as they enter the combustion chamber). Thus each zone, during its growth and motion in the combustion chamber, bears a single number. This is related to any other variable of the zone (stored at the beginning and end of each time-step), through the zone labels along and across the jet (K, L and K1, L1 as in Chapter 3, section 3.32), i.e.

NUMZ2 (K,L) = NUMZ1 (K1,L1)

Prior to the creation of any batch of KR^2 zones, the numbers NUMZ1 are given to the zones in that batch following the last number of the previous batch. These zones are hypothetically considered to form layers prior to injection with 2K-1 zones in each layer. The zones near the fringe (to become slow moving zones) receive the low numbers and the zones near the centreline (to become fast moving zones) receive the higher numbers through the following package in the computer program:

```
      DO 103 L = 1,KR
      DO 102 K = 1,KR
      NUMZ1 (K, LX + KR +1 - L) = KR* (LX - KR + 2) +
                K^2 - 2K - L + 2
      NUMZ1 (K, LX + 1 - L) = KR* (LX + 2) + K^2 -
                2K - L + 2
102   CONTINUE
103   CONTINUE
```

In Fig. 6.34 and 6.35 (for the history of bz in case 3) the output of the computer program is shown with KR = 3, i.e. nine zones in each batch. Thus the total number of zones is 8 x 9 = 72 (injection duration = 8 deg. CA). The first half of the zones are accommodated in Fig. 6.34 and the rest in Fig. 6.35. In this way a moderate size matrix is obtained for plotting (36 zones x 24 degrees crank angle).

Similarly, for case 8 due to the length of the injection duration (18 degrees) the computer program is run choosing KR = 2 (i.e. 4 zones in a batch only) which again gives a total of 4 x 18 = 72 zones to construct the diagrams in Fig. 6.36 and 6.37.

In case 3, at 24^{o} after the start of injection, except for the slow moving zones, most zones have attained nearly complete combustion. In case 8 however, due to the length of the injection period, only some of the zones created during the first half of injection (Fig. 6.36) have attained complete combustion.

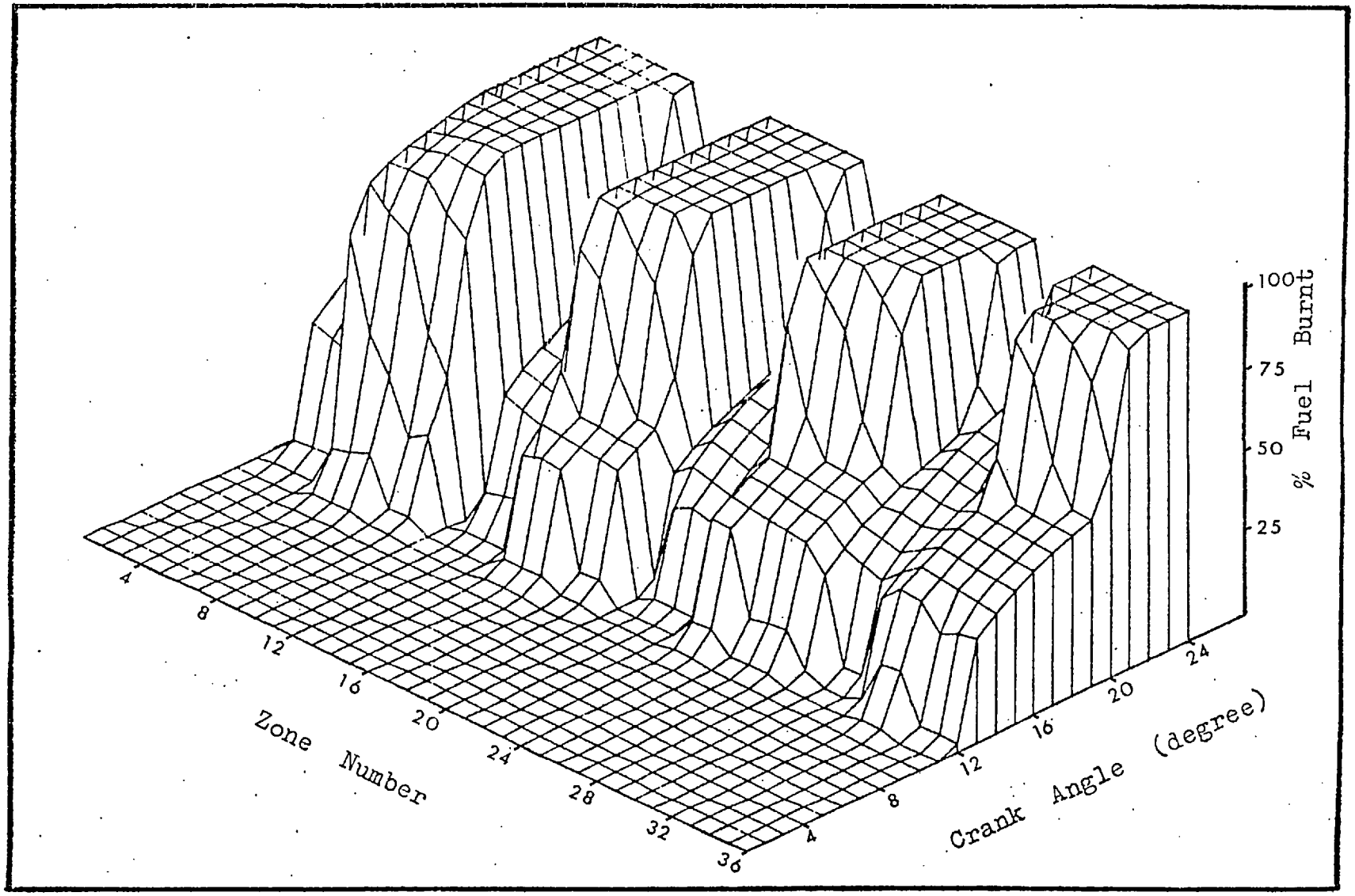

Fig. 6.34. Precentage of fuel burnt vs crank angle for individual zones created during the first half of injection (case 3).

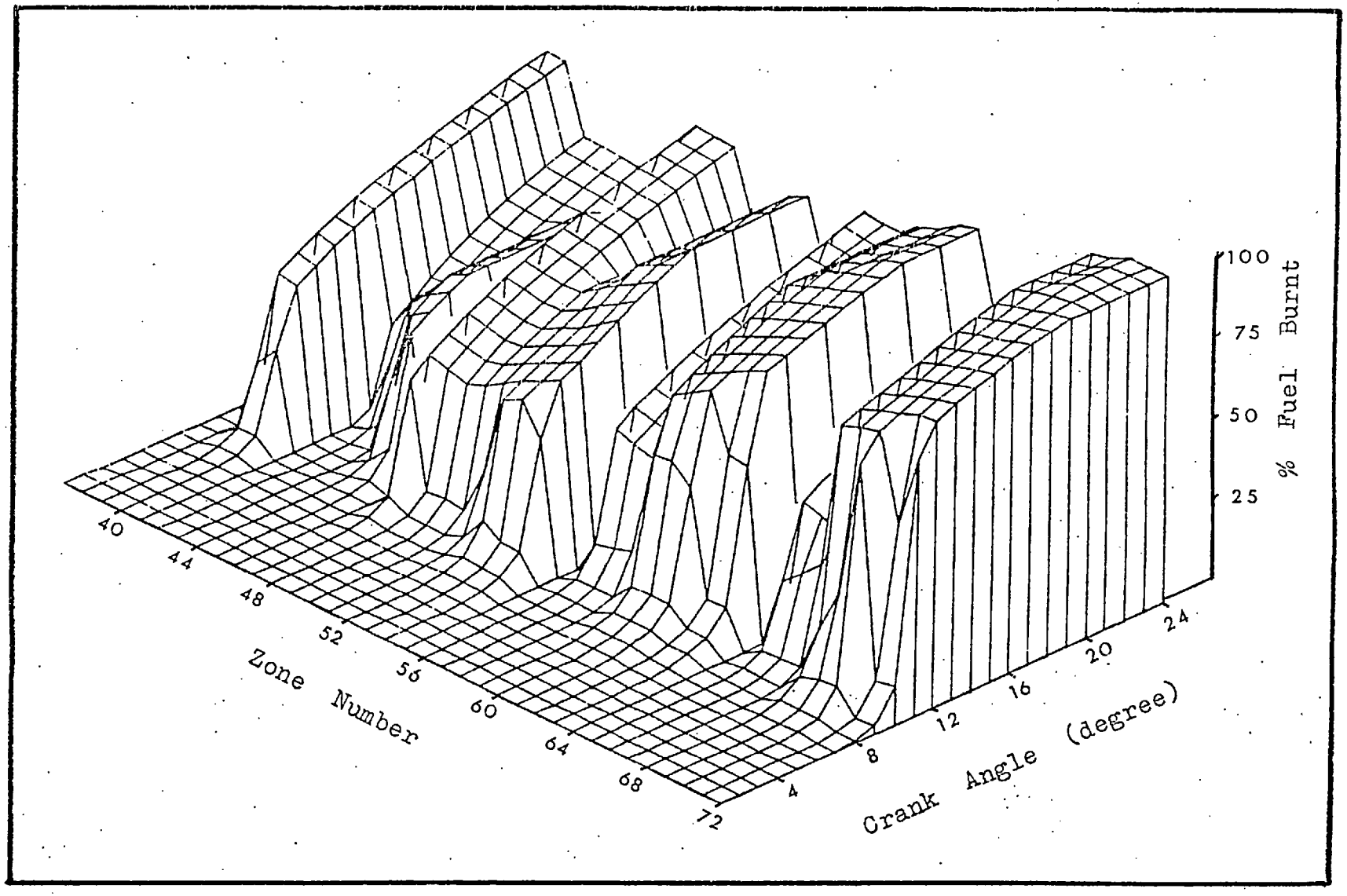

Fig. 6.35. Percentage of fuel burnt vs crank angle for individual zones created during the second half of injection (case 3).

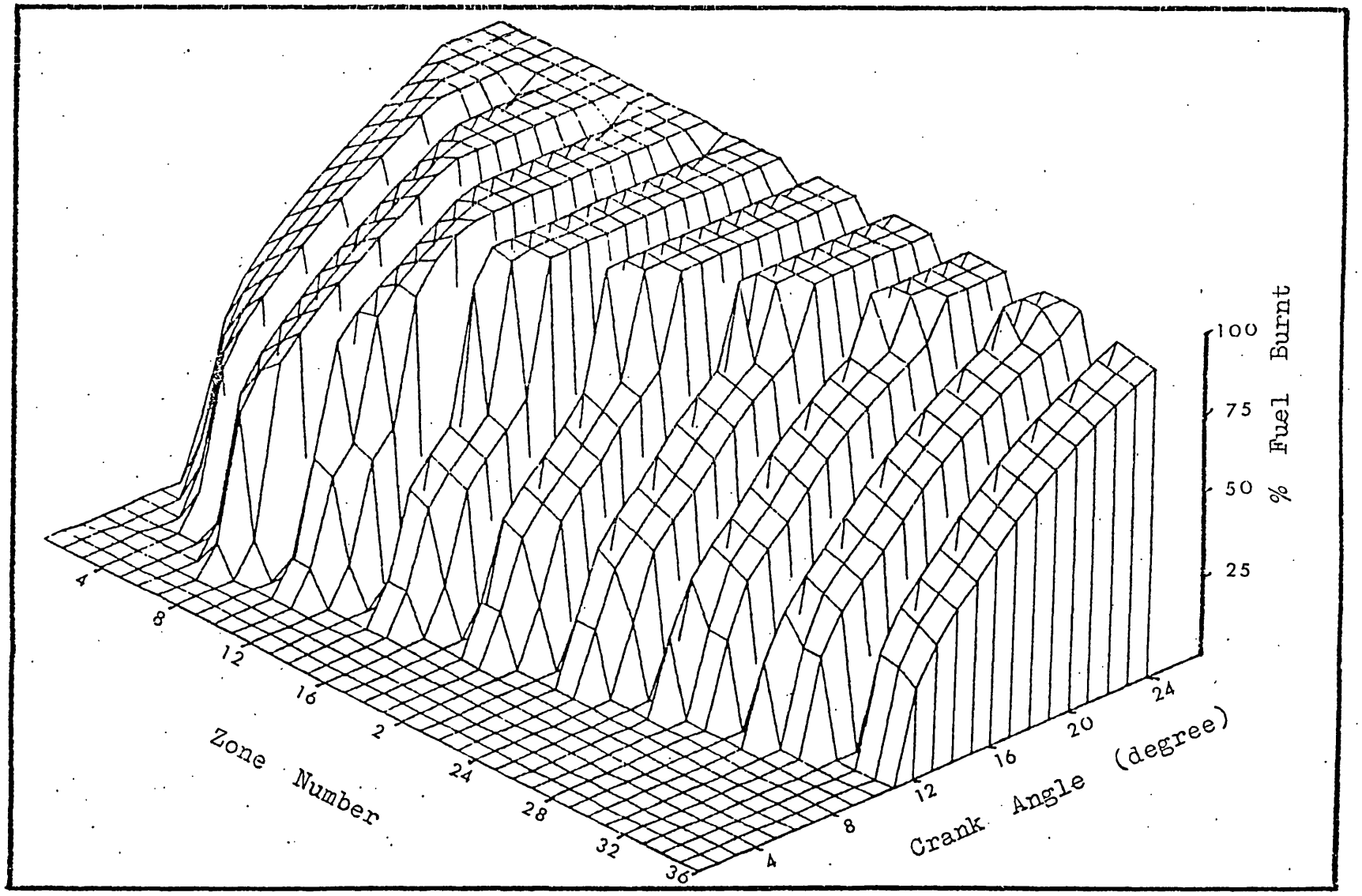

Fig. 6.36. Percentage of fuel burnt vs crank angle for individual zones created during the first half of injection (case 8).

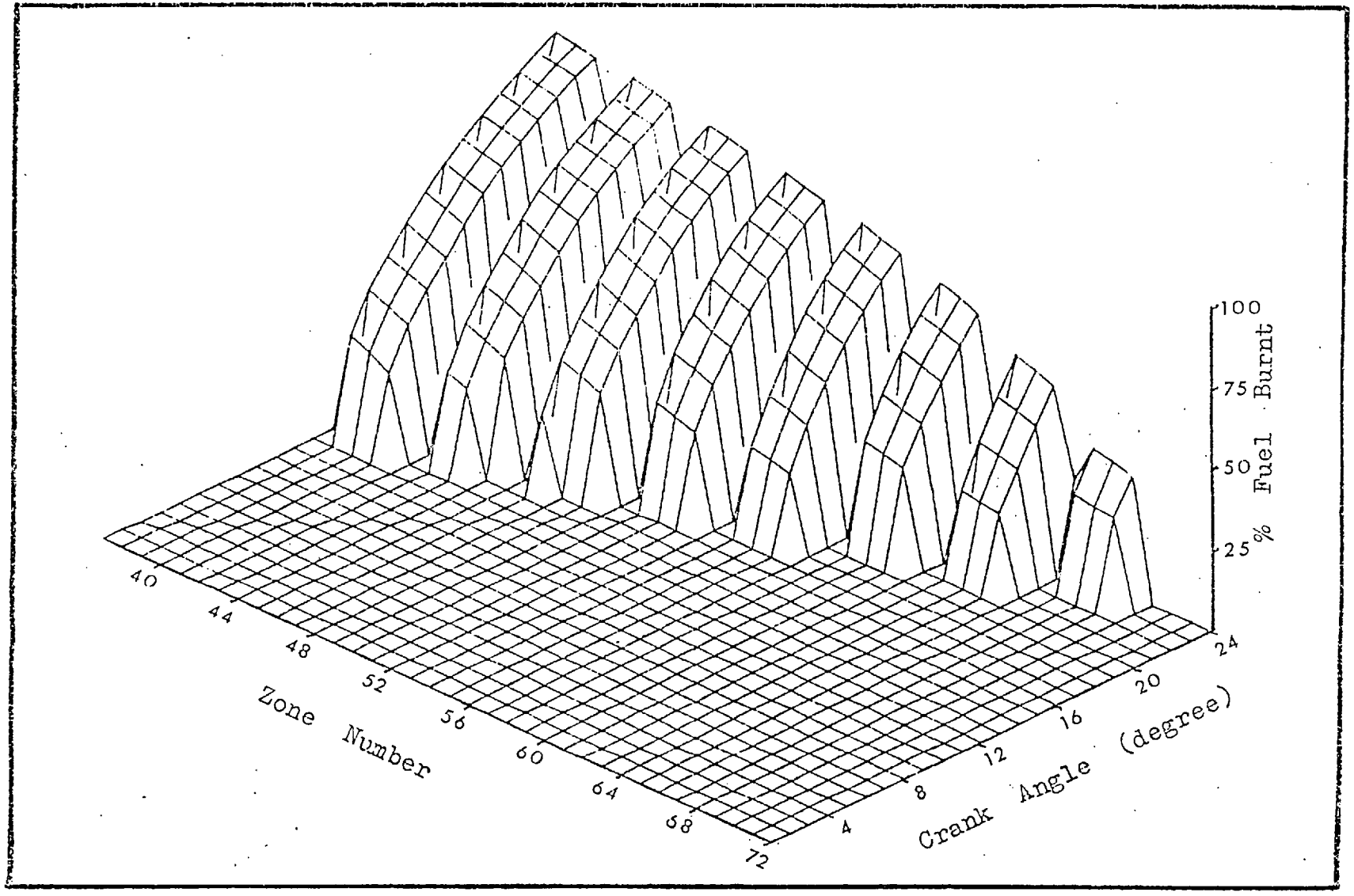

Fig. 6.37. Percentage of fuel burnt vs crank angle for individual zones created during the second half of injection (case 8).

Thus the burning pattern and other variables of the individual zones provide useful information concerning the initiation and development of combustion in the present model.

It has been shown that the model is capable of predicting realistic heat release rates and responds sensibly to changes in various parameters. However, since correct prediction of the moment of ignition is critical, and involves all aspects of the model, this will be discussed further.

Mixture formation, chemical kinetics as well as most other aspects related to the general structure and the assumptions in this model affect ignition.

The equations determining the reaction rates and temperature change leading to ignition are the same as those determining the state of each zone up to the end of combustion. Thus at all times there are two main factors, namely the zone temperature and concentration, which influence the rate of reaction in the zone.

Initially the mixture in the zone is too rich to allow any burning to take place. After the zone has crossed the inflammability limit, temperature becomes the decisive factor. If the temperature is very high, ignition occurs as soon as the zone crosses the rich limit. In such a case, the mixture formation aspect of the process becomes the dominating factor in determining ignition. Otherwise the increase in temperature due to compression decides the timing of ignition.

Thus potential for improving the accuracy of the model lies in future development of the physical aspects of the process, namely the jet-mixing pattern.

The model, at its present stage, shows closer agreement between predicted and measured ignition delay at those running conditions which have relatively low initial cylinder temperatures (case 1 and 3, Fig. 6.1 and 6.3). At higher initial cylinder temperatures. where the process is dominated by the mixing pattern, the error in the prediction of ignition delay is greater. This means that the model responds better to the influence of temperature than to the influence of the mixing pattern.

The above argument suggests that the formulation of the chemical kinetics aspects of the model is satisfactory. This view is probably further supported by the fact that changing the constants of the Arrhenious equation in any direction from the published values used, increases the disparity between the predicted and measured cylinder pressure diagrams. On the other hand changing the physical factors (e.g. Patrick's correlation for the concentration distribution of the deflected jet) in some cases improves the predictions. More work needs to be done on formulating the fuel-air mixing process in burning fuel sprays. It may be possible to improve the concentration distribution of the present model on the basis of information available from the mixture formation model of Whitehouse (1975). In any case the structure of the zone formation pattern in the present model is such that it can be improved as further information on deflected jets becomes available.

For improvements concerning the thermodynamic aspect of the process, Shahed's (1975) model may be considered useful, despite the fact that it is unsuitable for the early stages of the heat release period. This model does not predict ignition, but contains certain assumptions that may be beneficial in trying to predict the rich mixture combustion products based on chemical equilibrium during a part of the combustion duration.

However, the more detailed zone division pattern in the present model, compared to others, is a major potential benefit.

CHAPTER 7

SUMMARY, CONCLUSIONS AND RECOMMENDATIONS

7.1 Summary

A mathematical model for predicting the rate of heat release and cylinder pressure diagrams in direct injection diesel engines has been developed.

It was decided to devise a multi-zone structure for the model due to the importance of detailed information required on air entrainment in different parts of the fuel spray. It is also believed that a multi-zone structure will be of immense benefit in future applications of the model to pollutant formation studies.

Zone motion and concentration changes are dealt with on the basis of a jet-mixing model. Attention was paid to incorporate a detailed zone division pattern in an intermittent spray that allowed transition to a wall-jet and accounted for the air swirl present in the combustion chamber.

Due to the lack of sufficient information on jets in the presence of air swirl, a direct calculation of the zone formation pattern in such a jet was avoided. Instead, initially, a zone-formation pattern was calculated for an impulsively starting circular jet and a radial wall jet in the absence of swirl. The effect of swirl on reducing the fuel concentration in each zone was added to the model on the basis of experimental correlations and simplifying assumptions.

The mixture formation model thus obtained was assumed to exclusively supply the required information on air entrainment by individual zones.

Thermodynamic equations were applied to individual zones to compute zone heat release and temperature change resulting in the overall pressure change for the cylinder contents.

It was decided that fuel evaporation is relatively fast and its effect can be neglected. The first law of thermodynamics, the equation of state and the burning rate equation are applied to individual zones. The zone division pattern provides the essential structure for a step-by-step calculation of the time-dependent zone variables. Pressure is assumed to be equal in all zones at any time. The fuel mass burning rate is calculated by the Arrhenius equation, for all zones from the rich to the lean limits of inflammability. Constant values of activation energy and steric factor are used throughout the computations. The total rate of heat transfer is calculated using Eichelberg's correlation and is assumed to be shared among individual zones according to their mass and temperature.

The ability of the model to predict cylinder pressure diagrams has been verified experimentally and theoretical predictions, of for example, the distribution of temperature and burning rates have been investigated and discussed.

Eight test conditions covering the complete operating range of a turbocharged, direct injection, 4-stroke truck engine from 1000 to 2500 rev/min, medium to high

load, zero to full boost pressure (100 to 200 kN/m^2) have been considered for comparison between predicted and measured cylinder pressure diagrams.

The response of the model to changes in injection timing, swirl ratio, air temperature and injection rate has been investigated and discussed.

Spatial and temporal distributions of six variables have been displayed to demonstrate the initiation and development of combustion in two different cases.

7.2 Conclusions

A multi-zone model for the mixture formation and heat release in direct injection diesel engines has been developed.

Dependence on empirical correlations is not eliminated but has been substantially reduced in relation to other models. In particular the use of an ignition delay correlation is avoided by direct prediction of the timing and location of ignition and subsequent propagation of combustion.

It has been shown to be possible to predict ignition on the basis of two phenomena, namely the jet mixing process and temperature dependant reaction rates.

The model predicts the rapid pressure rise during the early stages of combustion and is therefore a valuable starting point for analytical combustion generated noise studies.

More work needs to be done on air-fuel mixing in burning fuel sprays. The accuracy in predicting timing of ignition needs improving. However, with the simplifying assumptions used in the model, reasonable predictions of the cylinder pressure diagram have been obtained.

The trends predicted by the model when changing controlling parameters, such as injection timing, swirl, air temperature and injection rate agree with those observed experimentally.

The multi-zone structure of the model enables the spatial and temporal history of burning rates, temperature, air fuel ratio, etc. to be investigated. It is believed that this structure will prove to be ideal for predicting the formation of various pollutants in diesel combustion chambers. In this respect, the potential resolution of mixture and temperature distribution will be a major asset.

7.3 Recommendations

The computer program developed for the present model may easily replace the heat release prediction package in a complete cycle simulation program used for direct injection diesel engines with few modifications. In this application, the response of the present heat release model in predicting b.m.e.p. for different engines can be investigated without requiring detailed data from the engines. This approach is recommended as a first step for further investigation of the overall predictive capability of the model.

More work is recommended to improve the physical aspects of the model in predicting the initiation and

development of combustion. This may include changing the correlation for the distribution of centreline concentration for jets in cross flow. It may also be useful to reconsider the assumption which relates the concentration distribution of jets in the presence and absence of cross flow, and in particular, the wall jet.

Work may be carried out towards extending the chemical kinetics and thermodynamic aspects of the chemical equilibrium in the combustion products during certain parts of the process.

The general structure of the model will provide detailed information on any variable required for pollutant calculations. This will make it relatively easy to add the mechanism of formation of Nitric Oxides, for example. The same applies to the prediction of CO. Soot formation, however, may be predicted with relatively more effort, although the changes required in the model have not been studied. Unburnt hydrocarbons could also be predicted, except that a better resolution of distribution across the jet will be required. Increasing the number of zones across the jet to obtain individual zones of very low fuel-to-air ratios is easily achieved in the present model.

APPENDIX A

Values of integrals $I_n(y)$ used in the text:

$$I_{fn}(y) = 2 \cdot \int_o^I (1 - y^{1.5})^n \, y \, dy$$

$$I_{f1}(y) = y^2 - \frac{4}{7} y^{3.5}$$

$$I_{f2}(y) = y^2 - \frac{8}{7} y^{3.5} + \frac{2}{5} y^5$$

$$I_{f3}(y) = y^2 - \frac{12}{7} y^{3.5} + \frac{6}{5} y^5 - \frac{4}{13} y^{6.5}$$

$$I_{f4}(y) = y^2 - \frac{16}{7} y^{3.5} + \frac{12}{5} y^5 - \frac{16}{13} y^{6.5} + \frac{1}{4} y^8$$

$$I_{f5}(y) = y^2 - \frac{20}{7} y^{3.5} + \frac{20}{7} y^{3.5} + \frac{20}{5} y^5 - \frac{40}{13} y^{6.5}$$

$$+ \frac{5}{4} y^8 - \frac{4}{19} y^{9.5}$$

$$I_{fn}(y) = 2. \sum_{m=0}^{m=n} (-1)^m \frac{n! \, y^{1.5m+2}}{(1.5m + 2) \cdot m!(n-m)!}$$

$I_{f1}(1.) = 0.430$ $\qquad$ $I_{f1}(0.5) = 0.199$

$I_{f2}(1.) = 0.257$ $\qquad$ $I_{f2}(0.5) = 0.161$

$I_{f3}(1.) = 0.180$ $\qquad$ $I_{f3}(0.5) = 0.132$

$I_{f4}(1.) = 0.134$ $\qquad$ $I_{f4}(0.5) = 0.110$

$I_{f5}(1.) = 0.108$ $\qquad$ $I_{f5}(0.5) = 0.093$

$$I_{wn}(y) = \int_o^I (1 - y^{1.5}) \, dy$$

$$I_{w1}(y) = y - \frac{1}{2.5}y^{2.5}$$

$$I_{w2}(y) = y - \frac{2}{2.5}y^{2.5} + \frac{1}{4}y^{4}$$

$$I_{w3}(y) = y - \frac{3}{2.5}y^{2.5} + \frac{3}{4}y^{4} - \frac{1}{5.5}y^{5.5}$$

$$I_{w4}(y) = y - \frac{4}{2.5}y^{2.5} + \frac{6}{4}y^{4} - \frac{4}{5.5}y^{5.5} + \frac{1}{7}y^{7}$$

$$I_{w5}(y) = y - \frac{5}{2.5}y^{2.5} + \frac{10}{4}y^{4} - \frac{10}{5.5}y^{5.5} + \frac{5}{7}y^{7} - \frac{1}{8.5}y^{8.5}$$

$$I_{wn}(y) = \sum_{m=0}^{m=n} (-1)^{m} \frac{n!\, y^{1.5m+1}}{(1.5m + 1)m!(n - m!)}$$

$I_{w1}(1.) = 0.600$ $\qquad$ $I_{w1}(0.5) = 0.429$

$I_{w2}(1.) = 0.450$ $\qquad$ $I_{w2}(0.5) = 0.374$

$I_{w3}(1.) = 0.368$ $\qquad$ $I_{w3}(0.5) = 0.330$

$I_{w4}(1.) = 0.316$ $\qquad$ $I_{w4}(0.5) = 0.296$

$I_{w5}(1.) = 0.278$ $\qquad$ $I_{w5}(0.5) = 0.267$

Appendix B

The exposed surface area of the cylinder liner (A_ℓ) and the cylinder volume $V(\theta)$ in terms of crank angle (θ) are calculated from the following relations:

$$A_\ell(\theta) = \pi \cdot B \cdot S_x(\theta)$$

$$V(\theta) = \pi \cdot \frac{B^2}{4} \cdot S_x(\theta) + V_{c\ell}$$

The angle (θ) is zero at T.D.C. (firing) and $S_x(\theta)$ indicates the position of the piston crown relative to T.D.C. in terms of the connecting rod length (ℓ) and the piston stroke (S).

$$S_x(\theta) = \ell + 0.5S \cdot (1 - \text{Cos } \theta) - \left|\ell^2 - 0.25S^2 \cdot \text{Sin}^2\theta\right|^{\frac{1}{2}}$$

The crank angle (θ) should be -180 to 0 or 540 to 720 during compression and 0 to 180 during expansion (in any case S_x is positive).

Appendix C

Fuel specifications (Shell gas oil)

Aniline point	70
Cloud point (^{o}F)	15
Critical pressure (psig)	350
Critical temperature (^{o}F)	900
Distillation range (^{o}C)	180-360
Flash point (^{o}C)	77
Pour point (^{o}C)	-5.5
Specific gravity at 65^{o}C	0.83
Surface tension at 20^{o}C (dynes/cm^{2})	30
Thermal conductivity at 0^{o}C (BTU/hr/in/^{o}R)	1.0
Mean molecular weight	200

Analysis

Carbon wt	86.2
Hydrogen wt	13.0
Sulphur wt	0.8

PUBLICATIONS

Meguerdichian M. and Watson N. "Mixture Formation and Heat Release in Diesel Engines", S.A.E. Paper No. 780225, International Congress on Internal Combustion Engines Detroit, 1978.

REFERENCES

1. Abramovich G.N. "The Theory of Turbulent Jets". MIT Press, Cambridge, Massachusetts, 1963.

2. Albertson, Dai, Jensen and Rouse. "Diffusion of Submerged Jets". Proc. A.S.C.E., 74, 1948.

3. Beer J.M. and Chigier N. "Combustion Aerodynamics", Applied Science Publishers, pp.22-25, 1972.

4. Burt R. and Troth K. "Penetration and Vaporization of Diesel Fuel Sprays". Diesel Engine Combustion Proc., Inst.Mech.Engrs., Vol.184, Part 31, pp. 147 - 170, 1970.

5. Chiu W.S., Shahed S.M. and Lyn W.T. "A Transient Spray Mixing Model for Diesel Combustion". SAE Paper No. 760128, 1976.

6. Dent J.C. "A Basis for the Comparison of Various Experimental Methods for Studying Spray Penetration". SAE Paper No. 710571, 1971.

7. Dent J.C. and Derham J.A. "Air Motion in a Four Stroke Direct Injection Diesel Engine". Inst.Mech.Engrs. 1973.

8. Edson M.H. "A Mathematical Model for Combustion". Ind.Engineering Chem. 52(No.12), 1007, 1960.

9. Forstall W. and Shapiro A.H. "Momentum and Mass Transfer in Coaxial Gas Jets". Journal of Applied Mechanics, Dec. 1950.

10. Glauert M.B. "The Wall Jet". Journal of Fluid Mechanis, 1956.

11. Grigg H.C. and Syed M.H. "The Problem of Predicting Rate of Heat Release in Diesel Engines". Symposium on 'Diesel Engine Combustion', Inst.Mech.Engrs. 1970.

12. Hall A.R. and Diederichsen J. "An Experimental Study of the Burning of Single Drops of Fuel in Air at up to Twenty Atmospheres". IVth Symposium (Int.)

on Combustion (Williams and Wilkins; Baltimore). 837, 1953.

13 Hay N. and Jones P.L. "Comparison of the Various Correlations for Spray Penetration". SAE Paper No. 720776, 1972.

14. Hiroyasu H. and Kadota T. "Models for Combustion and Formation of Nitric Oxide and Soot in Direct Injection Diesel Engines". SAE Paper No. 760129, February 1976.

15. Hiroyasu H. and Kadota T. "Droplet Size Distributions in Diesel Engines". SAE Paper No. 740715, 1974.

16. Hodgetts D. and Shroff H.D. "More on the Formation of Nitric Oxide in a Diesel Engine". Conference on 'Combustion in Engines', Inst.Mech.Engrs., 1975.

17. Ikegami M. and Nagao F. "An Analysis of Combustion Knock in Diesel Engines". Proc.Inst.Mech.Engrs., 1969.

18. Jordinson R. "Flow in a Jet Directed Normal to the Wind". Aero.Res.Council, R & M., No. 3074, 1956.

19. Khan I.M., Greeves G. and Wong C.H.T. "Factors Affecting Smoke and Gaseous Emissions from Direct Injection Diesel Engines and a Method of Calculation". SAE Paper No. 730169, 1973.

20. Knight B.E. "Communication on the Performance of a Type of Swirl Atomiser". Proc.Inst.Mech.Engrs., 104, 1955.

21. Lyn W.T. "Study of the Burning Rate and Combustion in Diesel Engines". IXth Symposium (International) on Combustion, 1962.

22. Lyshevskiy A.S. "The Coefficient of Free Turbulence in a Jet of Atomised Liquid Fuel". NASA TTF-351, 1956.

23. Marzouk M. "Simulation of Turbocharged Diesel Engines under Transient Conditions". Ph.D. Thesis, University of London, 1976.

24. Morton B.R, and Middleton J.H. "Scale Diagrams for Forced Plumes", J.Fluid Mechanics, Vol.58, part 1, pp.165-176, 1973.

25. Middleton J.H. "The Asymptotic Behaviour of a Starting Plume". J.Fluid Mechanics, Vol.72, part 4, pp. 753-771, 1975.

26. Newman J.A, and Brzustowski T.A. "Behaviour of a Liquid Jet Near the Thermodynamic Critical Region". A.I.A.A. Journal, Vol.9, No.8, 1971.

27. Ogosawara M. and Sami H. "Study on the Behaviour of a Fuel Droplet Injected into the Combustion Chamber of a Diesel Engine". SAE Transactions, Vol.78, paper 670468, 1967.

28. Olikara C. and Borman G.L. "A Computer Program for Calculating Properties of Equilibrium Combustion Products with Some Applications to I.C. Engines". SAE Paper No. 750468, Feb. 1975.

29. Öz H.J. "Calculation of Spray Penetration in Diesel Engines", SAE Paper No. 690254, Jan. 1969.

30. Parks M., Polonski C., and Toye R. "Penetration of Diesel Fuel Sprays in Gases." Paper 660747, presented at SAE Combined Powerplant and Transportation Meetings, Chicago, Oct., 1966.

31. Patrick M.A "Experimental Investigation of Mixing and Flow in a Round Turbulent Jet Injected Perpendicularly into a Main Stream". Sheffied Univ., Fuel Soc. Bulletin, 1965.

32. Powell H.N. "Applications of an Enthalpy-Fuel/Air Ratio Diagram to 'First Law' Combustion Problems", ASME, Gas Turbine Power and Machine Design Divns., Semi-Annual Meeting, Cleveland, Ohio, June 1956.

33. Probert R.P. "The Influence of Spray Particle Size and Distribution in the Combustion of Oil Droplets". Phil.Mag. Ser.7, 37(No.265), 94, 1946.

34. Rusinov R,V. "Length of Atomised Fuel Jet in a Diesel Engine." Russian Engrg.Jrl. 43, 1963.

35. Savery W,C. and Borman G.L. "Experiments on Droplet Vaporization at Supercritical Pressures". A.I.A.A 8th Aerospace Science Meeting, Paper No. 70-6, 1970.

36. Shahed S.M., Chiu W.S. and Lyn W.T. "A Mathematical Model of Diesel Combustion". Conf, on 'Combustion in Engines', Inst.Mech.Engrs., 1975.

37. Shandorov G.S. "Calculation of a Jet Axis in a Drifting Flow". NASA, TTF-10, 638, 1966.

38. Shipinski J.H., Myers P.S. and Uyehara O.A. "A Spray Droplet Model for Diesel Combustion', Symposium on Diesel Engine Combustion', Inst.Mech.Engrs., 1970.

39. Schweitzer P.H. "Penetration of Oil Sprays". Penn. State College Engineering Experiment Station Bulletin No. 46, 1937.

40. Sitkei G. "Kraftstoffaufbereitung und Verbrennung bei Dieselmotoren". Springer-Verlag, 1964.

41. Smith J.M. "A Fixed Head Concept Diesel Engine". Proc.Inst.Mech.Engrs. Vol.186, 16/72, 1972,

42. Spalding D.B. "Some Fundamentals of Combustion" Butterworths, London, 1955.

43. Squire H.B. and Trouncer B.A. "Round Jets in a General Stream". A.R.C. Technical Report (R & M No. 1974) Jan., 1944.

44. Tanasawa Y. "On the Combustion Rate of a Group of Fuel Particles". Technology Reports of Tonoku Univ., 18 (No.1), 61, 1953.

45. Taylor D.H. and Walsham B.E. "Combustion Processes in a Medium Speed Diesel Engine". Diesel Engine Combustion, Proc.Inst.Mech.Engrs., Vol.184, Part 3, pp.67-76, 1970.

46. Turner J.S. "The 'Starting Plume' in Neutral Surroundings". J.Fluid Mechanics, 13, pp.356-368, 1962.

47. Wakuri Y., Fujii M., Amitari T. and Tsuneya R. "Studies of the Penetration of a Fuel Spray in a Diesel Engine". Bull.J.S.M.E., Vol.3, No.9, pp. 123-130, 1960.

48. Whitehouse N.D. and Abughres S.M. "Calculation of Fuel-Air Mixing in a Diesel Engine with Swirl for the Purpose of Heat Release Prediction". Conf. on 'Combustion in Engines' Inst.Mech.Engrs. 1975.

49. Whitehouse N.D. and Sareen B.K. "Prediction of Heat Release in a Quiescent Chamber Diesel Engine Allowing for Fuel/Air Mixing". SAE Paper No. 740084, 1974.

50. Whitehouse N.D. and Way R. "Rate of Heat Release in Diesel Engines and its Correlation with Fuel Injection Data". Proc.Inst.Mech.Engrs., 184, Pt.3J, 1960-1970.

51. Wiebe I. "Habempirische Formel für die Verbrennungsgeschwindigkeit". Verleg der Akademie der Wissenschaften der VdSSR. Moscow, 1956.

52. Williams A. "Combustion of Droplets of Liquid Fuels: A Review". Combustion and Flame, 21, 1-31, 1973.

53. Williams T.J. "On the Effect of Droplet Lifetime and Diameter Distribution on Vapour Production Rates in Diesel Fuel Jets". Proc.Inst.Mech.Engrs., Vol.190, 10/76, 1976.

54. Wolfer H.H. "Der Zundverzug im Dieselmotor". VDI-Forschungsheft, 392, pp.15-24, 1938.

E R R A T A

Page	Line	Error	Correct
vii	3	fract	fraction
47	4	$+\int_0^1(1-y^{1.6})^5 ydy$	$+c_m\int_0^1(1-y^{1.5})^5 ydy$
50	15	$1+1.5d_j$ $+0.25$	$\sqrt{1+1.5d_j}$ $+0.25$
51	1	$\sqrt{}\ 1+1.5d_j$	$\sqrt{1+1.5d_j}$
54	21	$0.18\ {}_aA$	$0.18\ \rho_a A$
74	5	$=\frac{u_m}{2.4}\ \Delta l=$	$=\frac{u_m}{2.4}\Delta t=$
76	22	$=\frac{u_m}{2.}\ \Delta t$	$=\frac{u_m}{2.4}\ \Delta t$
108	4	Parmeability	Permeability
124	2	dm_z/dt	dq_z/dt
125	8	kg/m^2	kg/m^3
127	15	$=\int_o^D -kdt$	$=\int_o^t -kdt$
131	last	$(\frac{1}{cz_2}\ \ \frac{1}{cz_2})$	$(\frac{1}{c_{z2}}-\frac{1}{c_{z1}})$
138	20	(15)	(5.1)
138	21	(16)	(5.2)
138	22	(17)	(5.3)
233	16	1970	1961

Page	Line	Error	Correct
x	5	ill tration	illustation
2	6	immidiate	immediate
2	16	invironmental	environmental
8	21	trancationg	truncating
10	7	preveil	prevail
16	12	Woffer	Wolfer
27	4	suplied	supplied
27	27	Arhenius	Arrhenius
32	19	furtherst	furthest
42	20	relience	reliance
51	8,9	r_{1c}/r_{2c}	r_{c1}/r_{c2}
57	6	b_1/b_m	b_2/b_m
57	9	b_2/b_n	b_1/b_n
65	16	$(r-r_i)/r_i$	$\sqrt{r^2-r_i^2}/r_i$
65	5	hypotetical	hypothetical
66	12	$(r_f-r_i)/r_i$	$\sqrt{r_f^2-r_i^2}/r_i$
66	14	$(r_f-r_i)/(r-r_i)$	$\sqrt{(r_f^2-r_i^2)/(r^2-r_i^2)}$
93	14	interia	inertia
100	15	"	"
100	24	(10)	(1)
101	13	(6)	(14)
101	14	(7) (8)	(13) (12)
123	8	explicitly supply	supply explicitly
133	14	polynomical	polynomial
133	23	misture	mixture

Page	Line	Error	Correct
146	8	is	are
148	6	baginning	beginning
150	16	buring	burning
151	14	This is ... ... that measured.	This causes inaccuracy in predicted cylinder pressure diagrams.
153	2	maximum pressure	pressure diagrams
170	1	effected	affected
170	14	an increased peak pressure	a different cylinder pressure
175	18	spacial	spatial